SEISMIC RESPONSE AND VULNERABILITY ASSESSMENT OF TUNNELS: A CASE STUDY ON BOLU TUNNELS

A THESIS SUBMITTED TO
THE GRADUATE SCHOOL OF NATURAL AND APPLIED SCIENCES
OF
MIDDLE EAST TECHNICAL UNIVERSITY

BY

SERKAN ÜÇER

IN PARTIAL FULFILLMENT OF THE REQUIREMENTS
FOR
THE DEGREE OF DOCTOR OF PHILOSOPHY
IN
CIVIL ENGINEERING

SEPTEMBER 2012

Approval of the thesis:

SEISMIC RESPONSE AND VULNERABILITY ASSESSMENT OF TUNNELS:
A CASE STUDY ON BOLU TUNNELS

submitted by **SERKAN ÜÇER** in partial fulfillment of the requirements for the degree of **Doctor of Philosophy in Civil Engineering Department, Middle East Technical University** by,

Prof. Dr. Canan Özgen ____________________
Dean, Graduate School of **Natural and Applied Sciences**

Prof. Dr. Güney Özcebe ____________________
Head of Department, **Civil Engineering**

Prof. Dr. B. Sadık Bakır ____________________
Supervisor, **Civil Engineering Dept., METU**

Examining Committee Members:

Prof. Dr. M. Semih Yücemen ____________________
Civil Engineering Dept., METU

Prof. Dr. B. Sadık Bakır ____________________
Civil Engineering Dept., METU

Prof. Dr. H. Şebnem Düzgün ____________________
Mining Engineering Dept., METU

Prof. Dr. Tamer Topal ____________________
Geological Engineering Dept., METU

Asst. Prof. Dr. Deniz Ülgen ____________________
Civil Engineering Dept., Muğla University

Date: 27.09.2012

I hereby declare that all information in this document has been obtained and presented in accordance with academic rules and ethical conduct. I also declare that, as required by these rules and conduct, I have fully cited and referenced all material and results that are not original to this work.

Name, Last name : Serkan, Üçer

Signature :

ABSTRACT

SEISMIC RESPONSE AND VULNERABILITY ASSESSMENT OF TUNNELS:
A CASE STUDY ON BOLU TUNNELS

ÜÇER, Serkan

Ph.D., Department of Civil Engineering

Supervisor: Prof.Dr. B. Sadık BAKIR

September 2012, 159 pages

The aim of the study is to develop new analytical fragility curves for the vulnerability assessment of tunnels based on actual damage data of tunnels obtained from past earthquakes. For this purpose, additional important damage data belonging to Bolu Tunnels, Turkey was utilized as a case study.

Bolu Tunnels constitute a very interesting case from the earthquake hazard point of view, since two major earthquakes, 17 August 1999 Marmara and 12 November 1999 Düzce, occurred during the construction of the tunnels. The August 17, 1999 earthquake was reported to have had minimal impact on the Bolu Tunnels. However, the November 12, 1999 earthquake caused some sections of both tunnels to collapse. The remaining sections of the tunnels survived with various damage states which were subsequently documented in detail. This valuable damage data was thoroughly utilized in this study.

To develop analytical fragility curves, the methodology described by Argyroudis et al. (2007) was followed. Seismic response of the Tunnels was assessed using analytical, pseudo-static and full-dynamic approaches. In this way, it was possible to make comparisons regarding the dynamic analysis methods of tunnels to predict the seismically induced damage. Compared to the pseudo-static and full-dynamic methods, the predictive capability of the analytical method is found to be relatively low due to limitations inherent to this method. The pseudo-static and full-dynamic solution results attained appear to be closer to each other and better represented the recorded damage states in general. Still, however, the predictive capability of the pseudo-static approach was observed to be limited for particular cases with reference to the full-dynamic method, especially for the sections with increasingly difficult ground conditions.

The final goal of this study is the improvement of damage indexes corresponding to the defined damage states which were proposed by Argyroudis et al. (2005) based on the previous experience of damages in tunnels and engineering judgment. These damage indexes were modified in accordance with the findings from the dynamic analyses and actual damage data documented from Bolu Tunnels following the Düzce earthquake. Three damage states were utilized to quantify the damage in this study.

Keywords: Bolu Tunnels, Fragility Curve, Seismic Response, Earthquake, Vulnerability Assessment

ÖZ

TÜNELLERİN SİSMİK DAVRANIŞI VE SİSMİK HASAR DEĞERLENDİRMESİ:
BOLU TÜNELLERİ ÜZERİNE BİR ÇALIŞMA

ÜÇER, Serkan
Doktora, İnşaat Mühendisliği Bölümü
Tez Yöneticisi: Prof.Dr. B. Sadık BAKIR

Eylül 2012, 159 sayfa

Bu çalışmanın amacı geçmiş depremlerde hasar görmüş tünellerin gerçek deprem hasar bilgilerinden yararlanarak tünellerin sismik hasar değerlerlendirilmesinde kullanılmak üzere yeni hasargörebilirlik eğrileri çıkartmaktır. Bu amaçla Bolu Tünelleri'ne ait çok önemli hasar bilgileri örnek bir çalışma olarak kullanılmıştır.

Bolu Tünelleri, tünellerde oluşan deprem hasarı açısından çok önemli bir örnektir. Çünkü, bu tüneller inşaatları sırasında 17 Ağustos 1999 Marmara ve 12 Kasım 1999 Düzce Depremleri'ne maruz kalmıştır. 17 Ağustos 1999 Marmara Depremi'nin Bolu Tünelleri üzerinde etkisi çok az olmuştur. Fakat, 12 Kasım 1999 Düzce Depremi, inşaat halindeki Bolu Tünelleri'nin çeşitli kesimlerinde çökmelerin de yaşandığı ağır hasara sebep olmuştur. Tünellerin çökme yaşanmayan kesimleri çeşitli hasar düzeyleri ile kurtulmuş ve bu bilgiler sonradan detaylı bir şekilde kayıt altına alınmıştır. Elde edilen kıymetli hasar bilgileri yapılan bu çalışmada detaylı bir şekilde değerlendirilmiştir.

Analitik hasargörebilirlik eğrilerini tanımlamak için Argyroudis vd. (2007) tarafından tarif edilen yöntem kullanılmıştır. Tünellerin sismik davranışı analitik, yarı-statik ve tam-dinamik analiz yöntemleri kullanılarak değerlendirilmiştir. Bu sayede, sismik hasarı tahmin etmekte kullanılan dinamik analiz yöntemlerinin performansları hakkında değerlendirme yapabilmek de mümkün olmuştur. Analitik metodun tahmin kapasitesi, metodun kendisinden kaynaklanan nedenlerden dolayı yarı-statik ve tam-dinamik metotlara göre düşüktür. Yarı-statik ve tam-dinamik metotlar birbirine yakın sonuçlar vermiş ve sahada gözlenen hasar durumlarını genelde daha iyi yansıtmışlardır. Ancak zorlu zemin koşulları gibi özel durumlarda yarı-statik yaklaşımın tahmin gücü tam dinamik metoda göre sınırlı kalmaktadır.

Bu çalışmanın son amacı ise, daha önce Argyroudis vd. (2005) tarafından önerilmiş, tünellerde oluşmuş hasarlara ve mühendislik tecrübesine dayanılarak oluşturulmuş hasar indislerinin iyileştirilmesidir. Bu hasar indisleri, Düzce depremi sırasında Bolu Tüneleri'nde oluşan kayıt altına alınmış hasarlara ve dinamik analiz sonuçlarına uygun olarak yenilenmiştir. Çalışmada hasarı tanımlamak için üç farklı hasar düzeyi kullanılmıştır.

Anahtar Kelimeler: Bolu Tüneli, Hasargörebilirlik Eğrisi, Sismik Davranış, Deprem, Sismik Hasar Değerlendirmesi

To my family

&

To those who devoted their youth to research...

ACKNOWLEDGEMENTS

The author wishes to express his deepest gratitude to his supervisor Prof. Dr. B. Sadık BAKIR for his guidance, advice, criticism, encouragements and insight throughout the research.

Special thanks are also to Prof. Dr. M. Semih YÜCEMEN and Prof. Dr. H. Şebnem DÜZGÜN for their valuable suggestions.

The author would like to extend his sincere thanks to the Members of the Examining Committee for their valuable suggestions, comments and help.

The author would also like to thank to Bolu Tunnel Project Manager Mr. Faik TOKGÖZOĞLU and to Mr. Selami IŞIK for their suggestions, comments and valuable help through site visits and meetings held in Bolu.

The technical assistance of Asst. Prof. Dr. M. Tolga YILMAZ, Asst. Prof. Dr. Deniz ÜLGEN, Asst. Prof. Dr. Burcu BURAK and Prof. Dr. Ahmet YAKUT are gratefully acknowledged.

The technical advice of Prof. Dr. D. Sinan AKKAR, Dr. A. Anıl Yunatcı, Res. Asst. Abdullah SANDIKKAYA and Res. Asst. Özkan KALE in engineering seismology are also appreciated.

Special thanks is also extended to the former researchers who made very informative studies about Bolu Tunnels and dynamic modelling of tunnels, especially Dr. Ebu Bekir AYGAR, Dr. Sotiris ARGYROUDIS and Res. Asst. Ciro VISONE.

Finally, the author would like to thank his family and friends. Without their moral support, would not have been possible.

TABLE OF CONTENTS

LIST OF TABLES

Tables

LIST OF FIGURES

Figures

CHAPTER 1

INTRODUCTION

1.1. Background

Underground structures have a profound effect on daily life in modern societies. As being a lifeline they can serve for traffic (railway, highway and subway tunnels) or conveyance (hydroelectric power station, water supply, sewer and public utility tunnels) purposes. These structures can be grouped into three broad categories, each having distinct design features and construction methods: (1) bored or mined tunnels; (2) cut-and-cover tunnels; and (3) immersed tube tunnels (Power et al., 1998). In the last two decades, high demand of mankind, especially for traffic purposes and due to the advancements in construction technology, has increased the number of tunnels through different kind of geological medium including seismic zones.

Tunnels seem to be less vulnerable to seismic shaking than surface facilities as being an embedded underground structure except for cases when a tunnel crosses a fault or when landslides occur along the route or at portals of a tunnel. In fact, subsurface structures have generally experienced low level damage during the earthquakes in comparison to the surface structures (Lanzano et al., 2008). As a result, most of the underground structures are designed for static loads only until the end of 80'ies. Nevertheless, some underground structures have experienced significant damage in recent large earthquakes, including 1995 Kobe, Japan earthquake, 1999 Chi-Chi, Taiwan earthquake and 1999 Kocaeli, Turkey earthquake (Hashash et al., 2001). These disasters show that seismic design of underground structures is a necessity in earthquake prone regions.

Seismic analysis of underground structures can be simply categorized into three groups: (1) simplified or analytical methods; (2) pseudo-static or seismic deformation methods; and (3) full-dynamic methods. Simple to complicated analytical methods are presented by St. John and Zahrah (1987), Wang (1993) and Hashash et al. (2001). These methods are useful for a quick check of the results obtained from the complicated computer programs and software. Seismic deformation methods are reviewed by Nishiyama et al. (1999). The main idea behind these methods is the assessment of the lateral seismic free-field deformations at the level of subsurface structure and subsequently static imposition on the underground structure. These excess horizontal ground deformations during earthquakes can be estimated by software like SHAKE91 (Idriss et al., 1992) and EERA (Bardet et al., 2000). Full-dynamic methods can be utilized with the aid of numeric analysis (finite element or finite difference) software. Despite being rigorous, full-dynamic methods are time consuming and expensive.

A fundamental requirement for the assessment of seismic performance of a system is the quantification of potential damage as a function of the level of seismic hazard intensity (Pitilakis et al., 2006). Fragility curves are employed for the vulnerability assessment of engineering structures. As ALA (2001) states, fragility curve is a mathematical expression that relates the probability of reaching or exceeding a particular damage state, given a particular earthquake hazard. Damage states are defined in HAZUS technical manual (FEMA, 2003) with five different levels including none, slight/minor, moderate, extensive and complete.

Fragility curves or vulnerability functions can be defined based on three different approaches: (1) expert opinion approach; (2) empirical approach; (3) analytical approach. Lack of rigorous damage data necessitated the use of expert opinion approach. For instance, ATC-13 (1985) produced damage probability matrices and fragility curves based on questionnaires, through which the experts were queried on the probability of a lifeline component being in a certain damage state for a given Modified-Mercalli Intensity value (Pitilakis et al., 2008). Empirical approach is based on statistical analysis of damage data from past seismic activities. As an example, ALA (2001) used part of the historic damage data of tunnels provided by Dowding and Rozen (1978), Owen and Scholl (1981), Sharma and Judd (1991) and Power et al. (1998). Analytical fragility curves are constructed for the predefined structural systems according to the strong motion records of actual earthquakes by employing seismic analysis methods mentioned earlier in this section of the chapter.

1.2. Scope and Purpose of the Study

The aim of the study is to develop new analytical fragility curves for the vulnerability assessment of tunnels based on actual damage data of tunnels obtained from past earthquakes. For this purpose, additional important damage data belonging to Bolu Tunnels, Turkey was utilized as a case study.

The case of Bolu Tunnels is one of the most interesting from the earthquake hazard point of view, since, two major earthquakes (17 August 1999 Marmara and 12 November 1999 Düzce earthquakes) occurred during the construction of the tunnels. The August 17, 1999 earthquake was reported to have had minimal impact on the Bolu Tunnels. However, the November 12, 1999 earthquake caused the total collapse of some sections in both tunnels. The remaining sections of the tunnels survived with various damage states. In this study, all this valuable damage data was incorporated for construction of novel fragility curves.

To develop fragility curves, methodology described by Argyroudis et al. (2007) was followed. In that study, the quantification of the damage states is based on a damage index (DI) that is defined as the ratio of the developing moment during earthquake (M_{eq}) to the moment resistance of the tunnel lining (M_{rd}). Then, these damage states are correlated with the peak ground accelerations to construct fragility curves. The analysis of the tunnels is realized utilizing the seismic analysis methodologies described in Section 1.1 of this chapter.

The second goal of this study is the improvement of damage indexes corresponding to the defined damage states which were proposed by Argyroudis et al. (2005) based on the previously observed damage in tunnels as well as the engineering judgment.

Furthermore, damage index is a term which is actually analogous to the reciprocal of factor of safety. Thus, with the improvement of damage indexes it is also possible to recommend factors of safety based on levels of seismic shaking damage state for tunnel construction and design. To conduct the analysis of the tunnels, seismic analysis of underground structures was employed. In this way, it is possible to make some comparisons on the dynamic analysis methods of tunnels.

The final goal of this study is the improvement of damage indexes corresponding to the defined damage states which were proposed by Argyroudis et al. (2005) based on the previous experience of damages in tunnels and engineering judgment. These damage indexes were modified in accordance with the findings from the dynamic analyses and actual damage data documented from Bolu Tunnels following the Düzce earthquake.

CHAPTER 2

DYNAMIC ANALYSES OF TUNNELS

Contrary to the case of surface structures, inertial forces do not govern the seismic design of underground structures. Free-field deformations of the subsurface actually govern the design for most of the underground structures with or without considering the soil-structure interaction.

The response of tunnels to seismic shaking may be demonstrated in terms of three principal types of deformations as shown in Figure 2.1 (Owen and Scholl, 1981): (1) axial deformations, (2) curvature deformations, and (3) ovaling (for circular tunnels) or racking (for rectangular tunnels) deformations. In this study, only the ovaling types of deformations are considered for dynamic analyses of tunnels, because the great majority of seismic damage to tunnels occurs as a result of this kind of deformations.

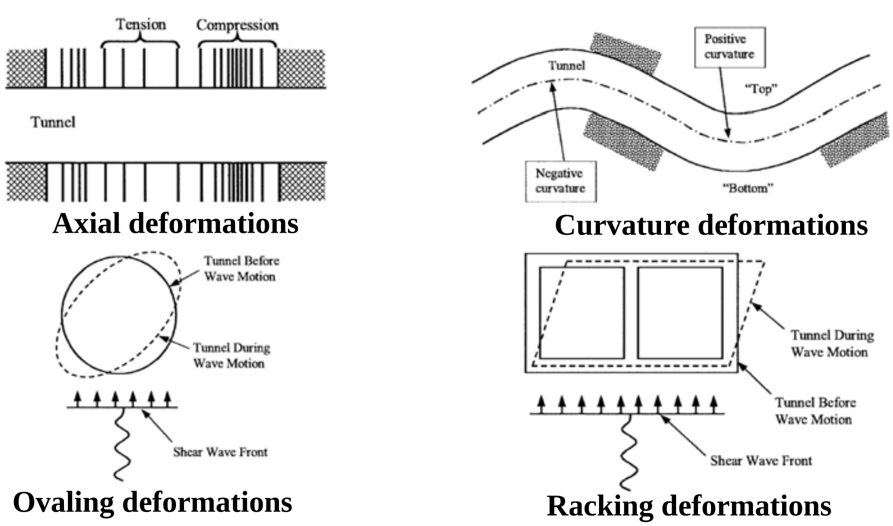

Figure 2.1 The response of tunnels to earthquakes (after Owen and Scholl, 1981)

2.1. Simplified (Analytical) Methods for Ovaling Deformations of Circular Tunnels

Analytical methods can be used for the preliminary design of underground structures. Furthermore, these simplified methods serve as a useful tool for approximate checking of the results obtained from the rigorous solutions. Ovaling of the circular tunnel is caused due to seismic waves propagating in planes perpendicular to the tunnel axis. As Penzien (2000) emphasized, the analytical procedures presented permit only the evaluation of the internal force components in a lining produced by ovaling during seismic loading. To check a design, these force components should be added to the corresponding components present in the lining prior to the seismic event.

2.1.1. Free-Field Deformation Method

In this method it is assumed that the tunnel conforms to the deformations that are imposed by the free-field. As Wang (1993) stated, there are two ultimate boundaries that exist for quantifying ovaling strains due to the free-field deformations. The first, the maximum diametric strain is found as a function of the maximum free-field shear strain with the assumption of non-perforated ground (tunnel excavation is not considered):

$$\frac{\Delta d}{d} = \pm \frac{\gamma_{\max}}{2} \tag{2.1}$$

where, Δd is the diameter change of the tunnel, d is the diameter of the tunnel and γ_{max} is the maximum free-field shear strain. This situation is a good example of tunnel lining which has a transversal sectional stiffness equal to the surrounding medium (tunnel construction in soil). The second situation consists of the assumption of perforated ground. That is the ground deformation derived considering a cavity due to tunnel excavation (see Figure 2.2). For this situation, the diametric strain for which the tunnel lining is to be designed can be defined as:

$$\frac{\Delta d}{d} = \pm 2\gamma_{\max}(1 - \nu_m) \tag{2.2}$$

where, ν_m is the Poisson's ratio of the medium. This situation is also corresponding to a case where the stiffness of the lining is small compared to that of the surrounding medium (tunnel construction in rock).

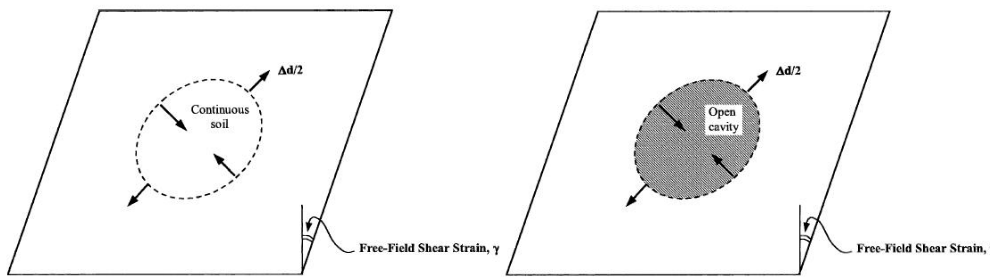

Figure 2.2 Free-field shear distortion of perforated and non-perforated ground for circular tunnel (after, Wang, 1993)

Maximum shear strain, γ_{max} of the ground can be estimated using the codes like SHAKE91 (Idriss et al., 1992) and EERA (Bardet et al., 2000). St John and Zahrah (1987) proposed a simple equation for calculating γ_{max}:

$$\gamma_{\max} = \frac{C_{peak}}{V_s} \tag{2.3}$$

where C_{peak} is the peak particle velocity; and V_s is the effective shear wave velocity. The values of C_{peak} can be estimated through in-situ and laboratory tests. An equation relating the effective propagation velocity of shear waves to effective shear modulus, G_m, is expressed as (Wang, 1993):

$$V_s = \sqrt{\frac{G_m}{\rho}} \tag{2.4}$$

where, ρ is the mass density of the ground.

Decision on how the tunnel lining behaves (perforated or non-perforated ground) can be given according to the dimensionless ratios namely the compressibility ratio, C, and flexibility ratio, F (Höeg, 1968):

$$C = \frac{E_m (1-\nu_l^2) d}{2 E_l t (1+\nu_m)(1-2\nu_m)} \tag{2.5}$$

$$F = \frac{E_m (1-\nu_l^2) d^3}{48 E_l I (1+\nu_m)} \tag{2.6}$$

where, E_m is the modulus of elasticity and ν_m is the Poisson's Ratio of the medium; E_l is the modulus of elasticity and ν_l is the Poisson's Ratio of the lining; d is the diameter; t is the thickness of the tunnel lining; and I is the moment of inertia of the tunnel lining per unit width.

2.1.2. Lining-Ground Interaction Method

Lining-ground interaction method can be further categorized into two as consideration of full-slip conditions and no-slip assumption. Assuming full-slip conditions, maximum thrust, bending moment and diametric strain can be expressed, respectively, as (Wang, 1993):

$$T_{\max} = \pm \frac{1}{12} K_1 \frac{E_m}{(1+\nu_m)} d \gamma_{\max} \tag{2.7}$$

$$M_{\max} = \pm \frac{1}{24} K_1 \frac{E_m}{(1+\nu_m)} d^2 \gamma_{\max} \tag{2.8}$$

$$\frac{\Delta d}{d} = \pm \frac{1}{3} K_1 F \gamma_{\max} \tag{2.9}$$

where,

$$K_1 = \frac{12(1-\nu_m)}{2F+5-6\nu_m} \tag{2.10}$$

Penzien (2000) solution for the full-slip condition:

$$\pm \Delta d^n_{lining} = \pm R^n \Delta d_{free-field} \tag{2.11}$$

$$T(\theta) = -\frac{12E_l I \Delta d^n_{lining}}{d^3(1-\nu_l^{\,2})} \cos 2\left(\theta + \frac{\pi}{4}\right) \tag{2.12}$$

$$M(\theta) = -\frac{6E_l I \Delta d^n_{lining}}{d^2(1-\nu_l^{\,2})} \cos 2\left(\theta + \frac{\pi}{4}\right) \tag{2.13}$$

$$V(\theta) = -\frac{24E_l I \Delta d^n_{lining}}{d^3(1-\nu_l^{\,2})} \sin 2\left(\theta + \frac{\pi}{4}\right) \tag{2.14}$$

$$R^n = \pm \frac{4(1-\nu_m)}{(\alpha^n + 1)} \tag{2.15}$$

$$\alpha^n = \frac{12E_l I(5-6\nu_m)}{d^3 G_m (1-\nu_l^{\,2})} \tag{2.16}$$

where, R is the lining rocking ratio which is a ratio of lining diametric deflection and free-field diametric deflection; $\Delta d_{free-field}$ is the free field diametric deflection in non-perforated ground; Δd_{lining} is lining diametric deflection; and α is the coefficient used in calculation of lining-soil racking ratio of circular tunnels. The superscript n implies the condition is under normal loading.

No-slip solution of Einstein and Schwartz (1979) based on study of Höeg (1968) for maximum thrust on the lining is:

$$T_{\max} = \pm K_2 \tau_{\max} R = \pm K_2 \frac{E_m}{2(1+\nu_m)} R \gamma_{\max} \tag{2.17}$$

where, τ_{max} is the maximum free-field shear stress and K_2 is the lining thrust response coefficient defined as:

$$K_2 = 1 + \frac{F\left[(1-2\nu_m)-(1-2\nu_m)C\right] - \frac{1}{2}(1-2\nu_m)^2 + 2}{F\left[(3-2\nu_m)+(1-2\nu_m)C\right] + C\left[\frac{5}{2} - 8\nu_m + 6\nu_m^{\ 2}\right] + 6 - 8\nu_m} \tag{2.18}$$

No-slip condition solution of Penzien (2000) is:

$$\pm \Delta d_{lining} = \pm R \Delta d_{free-field} \tag{2.19}$$

$$T(\theta) = -\frac{24 E_l I \Delta d_{lining}}{d^3(1-\nu_l^{\ 2})} \cos 2\left(\theta + \frac{\pi}{4}\right) \tag{2.20}$$

$$M(\theta) = -\frac{6 E_l I \Delta d_{lining}}{d^2(1-\nu_l^{\ 2})} \cos 2\left(\theta + \frac{\pi}{4}\right) \tag{2.21}$$

$$V(\theta) = -\frac{24 E_l I \Delta d_{lining}}{d^3(1-\nu_l^{\ 2})} \sin 2\left(\theta + \frac{\pi}{4}\right) \tag{2.22}$$

$$R = \pm \frac{4(1-\nu_m)}{(\alpha+1)} \tag{2.23}$$

$$\alpha = \frac{24 E_l I (3-4\nu_m)}{d^3 G_m (1-\nu_l^{\ 2})} \tag{2.24}$$

where, R is the lining rocking ratio which is a ratio of lining diametric deflection and free-field diametric deflection; $\Delta d_{free\text{-}field}$ is the free field diametric deflection in non-perforated ground; Δd_{lining} is lining diametric deflection; and α is the coefficient used in calculation of lining-soil racking ratio of circular tunnels.

2.2. Pseudo-Static (Seismic Deformation) Method

In this method, seismic ground deformation obtained from ground response analysis is imposed to the finite-element model of the tunnel statically. Seismic deformation of the ground due to vertically propagating shear waves reaching from the bedrock can be estimated through 1-D response analysis utilizing the software like SHAKE91 (Idriss et al., 1992) or EERA (Bardet et al., 2000). One-dimensional site response analyses are based on the assumption that all boundaries are horizontal and soil and bedrock surface is extending infinitely in the horizontal direction.

In Figure 2.3, resulting ovaling of the tunnel following the application of the free-field deformations to the finite-element model of the section can be seen. To determine the free-field deformations, EERA (Bardet et al., 2000) -a computer program for the Equivalent-linear Earthquake site Response Analyses of Layered Soil Deposits- was utilized in this study. Equivalent-linear method is an analysis technique to represent the nonlinear behavior of ground due to cyclic loading in which the modulus and damping factors used are compatible with the strains induced in the soil deposit or the earth structure.

One of the advantages of the pseudo-static method with regard to the analytical formulations is its capability of modeling irregular tunnel shapes other than those of circular. Another benefit of this method is the ability to see the effects of loads on linings which are generated due to the static loading combined with the dynamic loading. In analytic method, static loading is calculated separately and superimposed to the dynamic loading. In this study, static loading in analytical method is calculated with the method of Penzien and Wu (1998). See Appendix A for the example calculation spread sheet.

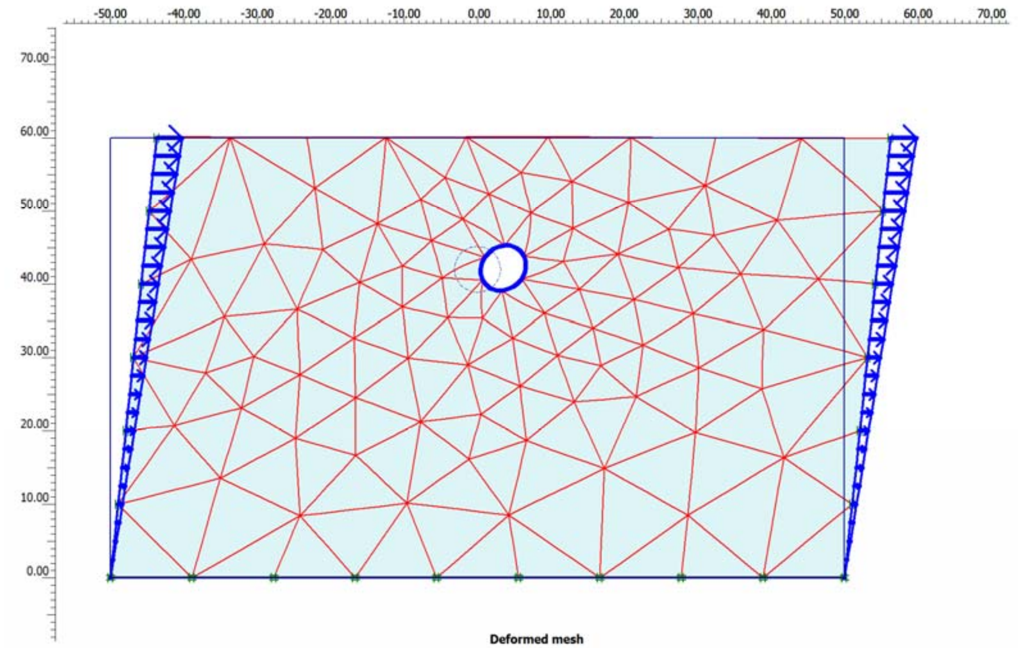

Figure 2.3 Application of seismic deformations to a circular tunnel through the finite-element model

2.3. Full-Dynamic Method

Thanks to the advancements in the numerical modeling techniques, researchers have many methods and tools to analyze the geotechnical earthquake engineering problems. Among these, the Finite Element Method and Finite Difference Method are well established and widely used. In this study, finite element method was utilized through the finite element code PLAXIS 2D V8.6 (PLAXIS bv, 2007) for the full-dynamic analyses.

In the analyses, dynamic excitation was applied from the base of the model as acceleration-time histories. Damping was implemented in the models utilizing Rayleigh damping and absorbent model boundaries. Damping in the PLAXIS code is defined by the damping tensor [C] through the linear combination of mass tensor [M] and the stiffness tensor [K]:

$$[C] = \alpha_R[M] + \beta_R[K] \qquad (2.25)$$

The two Rayleigh coefficients α_R and β_R were calculated according to the double frequency method as suggested by Lanzo et al. (2004) (quoted by Aversa et al., 2007) assuming that the soil damping ratio, D, is constant between the first natural frequency ω_1 of the deposit and a frequency $\omega_n = n\omega_1$, where n is the first odd integer larger than the ratio ω_{N1}/ω_1 between the fundamental frequency of the seismic signal (ω_{N1}) and the first natural frequency of the deposit (ω_1).

2.3.1 Details of Full-Dynamic Finite Element Analyses

Full-dynamic finite element analysis is the well established and the most comprehensive technique for studying the response of geotechnical earthquake engineering problems since it can provide detailed estimation of stresses and deformations of both geological media and structural components within, no matter how complete the model is. However, to conduct a complete dynamic finite element analysis, one must have to define the geometrical domain, mesh size, constitutive models, boundary conditions and the seismic input of the problem in detail properly.

Size of the geometrical domain is an important parameter while handling a dynamic finite element problem. To perform the dynamic analysis of a typical tunnel section, both horizontal and vertical model boundaries have to be determined. As the problem domain gets larger, solution time gets larger and hardware capabilities will become insufficient after some point. So, engineers prefer to reduce the problem domain with some techniques. In a tunneling problem, the upper horizontal boundary is determined according to the depth of cover (D_c) above the tunnel crown. While coping with deep tunneling problems, it becomes uneconomical to model the full D_c. In the first technique, D_c is reduced with an amount of ΔH by an equivalent distributed load $P_{\Delta H}$ that is equivalent to:

$$P_{\Delta H} = \gamma \cdot \Delta H \tag{2.25}$$

where γ is the unit weight of the geological media as shown in Figure 2.4. By utilizing this technique, it is possible to get successful results for static finite element problems. On the other hand, the same is not true for dynamic problems due to the omission of the mass. Therefore, a second technique can be introduced for reducing the horizontal upper boundary of the tunneling problems (see Figure 2.5). The equivalent distributed load in the first technique is replaced with a layer which has a thickness of ΔH' much smaller than ΔH. The decrease in ΔH is achieved by the increase in unit weight γ of the geological medium with the following equation:

$$\gamma' = \gamma \cdot \frac{\Delta H}{\Delta H'} \tag{2.26}$$

Shortcoming of this technique is the change in the center of gravity of the model. According to some parametric studies, this method gives satisfactory results for D_{c3}/D_{c1} ratios around 0.8. However, when D_{c3}/D_{c1} ratios are close to 0.5, the results of tunnel lining sectional forces are underestimated. So, this technique seems to be a very last alternative.

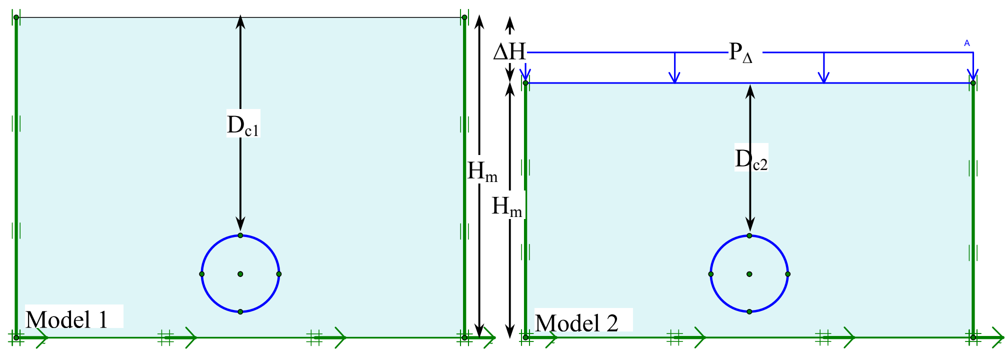

Figure 2.4 First technique reducing the depth of cover

Another important parameter which defines the size of the geometrical domain is the distance to the lateral boundaries L_b from the center of the problem as shown in Figure 2.6. There is no general rule for choosing L_b in dynamic analyses of underground structures. If absorbing or viscous boundary conditions are not used in the finite element model, a model wide enough to prevent the reflection of impinging waves which is computationally very inefficient is to be used. According to this approach, if one uses absorbing boundaries, the results of the tunnel lining sectional forces must be converging to a value with the increase of L_b. This method is converging for the ratios of L_b/H_m greater than 4 resulting in an uneconomical geometrical domain dimensions. Thus, another type of lateral boundaries suggested by Christian et al. (1977) (quoted by Visone et al., 2010) was used in this study resulting in a proper geometrical domain dimensions for the L_b/H_m ratios smaller than 4. According to him, the best lateral boundary conditions for S-waves polarized in the horizontal plane and propagating vertically are the vertical fixities. Horizontal displacements must be allowed. In order to equilibrate the horizontal lithostatic stresses acting on the lateral boundaries, it is suitable to introduce load distributions at left-hand and right-hand vertical boundaries (Visone et al., 2010). Comparison of the models can be seen in Figure 2.6. In the literature, there are also recommendations that L_b should be at least 5D far away from the underground opening, where D is the greatest dimension of the underground opening.

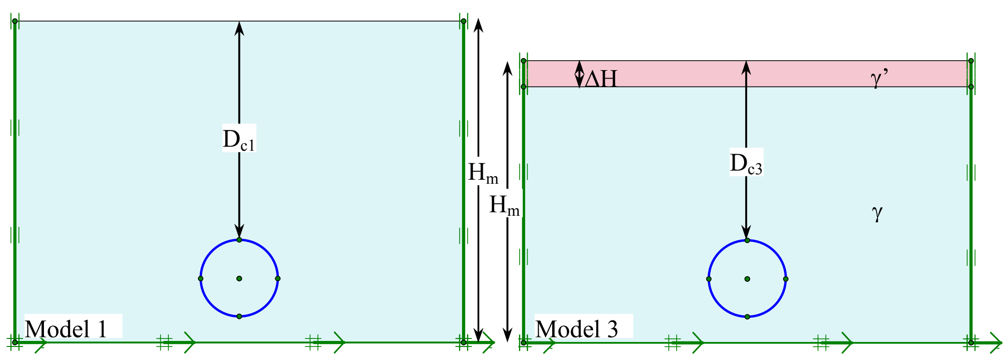

Figure 2.5 Second technique reducing the depth of cover

If it is not known, defining the distance to lower horizontal boundary conditions is not as simple as defining the upper horizontal boundary conditions. In soil profiles, the point where the rock starts is assumed as bedrock and this will be enough for the lower horizontal boundary condition. However, sections in fully rock conditions could also be faced during modeling. Therefore, trial error procedure is followed to determine the depth of bedrock or lower horizontal boundary condition for the rock profiles.

Mesh size is another important factor that defines the solution time of the finite element problem. Kuhlemeyer and Lysmer (1973) observed that the finite element models behave like low pass filters having definite passing bands and cutoff frequencies and that the cutoff frequencies depend upon the wave type and finite element mesh. For these reasons, they suggested to assume an element size not larger than λ/8, where λ is the wave length corresponding to the maximum frequency of interest. Additionally, element sizes must be refined around underground openings to take into consideration of the stress concentrations.

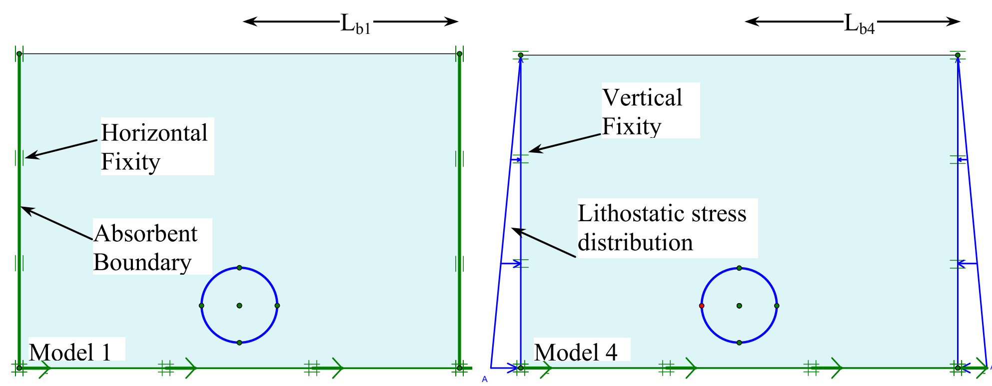

Figure 2.6 Model boundary conditions

Definition of seismic input plays a key role in the response of the system. Therefore, one must be careful while defining a seismic input to a geotechnical earthquake engineering problem in any finite element software. Furthermore, the user must be aware of limitations and capabilities of the utilized software. As also stated in the previous sections, in this study, finite element method was utilized through the finite element code PLAXIS 2D V8.6 (PLAXIS bv, 2007) for the full-dynamic analyses. In order to avoid loss of information due to some limitations of the FE code PLAXIS, the input signal had to be divided to n-parts each having a maximum number of data points limited with 1000.

PLAXIS code generates solutions for earthquake problems in time domain. For modeling material damping in FE code, Rayleigh formulation was utilized. However, Rayleigh formulation is frequency dependent. For this reason, engineers must be careful while defining constitutive models for earthquake engineering problems. Some well established FE model calibration procedures taking the material damping into account can be found in Park and Hashash (2004) and Visone et al. (2010).

CHAPTER 3

BOLU TUNNELS AND DAMAGE DUE TO 1999 EARTHQUAKES

3.1. Introduction

The Bolu Tunnels lie along Trans European Motorway (TEM) which connects Eastern Europe with the Middle East (see Figure 3.1). The tunnels are approximately 3.0 km long in total, 40 m apart and have excavated cross sections more than 200 m^2. The tunnels generally have an excavated arch section of 15 m height and 16 m width. New Austrian Tunneling Method (NATM) was utilized during construction. Construction was unusually challenging because the alignment crossed several minor faults parallel to the North Anatolian Fault (see Figure 3.2). Due to the challenging ground conditions, several problems were encountered during the excavation of the tunnels.

The tunnels were designed following the NATM principles according to ÖNORM B 2203 with some modifications to account for the local conditions. The original design, based on the investigations, consisted of seven ground classes and associated typical support designs, five for rocks (A2, B1, B2, C1 and C2) and for soils (L1 and L2) (Schubert et al., 1997). Before the 1999 Düzce earthquake, the unfavorable conditions at the tunnel route resulted in deformations of lining and heave of the invert as much as 1.0 m. As a result, construction was temporarily halted and a detailed investigation program was launched including pilot tunnel drives. At the end of the detailed analysis program, new construction methodologies, named CM, Option-3 and Option-4, were developed and started to be implemented (see Appendix B for geometrical details of the all mentioned tunnel sections).

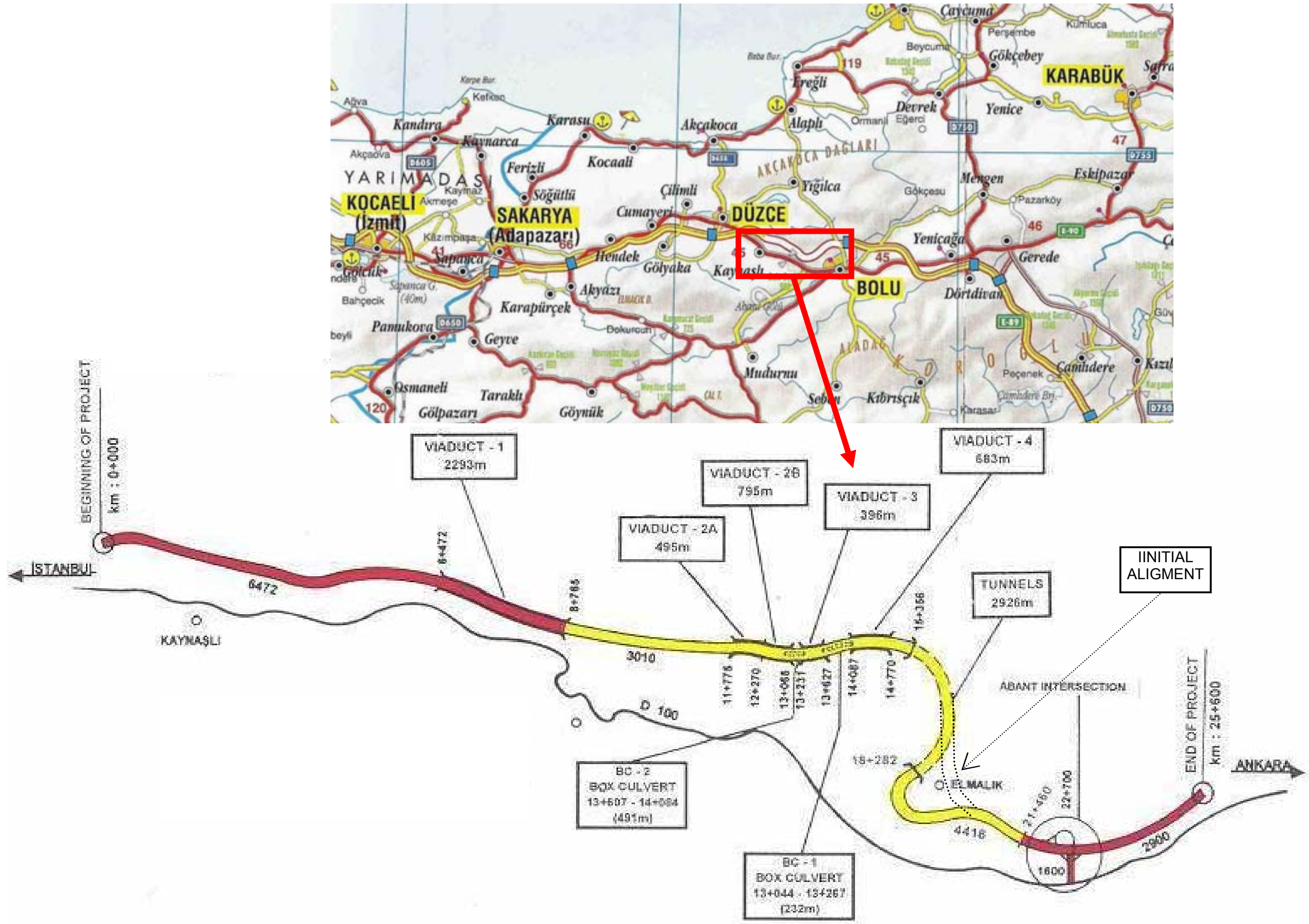

Figure 3.1 Map showing location of the Bolu Tunnels (modified after Tokgözoğlu and Işık, 2002)

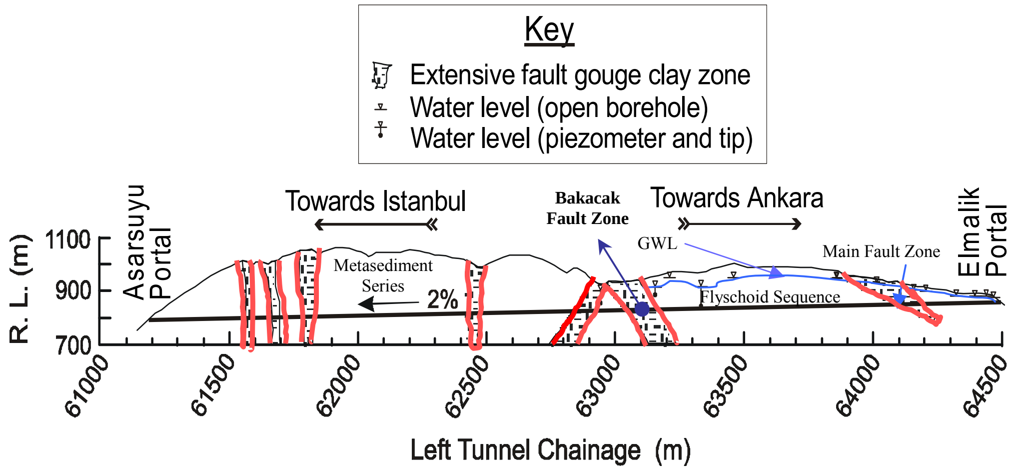

Figure 3.2 Simplified geological profile of the tunnel alignment (after Işık and Özben, 2007)

As it can be understood, Bolu Tunnels consist of different tunnel sections each having different support types and geologic sections including pilot tunnels (see Figure 3.3). Based on the geological reports and available construction details, several sections of the tunnels were analyzed. Comparison of the outcome of such analyses with the observed damage over the tunnels following the earthquakes provides a valuable opportunity for the assessment of the predictive capability of the dynamic analysis procedures. In the proceeding chapters of this study, dynamic analyses of the tunnel sections implemented during the construction of the Bolu Tunnels are presented.

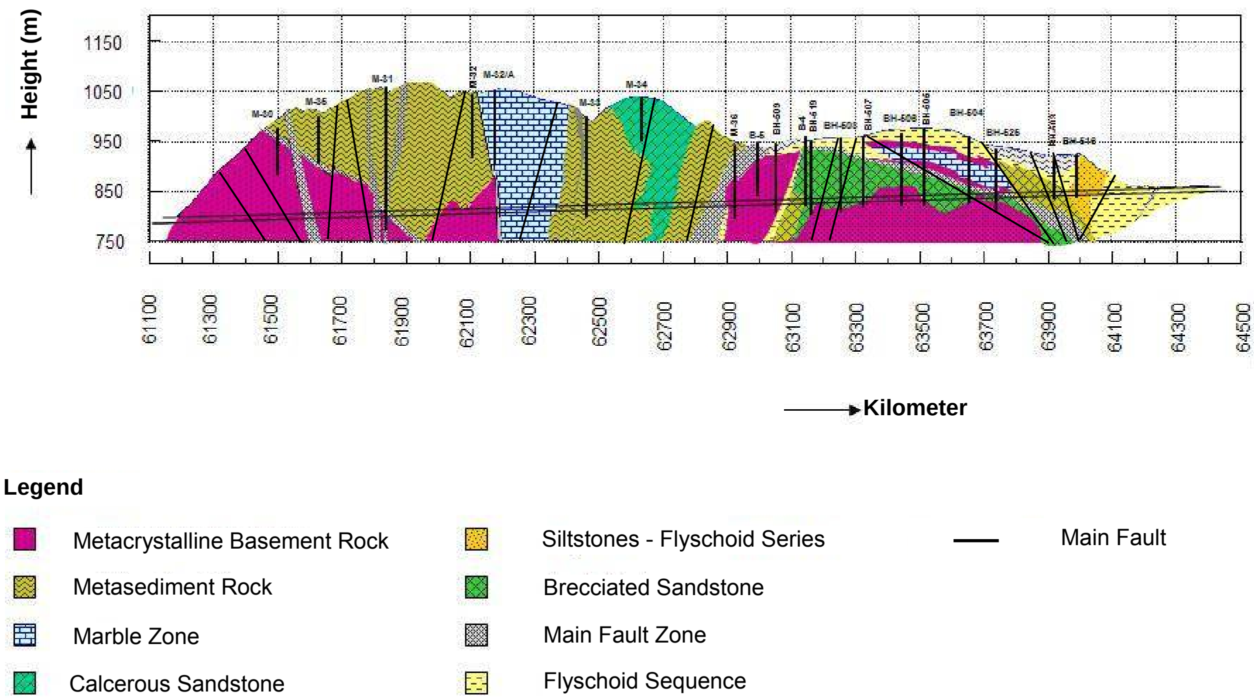

Figure 3.3 Simplified geological cross-section of Bolu Tunnels showing rock formations (Işık, 2009)

3.2. Damage in Bolu Tunnels Due to 1999 Earthquakes

In 1999 two major earthquakes struck Turkey (see Figure 3.4). On August 17, 1999 a magnitude M_w 7.4 earthquake hit Kocaeli and Sakarya provinces in northwestern Turkey, a densely populated region in the heavily industrial part of Turkey. The epicenter of earthquake was located at a depth of about 15 km and about 10 km east of the town of Gölcük. The length of the right-lateral strike-slip fault was 120 km and involving four distinct fault segments on the northernmost strand of the western extension of the 1300 km-long North Anatolian fault system (Erdik, 2001). The second one, the M_w 7.1 Düzce earthquake, occurred on 12 November 1999 along the North Anatolian Fault in northwestern Turkey (see Figure 3.5). The Düzce earthquake was a right-lateral strike-slip event that ruptured a section of the North Anatolian Fault immediately to the east of the fault rupture from the 17 August Kocaeli (M_w 7.4) earthquake (Rathje et al., 2006). As Akyüz et al. (2002) stated the Düzce earthquake formed a 40 km long surface rupture zone starting from Eften (Melen) lake and terminating near Kaynaşlı town. Faccioli et al. (2002) reported that the Düzce fault rupture crossed the so-called Bolu viaduct no.1, on a stretch under construction of the Trans European Motorway (TEM) (see Figure 3.6 through Figure 3.9).

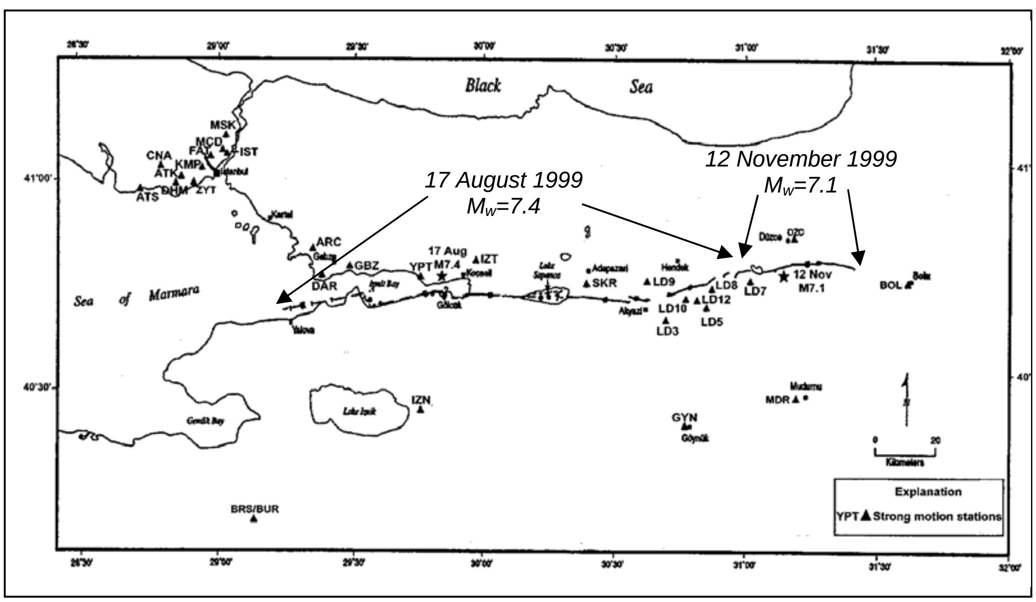

Figure 3.4 Map showing the location of strong motion stations and the extent of 1999 ruptures (after Rathje et al., 2003)

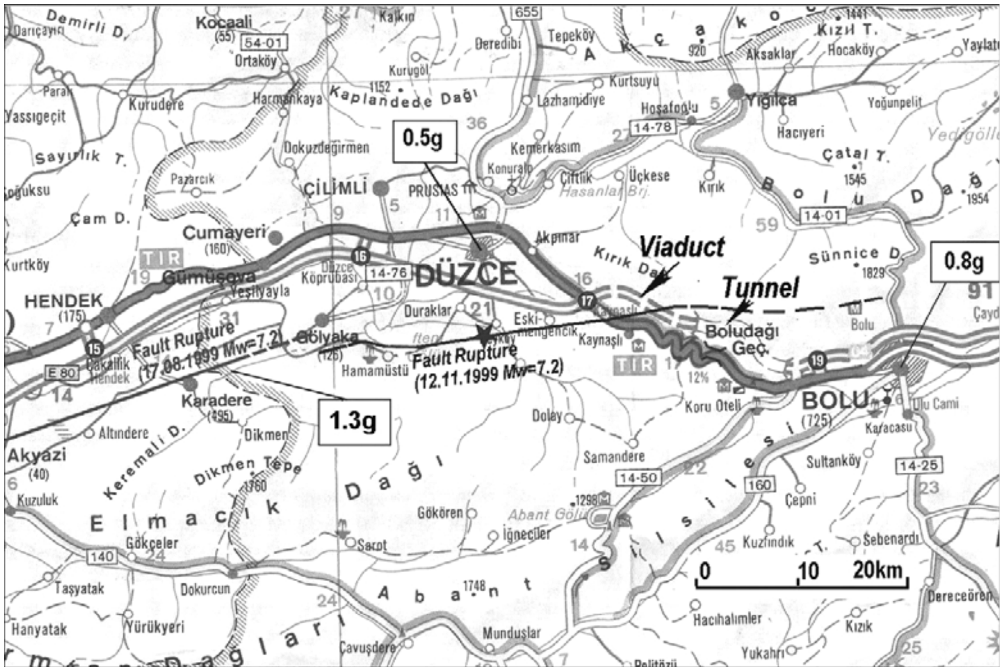

Figure 3.5 Closer view of surface rupture and peak horizontal accelerations recorded in the 1999 Düzce earthquake (after Durukal, 2002)

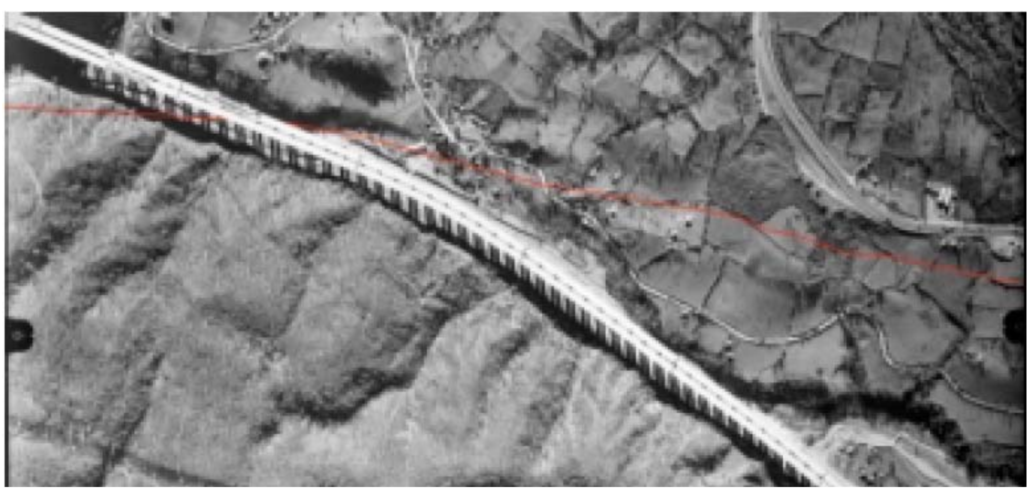

Figure 3.6 Aerial view of the Bolu 1 Viaduct. The fault rupture is indicated by the red line. (after Erdik, 2001)

Figure 3.7 General view (from SW) of the Bolu viaducts (after Faccioli et al., 2002)

Figure 3.8 Fault rupture (indicated by arrows) crossing through the viaduct piers. Courtesy G. Macchi. (after Faccioli et al., 2002)

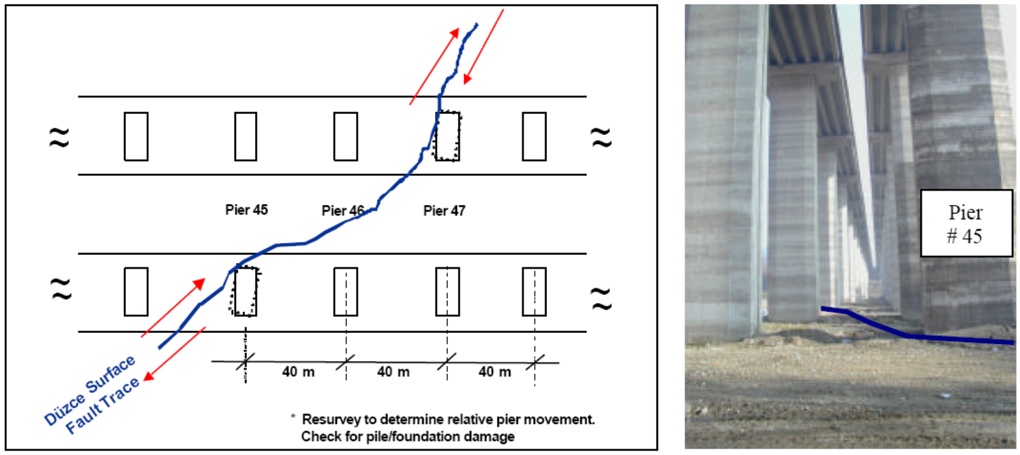

Figure 3.9 Fault trace at Bolu Viaduct No.1 (after Ghasemi et al., 2000)

The epicenter of the Kocaeli earthquake was located approximately to the west of Bolu Tunnels construction site. As Unterberger and Brandl (2000) pointed, structures at the project site experienced loading of 0.2g to 0.3g with no damage to the tunnels and other structures as opposed to the extensive damage experienced close to the epicenter (see Figure 3.10).

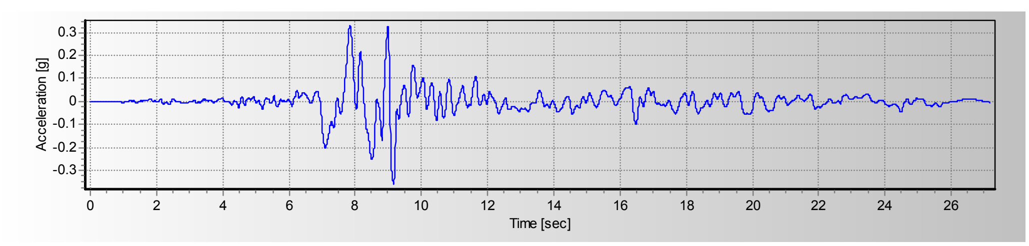

Figure 3.10 Time history of Kocaeli earthquake recorded at Düzce Station, E-W, pga=0.358g

Significant damage was induced in the Bolu Tunnels by the Düzce earthquake. The epicenter of the earthquake was only 20 km far away from west of the site. As it is seen from time histories of the earthquake records in Figure 3.11 and Figure 3.12, accelerations of 0.6g to 0.8g were measured at the stations in the vicinity of the site, far in excess of the 0.4g design earthquake (Unterberger and Brandl, 2000). Generally, it was observed that completed sections of the tunnels (where the inner lining had been installed) survived the earthquake intact with minor damage. However, some partly completed sections of the tunnels (temporarily supported by a shotcrete lining) suffered significant damage. The degree of the damage was noted to be dependent on the ground conditions (Yüksel-Rendel Engineers, 1999). Due to the collapsed sections, Bolu Tunnel Project was completed after realignment of the tunnel route as shown in Figure 3.13. Figure 3.14 summarizes the general status of the Bolu Tunnels after the 12 November Düzce earthquake.

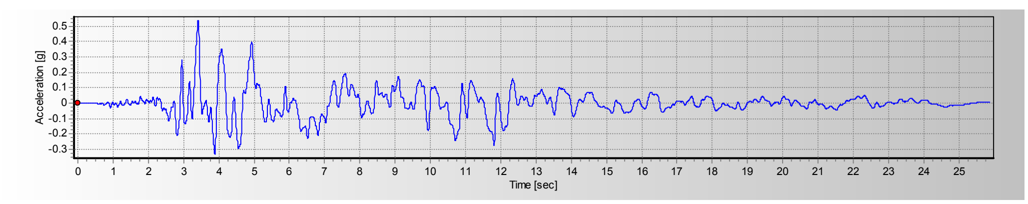

Figure 3.11 Time history of Düzce earthquake recorded at Düzce Station, E-W, pga=0.535g

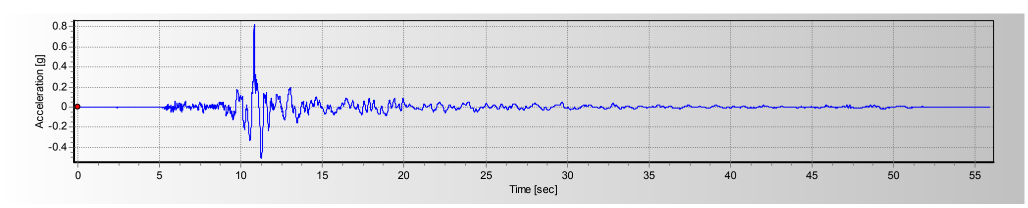

Figure 3.12 Time history of Düzce earthquake recorded at Bolu Station, E-W, pga=0.822g

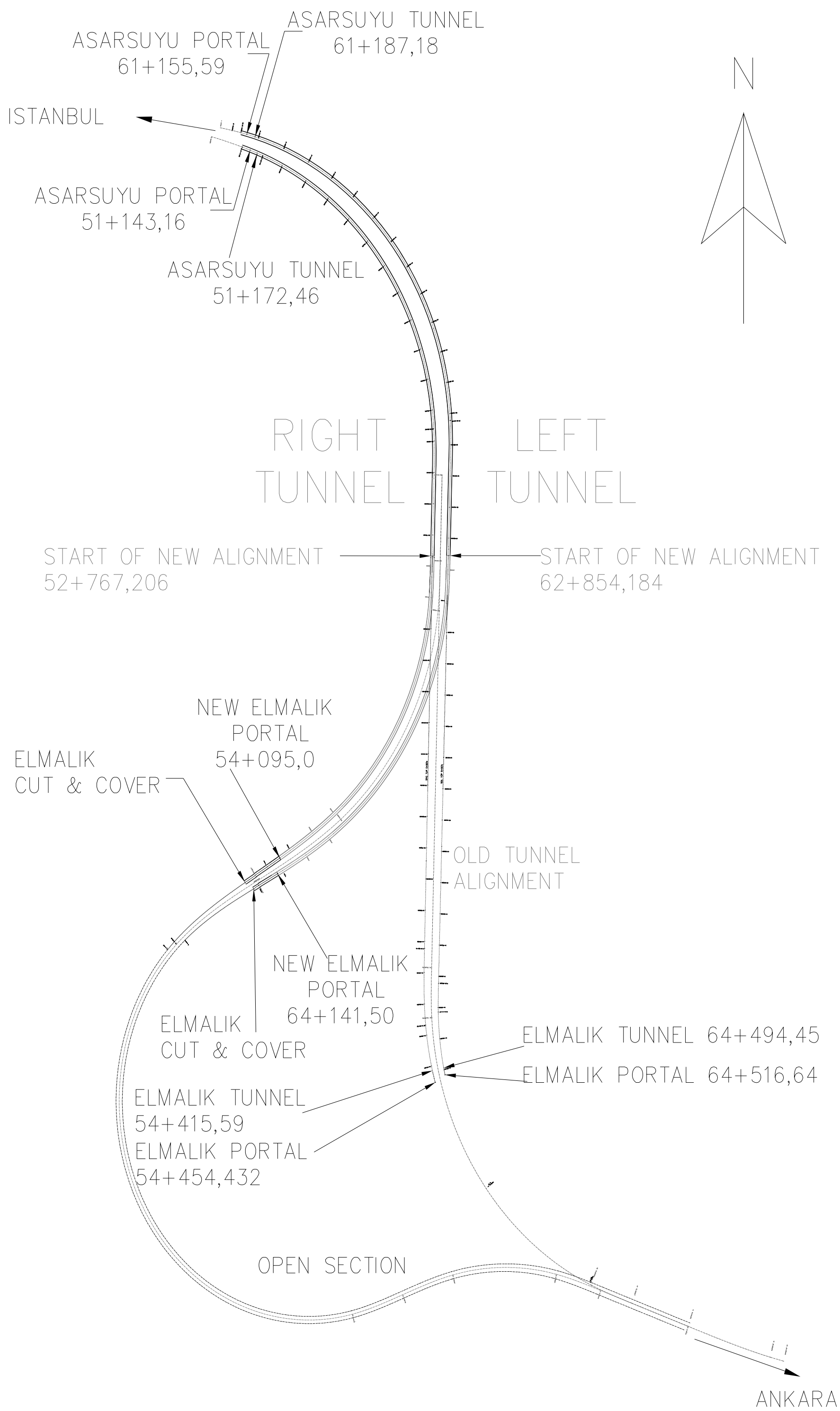

Figure 3.13 Initial and final alignments of Bolu Tunnels (after Astaldi Spa, 1993-2006)

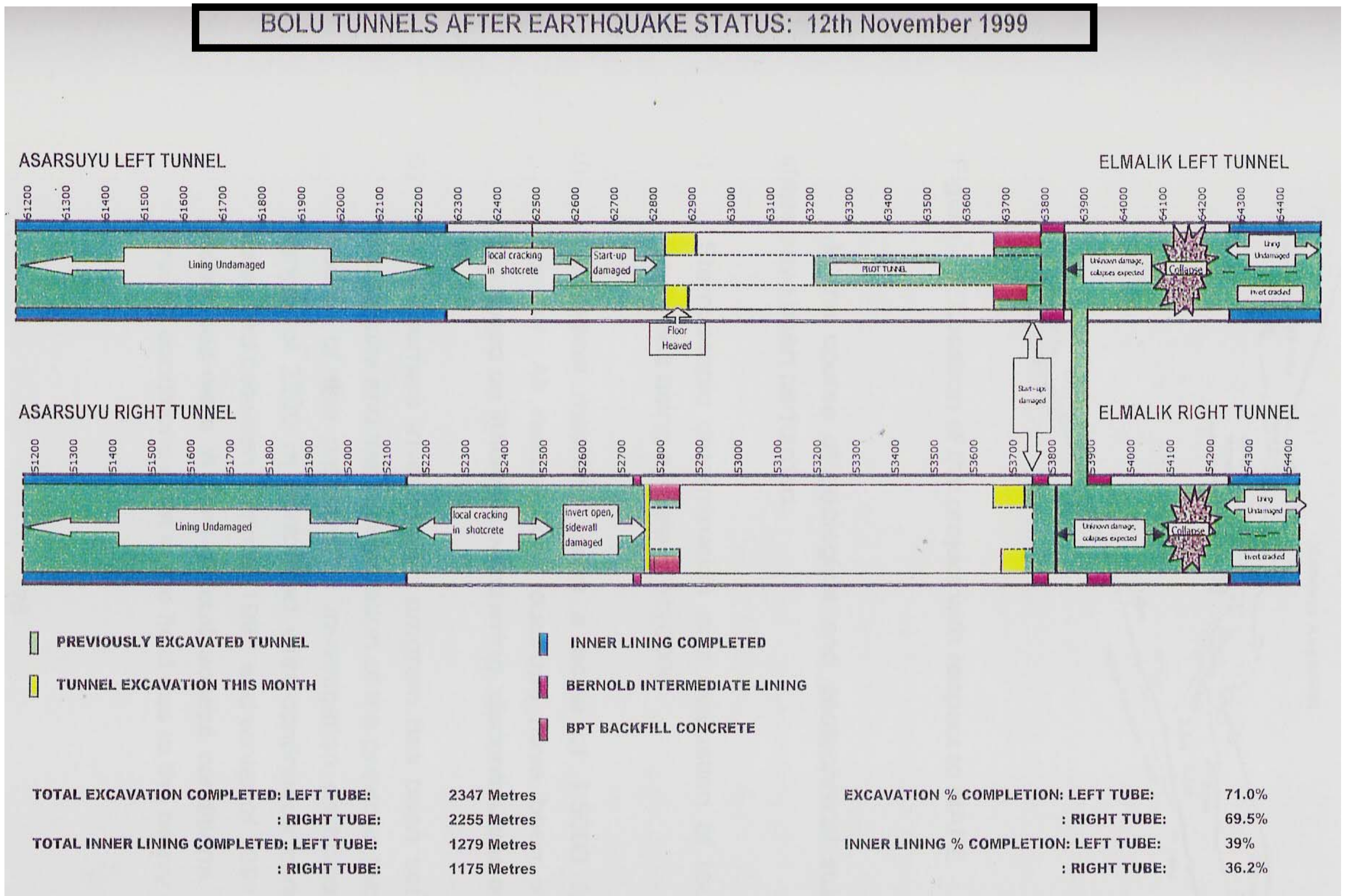

Figure 3.14 Situation of Bolu Tunnels after 12th November 1999 earthquake (after Yüksel-Rendel Engineers, 1999)

According to the reports of Yüksel-Rendel Engineers (1999) and Ghasemi et al. (2000), in Elmalık Tunnels, where the concrete lining had been installed, no damage was observed in the first 200-250 m section of the tunnels. Complete closure of both tunnel bores and in-rush of material was noted about 200 to 300 m from the Elmalik portal entrances. Longitudinal cracking along a segment above the tunnel invert, near the collapsed face, was noted. It was reported by the consultant that the invert had heaved upwards as much as 1 m. The collapses occurred in a section of tunnel passing through a clay/weak rock zone where a temporary shotcrete lining system was in place. The collapse of the tunnels occurred about 50 to 75 m beyond a structurally complete tunnel liner system. According to eyewitness reports, in front of this section (250 m) there was no major damage reported. However, there is no access to confirm these reports due to blockage collapse debris. Details of the damage to sections of the Elmalık Left Tunnel, supported only by the temporary lining are illustrated in Figure 3.15. Eye witness accounts of miners who were in the tunnel during the earthquake indicate that collapse began in the right tube and propagated to the left tube. In the right tube, the collapse was noted to have propagated to the surface and to have formed a sinkhole of dimensions $4^m x 6^m x 4^m$ deep at the ground level (see Figure 3.16 and Figure 3.17).

Significantly less damage occurred to the Asarsuyu tunnels due to the more favorable ground conditions that generally exist there according to the reports of Yüksel-Rendel Engineers (1999). It was observed that the sections of the tunnel where the permanent lining had been installed before the earthquake were undamaged (~1000 m). One-millimeter wide longitudinal and radial cracks were observed in the structurally complete reinforced concrete liner following the earthquake. Sections of the tunnels that were only supported by the shotcrete shell (~700 m) performed well, depending on the ground conditions. In the better ground conditions leading up to the Asarsuyu/Elmalık interface zone, only small and easily repairable damage was occurred. In that section, consistent cracking of the shotcrete at the construction joint between the top heading and bench sections occurred. Furthermore, localized slabbing and spalling of the shotcrete was noted to have been induced by the earthquake (see Figure 3.18). Overall, the shotcrete lining was still essentially intact.

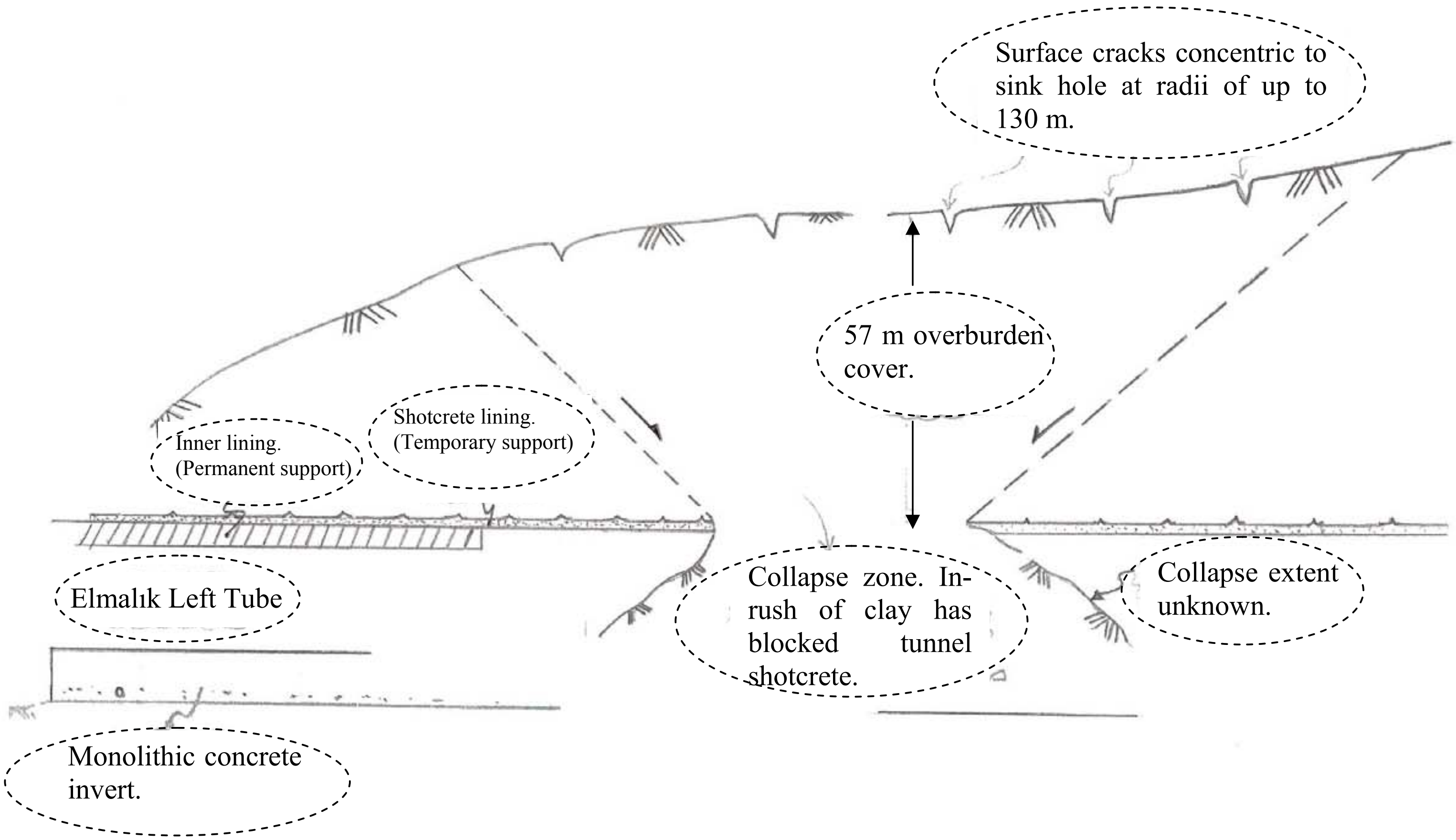

Figure 3.15 Schematic representation of collapse in Elmalık Left Tube (modified after Yüksel-Rendel Engineers, 1999)

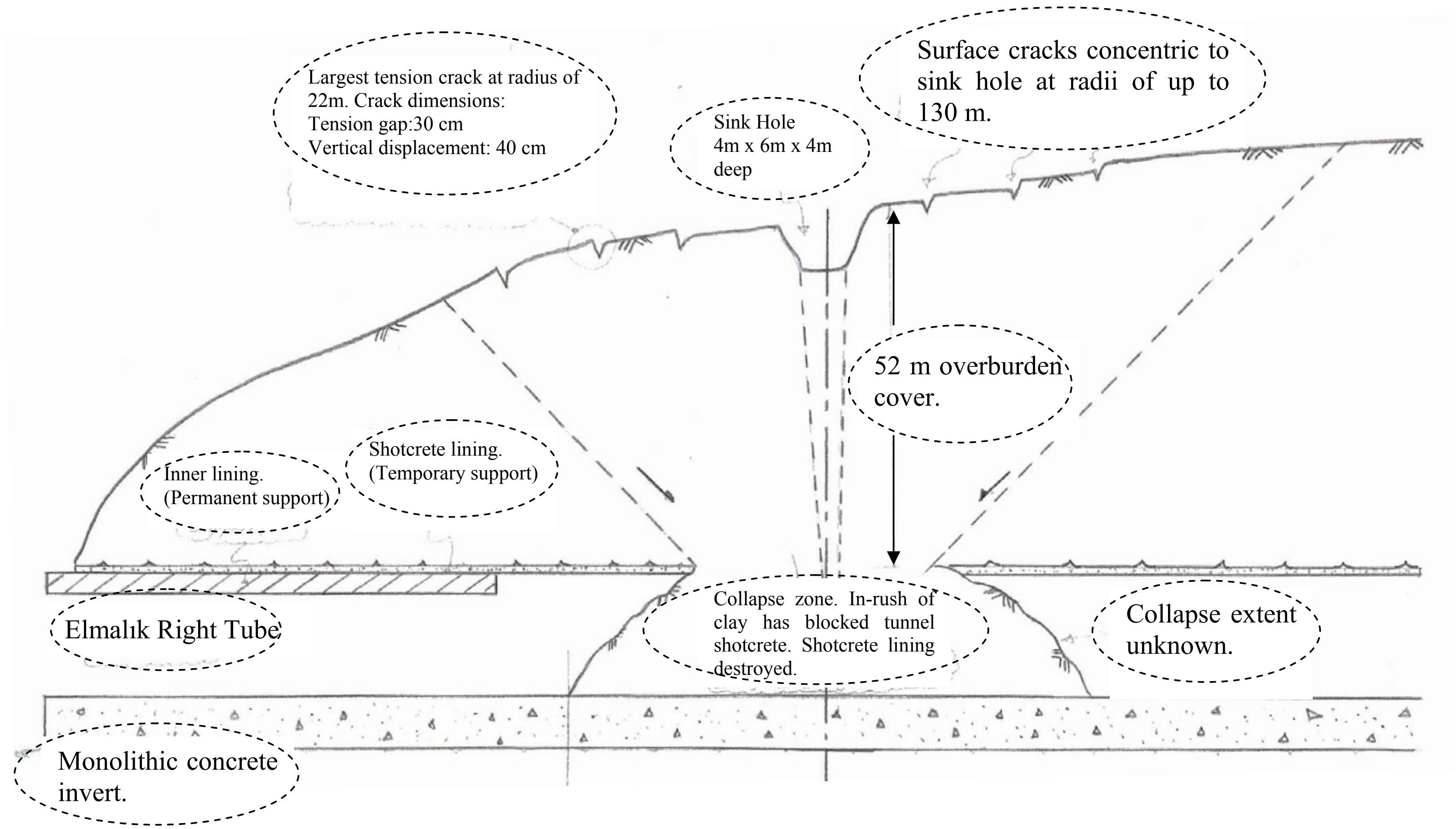

Figure 3.16 Schematic representation of collapse in Elmalık Right Tube (modified after Yüksel-Rendel Engineers, 1999)

Closer to the face on the Elmalık side, where the tunnel had been excavated through poor fault gouge clay, significant damage occurred. The Asarsuyu Left Tube Bench Pilot Tunnels (BPTs) were under construction through the fault gouge clay at the Asarsuyu/Elmalık interface zone when the earthquake occurred. Tunnels were observed to have suffered consistent crushing and cracking of the shotcrete shell together with the invert failure and heave up to 1 m (see Figure 3.19). This pattern of failure was continuous along the length of the BPTs. The Asarsuyu Right BPTs appeared to be undamaged since they had been completed and backfilled with reinforced concrete.

Figure 3.17 Sinkhole formed due to Bolu Tunnel collapse at Elmalık Right Tube (after Yüksel-Rendel Engineers, 1999)

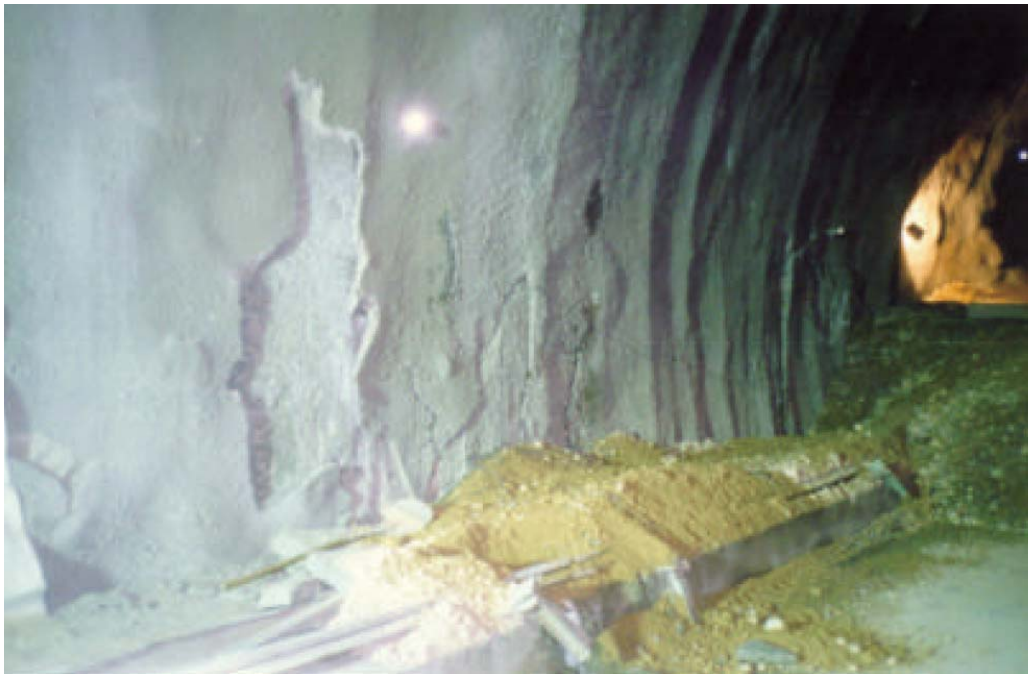

Figure 3.18 Spalled shotcrete liner segment (after Ghasemi et al., 2000)

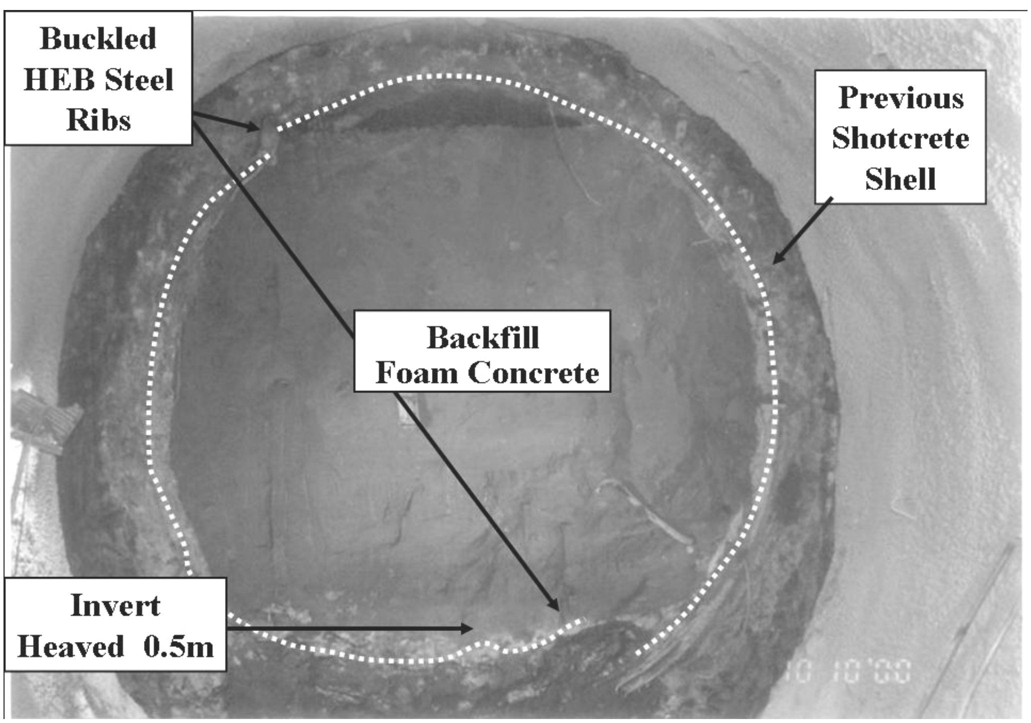

Figure 3.19 Damage observed at Asarsuyu Left Tube Bench Pilot Tunnels (after Işık and Özben, 2007)

3.3. Sections of Bolu Tunnels and Site Properties

According to the reports and papers referenced in the previous sections, 35 different tunnel sections have been evaluated for the damage analyses of Bolu Tunnels as a result of 1999 earthquakes with their respective damage states. Details of each section are given in Table 3.1 and Table 3.2 with the corresponding chainage and site characteristics considered in the assessment of the dynamic response. Average cover depth over the tunnel crown, type of rock formation, weathering grade and strength of these rock formations were determined for each section from the geological profile along the tunnel route (see Appendix C). While the tunnel was in construction at the time of the earthquakes, the state of construction for the corresponding time is also given in these tables.

Based on the information provided in the project documents, the coefficient of lateral earth pressure (K_o) was assumed to be 1.0 in the analyses. Ground water level above the tunnel axis varied within a range of 45% to 85% of the overburden cover according to the site-specific pieozometer readings. Accordingly, in the analyses, ground water table was assumed to be 80% of the overburden cover where applicable.

Table 3.1 Properties of sections to be analyzed in the Bolu Tunnels

	Section Type	Type No.	Starting Chainage KM:	Starting Chainage Depth of Cover (m)	Ending Chainage KM:	Ending Chainage Depth of Cover (m)	Average Depth of Cover (m)	Rock Formation Surrounding Tunnel *	Weathering Grade of Rock	Rock Strength *	Construction Stage	Damage State (Bolu EQ)
1	A2	1	61+222	20	61+240	34	27	metacrystalline	slightly w.	very strong - strong	inner lining completed	undamaged
2		2	61+197	9	61+215	18	13.5	metacrystalline	slightly w.	very strong - strong	inner lining completed	undamaged
3	B1	1	61+309	85	61+519	195	140	metacrystalline	slightly-medium w.	very strong - strong	inner lining completed	undamaged
4		2	61+523	197	61+590	201	199	metacrystalline	slightly-medium w.	very strong - strong	inner lining completed	undamaged
5		3	62+227	234	62+275	223	228.5	marble	slightly-medium w.	very strong - strong	inner lining completed	undamaged
6		4	62+275	223	62+326	211	217	marble	slightly-medium w.	very strong - strong	supports completed	local cracking in shotcrete
7	B2	1	61+251	40	61+309	85	62.5	metacrystalline	slightly-medium w.	strong - medium strong	inner lining completed	undamaged
8		2	61+665	207	61+760	239	223	metacrystalline	slightly-medium w.	strong - medium strong	inner lining completed	undamaged
9		3	62+200	237	62+227	234	235.5	marble	slightly-medium w.	very strong - strong	inner lining completed	undamaged
10	B2_invert	1	61+764	239	61+799	242	240.5	metacrystalline	slightly-highly w.	strong - weak	inner lining completed	undamaged
11	C1	1	61+600	207	61+633	200	203.5	fault gouge clay	medium- completely w.	medium strong - very weak	inner lining completed	undamaged
12		2	62+678	205	62+716	194	199.5	brecciated sandstone	slightly-highly w.	strong - weak	supports completed	local cracking in shotcrete
13	C2	1	62+644	210	62+678	205	207.5	brecciated sandstone	slightly-completely w.	strong - very weak	supports completed	local cracking in shotcrete
14		2	61+806	243	61+923	252	247.5	fault gouge clay	medium- completely w.	medium strong - very weak	inner lining completed	undamaged
15		3	64+340	32	64+475	28	30	high PI flyschoid	medium- completely w.	strong - very weak	inner lining completed	undamaged
16	C2M	1	61+923	252	61+978	248	250	metasediment	medium- completely w.	weak - extremely weak	inner lining completed	undamaged
17		2	62+000	239	62+030	223	231	heavily faulted metacrystalline	medium- completely w.	weak - extremely weak	inner lining completed	undamaged
18		3	62+030	223	62+070	230	226.5	metasediment	highly weathered-residual soil	weak - extremely weak	inner lining completed	undamaged
19		4	62+070	230	62+106	230	230	metacrystalline	medium- completely w.	medium strong - very weak	inner lining completed	undamaged
20		5	64+260	50	64+340	33	41.5	heavily faulted metacrystalline	medium- completely w.	weak - very weak	inner lining completed	undamaged
21		6	64+150	70	64+260	50	60	fault gouge clay	medium w.- residual soil	medium strong - extremely weak	supports completed	failed

Table 3.1 Continued.

	Section Type	Type No.	Starting Chainage KM:	Starting Chainage Depth of Cover (m)	Ending Chainage KM:	Ending Chainage Depth of Cover (m)	Average Depth of Cover (m)	Rock Formation Surrounding Tunnel *	Weathering Grade of Rock	Rock Strength *	Construction Stage	Damage State (Bolu EQ)
22	CM	1	62+106	230	62+200	237	233.5	metacrystalline	medium- completely w.	medium strong - very weak	inner lining completed	undamaged
23		2	62+347	208	62+644	210	209	metasediment	medium- completely w.	medium strong - very weak	supports completed	local cracking in shotcrete
24		3	62+721	192	62+825	146	169	metasediment	medium- completely w.	weak - extremely weak	supports completed	local cracking in shotcrete
25		4	64+050	98	64+150	71	84.5	heavily faulted metacrystalline	medium- completely w.	medium strong - very weak	supports completed	failed
26		5	63+940	132	64+050	98	115	high PI fault gouge clay	medium- completely w.	medium strong - very weak	supports completed	anticipated heavy damage
27		6	63+880	155	63+940	132	143.5	high PI fault gouge clay	medium- completely w.	medium strong - very weak	supports completed	anticipated heavy damage
28	L2	1	64+475	10	64+494	2	6	flyschoid	medium- completely w.	strong - very weak	inner lining completed	invert cracked
29	Option-3	1	52+729	164	52+752	173	168.5	metasediment	medium- completely w.	very weak - extremely weak	supports completed	sidewall damaged
30		2	63+800	162	63+850	158	160	high PI fault gouge clay	highly weathered-residual soil	weak - extremely weak	supports completed	anticipated heavy damage
31		3	53+900	155	53+950	132	143.5	high PI fault gouge clay	medium- completely w.	medium strong - very weak	supports completed	anticipated heavy damage
32	Option-4	1	63+680	162	63+800	162	162	high PI flyschoid	medium- completely w.	medium strong - very weak	supports completed	anticipated heavy damage
33	Pilot T.	1	62+820	146	62+900	119	132.5	fault gouge clay	completely weathered-residual soil	weak - very weak	supports completed	floor heaved
34		2	53+650	162	53+720	162	162	high PI flyschoid	medium- completely w.	medium strong - very weak	supports completed	anticipated heavy damage
35		3	63+600	162	63+660	162	162	brecciated sandstone	medium- completely w.	medium strong - very weak	supports completed	undamaged

***See explanations below. Detailed geological profiles of the analyzed sections can be found in Section 4.3.**

Formation	γ (kN/m^3)	ϕ	c (kPa)	ν	E (MPa)	G_o/σ'_v
Metacrystalline	23	40	600	0.3	2000	950
Heavily Faulted Metacrystalline	23	25	50	0.3	300	600
Marble	25	40	500	0.25	4000	High
Metasediment	23	20	25	0.3	$0.2(\sigma')$	825
High PI Flyschoid	23	17	100	0.3	$0.386(\sigma')^{0.91}$	500
Low PI Flyschoid	23	22	100	0.3	$0.386(\sigma')^{0.91}$	650
Brecciated Sandstone	23	21	150	0.3	550	700
Calcerous Sandstone	23	30	50	0.3	$0.386(\sigma')^{0.91}$	825
Fault Gouge Clay	20	21	75	0.3	200	700
High PI Fault Gouge Clay	23	24	100	0.3	250	600

ROCK STRENGTH
(ESTIMATED UCS IN MPa)

>250	**Extremely Strong**
100-250	**Very Strong**
50-100	**Strong**
25-50	**Moderately Strong**
5-25	**Weak**
1-5	**Very Weak**
0.25-1	**Extremely Weak**

Table 3.2 Support and excavation properties of the sections at the Bolu Tunnels

ASARSUYU LEFT TUNNEL					
Type	Chainage KM		Round Length (m)	Steel Ribs	Rock Anchor Density (m/m)
A2	61+200	61+220	2.90 - 3.50	-	7.5
A2	61+230	61+250	2.80 - 3.50	-	8
B1	61+250	61+260	2.00 - 3.50	-	20
B1	61+310	61+520	2.30 - 3.75	-	13
B1	61+520	61+530	2.25 - 3.50	-	14
B1	62+230	62+320	2.50 - 3.00	-	13
B1	63+330	62+340	2.00 - 3.00	-	14
B2	61+220	61+230	1.20 - 2.00	HEB100	30
B2	61+260	61+310	1.50 - 3.50	HEB100	19
B2	61+520	61+530	1.50 - 2.00	HEB100	31
B2	61+590	61+600	1.50 - 2.00	HEB100	47
B2	61+655	61+760	1.50 - 2.50	HEB100	24
B2	61+770	61+880	2.30 - 2.50	HEB100	23
B2	62+200	62+230	2.00 - 2.50	HEB100	34
C1	61+600	61+635	1.30 - 1.50	HEB100	135
C1	61+645	61+655	1.30 - 1.80	HEB100	74
C1	61+760	61+770	1.50 - 2.10	HEB100	71
C1	61+800	61+810	1.00 - 1.50	HEB100	83
C2	61+635	61+645	1.00 - 1.20	HEB100	109
C2	61+810	61+930	0.80 - 1.20	HEB100	467
C2	62+320	62+330	1.00 - 1.50	HEB100	91
C2M	61+930	62+100	0.80 - 1.20	HEB100-INP200-INP160	696
CM	62+100	62+200	1.10 - 1.15	HEB100-HEB140	336
CM	62+340	62+440	1.00 - 1.35	TH29	340

ASARSUYU RIGHT TUNNEL					
Type	Chainage KM		Round Length (m)	Steel Ribs	Rock Anchor Density (m/m)
B1	51+205	51+490	1.25 - 3.50	-	17
B1	51+645	51+665	2.10 - 3.50	-	13
B1	51+675	51+720	2.25 - 3.00	-	14
B1	52+115	51+240	2.00 - 3.00	-	15
B2	51+175	51+205	2.00	HEB100	28
B2	51+490	51+515	0.75 - 2.00	HEB100	31
B2	51+555	51+645	2.00 - 2.50	HEB100	24
B2	51+665	51+675	1.15 - 2.50	HEB100	23
B2	51+720	51+725	1.40 - 2.50	HEB100	38
B2	52+090	52+115	1.50 - 2.00	HEB100	39
C1	51+515	51+535	0.90 - 1.30	HEB100	86
C1	51+545	51+555	1.30	HEB100	86
C1	51+725	51+730	1.20 - 1.30	HEB100	88
C1	51+760	51+785	1.40 - 1.50	HEB100	114
C2	51+535	51+545	1.10 - 1.20	HEB100	94
C2	51+730	51+760	1.10 - 1.30	HEB100	162
C2	51+785	51+805	0.90 - 1.20	HEB100	353
C2M	51+805	51+960	0.80 - 1.50	HEB100-INP160x2-INP200x2	350
CM	51+960	52+090	1.05 - 1.20	HEB140-INP200-HEB100	298
CM	52+240	52+320	1.10 - 1.20	HEB140-TH29	305

ELMALIK LEFT TUNNEL					
Type	Chainage KM		Round Length (m)	Steel Ribs	Rock Anchor Density (m/m)
L2	64+494	64+474	1.00	HEB100-HEB100X2	118
C2	64+474	64+340	1.10 - 1.20	HEB100-HEB100X2	109
C2M	64+150	64+260	1.10	HEB140	388
C2M	64+340	64+260	1.10	HEB140	185
CMR1	64+050	64+150	1.10	HEB140	305-356-375-310
CMR1	64+050	63+940	1.10	HEB140	392-403
CM	63+975	63+880	1.10	TH29	403
CM	63+880	63+784	1.10	TH29	403-496-538

ELMALIK RIGHT TUNNEL					
Type	Chainage KM		Round Length (m)	Steel Ribs	Rock Anchor Density (m/m)
L2	54+415	54+410	1.00	HEB100	122
C2	54+410	54+245	1.10 - 1.20	HEB100-HEB100X2	133
C2M	54+245	54+170	1.10	HEB100-HEB100X2	133-367

CHAPTER 4

SEISMIC RESPONSE ANALYSES OF BOLU TUNNELS

In this part of the study, dynamic analysis methods are applied to the selected sections of the Bolu Tunnels accordingly.

4.1. Selection of Dynamic Loadings for Vulnerability Assessment

Four actual earthquake time history records having response spectra consistent with the design spectra for rock were selected as scenario events for the dynamic analyses. The records were selected in accordance with the requirements set forth by Eurocode 8 (CEN, 2004), Seed and Idriss (1982) and Turkish seismic design provisions (TEC, 2007). Relevant characteristics of these earthquakes are presented in Table 4.1 and Figure 4.1. According to these characteristics, response spectra of these earthquakes are drawn in Figure 4.2 for comparison. Since dynamic excitation is presumed to act at the base of the model which is considered to be the bedrock, records obtained in rock or stiff-soil site conditions were preferred. Damping ratio of 5% was used in evaluation for all of the response spectra. All response spectra were normalized with respect to the peak ground acceleration (PGA).

Table 4.1 Characteristics of the selected earthquakes

Earthquake	Date	distance (km)	M_w	PGA (g)	PGV (cm/s)	PGD (cm)	Site Condition
Coyote Lake, USA	08.06.1979	3.1	5.7	0.434	49.2	7.77	360<Vs<750
Mammoth Lake, USA	06.28.1992	19.7	7.3	0.484	14.2	1.77	750<Vs
Supersitition Hills, USA	24.11.1987	0.7	6.7	0.377	43.9	15.2	360<Vs<750
Morgan Hill, USA	04.24.1984	2.6	6.2	0.423	25.3	4.58	360<Vs<750

For the fragility analysis, a complete data set of earthquakes is required with peak ground accelerations ranging between 0.1g and 1.0g. Due to the difficulties involved in finding earthquake time histories with such properties, selected earthquake records were scaled to the desired peak ground acceleration values to represent a specific earthquake scenario. Kramer (1996) states that the recommendation of Krinitszky and Chang (1979) that the scaling factor (the ratio of the target amplitude to the amplitude of the record being scaled) should be kept as close to 1 as possible, and always between 0.25 and 4.0, and the analyses be conducted with several scaled records. Following this recommendation, peak ground accelerations of the scenario earthquakes were selected from the database within a range of 0.30g and 0.50g to generate the earthquakes in the target range of 0.1g and 1.0g.

<u>Supersitition Hills EQ</u>
Maximum Acceleration: 0.3771807g
Maximum Velocity: 43.88013678cm/sec
Vmax / Amax: 116.33717414sec
Arias Intensity: 1.70204713m/sec
A95 parameter: 0.37052125g

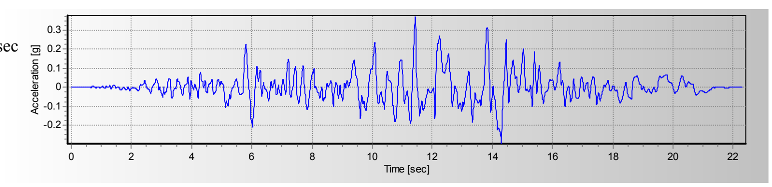

<u>Coyote Lake EQ</u>
Maximum Acceleration: 0.4339443g
Maximum Velocity: 49.2345923cm/sec
Vmax / Amax: 113.45832241sec
Arias Intensity: 0.77460281m/sec
A95 parameter: 0.43285808g

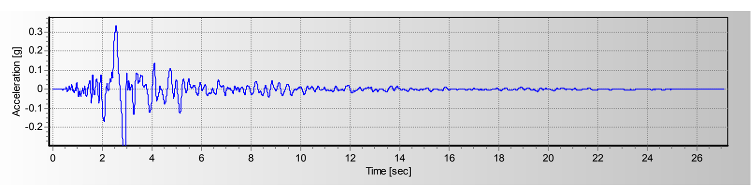

<u>Mammoth Lake EQ</u>
Maximum Acceleration: 0.4837399g
Maximum Velocity: 14.20836516cm/sec
Vmax / Amax: 29.37191072sec
Arias Intensity: 0.74510883m/sec
A95 parameter: 0.48009814g

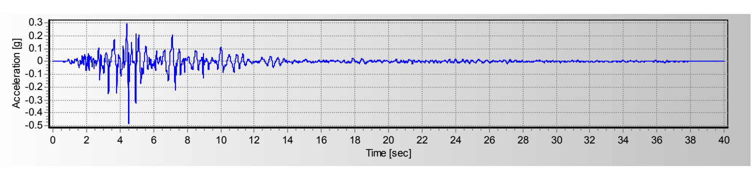

<u>Morgan Hill EQ</u>
Maximum Acceleration: 0.4230476g
Maximum Velocity: 25.27839093cm/sec
Vmax / Amax: 59.75306545sec
Arias Intensity: 0.68309056m/sec
A95 parameter: 0.42198866g

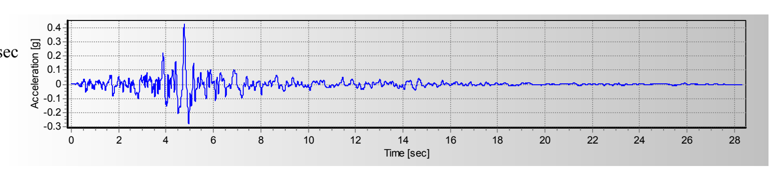

Figure 4.1 Time histories and some characteristics of the selected earthquakes

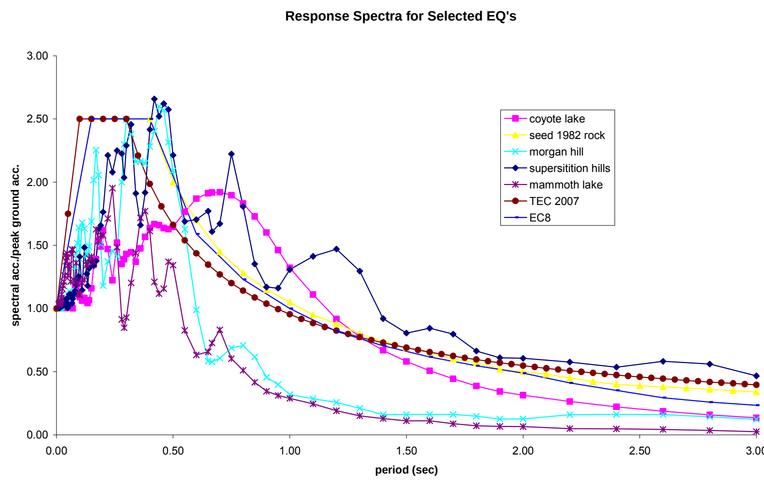

Figure 4.2 Comparison of response spectra of the selected earthquakes with the spectra for stiff soil and rock sites according to Eurocode 8, TEC (2007) and Seed and Idriss (1982)

4.2. Evaluation of Dynamic Loading for Actual Damage Study

In order to investigate the damage to the Bolu Tunnels during the 1999 earthquakes, it was necessary to estimate the characteristics of dynamic loading at the construction site of the tunnels. Since there is no bedrock ground motion record available close to the tunnels, surface accelerograms of strong motion recording stations had to be inspected in the affected region. Amongst the inspected strong motion recording stations, the ones which are close to fault rupture in the vicinity of the site and the ones having detailed subsurface ground properties available were considered to be used in the study. Then the surface accelerograms of these selected stations were deconvolved to bedrock motions. Finally, deconvolved ground motions were scaled with respect to distance by using an appropriate attenuation relationship. In the following paragraphs, the summarized process will be clarified.

Thirty ground motions were recorded during the 1999 Kocaeli earthquake and forty-eight ground motions were recorded during the 1999 Düzce earthquake. Ground motions were recorded by permanent recording stations operated by the Kandilli

Observatory and Earthquake Research Institute (KOERI), the Earthquake Research Department of the General Directorate of Disaster Affairs (ERD) and the Istanbul Technical University (ITU) in Turkey. Additionally, after the Kocaeli earthquake several international research institutes visited the affected area and installed temporary recording stations to catch the aftershocks of this event. Fortunately, these temporary stations caught the mainshock of the Düzce earthquake. These temporary stations were installed by the Lamont Doherty Earth Observatory of Columbia University (LD) and Observatoire de Grenoble of Joseph Fourier University. The data sets are presented in Table 4.2 and Table 4.3 for Kocaeli and Düzce earthquakes, respectively. As Durukal (2002) stated, the tables present station info, soil conditions at the stations classified as NEHRP site classes, 3D peak acceleration data and distances defined as the shortest distance to the surface fault rupture.

Table 4.2 Mw=7.4 Kocaeli earthquake strong motion data set (after Durukal, 2002)

Station	Operator	Soil type	NS PGA (mg)	EW PGA (mg)	UD PGA (mg)	Distance (km)
Afyon	ERD	Unknown	13.5	15.0	5.0	232.9
Arçelik	KOERI	C	2.09×10^2	1.32×10^2	7.45×10	21.6
Ataköy	ITU	D	1.02×10^2	1.67×10^2	6.76×10	67.6
Ambarlı	KOERI	D	2.53×10^2	1.86×10^2	7.88×10	79.0
Balıkesir	ERD	Unknown	1.78×10	1.82×10	7.60	192.0
Bursa	ERD	D	5.43×10	4.80	2.57×10	74.6
Botaş	KOERI	C	8.70×10	9.89×10	2.33×10	136.4
Bursa	KOERI	D	1.01×10^2	9.98×10	4.78×10	63.1
Çekmece	ERD	D	1.18×10^2	8.96×10	4.98×10	79.6
Çekmece	KOERI	D	1.77×10^2	1.32×10^2	5.81×10	76.1
Çanakkale	ERD	Unknown	2.46×10	2.86×10	7.90	279.2
Yesilkoy	KOERI	D	9.01×10	8.47×10	5.45×10	69.4
Düzce	ERD	D	3.74×10^2	3.15×10^2	4.80×10^2	12.7
Ereğli	ERD	Unknown	9.14×10	1.01×10^2	5.70×10	145.4
Fatih	KOERI	D	1.77×10^2	1.62×10^2	1.07×10^2	62.3
Gebze	ERD	B	2.65×10^2	1.42×10^2	1.99×10^2	15.6
Göynük	ERD	D	1.18×10^2	1.38×10^2	1.30×10^2	35.5
Heybeli	KOERI	C	5.17×10	1.12×10^2	1.39×10^2	43.6
Istanbul	ERD	D	6.07×10	4.27×10	3.62×10	56.5
İznik	ERD	D	9.18×10	1.23×10^2	8.23×10	29.7
İzmit	ERD	B	1.71×10^2	2.25×10^2	1.46×10^2	4.8
Koca Mustafa Paşa	KOERI	D	9.83×10	1.28×10^2	8.32×10	62.7
Kütahya	ERD	D	5.00×10	5.97×10	2.32×10	152.0
Mecidiyeköy	ITU	C	1.06×10^2	1.40×10^2	6.45×10	62.3
Maslak	ITU	B	1.07×10^2	7.56×10	6.01×10	64.0
Sakarya	ERD	C		4.07×10^2	2.59×10^2	3.1
Tekirdağ	ERD	Unknown	3.22×10	3.35×10	1.02×10	177.4
Usak	ERD	Unknown	8.90	7.20	3.40	232.0
Yarimca	KOERI	D	3.23×10^2	2.31×10^2	2.34×10^2	2.6
Zeytinburnu	ITU	D	2.38×10^2	2.18×10^2	9.45×10	63.2

Among the recording stations presented in Table 4.2 and Table 4.3, accelerograms from Bolu and Düzce Stations are chosen to use in the finite element analyses. Since these stations are not only close to the surface rupture of fault, but also close to the Bolu Tunnels site. Additionally, much more data is available in literature regarding to the site conditions of these stations and their basins. The chosen stations and surface ruptures of the earthquakes are shown in Figure 4.3 with respect to the Bolu Tunnels for comparison.

Table 4.3 Mw=7.1 Düzce earthquake strong motion data set (after Durukal, 2002)

Station	Operator	Soil type	NS PGA (mg)	EW PGA (mg)	UD PGA (mg)	Distance (km)
Afyon	ERD	Unknown	8.0	10.0	3.5	221.3
Arçelik	KOERI	C	7.80	7.85	6.72	134.4
Ataköy	ITU	D	1.64×10	1.63×10	5.45	178.9
Ambarli	KOERI	D	3.79×10	2.69×10	8.23	191.8
Bağlaraltı (Yalova)	KOERITEMP	D	2.27×10	2.14×10	9.54	163.6
Bahçevan (Yalova)	KOERITEMP	D	2.65×10	2.04×10	1.09×10	141.4
Balikesir	ERD	Unknown	2.70	2.40	1.70	290.4
Bolu	ERD	D	7.40×10^2	8.06×10^2	2.00×10^2	19.9
Bornova	ERD	Unknown	1.80	1.50	8.00×10^{-1}	409.4
Bursa	ERD	D	9.30	8.00	4.80	167.0
Botas	KOERI	C	4.29	3.70	1.68	251.6
Bursa	ERD	D	1.79×10	1.69×10	1.15×10	168.8
Cekmece	KOERI	D	1.54×10	1.69×10	7.25	186.9
Darica	KOERI	D	8.17	1.51×10	6.32	133.7
Yesilkoy	KOERI	D	1.76×10	1.79×10	7.33	181.2
Düzce	ERD	D	4.08×10^2	5.14×10^2	3.40×10^2	8.3
Fatih	KOERI	D	3.57×10	2.47×10	7.58	171.0
Galata Bridge	KOERI	D	1.39×10	1.52×10	9.30	169.4
Gime (Yalova)	KOERITEMP	D	1.69×10	1.47×10	5.78	140.3
Gölcük	ITU	D	3.55×10	4.09×10	1.94×10	96.0
Göynük	ERD	D	2.78×10	2.48×10	2.49×10	45.8
Hastane (Yalova)	KOERITEMP	D	3.86×10	4.25×10	1.71×10	143.0
Heybeli	KOERI	C	1.84×10	2.62×10	2.01×10	157.6
Hilal (Yalova)	KOERITEMP	D	4.68×10	5.39×10	1.97×10	143.0
İstanbul	ERD	D	9.00	5.20	8.20	160.7
İznik	ERD	D	2.20×10	2.14×10	9.80	125.0
İzmit	ERD	B	2.22×10	2.38×10	2.24×10	114.1
Kaşif (Yalova)	KOERITEMP	D	2.68×10	2.48×10	9.53	140.6
Koca Mustafa Paša	KOERI	D	1.48×10	1.79×10	7.67	172.5
Kutahya	ERD	D	1.71×10	2.06×10	9.40	169.8
Mudurnu	ERD	B	1.21×10^2	5.83×10	6.31×10	33.6
Radar (Yalova)	KOERITEMP	D	2.52×10	2.74×10	9.05	159.4
Ruzgar (Yalova)	KOERITEMP	D	3.50×10	3.42×10	1.78×10	141.9
Sakarya	ERD	C	1.73×10	2.47×10	1.15×10	48.0
Tar (Yalova)	KOERITEMP	D	2.60×10	2.64×10	1.11×10	144.3
Tekirdağ	ERD	Unknown	5.70	6.10	1.80	290.4
Tosya	ERD	Unknown	7.90	7.60	4.10	222.6
Uşak	ERD	Unknown	3.10	3.10	1.40	267.4
Yarimca	KOERI	D	1.80×10	1.61×10	1.37×10	100.4
Zeytinbumu	ITU	D	4.52×10	5.83×10	2.13×10	174.0
VO-375-Karadere	LD	B	890	510	190	10.0
FP-1059-Karadere	LD	–	150	140	100	10.0
WF-531-Karadere	LD	–	160	120	60	14.0
FI-1062-Karadere	LD	–	120	260	90	15.0
LS-1061-Karadere	LD	C	100	130	50	17.0
CH-362-Karadere	LD	C	40	30	20	28.0
BU-1060-Karadere	LD	B	30	50	20	31.0
St 496	FG	–	736	736	324	–

Düzce is located close to the epicenter of the Düzce earthquake. It is located approximately 7 km north of the fault rupture surface. Dönmez and Pujol (2005)

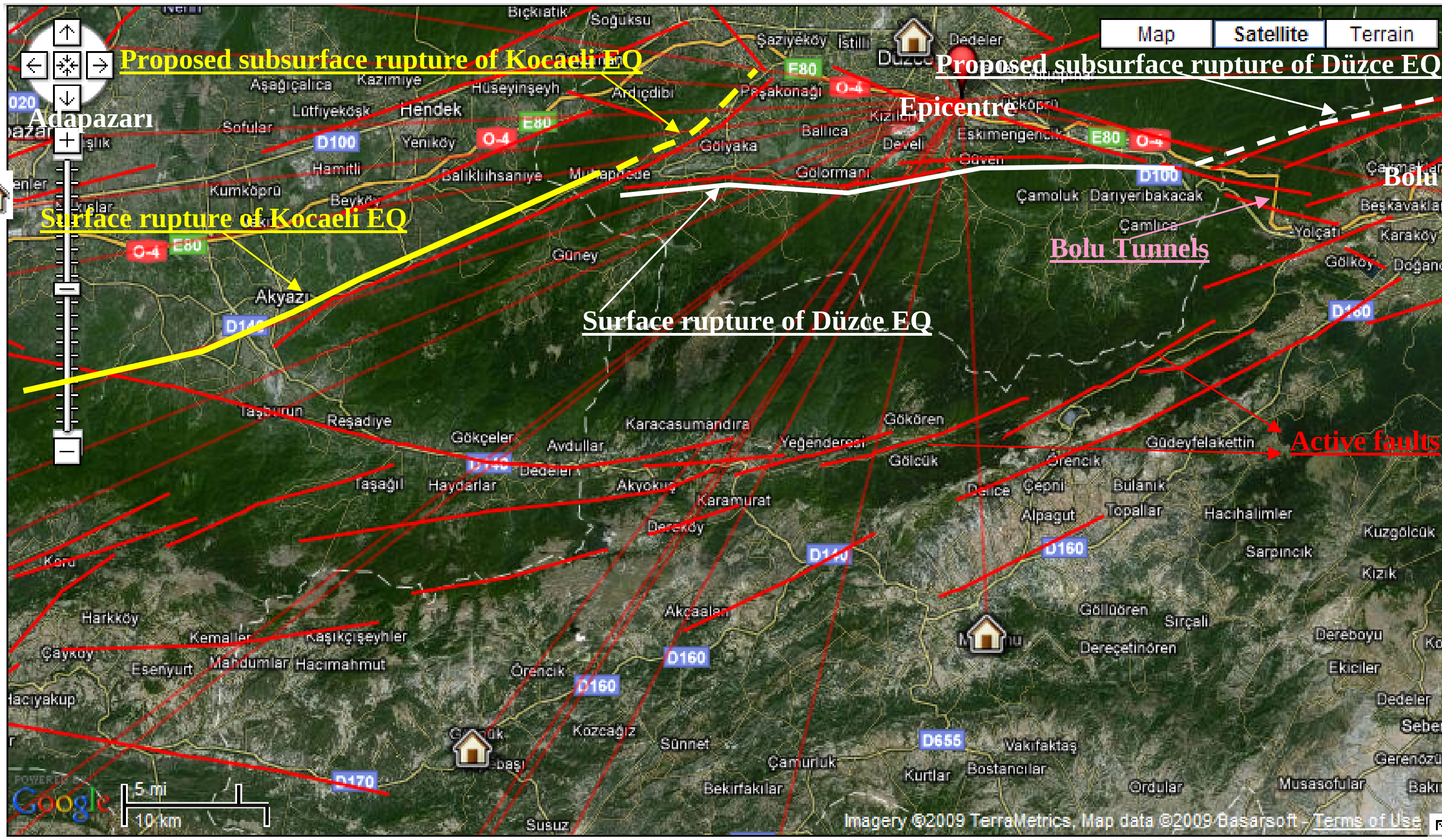

Figure 4.3 Map showing ruptures of the 1999 earthquakes, strong motion recording stations and the Bolu Tunnels (ERD and EERC, 2009)

stated that the city is situated in a basin that is filled with colluvial deposits. According to their investigations, these deposits are composed of clay, sand and gravel. The average depth to bedrock varies between 200 and 250 meters (see Figure 4.4). Rathje et al. (2006) also reported that, the thickness of these sediments is approximately between 175 to 225 meters according to the studies of ERD and TUBİTAK. To study the site effects, several researchers investigated the geotechnical conditions and shear wave profiles under the Düzce strong motion station. Kudo et al. (2002) investigated the shear wave velocities under the station up to 1.5 km depth with array observations of microtremors and aftershocks. Rathje et al. (2003) utilized the spectral-analysis-of-surface-waves (SASW) method up to 42 m. Additionally, Scandella et al. (2007) studied the Düzce basin and proposed a shear wave profile up to 1 km with the help of deep borings and past geophysics studies of the site. In the latest research, with the cooperation of ERD and EERC (Earthquake Engineering Research Center) of METU (Middle East Technical University) in 2009, shear wave profiles up to 30 m were investigated with down-hole measurements. In their study, ERD and EERC also provided the borehole logs (see Appendix D). According to these borehole logs, first 10 meters of the profile is composed of low plastic clays and the remaining 200 meters composed of sand and gravelly sand. According to these detailed data shear wave velocity profiles are drawn for Düzce station in Figure 4.6 and the adopted shear wave profile by engineering judgment used in this study is shown with red lines.

Similar to Düzce, Bolu is also situated in a basin that is filled with colluvial deposits. Information from the limited number of boreholes available indicates that the depth to bedrock is of the order of 100 meters (see Figure 4.5). Deep and shallow borings show that the soils in Bolu are composed of clay, sand and gravel layers (Dönmez and Pujol, 2005). Rathje et al. (2006) reported that there is an outcropping Pliocene bedrock in the center of town. To study the site effects, several researchers investigated the geotechnical conditions and shear wave profiles under the Bolu strong motion station. Rathje et al. (2003) utilized the spectral-analysis-of-surface-waves (SASW) method up to 40 m. Başokur (2005) used Refraction-Microtremor (ReMi) method investigating shear wave profiles up to 64 meters. Finally, ERD and

EERC (2009) investigated shear wave profiles up to 30 m with down-hole measurements. In their study, ERD and EERC also provided the borehole logs (see Appendix E). According to these borehole logs, the whole profile is composed of low to high plastic clays. With respect to the detailed shear wave velocity information for Bolu station, shear wave profiles are drawn in Figure 4.7 and the profile adopted for this study by engineering judgment is shown with red lines.

With the available shear wave profiles and geotechnical information, the surface accelerograms of Düzce and Bolu stations are deconvolved to bedrock motions by using equivalent linear method. Software like SHAKE91 (Idriss et al., 1992) and EERA (Bardet et al., 2000) were utilized for the analyses. For the clays, in the analyzed profiles, modulus and damping degradation curves proposed by Vucetic and Dobry (1991) and Sun et al. (1988) were used for comparison. For the sands, modulus and damping degradation curves proposed by Seed et al. (1986) were utilized. According to the results of the analyses, bedrock motions with PGA ranging between 0.3-0.7g and 0.3-0.5g were evaluated for Bolu and Düzce, respectively. Example outputs for variation of maximum acceleration with depth for Düzce and Bolu stations are presented in Figure 4.8.

For the final scaling of calculated rock motions obtained from the equivalent linear analysis, attenuation relationship proposed by Abrahamson and Silva (2008) was employed. According to the appropriate Joyner-Boore distances together with the average shear wave velocities, proposed PGAs on rock were calculated for Düzce station, Bolu station and chainages of Bolu Tunnels site, respectively. Results are presented in Table 4.4 and Table 4.5 for Düzce and Kocaeli earthquakes, respectively. While calculating the Joyner-Boore distances, surface faults and subsurface faults were utilized according to the study of Lettis and Barka (2000) and Barka et al. (2002). Subsurface faults were also considered according to their study, because this study is compliant with the mainshock and aftershock epicenters map published in the study of Sucuoğlu and Yılmaz (2001) which is shown in Figure 4.9. Summary of the general calculation scheme for the evaluation of dynamic loading for the tunnels is shown in Figure 4.10.

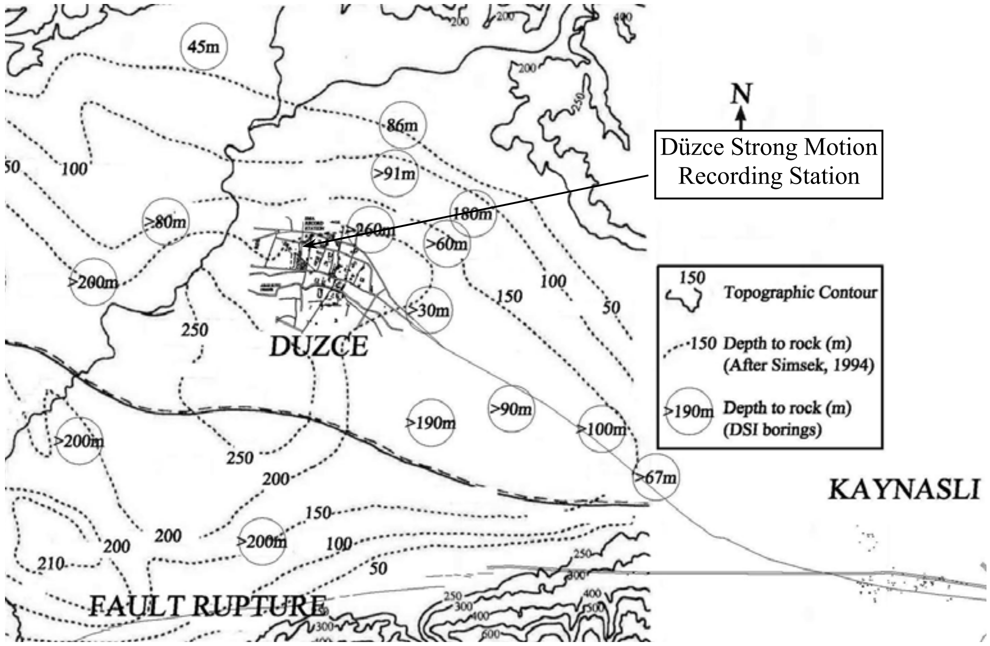

Figure 4.4 Site information about Düzce (after Dönmez and Pujol, 2005)

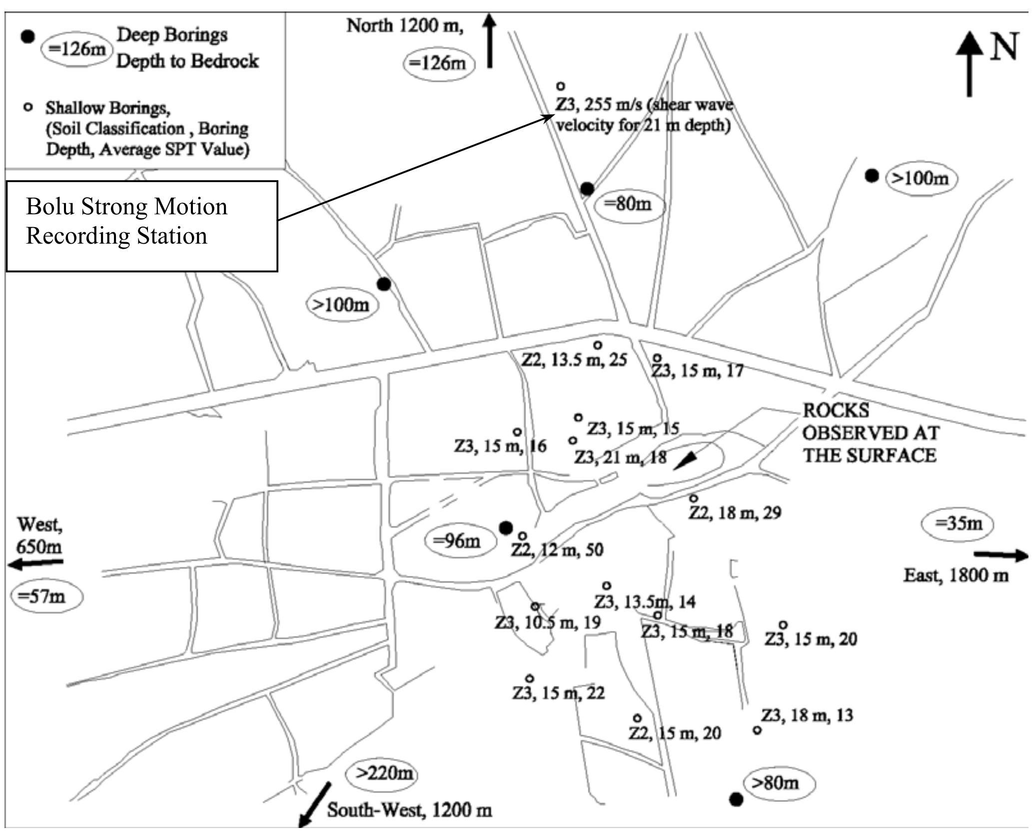

Figure 4.5 Site information about Bolu (after Dönmez and Pujol, 2005)

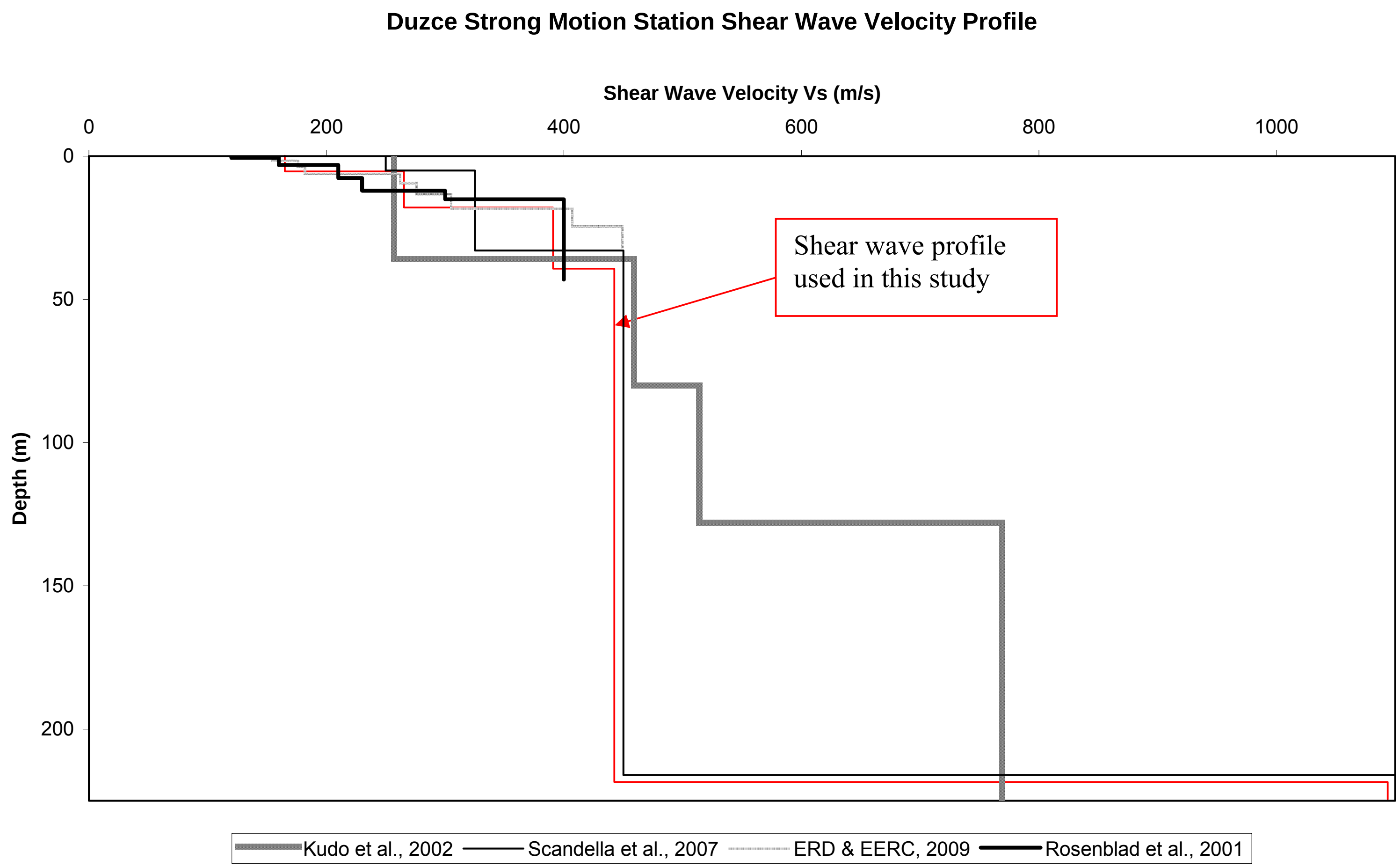

Figure 4.6 Shear wave profiles proposed by several researchers and the one used in this study for Düzce Station

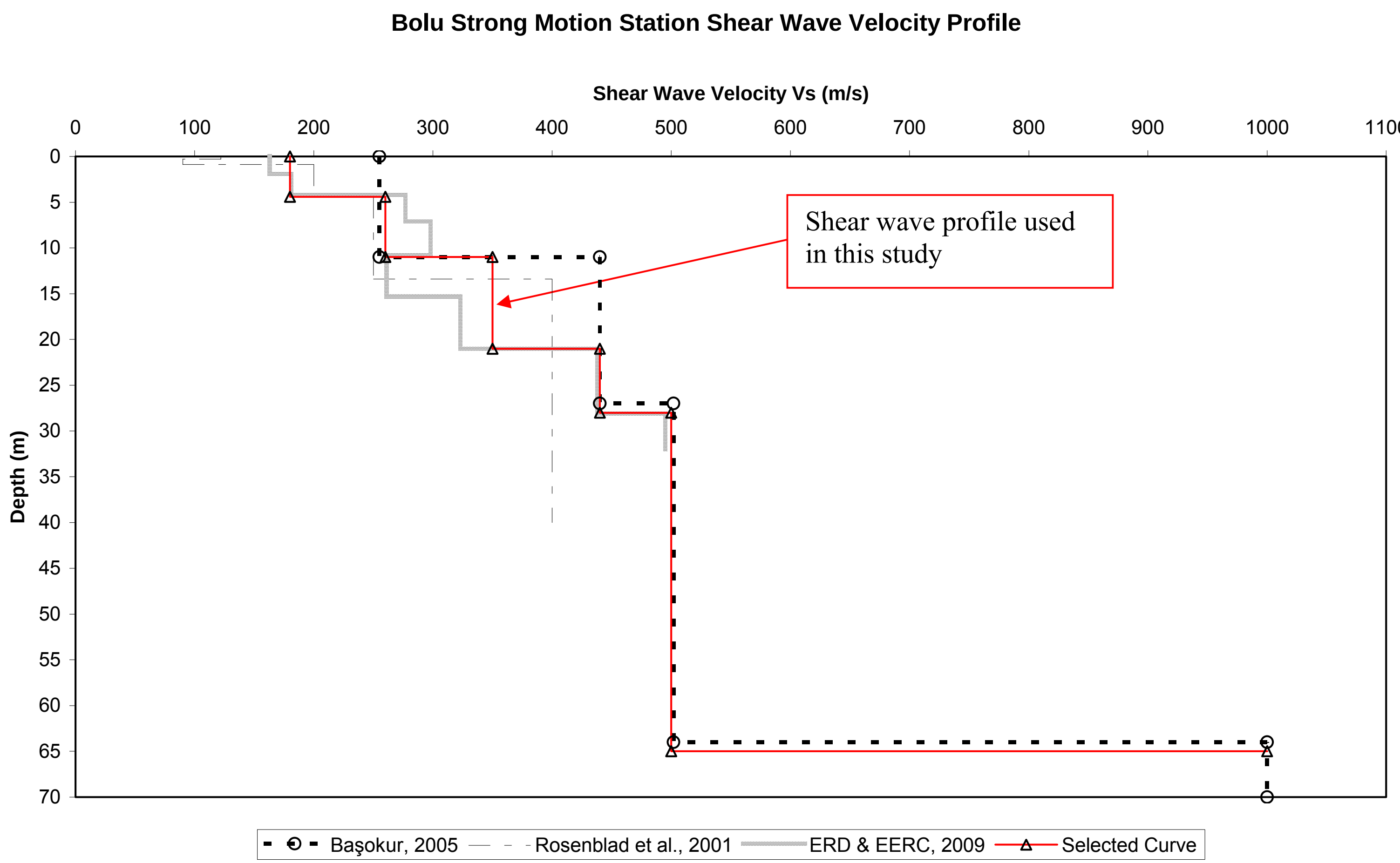

Figure 4.7 Shear wave profiles proposed by several researchers and the one used in this study for Bolu Station

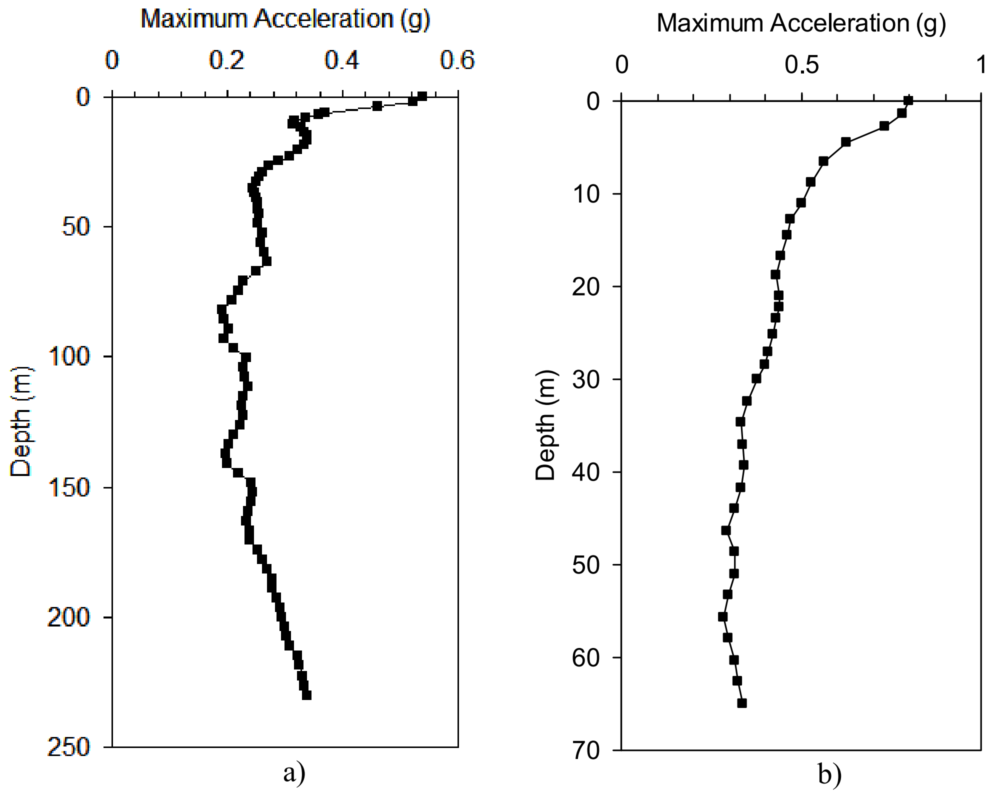

Figure 4.8 Variation of maximum acceleration with depth for a) Düzce and b) Bolu stations as a result of Düzce earthquake

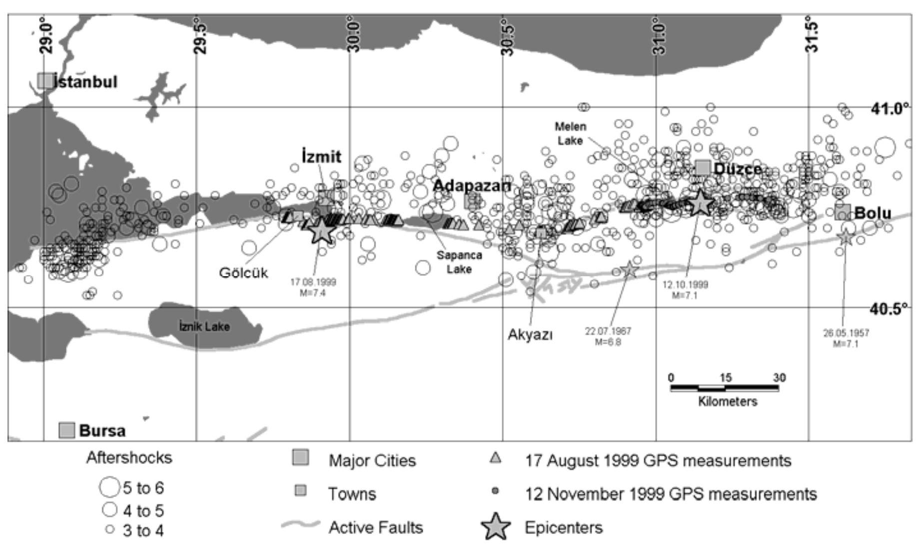

Figure 4.9 17 August Kocaeli and 12 November Düzce earthquakes, mainshock and aftershock epicenters, surface faulting (after Sucuoğlu and Yılmaz, 2001)

Table 4.4 Calculation of distance scaling as a result of Düzce earthquake

	Section Type	Type No.	Starting Chainage		Ending Chainage		Calculations for Distance Scaling According to Abrahamson & Silva (2008) for Bolu and Düzce Stations as result of Düzce EQ					
			KM:	Depth of Cover (m)	KM:	Depth of Cover (m)	R_{JB}	R_{RUP}	R_X	Vs=760	Amp_B	Amp_D
1	A2	1	61+222	20	61+240	34	2.28	2.28	-2.28	0.3197	1.6746988	0.73443602
2		2	61+197	9	61+215	18	2.28	2.28	-2.28	0.3197	1.6746988	0.73443602
3	B1	1	61+309	85	61+519	195	2.44	2.44	-2.44	0.3157	1.65374542	0.72524696
4		2	61+523	197	61+590	201	2.56	2.56	-2.56	0.3127	1.63803038	0.71835516
5		3	62+227	234	62+275	223	3.17	3.17	-3.17	0.2967	1.55421687	0.6815989
6		4	62+275	223	62+326	211	3.22	3.22	-3.22	0.2953	1.54688318	0.67838272
7	B2	1	61+251	40	61+309	85	2.33	2.33	-2.33	0.3184	1.66788895	0.73144958
8		2	61+665	207	61+760	239	2.67	2.67	-2.67	0.3098	1.62283918	0.71169309
9		3	62+200	237	62+227	234	3.17	3.17	-3.17	0.2967	1.55421687	0.6815989
10	B2_invert	1	61+764	239	61+799	242	2.72	2.72	-2.72	0.3085	1.61602933	0.70870664
11	C1	1	61+600	207	61+633	200	2.61	2.61	-2.61	0.3144	1.64693557	0.72226051
12		2	62+678	205	62+716	194	3.56	3.56	-3.56	0.2863	1.49973808	0.65770733
13	C2	1	62+644	210	62+678	205	3.5	3.5	-3.5	0.2879	1.50811943	0.66138295
14		2	61+806	243	61+923	252	2.78	2.78	-2.78	0.307	1.60817182	0.70526074
15		3	64+340	32	64+475	28	5.11	5.11	-5.11	0.2471	1.29439497	0.56765449
16	C2M	1	61+923	252	61+978	248	2.89	2.89	-2.89	0.3041	1.59298062	0.69859867
17		2	62+000	239	62+030	223	2.94	2.94	-2.94	0.3028	1.58617077	0.69561222
18		3	62+030	223	62+070	230	3.06	3.06	-3.06	0.2996	1.56940807	0.68826097
19		4	62+070	230	62+106	230	3.06	3.06	-3.06	0.2996	1.56940807	0.68826097
20		5	64+260	50	64+340	33	5	5	-5	0.2497	1.30801467	0.57362738
21		6	64+150	70	64+260	50	4.94	4.94	-4.94	0.2512	1.31587218	0.57707328
22	CM	1	62+106	230	62+200	237	3.11	3.11	-3.11	0.2982	1.56207438	0.6850448
23		2	62+347	208	62+644	210	3.39	3.39	-3.39	0.2908	1.52331063	0.66804503
24		3	62+721	192	62+825	146	3.64	3.64	-3.64	0.2841	1.48821372	0.65265334
25		4	64+050	98	64+150	71	4.83	4.83	-4.83	0.2538	1.32949188	0.58304618
26		5	63+940	132	64+050	98	4.78	4.78	-4.78	0.255	1.33577789	0.58580289
27		6	63+880	155	63+940	132	4.72	4.72	-4.72	0.2565	1.34363541	0.58924879
28	L2	1	64+475	10	64+494	2	5.17	5.17	-5.17	0.2457	1.28706129	0.56443832
29	Option-3	1	52+729	164	52+752	173	3.67	3.67	-3.67	0.2834	1.48454688	0.65104526
30		2	63+800	162	63+850	158	4.67	4.67	-4.67	0.2577	1.34992142	0.59200551
31		3	53+900	155	53+950	132	4.83	4.83	-4.83	0.2538	1.32949188	0.58304618
32	Option-4	1	63+680	162	63+800	162	4.56	4.56	-4.56	0.2604	1.36406496	0.59820813
33	Pilot T.	1	62+820	146	62+900	119	3.72	3.72	-3.72	0.282	1.4772132	0.64782908
34		2	53+650	162	53+720	162	4.61	4.61	-4.61	0.2592	1.35777894	0.59545141
35		3	63+600	162	63+660	162	4.33	4.33	-4.33	0.2662	1.39444735	0.61153228
36	Bolu S.						8.01	8.01	-8.01	0.1909		
37	Düzce S.						0	9.71	8.7	0.4353		

Table 4.5 Calculation of distance scaling as a result of Kocaeli earthquake

	Section Type	Type No.	Starting Chainage		Ending Chainage		Calculations for Distance Scaling According to Abrahamson & Silva (2008) for Bolu and Düzce Stations as result of Kocaeli EQ					
			KM:	Depth of Cover (m)	KM:	Depth of Cover (m)	R_{JB}	R_{RUP}	R_X	Vs=760	Amp_B	Amp_D
1	A2	1	61+222	20	61+240	34	44.4	51.3	44.4	0.07552	1.07211811	0.33050328
2		2	61+197	9	61+215	18	44.4	51.3	44.4	0.07552	1.07211811	0.33050328
3	B1	1	61+309	85	61+519	195	44.4	51.3	44.4	0.07552	1.07211811	0.33050328
4		2	61+523	197	61+590	201	44.4	51.3	44.4	0.07552	1.07211811	0.33050328
5		3	62+227	234	62+275	223	45.1	52.1	45.1	0.07461	1.05919932	0.32652079
6		4	62+275	223	62+326	211	45.1	52.1	45.1	0.07461	1.05919932	0.32652079
7	B2	1	61+251	40	61+309	85	44.4	51.3	44.4	0.07552	1.07211811	0.33050328
8		2	61+665	207	61+760	239	44.4	51.3	44.4	0.07552	1.07211811	0.33050328
9		3	62+200	237	62+227	234	45.1	52.1	45.1	0.07461	1.05919932	0.32652079
10	B2_invert	1	61+764	239	61+799	242	45.1	52.1	45.1	0.07461	1.05919932	0.32652079
11	C1	1	61+600	207	61+633	200	44.4	51.3	44.4	0.07552	1.07211811	0.33050328
12		2	62+678	205	62+716	194	45.7	52.8	45.7	0.07383	1.04812606	0.32310722
13	C2	1	62+644	210	62+678	205	45.7	52.8	45.7	0.07383	1.04812606	0.32310722
14		2	61+806	243	61+923	252	45.1	52.1	45.1	0.07461	1.05919932	0.32652079
15		3	64+340	32	64+475	28	46	53.1	46	0.07351	1.04358319	0.32170678
16	C2M	1	61+923	252	61+978	248	45.1	52.1	45.1	0.07461	1.05919932	0.32652079
17		2	62+000	239	62+030	223	45.1	52.1	45.1	0.07461	1.05919932	0.32652079
18		3	62+030	223	62+070	230	45.1	52.1	45.1	0.07461	1.05919932	0.32652079
19		4	62+070	230	62+106	230	45.1	52.1	45.1	0.07461	1.05919932	0.32652079
20		5	64+260	50	64+340	33	46	53.1	46	0.07351	1.04358319	0.32170678
21		6	64+150	70	64+260	50	46	53.1	46	0.07351	1.04358319	0.32170678
22	CM	1	62+106	230	62+200	237	45.1	52.1	45.1	0.07461	1.05919932	0.32652079
23		2	62+347	208	62+644	210	45.7	52.8	45.7	0.07383	1.04812606	0.32310722
24		3	62+721	192	62+825	146	45.7	52.8	45.7	0.07383	1.04812606	0.32310722
25		4	64+050	98	64+150	71	46	53.1	46	0.07351	1.04358319	0.32170678
26		5	63+940	132	64+050	98	46	53.1	46	0.07351	1.04358319	0.32170678
27		6	63+880	155	63+940	132	46	53.1	46	0.07351	1.04358319	0.32170678
28	L2	1	64+475	10	64+494	2	46	53.1	46	0.07351	1.04358319	0.32170678
29	Option-3	1	52+729	164	52+752	173	45.7	52.8	45.7	0.07383	1.04812606	0.32310722
30		2	63+800	162	63+850	158	46	53.1	46	0.07351	1.04358319	0.32170678
31		3	53+900	155	53+950	132	46	53.1	46	0.07351	1.04358319	0.32170678
32	Option-4	1	63+680	162	63+800	162	46	53.1	46	0.07351	1.04358319	0.32170678
33	Pilot T.	1	62+820	146	62+900	119	45.7	52.8	45.7	0.07383	1.04812606	0.32310722
34		2	53+650	162	53+720	162	46	53.1	46	0.07351	1.04358319	0.32170678
35		3	63+600	162	63+660	162	46	53.1	46	0.07351	1.04358319	0.32170678
36	Bolu S.						48.56	56.06	48.56	0.07044		
37	Düzce S.						8.3	11.79	8.3	0.2285		

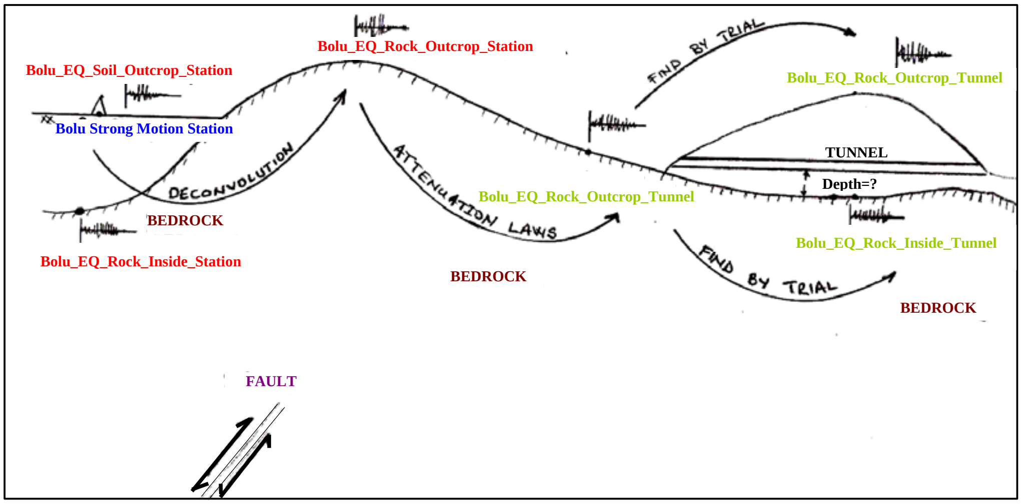

Figure 4.10 Summary of the general calculation scheme for the evaluation of dynamic loading for the tunnels

4.3. Evaluation of Geotechnical Properties for Sections of Bolu Tunnels and Dynamic Analyses

Bolu Tunnel is a well-instrumented case among the tunnels built in Turkey. Geological and geotechnical characteristics of soil and rock formations were documented in a detailed manner in various sources. Engineering properties of the in-situ materials were also published in literature as well as geotechnical properties given in design documents. However, missing properties related to Bolu Tunnels were adopted from the literature for the same materials and behavior. Among these, static parameters were evaluated on the basis of classical soil and rock mechanics principles. On the other hand, deformability parameters at low strain were used for the dynamic analyses. Utilized modulus and damping factors compatible with the strains induced in the soil deposit and the earth structures can be found in Appendix F. Through the analyses, all the material properties published in Aygar (2000), Çakan (2000), Aygar (2007), Dalgıç (1997) and Aşçıoğlu (2007) were reviewed and utilized.

Since there is no shear wave velocity measurement at the site, shear wave velocity profiling was done by the help of literature. To achieve this, equations of shear wave velocity change with respect to depth proposed by Boore and Joyner (1997) for generic rock sites were utilized (see Table 4.6). As it is seen in Figure 4.11, shear wave velocity for generic rock sites (heavy solid line) are plotted with the equations that they proposed. Velocity model proposed by Boore (1986) and shear wave velocity profile for very hard rock sites are also plotted in the same figure for comparison.

Table 4.6 Velocity for generic rock site (after Boore and Joyner ,1997)

Depth (km)	Shear Velocity (km/sec)*
$z \leqq 0.001$	0.245
$0.001 < z \leqq 0.03$	$2.206z^{0.272}$
$0.03 < z \leqq 0.19$	$3.542z^{0.407}$
$0.19 < z \leqq 4.00$	$2.505z^{0.199}$
$4.00 < z \leqq 8.00$	$2.927z^{0.086}$

$*\bar{V}_{30} = 0.618$ km/sec.

Normalized secant stiffness graphs of the materials in Bolu Tunnels are given in Figure 4.12. The curves can be used in the equivalent linear analyses after factorizing with initial effective vertical stresses. However, these curves are not enough for the complete equivalent linear analyses since, damping reduction curves are missing. In literature, studies on modulus and damping reduction curves for rocks are limited with respect to soil classes. Thus, modulus damping reduction curves for rock used in EPRI (1993) as quoted by the study of Hartzell et al. (2004) were utilized in this study (see Appendix F). These modulus and damping reduction curves change with respect to depth. Curves are divided into 8 depth groups, ranging between 0 to 20 ft, 21 to 50 ft, 51 to 120 ft, 121 to 250 ft, 251 to 500 ft, 501 to 1000 ft, 1001 to 2000 ft and 2001 to 5000 ft. Instead of assigning an average shear wave velocity and using one set of modulus and damping reduction curve in the equivalent linear analyses, shear wave velocities calculated for the mentioned depth intervals are adopted for the analyzed rock profile. In Figure 4.13, shear wave velocity versus depth curves are drawn with the methods and procedures mentioned in the previous paragraphs.

As it seen from Figure 4.13, the shear wave velocity profile proposed by Astaldi (2000) is lower than the profile proposed by Boore and Joyner (1997). The profile of Astaldi (2000) seems to be an underestimate of Boore and Joyner (1997). However, the curves of Astaldi (2000) are the results of experiments done for a more faulted section of the Bolu Tunnels at the Elmalık side than for the sections which are located at the Asarsuyu side of the tunnels. Therefore, through the analyses, a shear wave profile which is a little bit lower than the average profile of Boore and Joyner (1997) was utilized for rock sections on Asarsuyu side. For the sections on Elmalık side, shear wave velocity profiles calculated by Astaldi (2000) were utilized for rather soft materials.

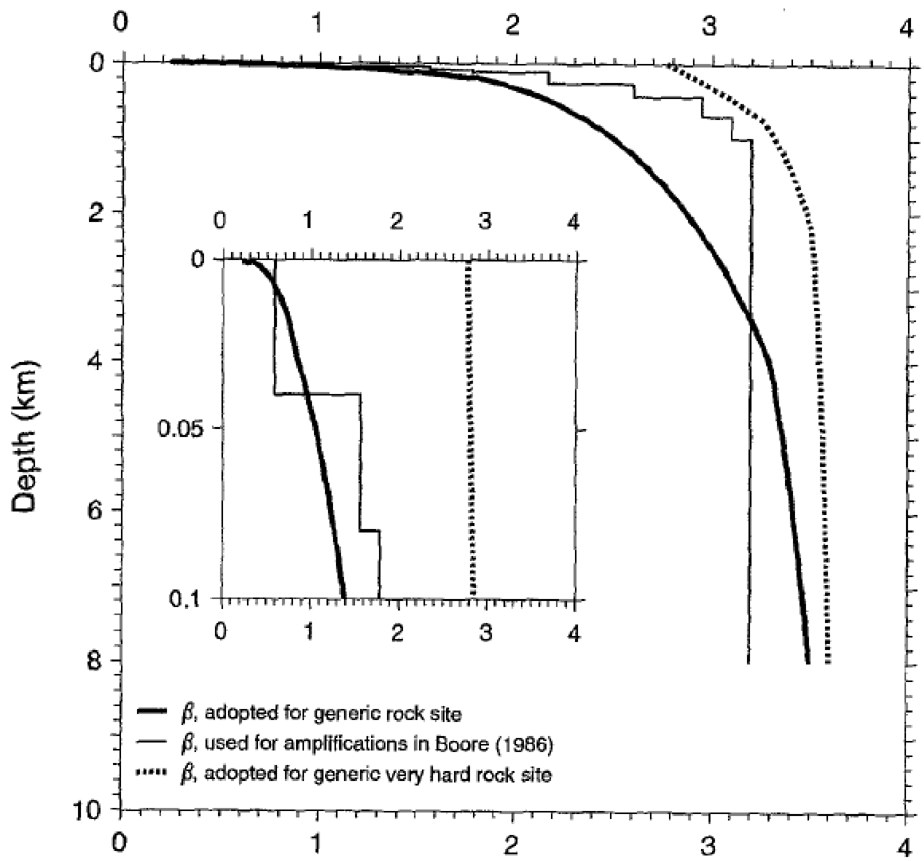

Figure 4.11 Shear wave velocity versus depth (after Boore and Joyner ,1997)

It is very difficult to determine the bedrock depth to use in the dynamic analyses. There is no clear borehole data or seismic measurement available. So, depth to bedrock had to be forecasted by utilizing the available geotechnical information related to site and literature. By using the adopted shear wave velocity profile shown in Figure 4.13, dynamic analyses were made for a sample section with ordinal number 1 as shown on Table 3.1 assuming the depth to bedrock below tunnel is 5 m, 10 m, 15 m, 30 m, 50 m, 75 m and 100 m, respectively. The horizontal displacements of the soil profiles due to dynamic excitation are shown in Figure 4.14. The order of the horizontal displacement difference between the tunnel crown and invert seems to be between 3-5 mm. The curves display a quite similar trend. However, when Figure 4.15 is carefully examined, a clue can be found to obtain the real bedrock depth.

According to Boore and Joyner (1997), the amplifications on rock sites can be in excess of 3.5 at high frequencies, in contrast to the amplifications of less than 1.2 on very hard rock sites. The site effect for the soil sites exceeds a factor of 2 over a wide range of frequencies of importance in engineering (see Table 4.7 and Table 4.8).

Table 4.7 Node points for amplification **a)** for generic rock site (V_{s30}=620 m/s) **b)** for generic very hard rock site (V_{s30}=2900 m/s) (after Boore and Joyner ,1997)

Frequency (Hz)	Amplification*
0.01	1.00
0.09	1.10
0.16	1.18
0.51	1.42
0.84	1.58
1.25	1.74
2.26	2.06
3.17	2.25
6.05	2.58
16.6	3.13
61.2	4.00

*Amplifications at other frequencies are obtained by interpolation, assuming a linear dependence between log frequency and log amplification (e.g., function *site_amp_factor* in *rvtdsubs.for* of Boore, 1996).

a)

Table 4.7 Continued

Frequency (Hz)	Amplification*
0.01	1.00
0.10	1.02
0.20	1.03
0.30	1.05
0.50	1.07
0.90	1.09
1.25	1.11
1.80	1.12
3.00	1.13
5.30	1.14
8.00	1.15
14.00	1.15

*Amplifications at other frequencies are obtained by interpolation, assuming a linear dependence between log frequency and log amplification (e.g., function *site_amp_factor* in *rvtdsubs.for* of Boore, 1996).

b)

With the amplification values in mind, it can be said easily that the bedrock depths under the tunnels can not be smaller than 15 m, because the amplification values of the profiles with depths 5 m and 10 m are closer to that of the very hard rock sites. However, the site concerned in this study is not a very hard rock site. Thus, 4 choices were left. Furthermore, because in rock profiles it is expected that after a certain depth, the value of peak ground acceleration (PGA) had to be fixed. This behavior can be seen in the profiles with the depths of 30 m and 50 m. However, the pseudo-static and full-dynamic analyses results of the 50 m bedrock depth were not close to each other. The final decision was made according to comparison with the results of pseudo-static and full-dynamic analyses. Only for the 30 m bedrock depth, the results of the dynamic analyses came closer to each other. So, bedrock depth was chosen as 30 m in the analyses. Dynamic analyses results of the mentioned study above can be seen in Table 4.10. Shear wave velocity profile and finite element models can also be seen in Appendix G and Appendix H, respectively.

Table 4.8 Node points of amplification for various sites characterized by the average shear-wave velocity over the upper 30 m (after Boore and Joyner ,1997)

	Amplification*		
Freq. (Hz)	$\bar{V}_{30}$ = 520 m/sec (NEHRP class C)	$\bar{V}_{30}$ = 310 m/sec (generic soil)	$\bar{V}_{30}$ = 255 m/sec (NEHRP class D)
0.01	1.00	1.00	1.00
0.09	1.21	1.34	1.43
0.16	1.32	1.57	1.71
0.51	1.59	2.24	2.51
0.84	1.77	2.57	2.92
1.25	1.96	2.76	3.10
2.26	2.25	2.98	3.23
3.17	2.42	2.95	3.18
6.05	2.70	3.05	3.18
16.60	3.25	3.18	3.18
61.20	4.15	3.21	3.18

*Values assume κ_0 = 0.035 sec and are based on the generic rock amplifications (Table 3), modified by the Boore *et al.* (1994) site factors for frequencies between 0.5 and 10 Hz. The modifications for frequencies outside this range are based on subjective judgment and are not constrained by data. Amplifications at frequencies other than those tabulated are obtained by interpolation, assuming a linear dependence between log frequency and log amplification (e.g., function *site_amp_factor* in *rvtdsubs.for* of Boore, 1996).

Finite Element code PLAXIS was utilized through all dynamic analyses. To model the behavior of geomaterials, Mohr-Coulomb model was used. For comparison, the resultant forces are plotted on a moment interaction diagram. Moment interaction diagrams of the analyzed tunnel sections are calculated with the code named Response2000 (Bentz, 2001).

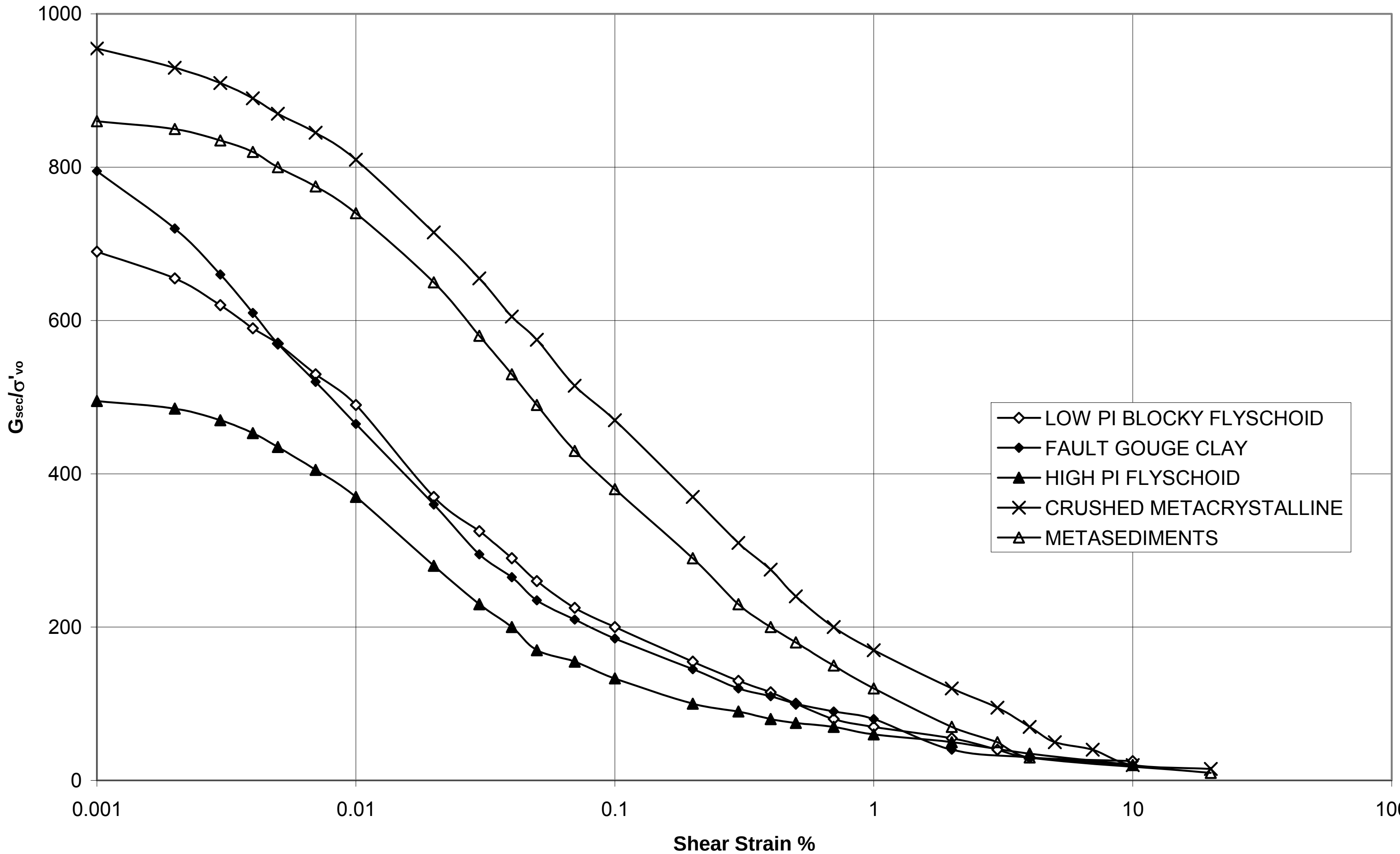

Figure 4.12 Bolu Tunnels normalized secant stiffness for all materials (Astaldi, 2000)

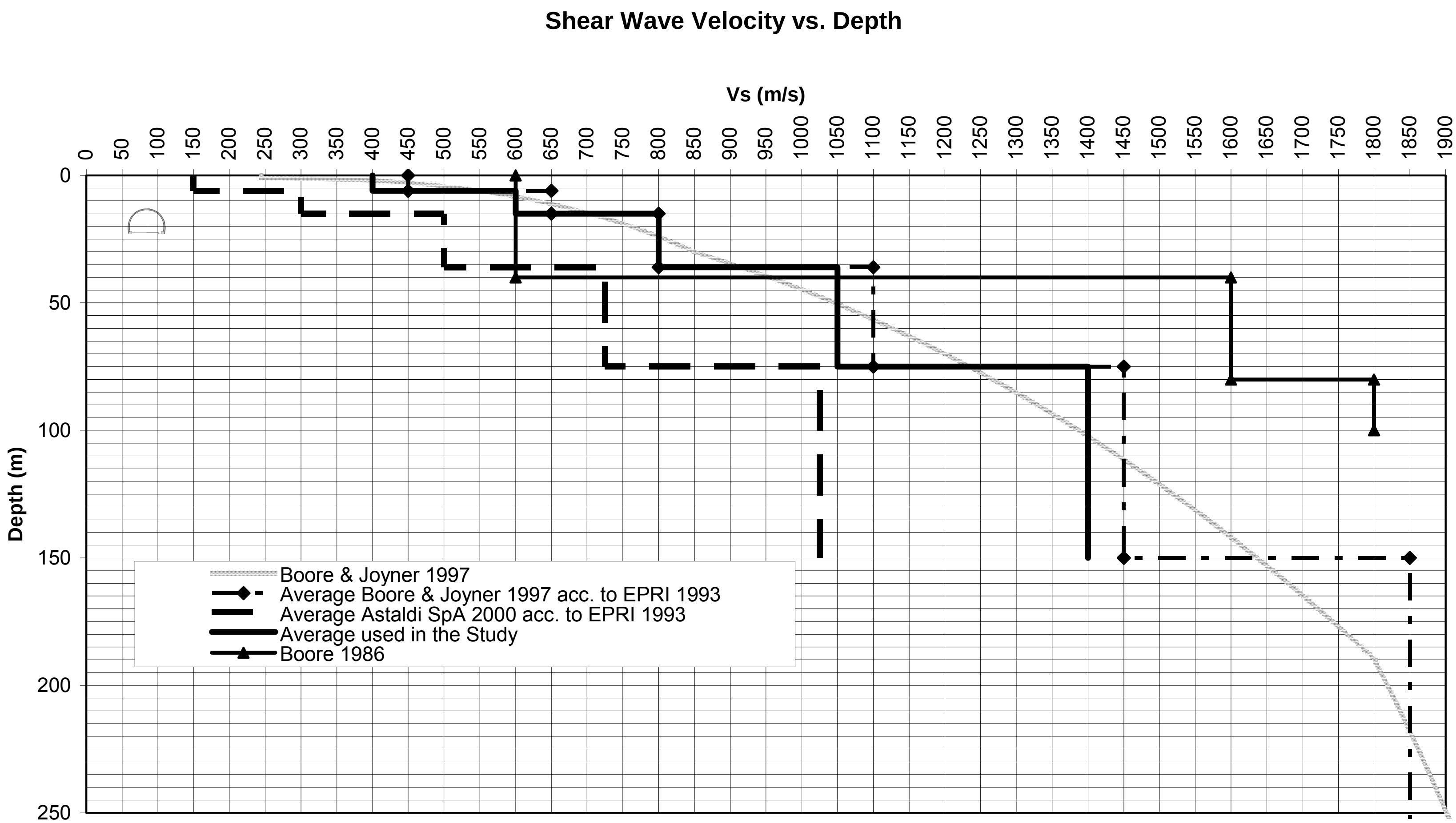

Figure 4.13 Adopted shear wave profile for Section No.1

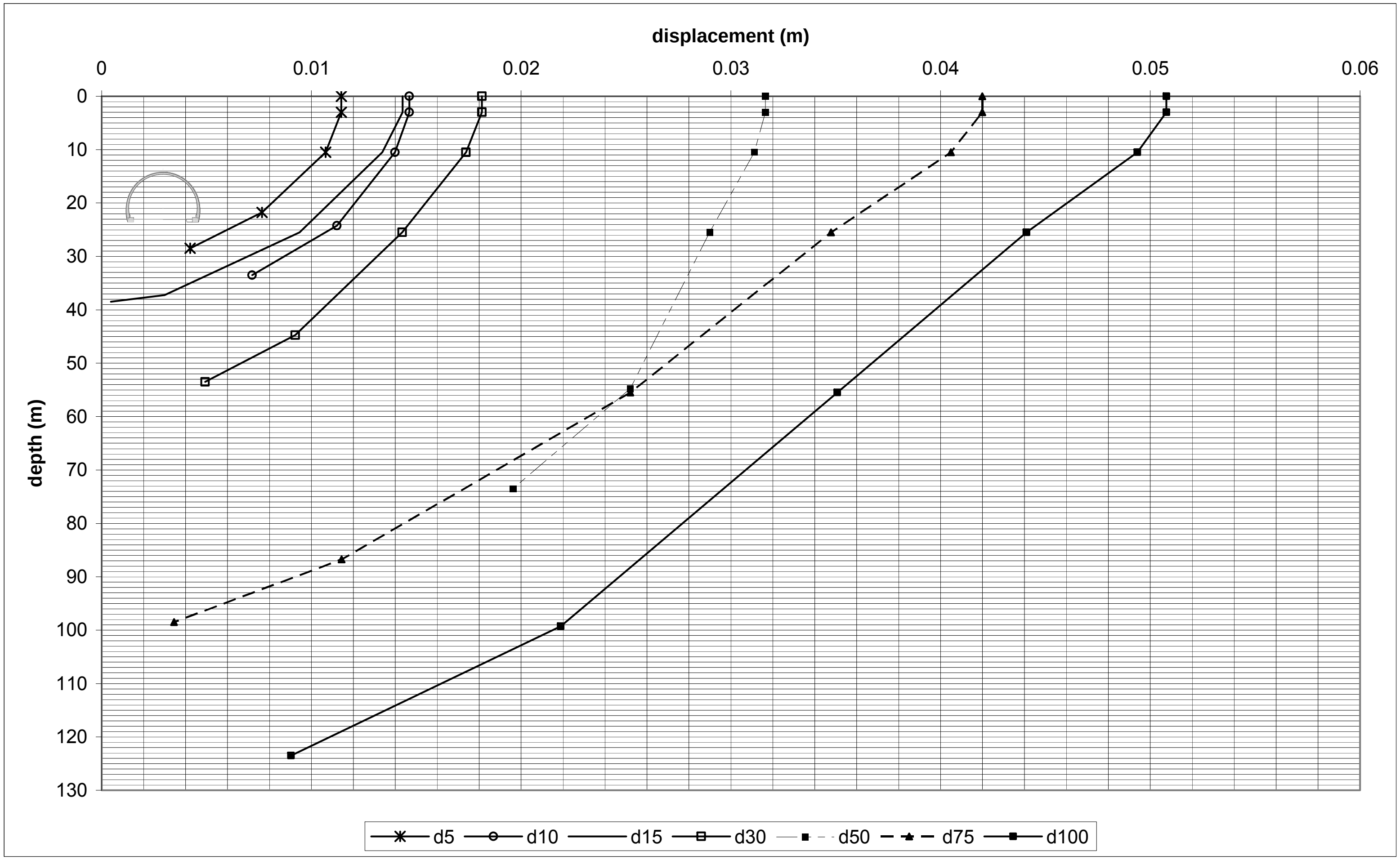

Figure 4.14 Horizontal displacement of soil profiles due to dynamic excitation according to the selected bedrock depths

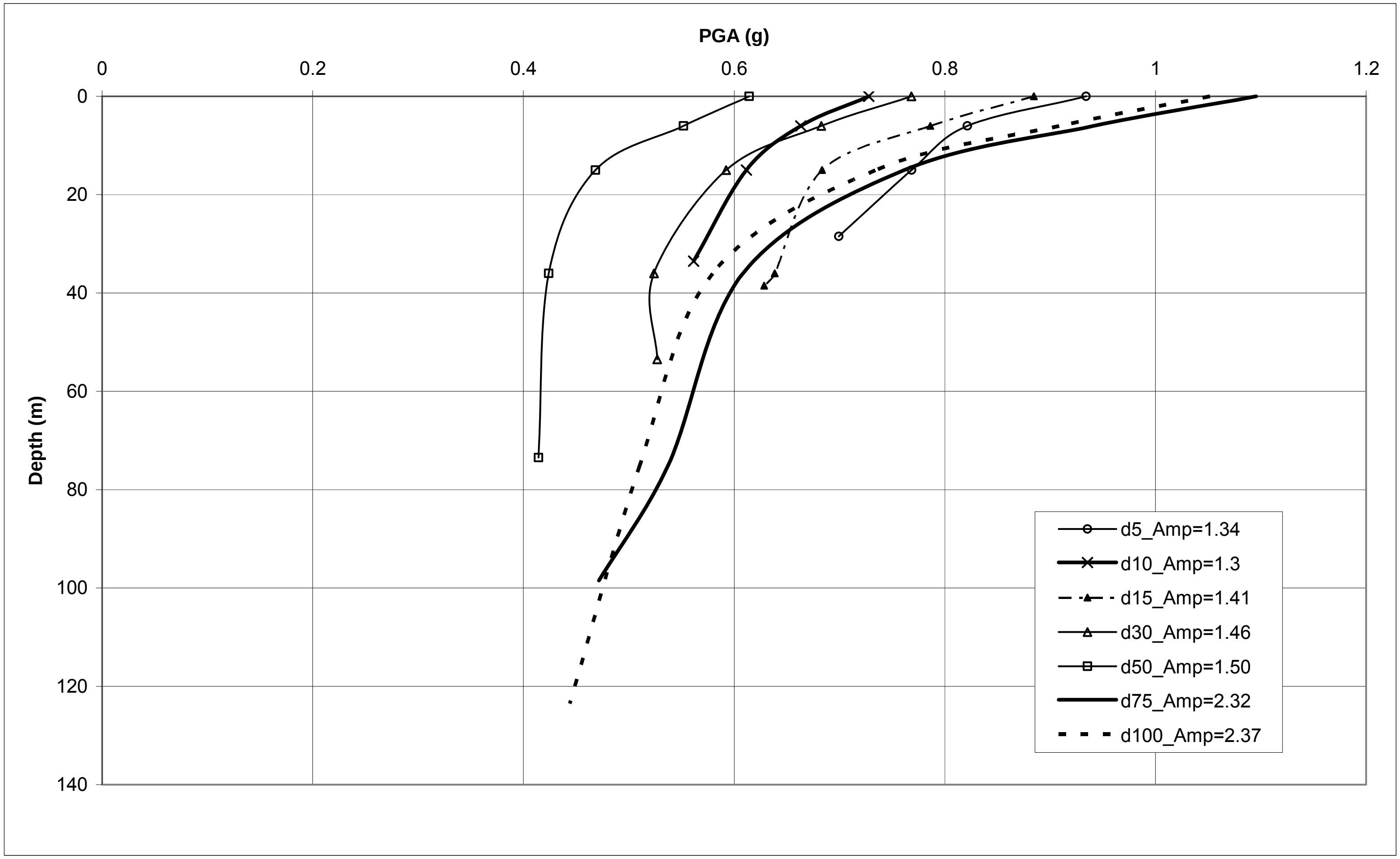

Figure 4.15 Change of peak ground acceleration with depth

4.3.1. Section for A2

A2 support class is developed especially for competent rock classes. This type of support classes were implemented at the Asarsuyu Portals of the Bolu Tunnels, where competent rock conditions are prevailing. In this type of rock class, rock is stable and behaves nearly elastic. There is a possibility of local rock spalling due to joints and gravity. Rock bolts together with shotcrete can be used to prevent local rock spallings (see Figure 4.16). Excavation is made in stages with conventional drill & ballast method. Deformations due to excavation are small. Detailed geometry and properties of the section for A2 support class is given in Figure B.1.

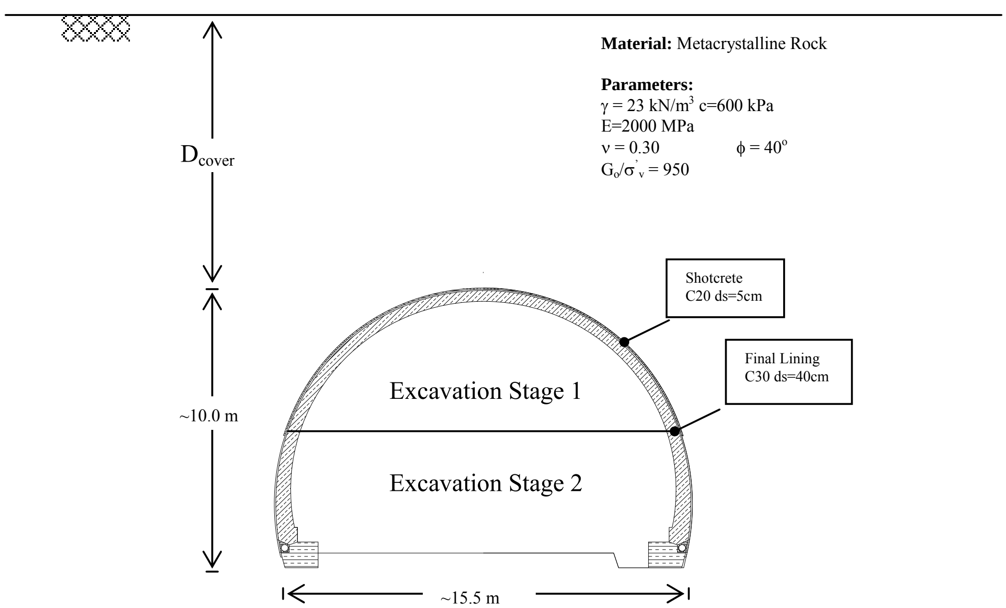

Figure 4.16 General properties of section A2

Geotechnical properties and support details of the analyzed sections are also given in Table 3.1 and Table 3.2 in addition to Figure 4.16. In this part of the chapter, sections with the ordinal number 1 and 2 as shown in these tables were analyzed. According to the drawings, the average rock cover, D_{cover}, above the tunnel crown which is considered in the finite element analyses are 27.0 m and 13.5 m, respectively. In these sections, rock formation is classified as metacrystalline and it is slightly weathered. A summary of details is given in Table 4.9 for the analyzed tunnel sections. Rock strength ranges from strong to very strong having an unconfined compressive strength ranging between 50-100 MPa to 100-250 MPa. Parameters used in the dynamic analyses are also shown in Figure 4.16. Shear wave velocity profiles used in the dynamic analyses are presented respectively in Figure G.1 and Figure G.2.

Table 4.9 Summary of details for the analyzed sections (A2 Rock Class)

Analyzed sections	D_{cover} Depth (m)	Number of rock layers	Depth and Type of Rock Layers in the FE Model: Layer-1 Type	Layer-1 Depth (m)	Layer-2 Type	Layer-2 Depth (m)	Layer-3 Type	Layer-3 Depth (m)
Section-1	27	1	Metacrystalline	67	-	-	-	-
Section-2	13.5	1	Metacrystalline	53.5	-	-	-	-

Finite element models constructed with the aid of PLAXIS software are presented in Appendix H. As it is also seen from the previous parts of this study, results of dynamic analyses of section A2 also correlates well with the damage data. These sections of the tunnels survived from the 1999 earthquakes with no damage. Resulting internal force components of the final lining obtained from the simplified, pseudo-static and full-dynamic analyses are shown in Table 4.10. Moment interaction diagrams of the related sections are presented in Figure I.1 and Figure I.2, respectively.

Table 4.10 Final results (envelope of maximum values)

	Simplified Solution, Penzien (2000), No-Slip			Pseudo-static Solution			Full Dynamic Solution		
Section No.	*N(kN/m)*	*V(kN/m)*	*M(kN.m/m)*	*N(kN/m)*	*V(kN/m)*	*M(kN.m/m)*	*N(kN/m)*	*V(kN/m)*	*M(kN.m/m)*
1	-2191.75	12.45	24.9	-2150	-99.01	54.92	-2290	343	50.75
2	-1244.95	18.55	37.1	-1170	95.32	32.77	-1430	280	43.95

4.3.2. Section for B1

B1 support class is developed especially for tunnels in competent rock classes with high overburden or intermediate rock classes at shallow depths. This type of support class was implemented at the Asarsuyu side of the Bolu Tunnels, where these types of rock conditions are prevailing. In this type of rock class, rock is friable. There is a possibility of rock spalling. Rock bolts together with shotcrete can be used to prevent rock spallings (see Figure 4.17). Excavation is made with classical drill & ballast method in stages. Deformations due to excavation rapidly decrease. Detailed geometry and properties of the section for B1 support class is given in Figure B.2.

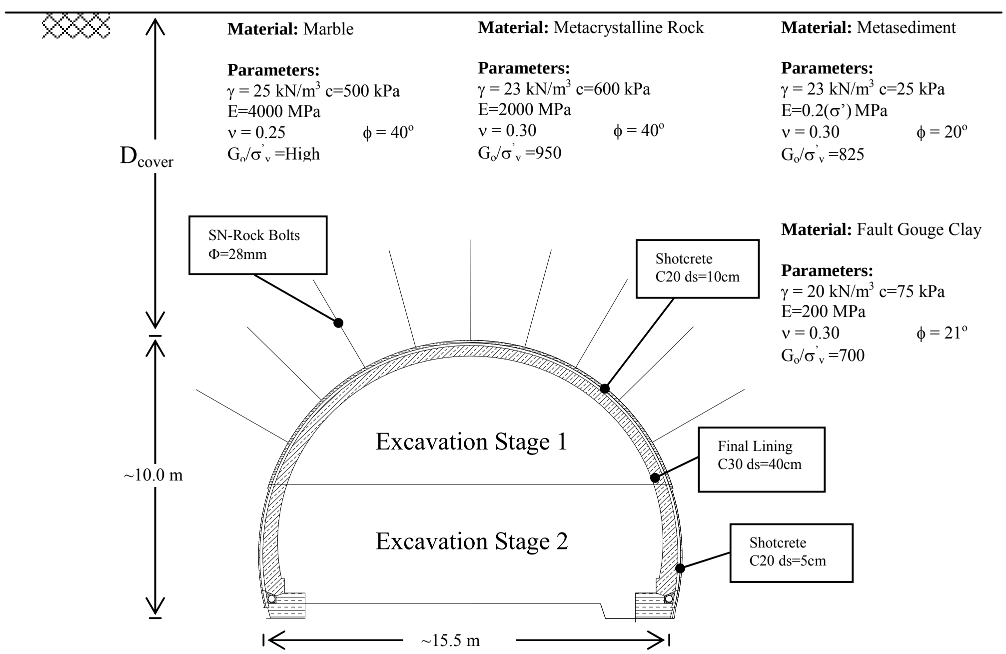

Figure 4.17 General properties of section B1

Geotechnical properties and support details of the analyzed sections are also given in Table 3.1 and Table 3.2 in addition to Figure 4.17. In this part of the chapter, sections with the ordinal number 3, 4 and 5 as shown in these tables were analyzed. According to the drawings, the average rock cover, D_{cover}, above the tunnel crown which is considered in the finite element analyses are 130.0 m, 201.0 m and 229.0 m, respectively. In sections 3 and 4, rock formation is classified as metacrystalline and it is slightly to moderately weathered. Rock strength can be ranged from strong to very strong having an unconfined compressive strength ranging between 50-100 MPa to 100-250 MPa. Additionally, only for section 4, there is a metasediment rock layer at the top of metacrystalline layer. These layers are separated with gouge clay formation. In section 5, rock formation is classified as marble and it is slightly to moderately weathered. Rock strength ranges from strong to very strong having an unconfined compressive strength ranging between 50-100 MPa to 100-250 MPa. Parameters used in the dynamic analyses are also shown in Figure 4.17. A summary of details is given in Table 4.11 for the analyzed tunnel sections. Shear wave velocity profiles used in the dynamic analyses are presented in Figure G.3, Figure G.4 and Figure G.5, respectively.

Table 4.11 Summary of details for the analyzed sections (B1 Rock Class)

Analyzed sections	D_{cover} Depth (m)	Number of rock layers	Depth and Type of Rock Layers in the FE Model: Layer-1 Type	Layer-1 Depth (m)	Layer-2 Type	Layer-2 Depth (m)	Layer-3 Type	Layer-3 Depth (m)
Section-3	130	1	Metacrystalline	170	-	-	-	-
Section-4	201	3	Metasediment	75	Fault Gouge Clay	5	Metacrystalline	161
Section-5	229	1	Marble	269	-	-	-	-

Finite element models constructed with the aid of PLAXIS software are presented in Appendix H. As it is also seen from the previous parts of this study, results of dynamic analyses of section B1 also correlates well with the damage data. These sections of the tunnels survived from the 1999 earthquakes with no damage. Resulting internal force components of the final lining obtained from the simplified, pseudo-static and full-dynamic analyses are shown in Table 4.12. Moment interaction diagrams of the related sections are presented in Figure I.3, Figure I.4 and Figure I.5, respectively.

Table 4.12 Final results (envelope of maximum values)

	Simplified Solution, Penzien (2000), No-Slip			Pseudo-static Solution			Full Dynamic Solution		
Section No.	***N(kN/m)***	***V(kN/m)***	***M(kN.m/m)***	***N(kN/m)***	***V(kN/m)***	***M(kN.m/m)***	***N(kN/m)***	***V(kN/m)***	***M(kN.m/m)***
3	-5341.06	-14.18	-28.37	-6580	-520.57	179.66	-5840	-617.3	180.03
4	-5876.22	-10.64	-21.28	-5490	410.37	131.29	-4530	874.04	195.78
5	-5950.44	-13.24	-26.48	-7480	871	167	-4880	-494.43	145.45

4.3.3. Section for B2

B2 support class is developed especially for tunnels in intermediate rock classes with high overburden or weak rock classes at shallow depths. This type of support class was implemented at the Asarsuyu side of the Bolu Tunnels, where these types of rock conditions are prevailing. In this type of rock class, rock is heavily friable. Stand-up time of unsupported span is short. A systematic support pattern is required with rock bolts and shotcrete (see Figure 4.18). Excavation is made with drill and ballast method or mechanical excavation equipments in stages. There is a potential of deep and sudden failures if systematic support installation is delayed. Detailed geometry and properties of the section for B2 support class is given in Figure B.3.

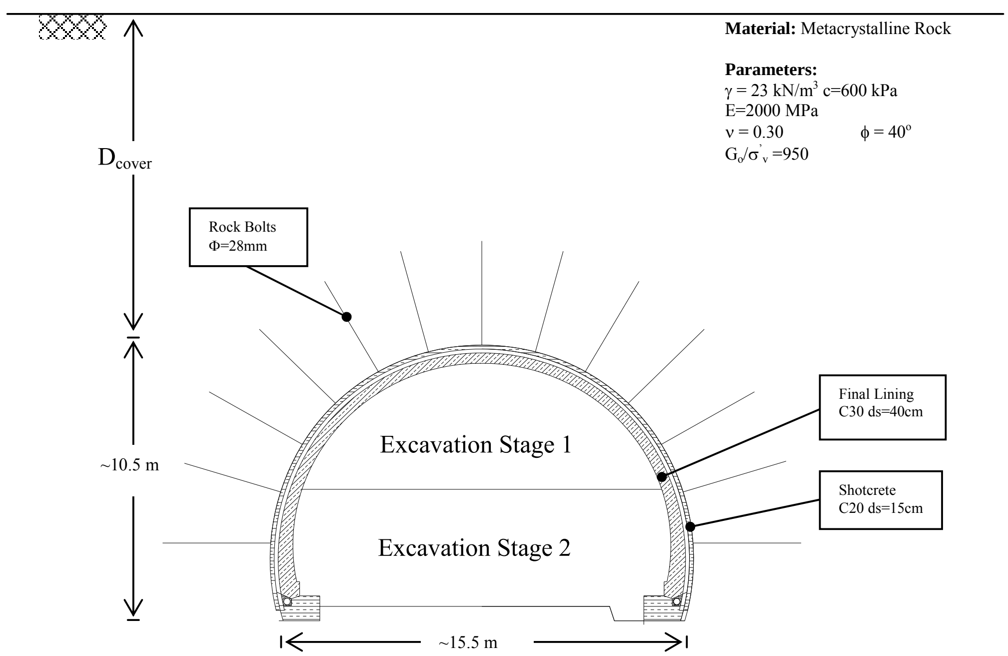

Figure 4.18 General properties of section B2

Geotechnical properties and support details of the analyzed sections are also given in Table 3.1 and Table 3.2 in addition to Figure 4.18. In this part of the chapter, section with the ordinal number 7 as shown in these tables was analyzed. According to the drawings, the average rock cover, D_{cover}, above the tunnel crown considered in the finite element analyses is 62.5 m. In section 7, rock formation is classified as metacrystalline and it is slightly to moderately weathered. Rock strength ranges from medium strong to strong having an unconfined compressive strength ranging between 25-50 MPa to 50-100 MPa. Parameters used in the dynamic analyses are also shown in Figure 4.18. A summary of details is given in Table 4.13 for the analyzed tunnel section. Shear wave velocity profile used in the dynamic analyses is presented in Figure G.6.

Table 4.13 Summary of details for the analyzed sections (B2 Rock Class)

	D_{cover}		Depth and Type of Rock Layers in the FE Model					
Analyzed sections	Depth (m)	Number of rock layers	Layer-1		Layer-2		Layer-3	
			Type	Depth (m)	Type	Depth (m)	Type	Depth (m)
Section-7	62.5	1	Metacrystalline	102.5	-	-	-	-

Finite element models constructed with the aid of PLAXIS software are presented in Appendix H. As it is also seen from the previous parts of this study, results of dynamic analyses of section B2 also correlates well with the damage data. This section of the tunnels survived from the 1999 earthquakes with no damage. Resulting internal force components of the final lining obtained from the simplified, pseudo-static and full-dynamic analyses are shown in Table 4.14. Moment interaction diagrams of the related section are presented in Figure I.6.

Table 4.14 Final results (envelope of maximum values)

	Simplified Solution, Penzien (2000), No-Slip			Pseudo-static Solution			Full Dynamic Solution		
Section No.	N(kN/m)	V(kN/m)	M(kN.m/m)	N(kN/m)	V(kN/m)	M(kN.m/m)	N(kN/m)	V(kN/m)	M(kN.m/m)
7	3114.91	-18.63	-37.25	-3930	-382.83	99.63	-3020	-489.76	65.3

4.3.4 Section for CM

Generally C support classes are developed especially for tunnels in highly pressure exerting rock masses. As Aşçıoğlu (2007) summarizes, this kind of rock masses are characterized by plastic and deep failure zones extending far into the rock masses. However, C support classes had to be modified during the construction of the tunnels due to the long lasting deformation rates. Aygar (2000) stated that the solution to this problem was to design a more rigid lining system. With this idea, CM (C modified) support classes started to be implemented at Bolu Tunnels. In his thesis, he called all the support types which were out of NATM principles as CM support classes including Option-3 and Option-4. This type support class was implemented at the Asarsuyu metasediments, Elmalık flyschoid series and clayey fault zones. A heavy systematic support pattern is required with rock bolts in a dense pattern and a thick shotcrete (see Figure 4.19). Excavation is made with smooth blasting method and conventional excavators in a top heading, bench and invert sequences. Detailed geometry and properties of the section for CM support class is given in Figure B.4.

Geotechnical properties and support details of the analyzed sections are also given in Table 3.1 and Table 3.2 in addition to Figure 4.19. In this part of the study, sections with the ordinal number 25, 26 and 27 as shown in these tables were analyzed. According to the drawings, the average rock cover, D_{cover}, above the tunnel crown which is considered in the finite element analyses are 75 m, 105 m and 120 m, respectively. In section 25 rock formation is classified as metacrystalline and it is moderately to completely weathered. Rock strength ranges from medium strong to very weak having an unconfined compressive strength ranging between 1-5 MPa to 25-50 MPa. Additionally, there are fault gouge clay and flyschoid layers at the top of metacrystalline layer. In sections 26 and 27, rock formation is classified as highly plastic brown to red and black fault gouge clay. Weathering grade of the rock masses ranges from residual soil to highly weathered. Rock strength ranges from extremely weak to weak having an unconfined compressive strength ranging between 0.25-1 MPa to 5-25 MPa. Parameters used in the dynamic analyses are also shown in Figure 4.19. A summary of details is given in Table 4.15 for the analyzed tunnel sections. Shear wave velocity profiles used in the dynamic analyses are presented in Figure G.7, Figure G.8 and Figure G.9, respectively.

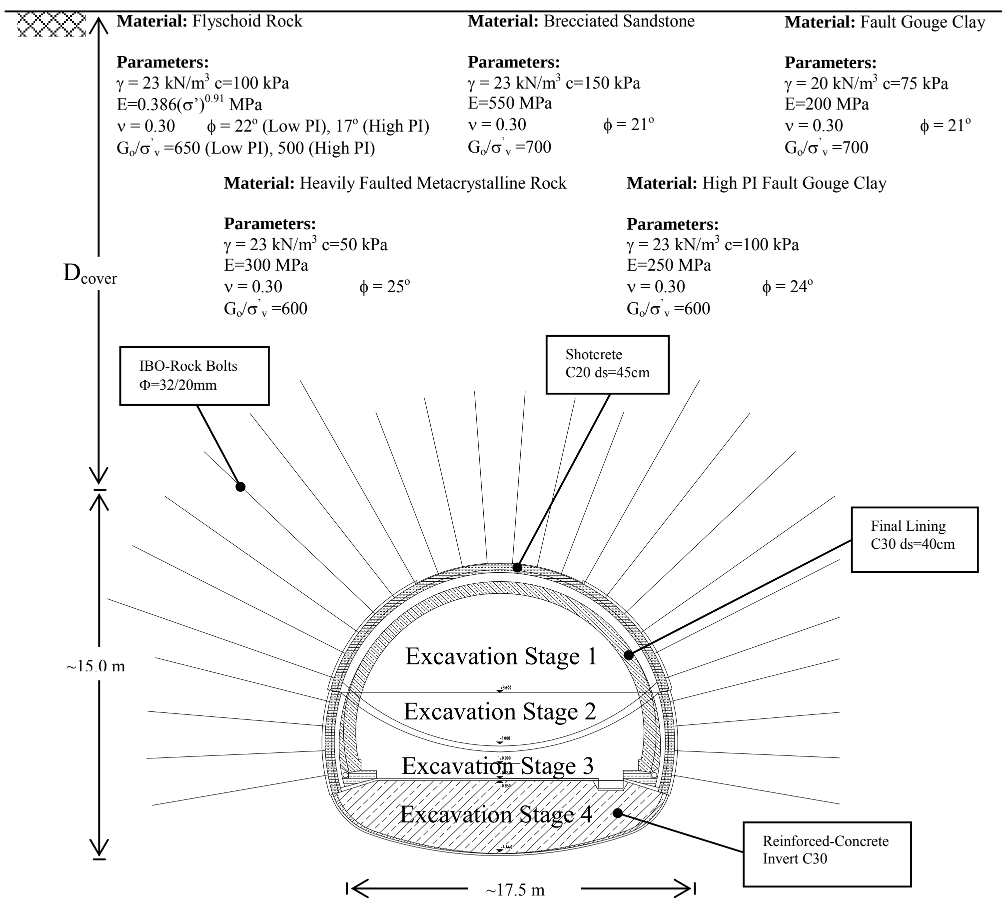

Figure 4.19 General properties of section CM

Detailed construction sequences and geotechnical properties are also found in Çakan (2000), Aşçıoğlu (2007) and Aygar (2007).

Table 4.15 Summary of details for the analyzed sections (CM Rock Class)

	D_{cover}		Depth and Type of Rock Layers in the FE Model									
Analyzed sections	Depth (m)	Number of rock layers	Layer-1		Layer-2		Layer-3		Layer-4		Layer-5	
			Type	Depth (m)	Type	Depth (m)	Type	Depth (m)	Type	Depth (m)	Type	Depth (m)
Section-25	75	3	High PI Flyschoid	15	Fault Gouge Clay	47.5	Heavily Faulted Metacrystalline Rock	58	-	-	-	-
Section-26	105	4	Fault Gouge Clay	22	Brecciated Sandstone	14	High PI Flyshoid	44	High PI Fault Gouge Clay	78	-	-
Section-27	120	5	Low PI Flyschoid	31	Fault Gouge Clay	3	Brecciated Sandstone	20	High PI Flyschoid	53	High PI Fault Gouge Clay	58

Finite element models constructed with the aid of PLAXIS software can be seen in Appendix H. As it is also seen from the previous parts of the study, results of dynamic analyses of section CM also correlates well with the damage data. These sections of the tunnels collapsed during the 1999 earthquakes. Resulting internal force components of the shotcrete lining obtained from the simplified, pseudo-static and full-dynamic analyses are shown in Table 4.16. Moment interaction diagrams of the related sections are presented in Figure I.7, Figure I.8 and Figure I.9, respectively.

Table 4.16 Final results (envelope of maximum values)

	Simplified Solution, Penzien (2000), No-Slip			Pseudo-static Solution			Full Dynamic Solution		
Section No.	*N(kN/m)*	*V(kN/m)*	*M(kN.m/m)*	*N(kN/m)*	*V(kN/m)*	*M(kN.m/m)*	*N(kN/m)*	*V(kN/m)*	*M(kN.m/m)*
25	-7924.65	-37.39	-74.79	-11020	-1750	787	-28790	-2400	861.94
26	-10757.38	-30.12	-60.25	-12540	-2280	833.8	-36500	-3350	813.79
27	-11274.05	-30.13	-60.26	-12280	-2160	670.22	-35770	-3280	1530

4.3.5. Section for Option-3

Option-3 is a construction technique developed particularly for the excavation of flyschoid sequences and clay gouge zones not longer than 20 m. As Çakan (2000) stated, this type of support class was implemented at the Elmalık side of the Bolu Tunnels, where long term creep deformation was expected, but no sudden deformation close to the face was predicted. Rock, where this type of support was implemented, is unstable and shows plastic behavior. Excavation is performed with conventional excavators and back-hoes in top heading, bench and invert sequence using shotcrete and rock bolts. Initial support system involves advancing top heading face with a shotcrete thickness of 40 cm. There is an additional temporary shotcrete invert of 50 cm to stabilize the fast ground deformations. The lengths of rock bolts used were 9.0 m and 12.0 m. Following the ring closure with a deep monolithic concrete invert, initial support system was fortified by 60 cm thick cast in-situ C40 concrete intermediary (Bernold) lining. Ductility of the lining was increased with addition of steel fibers. Detailed geometry and properties of the section for Option-3 is given in Figure B.5.

Geotechnical properties and support details of the analyzed sections are also given in Table 3.1 and Table 3.2 in addition to Figure 4.20. In this part of the chapter, sections with the ordinal number 29, 30 and 31 as shown in these tables were analyzed. According to the drawings, the average rock cover, D_{cover}, above the tunnel crown which is considered in the finite element analyses are 170.0 m, 147.0 m and 97.0 m, respectively. In Section-29, rock formation is classified as metasediment underlain by fault gouge clay and it is moderately to completely weathered. Rock strength can be ranged from extremely weak to very weak having an unconfined compressive strength ranging between 0.25-1 MPa to 1-5 MPa. Section-30 is composed of 5 different rock types and Section-31 is composed of 3 different rock types as shown in Table 4.17. Tunnel was excavated through highly faulted rock series. Rock strength ranges from very weak to extremely weak having an unconfined compressive strength ranging between 0.25-1 MPa to 1-5 MPa. Parameters used in the dynamic analyses are also shown in Figure 4.17. A summary of details is given in Table 4.17 for the analyzed tunnel sections. Shear wave velocity profiles used in the dynamic analyses are presented in Figure G.10, Figure G.11 and Figure G.12, respectively.

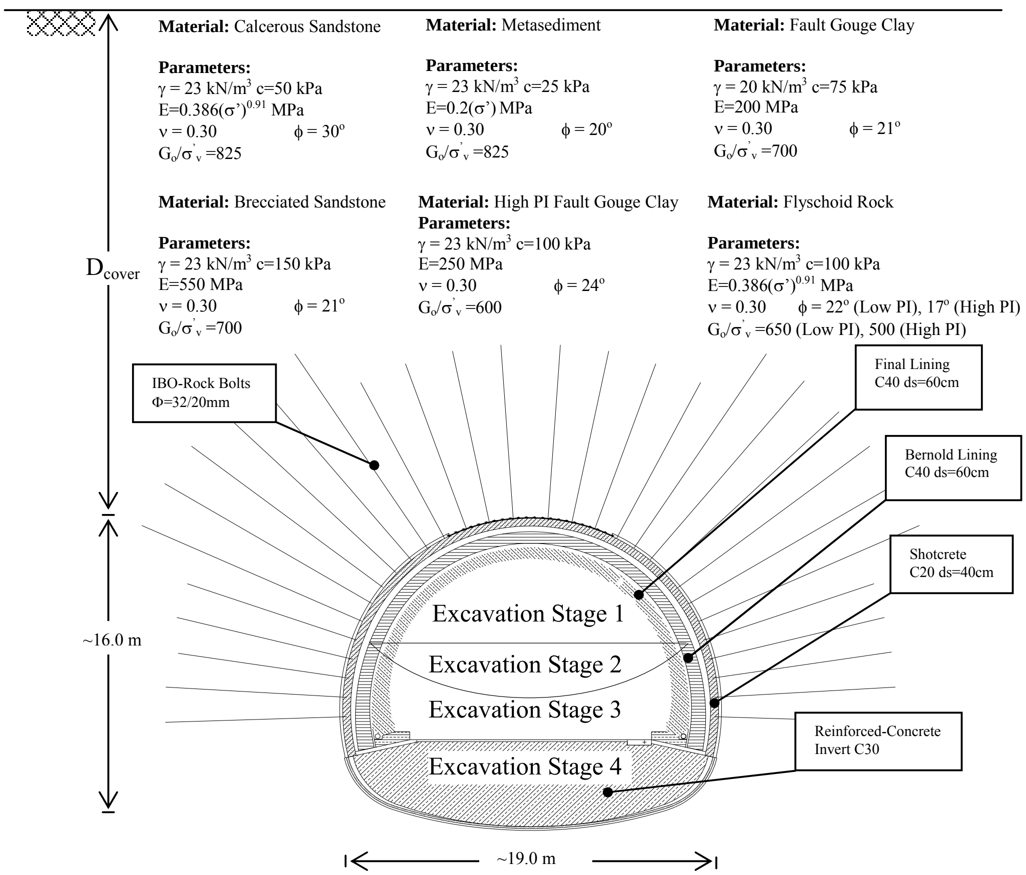

Figure 4.20 General properties of Option-3

Detailed construction sequences and geotechnical properties are also found in Çakan (2000), Aşçıoğlu (2007) and Aygar (2007).

Table 4.17 Summary of details for the analyzed sections (Option-3 Rock Class)

	D_{cover}		Depth and Type of Rock Layers in the FE Model									
Analyzed sections	Depth (m)	Number of rock layers	Layer-1		Layer-2		Layer-3		Layer-4		Layer-5	
			Type	Depth (m)	Type	Depth (m)	Type	Depth (m)	Type	Depth (m)	Type	Depth (m)
Section-29	170	3	Calcerous Sandstone	42	Metasediment	141	Fault Gouge Clay	33	-	-	-	-
Section-30	147	5	Low PI Flyschoid	59	Fault Gouge Clay	5	Brecciated Sandstone	19	High PI Flyschoid	52	High PI Fault Gouge Clay	58
Section-31	97	3	Fault Gouge Clay	34	High PI Flyschoid	50	High PI Fault Gouge Clay	59	-	-	-	-

Finite element models constructed with the aid of PLAXIS software can be seen in Appendix H. As it is also seen from the previous parts of the study, results of dynamic analyses of Option-3 also correlates well with the damage data. These sections of the tunnels collapsed during the 1999 earthquakes. Resulting internal force components of the Bernold lining obtained from the simplified, pseudo-static and full-dynamic analyses are shown in Table 4.18. Moment interaction diagrams of the related sections are presented in Figure I.10, Figure I.11 and Figure I.12, respectively.

Table 4.18 Final results (envelope of maximum values)

	Simplified Solution, Penzien (2000), No-Slip			Pseudo-static Solution			Full Dynamic Solution		
Section No.	*N(kN/m)*	*V(kN/m)*	*M(kN.m/m)*	*N(kN/m)*	*V(kN/m)*	*M(kN.m/m)*	*N(kN/m)*	*V(kN/m)*	*M(kN.m/m)*
29	-13730.21	-47.71	-95.42	-12590	-3160	1410	-43240	4720	1570
30	-14994.94	-62.25	124.49	-11410	-2750	1360	-28480	5270	2570
31	-12119.8	-81.48	-162.96	-13060	-2340	1820	-23450	2640	2280

4.3.6. Section for Option-4

Option-4 is the only solution for the unfavorable ground conditions. It is a construction technique developed particularly for the excavation of clay gouge zones longer than 20 m which was a case at the Elmalık side of the Bolu Tunnels. As Çakan (2000) stated, the main philosophy is the precreation of a stiff abutment for the top heading prior to main tunnel advance. For this reason, two 5 m diameter pilot tunnels were excavated at bench level. Then these bench pilot tunnels were backfilled with C30 reinforced concrete. Excavation was performed with conventional excavators and back-hoes in top heading, bench and invert sequence. Due to the rather stiff support system, rock bolts were not installed. Detailed geometry and properties of the section for Option-4 is given in Figure B.6.

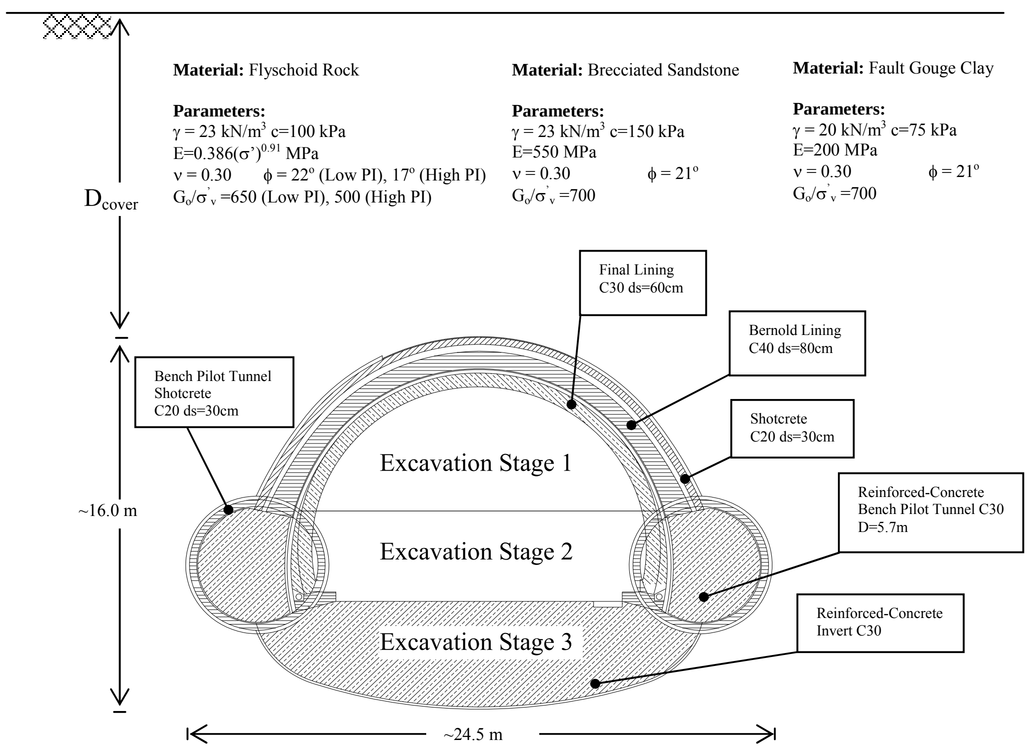

Figure 4.21 General properties of Option-4

Geotechnical properties and support details of the analyzed sections are also given in Table 3.1 and Table 3.2 in addition to Figure 4.21. In this part of the chapter, section with the ordinal number 32 as shown in these tables is analyzed. According to the drawings, the average rock cover, D_{cover}, above the tunnel crown which is considered in the finite element analyses is 156.5 m. In Section-32, rock formation is classified as flyschoid and it is moderately to completely weathered. Rock strength ranges from extremely weak to very weak having an unconfined compressive strength ranging between 0.25-1 MPa to 1-5 MPa. Parameters used in the dynamic analyses are also shown in Figure 4.21. A summary of details is given in Table 4.19 for the analyzed tunnel sections. Shear wave velocity profile used in the dynamic analyses is presented in Figure G.13.

Table 4.19 Summary of details for the analyzed section (Option-4 Rock Class)

	D_{cover}		Depth and Type of Rock Layers in the FE Model							
Analyzed sections	Depth (m)	number of rock layers	Layer-1		Layer-2		Layer-3		Layer-4	
			Type	Depth (m)	Type	Depth (m)	Type	Depth (m)	Type	Depth (m)
Section-32	156.5	4	Low PI Flyschoid	78	Fault Gouge Clay	6	Brecciated Sandstone	35	High PI Flyschoid	83

Detailed construction sequences and geotechnical properties are also found in Çakan (2000), Aşçıoğlu (2007) and Aygar (2007).

Finite element models constructed with the aid of PLAXIS software can be seen in Appendix H. As it is also seen from the previous parts of this study, results of dynamic analyses of Option-4 also correlates well with the damage data. These sections of the tunnels collapsed during the 1999 earthquakes. Resulting internal force components of the Bernold lining obtained from the simplified, pseudo-static and full-dynamic analyses are shown in Table 4.20. Moment interaction diagrams of the related section are presented in Figure I.13.

Table 4.20 Final results (envelope of maximum values)

	Simplified Solution, Penzien (2000), No-Slip			Pseudo-static Solution			Full Dynamic Solution		
Section No.	*N(kN/m)*	*V(kN/m)*	*M(kN.m/m)*	*N(kN/m)*	*V(kN/m)*	*M(kN.m/m)*	*N(kN/m)*	*V(kN/m)*	*M(kN.m/m)*
32	-15439	-125.13	-250.26	-16900	-2330	4300	-30610	5850	5780

4.3.7. Section for Pilot Tunnels

Pilot tunnel was driven due to the unfavorable ground conditions for ground investigation purposes. This tunnel was excavated in full face within the left tube of Bolu Tunnels. By the help of this pilot tunnel sufficient geotechnical data was gained for the excavation of the problematic sections of the Bolu Tunnels. Pilot Tunnel has a 4.6 m inner diameter. The supporting element is shotcrete.

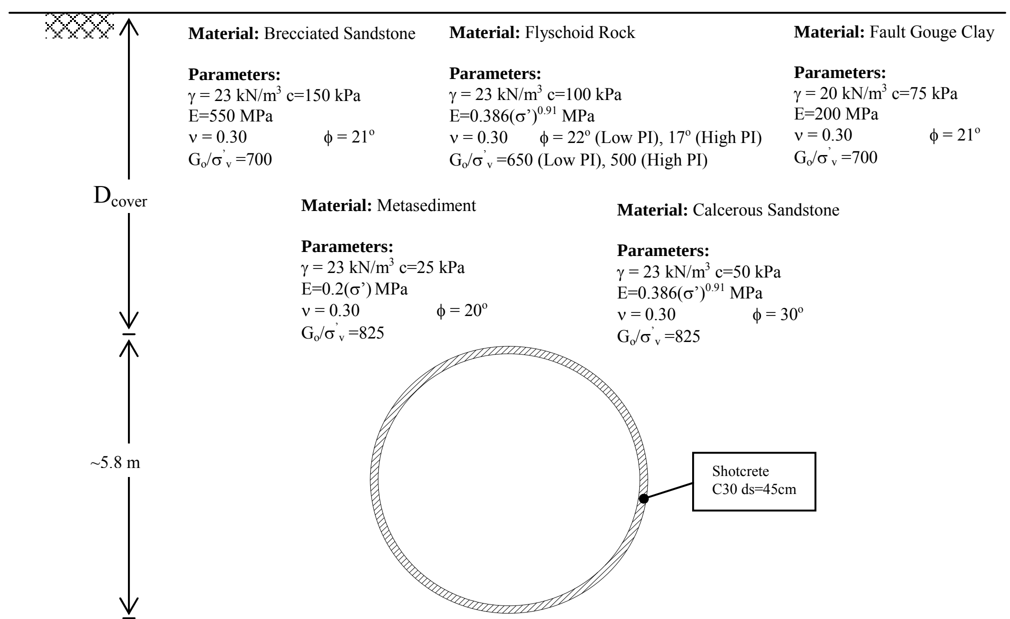

Figure 4.22 General properties of Pilot Tunnel

Geotechnical properties and support details of the analyzed sections are also given in Table 3.1 and Table 3.2 in addition to Figure 4.22. In this part of the chapter, section with the ordinal number 33 and 34 as shown in these tables are analyzed. According to the drawings, the average rock cover, D_{cover}, above the tunnel crown which is considered in the finite element analyses are 147 m and 163 m, respectively. In Section-33, rock formation is classified as high PI fault gouge clay and it is moderately to completely weathered. In Section-34, rock formation is classified as flyschoid and it is moderately to completely weathered. For both rock formations, rock strength ranges from extremely weak to very weak having an unconfined compressive strength ranging between 0.25-1 MPa to 1-5 MPa. Parameters used in the dynamic analyses are also shown in Figure 4.22. A summary of details is given in Table 4.22 for the analyzed tunnel sections. Shear wave velocity profiles used in the dynamic analyses are presented in Figure G.14 and Figure G.15, respectively.

Table 4.21 Summary of details for the analyzed section (Pilot Tunnel)

	D_{cover}		Depth and Type of Rock Layers in the FE Model							
Analyzed sections	Depth (m)	number of rock layers	Layer-1		Layer-2		Layer-3		Layer-4	
			Type	Depth (m)	Type	Depth (m)	Type	Depth (m)	Type	Depth (m)
Section-33	147	3	Calcerous Sandstone	63	Metasediment	56	Fault Gouge Clay	64	-	-
Section-34	163	4	Low PI Flyschoid	78	Fault Gouge Clay	6	Brecciated Sandstone	35	High PI Flyschoid	83

Finite element models constructed with the aid of PLAXIS software can be seen in Appendix H. As it is also seen from the previous parts of the study, results of dynamic analyses of pilot tunnels also correlates well with the damage data. These sections of the tunnels were heavily damaged and collapsed during the 1999 earthquakes. Resulting internal force components of the shotcrete lining obtained from the simplified, pseudo-static and full-dynamic analyses are shown in Table 4.22. Moment interaction diagrams of the related sections are presented in Figure I.14 and Figure I.15, respectively.

Table 4.22 Final results (envelope of maximum values)

	Simplified Solution, Penzien (2000), No-Slip			Pseudo-static Solution			Full Dynamic Solution		
Section No.	*N(kN/m)*	*V(kN/m)*	*M(kN.m/m)*	*N(kN/m)*	*V(kN/m)*	*M(kN.m/m)*	*N(kN/m)*	*V(kN/m)*	*M(kN.m/m)*
33	-6377.45	-57.38	-114.75	-10370	-568.09	455.9	-15170	2060	2500
34	-7630.86	-79.15	-158.29	-10580	-447.37	416.27	-13130	1190	1180

4.4. Seismic Response Analysis Results for Vulnerability Assessment

To make vulnerability assessment and to construct the respective fragility curves pseudo-static dynamic analyses of the selected sections were repeated in this part for the preselected earthquakes as explained at the beginning of this chapter. Tunnel sections used in this vulnerability assessment were selected amongst the collapsed and heavily damaged ones. Totally 5 sections were prepared and these were analyzed with 4 different earthquakes each scaled to peak ground accelerations of 0.2g, 0.4g, 0.6g, 0.8g and 1.0g, respectively. Hence, each tunnel section was analyzed with 20 time histories and a total of 100 pseudo-static dynamic analyses were performed. For each time history, free-field displacements were calculated, and then these horizontal displacements are applied to the calibrated finite-element models.

Displacements applied to the finite element models and calculated damage indexes for the selected 5 sections are presented in Appendix J.

CHAPTER 5

ASSESSMENT OF FRAGILITY CURVES FOR TUNNELS

In this part, analytical fragility curves are developed based on the approach of Argyroudis et al. (2007). In the fragility formulations, lognormal distribution is assumed as recommended by ALA (2001). Fragility curves are generated using the expression given below:

$$F(S_a) = \Phi\left[\frac{1}{\beta}\ln(\frac{S_a}{A_i})\right] \tag{5.1}$$

where, F is the cumulative distribution function, Φ is the standard cumulative distribution function showing the probability of i^{th} damage state to occur for a given peak ground acceleration of S_a, β is the logarithmic standard deviation of S_a and A_i is the median spectral acceleration necessary to cause the i^{th} damage state.

For the construction of fragility curves, the damage index ranges presented in Table 5.1 corresponding to the defined damage states proposed by Argyroudis et al. (2005) based on the past experience of observed damage in tunnels and the engineering judgment were studied as a reference together with his methodology. In this study, as previously stated, quantification of the damage states was based on a damage index (DI) that is defined as the ratio of the developing moment as a result of the earthquake loading (M_{eq}) to the moment resistance of the tunnel lining (M_{rd}). The ranges of damage index which were used for the construction of fragility curves in this study are shown in Table 5.2.

Table 5.1 Relationship between damage index ($DI=M_{eq}/M_{rd}$) and the damage state (after Argyroudis et al., 2005)

Damage Index-DI	**Damage State**
$DI \leq 0.70$	No Damage
$0.70 < DI \leq 1.00$	Minor Damage
$1.00 < DI \leq 1.30$	Moderate Damage
$1.30 < DI \leq 1.80$	Extensive Damage

In the literature, damage is defined based on four or five states as similar to Argyroudis et al. (2005) in Table 5.1, which are identified as from no damage to failure damage state. Due to the difficulty involved in quantification between the minor and moderate damage states for tunnels, damage was categorized into 3 states in this study. New damage indexes as a result of this study with the modification of Argyroudis et al. (2005) are presented in Table 5.2.

Table 5.2 Proposed ranges of damage index and the corresponding damage states

Damage Index-DI	**Damage State**
$DI \leq 0.65$	No Damage
$0.65 < DI \leq 1.00$	Minor and Moderate Damage
$1.00 < DI \leq 1.50$	Extensive Damage and Failure

The upper limit damage index value of 0.65 corresponding to no damage state was evaluated through the seismic response analyses of the undamaged sections as summarized in Table 3.1. The evaluation of the damage index value is based on the moment-interaction diagrams which were calculated from the pseudo-static seismic response analyses of the tunnel sections. Damage index value of 0.65 can also be checked from the moment interaction diagrams presented in Appendix I (see Figure I.1 through Figure I.6).

The lower limit damage index value of 1.00 corresponding to extensive damage and failure was evaluated through the seismic response analyses of heavily damaged and failed sections as summarized in Table 3.1. The value is based on the moment-interaction diagrams which were developed utilizing the outcome of the pseudo-static seismic response analyses of the tunnel sections. Damage index value of 1.00 can also be checked from the moment interaction diagrams presented in Appendix I (see Figure I.7 through Figure I.13).

The upper limit damage index value of 1.50 corresponding to extensive damage and failure was evaluated graphically by the methodology proposed by Argyroudis et al. (2007). Following this methodology, seismic response was calculated at the tunnel sections by the pseudo-static method for a set of 100 time histories using finite element models as explained in detail in Chapter 4 of this study. The finite element models and the calculated pseudo-static deformations are presented in Appendices H and J, respectively. Finally, the damage indexes are calculated in Appendix J and plotted in Figure 5.1 for calculating the median damage spectral acceleration for extensive damage and failure.

Three curves were fitted to the data presented in Figure 5.1 for comparison. To remain on the safe side exponential fit was selected amongst, which yields higher damage index values. An upper value of damage index for extensive damage and failure was needed to quantify the median spectral acceleration for this damage state. The upper value was selected as that corresponding to the possible maximum value of peak ground acceleration on rock (PGA_{Rock}). Although quite uncommon, values in excess of 1.0g are reported in literature for PGA_{Rock}. As an upper limit for the PGA of graph in Figure 5.1, 1.2g was selected based on Strasser and Bommer (2009). When the best fit curves in Figure 5.1 are examined, it is observed that the damage index values corresponding to 1.2g exceed 1.5 in all of the curves. Therefore, 1.5 was selected for an upper boundary.

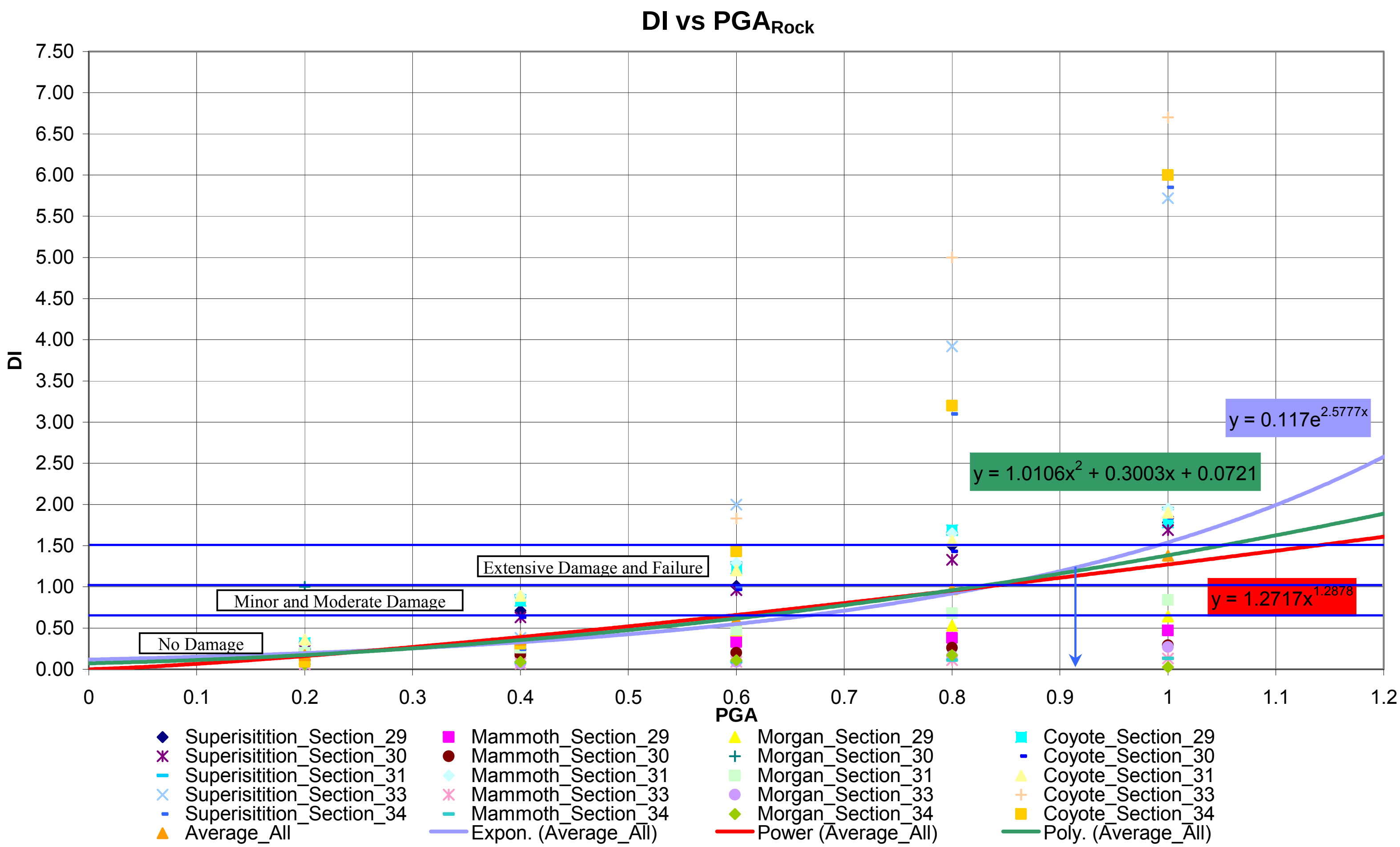

Figure 5.1 Damage index (DI) versus peak ground acceleration on rock (PGA_{Rock})

As it is observed in Figure 5.1, median spectral acceleration for extensive damage and failure was determined as 0.91g. With this value in hand, corresponding fragility curve is finally generated in Figure 5.2. Lognormal standard deviation value β, was taken as 0.5 as recommended by ALA (2000) in plotting of the curve.

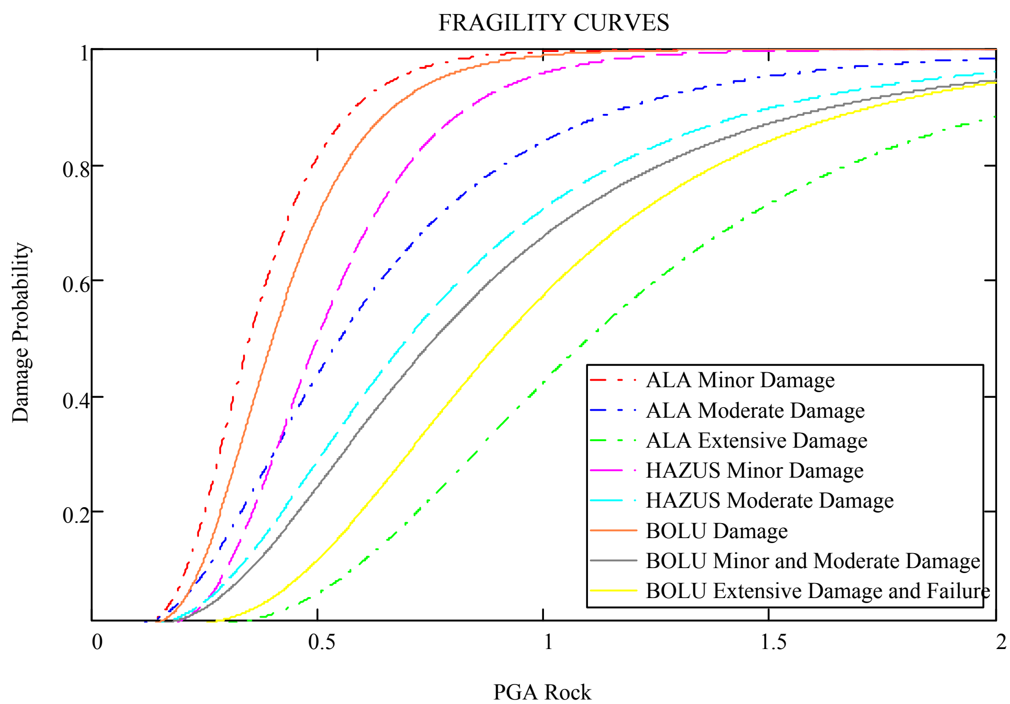

Figure 5.2 Comparison of fragility curves

To compare with the fragility curves which existing in literature, fragility curves for no damage and minor and moderate damage states can also be generated with the derived data. The fragility curve corresponding to the no damage state is the damage curve. From Figure 5.1, median spectral acceleration for no damage and minor and moderate damage states can be determined as 0.40g and 0.76g, respectively. Lognormal standard deviation values β, were taken as 0.4 and 0.6 as recommended by ALA (2000). With these values, corresponding fragility curves are generated in Figure 5.2 by utilizing Equation 5.1.

CHAPTER 6

RESULTS AND DISCUSSION

While evaluating the bedrock motions for the stations, a wide range of PGA values were calculated especially for the Bolu station. This can be attributed to the broad variability of the ground properties. Additionally, selection of modulus and damping curves used in the analyses of site response affects the results. Using the PGA values in that wide range, representative realistic bedrock accelerograms can be derived based on comparisons with the inflicted damage recorded in Bolu Tunnels. This approach was used for the analyzed sections of Bolu Tunnels in Chapter 4.

Due to the process of deconvolution, shown schematically in Figure 4.10, at the depth of tunnels peak accelerations in Bolu and Düzce earthquake records were reduced with respect to PGA. This observation is in compliance with the findings of the study by Shimizu et al. (1996), which consisted of monitoring distant earthquake strong motion vibrations in the underground test facility at the Kamaishi Mine, Japan. They concluded that, the accelerations at 650 m and 150 m below the ground surface were in the range of 50-25% and 100-50% of the surface value, respectively.

Based on the results attained in the dynamic analyses, it can be said that the methods performed better for shallow tunnels with respect to deep tunnels. Compared to the pseudo-static and full-dynamic methods, the predictive capability of the analytical (simplified) method is low due to limitations relating to the tunnel geometry and excavation phases involved in the construction process. However, with the approach used in this study, the predictive capability of the analytical method under dynamic excitation was enhanced particularly for the case of axial forces in the lining. For this purpose, the average dynamic modulus of elasticity $(E_{dyn})_{ave}$ was utilized in place of the average static modulus of elasticity of the medium $(E_{med})_{ave}$ into which the tunnel is built, as proposed by Penzien and Wu (1998). In this study, $(E_{dyn})_{ave}$ is calculated based on the average shear wave velocity profile of the geotechnical model. A typical calculation spread-sheet is shown in Appendix A. On the other hand, enhancement in the prediction capability of the analytical method for the shear forces and moments developing in the liner was not as much that for the axial forces.

The shear forces and moments estimated by the simplified solution appear to be relatively smaller than those resulting from the pseudo-static and full-dynamic solutions. This difference can be attributed to the assumption that the internal forces caused only by the ovaling deformations, which means that the variations in the earth load triggered due to seismic activity is not taken into account in the analytical approach. If the ground is considered to be massless in the pseudo-static and full-dynamic solutions, results attained using simplified approach can be validated in terms of shear forces and moments as well, as it was also shown by Hashash (2005). For validating the dynamic sectional resultants calculated by the simplified method, Penzien (2000) recommends to add these resultants with those due to geostatic stresses which can be calculated roughly by the methods described by AFTES (1988). However, with the formulations used in this study for analytical solution, superposition of static and dynamic axial forces is not required. On the other hand, the results for shear forces and moments calculated with this methodology should be studied in greater detail.

The pseudo-static and full-dynamic solution results attained in this study appear to be closer to each other for each modeled section. The pseudo-static internal force resultants agree well with the full-dynamic solutions in general (see Figure I.1 through Figure I.6). This is a justified result for deep tunnels which was not reported earlier in the literature. Results agreed well with the observed damage levels in general. However, the predictive capability of the pseudo-static approach was observed to be limited for particular cases with reference to the full-dynamic method, especially for the sections with increasingly difficult ground conditions.

When moment interactions diagrams are compared for the extensively damaged and collapsed sections, collapse cases are observed to be clearly identified by the full-dynamic solutions as presented in Appendix I (see Figure I.7 through Figure I.13).

The run time, storage space and the effort required for the model preparation for a typical full-dynamic solution is rather high when compared to those for pseudo-static solution. Therefore, for ordinary projects, pseudo-static solution can be preferred. As a recommendation, however, both pseudo-static and full-dynamic solutions should be carried out and the outcomes should be compared as a cross-check.

Fragility curves provide a useful tool in assessing the seismic vulnerability for tunnel structures. To construct the fragility curves in the case of tunnels, the damage states are quantified based on a damage index (DI) which is by and large defined as the ratio of the developing moment as a result of earthquake loading (M_{eq}) to the moment resistance of the tunnel lining (M_{rd}). As it can be recognized from an overall evaluation of the dynamic analyses results presented in this study, using a definition of damage index based on the ratio of moments appears to be more reliable when compared to those of the normal and shear forces while developing fragility curves. Accordingly, the quantification of damage was based on the moment ratios by utilizing the pseudo-static dynamic analysis method as proposed by Argyroudis et al. (2007).

In the literature, damage is generally classified into four states, which are identified as from no damage to failure state. Due to the difficulty involved in quantification between the minor and moderate damage states for tunnels, three damage states were utilized to quantify the damage in this study. Hence, after moderate damage state tunnel structures go into extensive and failure damage state suddenly. The damage margins thus identified are presented in Table 5.2.

The limits presented in Table 5.2 are obtained without considering any safety factors. Safety factors, however, are incorporated in design and they are subject to variations depending on the country or region. Hence, when utilizing the vulnerability concept in design practice, the damage indexes in Table 5.2 should comprise the appropriate safety factors.

The fragility curves derived in this study are presented in Figure 5.2. The curves were developed by utilizing five different sections of the tunnels damaged during Düzce earthquake. Besides, the fragility curves for damage and minor/moderate damage states developed from the same sections are also presented to make a comparison. These curves can be improved by incorporation of additional sections, especially the undamaged sections of the tunnels. When compared with the empirical fragility curves of HAZUS (FEMA, 2003) and ALA (2001), the fragility curves developed in this study generally provide lower bounds and hence appear to be conservative with small margins, with the exception of moderate damage state when compared with ALA (2001). Extensive damage fragility curve provided by this study gives higher damage probability than ALA (2001), whereas the corresponding curve is not available in HAZUS (FEMA, 2003).

During 1999 Düzce earthquake, peak ground accelerations on rock at the site of Bolu Tunnels were calculated to be around 0.75g. Entering this value in Figure 5.2, damage probability is seen to exceed 40%, which is a rather high value. If such curves are incorporated with the site specific seismic hazard studies, catastrophic failures can be prevented. On the other hand, the design PGA_{rock} value for the Bolu Tunnels Project site was originally presumed as 0.40g in accordance with the requirements of Earthquake Code of Turkey (TEC). Entering this value in Figure 5.2, the corresponding damage probability remains below 10% which is acceptable. The PGA_{rock} was, however, 0.75g at the site during the Düzce earthquake.

Proposed fragility curves are to be used together with the corresponding damage indexes, because Figure 5.2 contains information neither about the structural condition of the tunnel and nor the geotechnical circumstances at the site. Hence Figure 5.2 should be used together with Table 5.2 to decide on the probability of the corresponding damage state to occur due to a seismic activity. To further clarify the case, the situation summarized in the previous paragraph can be taken as an example. With the PGA_{rock} value of 0.75g, there is a probability of 94% for damage, 49% for minor and moderate damage and 35% for extensive damage and failure. These probabilities are quite high from damage point of view, so the support system and geotechnical circumstances at the site should be checked. The site under consideration may consist of competent rock or the tunnel excavation might be provided with heavy support, either of which results in a low damage index. On the contrary, if there exist unfavorable geotechnical conditions at the site or the tunnel support is relatively weak, a higher damage index results and precautions must be taken.

CHAPTER 7

SUMMARY, CONCLUSIONS AND RECOMMENDATIONS

7.1. Summary

The analytical, pseudo-static and full-dynamic analysis methods are applied to Bolu Tunnels as a case study, which were under construction during the November 12, 1999 Düzce earthquake and experienced diverse levels of damage including collapse. The fragility curves are developed using the available damage data at a number of sections of the tunnels.

The available literature covering the dynamic analyses of tunnels was reviewed in detail. Besides, all geotechnical and structural data belonging to Bolu Tunnels was searched and collected both from literature and detailed project documents. Sifting through the collected data regarding the Bolu Tunnels required investigations in diverse fields including seismology and geology as well as geotechnical, structural and earthquake engineering.

7.2. Conclusions

Seismically induced damage levels at particular sections of the tunnels were back-analyzed with the three approaches. As it is reported in literature, the results of the all three methods yield more or less consistent results in the case of shallow tunnels. For deep tunnels, however, the results of the analytical method, particularly in terms of shear forces and moments, deviated from those of the other two as observed in this study. This was attributed to the limitations of the analytical method, in the case of modeling complex geometries and excavation phases involved in the construction process.

The results obtained from the pseudo-static and full-dynamic analyses methods were in well conformance with various damage levels observed at particular sections of the tunnels. However, the predictive capability of the pseudo-static approach was observed to be limited in certain cases with particular reference to the full-dynamic solution. This was further apparent for the sections with more difficult ground conditions. Accordingly, especially the cases of collapse were more clearly identified with the full-dynamic analysis.

Although the full-dynamic solution is superior in a number of ways to the other two methods, for ordinary projects which consist of shallow tunnels in competent ground conditions and preferably circular sectional geometries, analytical and pseudo-static solutions can be preferred due to the much lower run time and storage space requirements and the effort involved for the model preparation. On the other hand, that analytical solution appears to have some shortcomings in the case of deep tunnels and complex construction geometries. As a recommendation, however, both pseudo-static and full-dynamic solutions should be carried out and the outcomes should be compared as a cross-check.

Fragility curves provide a useful tool in assessing the seismic vulnerability for tunnel structures. Novel fragility curves were presented as a result of this study. Three damage states were utilized to quantify the damage, which are identified as from no damage to failure damage state.

The fragility curves were developed particularly for extensive damage and failure damage states by utilizing the five sections damaged during the Düzce earthquake. The fragility curves for damage and minor/moderate damage states developed from the same sections are also presented for the purpose of comparison.

When compared with the empirical fragility curves provided by HAZUS (FEMA, 2003) and ALA (2001), the fragility curves developed in this study generally yield lower bounds and seem to be conservative or approximately equal with respect to those available in literature due to the actual damage data utilized, except for the moderate damage state when compared with ALA (2001). Extensive damage fragility curve provided by this study gives higher damage probability than ALA (2001), whereas the corresponding curve is not available in HAZUS (FEMA, 2003).

If such curves are used with site specific seismic hazard studies, catastrophic accidents could be prevented. On the other hand, the presumed design PGA_{rock} value for the Bolu Tunnels Project site was 0.40g according to TEC. Entering this value in Figure 5.2, the corresponding damage probability is lower than 10%, which is reasonable. However, the Düzce earthquake struck the site with 0.75g.

7.3. Recommendations for Future Studies and Limitations

The analyses of some of the sections of Bolu Tunnels could not be carried out within the framework of this study due to time limitations. Analyses of the sections with 1999 Kocaeli earthquake are also missing due to the same reason. Those can be completed to improve the analytical fragility curves for damage and moderate damage states.

Additional observed seismic damage data of tunnels from the literature can be combined with this study for further improvement of the fragility curves and damage indexes. Example damage inventory is presented in Appendix K from ALA (2001) which was collected from earthquakes in Japan.

Bolu and Düzce stations were under forward directivity effect of fault rupture during the Kocaeli earthquake, whereas during the November 12 Düzce earthquake only the Bolu station experienced such effect. This was evidenced by the short duration and high intensity of the strong motion recorded at the Bolu Station compared to that of the Düzce record (Durukal, 2002). This effect, which can be decisive on the response, can be investigated further in the future studies.

Although, being a quite user-friendly software, PLAXIS has some limitations. One of these is that the control of the user over the mesh generation is limited and the mesh is generated automatically according to the predefined mesh fineness.

Furthermore, the upper limit of the elements that can be utilized in a model is 5000. Finally, the software does not provide a time-history of the sectional forces and moments but reports only the envelope of maximum values. More sophisticated software, free from such drawbacks is recommended to be used in future studies.

REFERENCES

Abrahamson, N., and Silva, W., 2008. Summary of the Abrahamson & Silva NGA Ground-Motion Relations. Earthquake Spectra, Vol.24, No.1, pp. 67-97.

AFTES Temporary Supports and Permanent Lining, Working Group No.7, 1988. Considerations on the usual methods of tunnel lining design. Tunnel et Ouvrages Souterrains, No.90.

Akyüz, H.S., Hartleb, R., Barka, A., Altunel, E., Sunal, G., Meyer, B., and Armijo, R, 2002. Surface Rupture and Slip Distribution of the 12 November 1999 Düzce Earthquake (M 7.1), North Anatolian Fault, Bolu, Turkey. Bulletin of the Seismological Society of America, Vol. 92, No. 1, pp. 61-66.

American Lifelines Alliance (ALA), 2001. Seismic fragility formulations for water tunnels.

Applied Technology Council, 1985. ATC-13: Earthquake damage evaluation data for California, Redwood City, California.

Argyroudis, S., Argyriou, N., Chatzis, I., and Pitilakis, K., 2005. Seismic fragility curves of shallow tunnels. Proceedings of the 11th International Conference on Computer Methods and Advances in Geomechanics (IACMAG).

Argyroudis, S., Pitilakis, K., Boussoulas, N., and Nakou, F., 2007. Vulnerability assessment of shallow metro tunnels in Greece. Proceedings of the Fourth International Conference on Earthquake Geotechnical Engineering.

Astaldi SpA, 1993-2006. Anatolian Motorway Gümüşova-Gerede Section – Stretch 2 Bolu Tunnel Bypass Drawings Album.

Astaldi SpA., 2000. Strecth-2 Bolu Tunnel – Seismic Design, Seismic Screening. Report No: 45.110/R/2251.

Aşçıoğlu, G., 2007. Analysis of Support Design Practice at Elmalık Portals of Bolu Tunnel. M.Sc. Thesis, Middle East Technical University, Department of Mining Engineering, Ankara, Turkey.

Aversa, S., Maiorano, R.M.S, and Tamagnini, C., 2007. Influence of damping and soil model on the computed seismic response of flexible retaining structures. Geotechnical Aspects of EC8, Madrid, 25 September 2007, BOLOGNA, Patron Editore.

Aygar, E.B., 2000. A Critical Approach to the New Austrian Tunnelling Method in Bolu Tunnels (in Turkish). M.Sc. Thesis, Hacettepe University, Department of Mining Engineering, Ankara, Turkey.

Aygar, E.B., 2007. Investigation of the Bolu Tunnel Stability by Means of Static and Dynamic Analyses (in Turkish). Ph.D. Thesis, Hacettepe University, Department of Mining Engineering, Ankara, Turkey.

Bardet, J.P., Ichii, K., and Lin, C.H., 2000. EERA: A computer program for Equivalent-linear Earthquake site Response Analyses of Layered Soil Deposits. University of Southern California, Department of Civil Engineering.

Barka, A., Akyüz, H.S., Altunel, E., Sunal, G., Çakır, Z., Dikbaş, A., Yerli, B., Armijo, R., Meyer, B., de Chabalier, J.B., Rockwell, T., Dolan, J.R., Hartleb, R., Dawson, T., Christoffersen, S., Tucker, A., Fumal, T., Langridge, R., Stenner, H., Lettis, W., Bachhuber, J., and Page, W., 2002. The Surface Rupture and Slip Distribution of the 17 August 1999 İzmit Earthquake (M 7.4), North Anatolian Fault. Bulletin of the Seismological Society of America, Vol. 92, No. 1, pp. 43-60.

Başokur, A.T., 2005. Yapı-Yeri İncelemelerinde Makaslama Dalgası Hız Kesitinin ReMi Yöntemi ile Saptanması. Proceedings of the Earthquake Symposium, March 23-25, 2005, Kocaeli University, Kocaeli, Turkey.

Bentz, E., 2001. Response-2000: A computer program for 2D sectional analysis of beams and columns. University of Toronto, Department of Civil Engineering, Toronto, Ontario Canada.

Boore, D. and Joyner, W., 1997. Site amplifications for generic rock sites. Bulletin of the Seismological Society of America, Vol. 87, No. 2, pp. 327-341.

CEN, 2004. Eurocode 8. Design of Structures for Earthquake Resistance-Part 1: general rules, seismic actions and rules for buildings, EN 1998-1:2004. Comite Europeen de Normalisation, Brussels.

Çakan, A.G., 2000. Analysis of Tunnel Advance in Soft Ground Using Finite Element Method: A Case Study on Bolu Tunnels. M.Sc. Thesis, Middle East Technical University, Department of Civil Engineering, Ankara, Turkey.

Dalgıç, S., 1997. Anadolu otoyolu Bolu tünelinde litolojik ve yapısal unsurların dağılımı. Türkiye Jeoloji Bülteni, C.40, S.2, pp. 39-47.

Dowding, C.H. and Rozen, A., 1978. Damage to Rock Tunnels from Earthquake Shaking. Journal of the Geotechnical Engineering Division, ASCE, Vol.104, No.GT2, pp.175-191.

Dönmez, C. and Pujol, S., 2005. Spatial Distribution of Damage Caused by the 1999 Earthquakes in Turkey. Earthquake Spectra, Vol.21, No.1, pp. 53-69.

Durukal, E., 2002. Critical evaluation of strong motion in Kocaeli and Düzce (Turkey) earthquakes. Soil Dynamics and Earthquake Engineering, Vol.22, pp.589-609.

Earthquake Research Department (ERD) of General Directorate of Disaster Affairs and Earthquake Engineering Research Center (EERC) of Middle East Technical University (METU), 2009. Turkish Strong Motion Database (1976-2007). The database has been compiled under the project of Compilation of National Strong-Motion Database in Accordance with International Standards in support by The Scientific and Technological Council of Turkey (TUBİTAK), Turkey.

Einstein, H.H. and Schwartz, C. W., 1979. Simplified analysis for tunnel supports. Journal of the Geotechnical Engineering Division, ASCE, Vol.105, No.GT4, pp.499-518.

Erdik, M., 2001. Report on 1999 Kocaeli and Düzce (Turkey) Earthquakes. Proceedings of the 3rd International Workshop on Structural Control, F. Casciati,G. Magonette (eds.). Structural Control for Civil and Infrastructure Engineering ,World Scientific, pp.149-186.

Faccioli, E., Paolucci, R. and Pessina, V. 2002. Engineering assessment of seismic hazard and long period ground motions at the Bolu Viaduct Site following the November 1999 earthquake. Journal of Seismology, 6, pp.307-327.

Federal Emergency Management Agency, FEMA, 2003. Multi Hazard Loss Estimation Methodology, Earthquake Model, HAZUS-MH MR3, Technical Manual.

Ghasemi, H., Cooper, J.D., Imbsen, R., Pişkin, H., Inal, F. and Tıraş, A., 2000. The November 1999 Düzce Earthquake: Post-earthquake investigation of the structures on the TEM. Federal Highway Agency, publication No.FHWA-RD-00-146.

Hartzell, S., Bonilla, L.F., and Williams, R.A., 2004. Prediction of Nonlinear Soil Effects. Bulletin of the Seismological Society of America, Vol. 94, No. 5, pp. 1609-1629.

Hashash, Y.M.A., Hook, J.J., Schmidt, B. and Yao, J.I-C., 2001. Seismic Design and Analysis of Underground Structures. Tunnelling and Underground Space Technology, Vol.16, pp. 247-293.

Hashash, Y.M.A., Park, D., and Yao, J.I-C., 2005. Ovaling deformations of circular tunnels under seismic loading, an update on seismic design and analysis of underground structures. Tunnelling and Underground Space Technology, Vol.20, pp. 435-441.

Höeg, K., 1968. Stresses against underground structural cylinders. Journal of the Soil Mechanics and Foundations Division, ASCE. Vol.94 No.SM4, pp. 835-858.

Işık, S. and Özben, M., 2007. Assessment of deformation effects of 12 November 1999 Düzce Earthquake on Bolu Tunnels and Seismic Design (in Turkish). Proceedings of the 6th National Conference on Earthquake Engineering, 16-20 October 2007, Istanbul, Turkey.

Işık, S., 2009. Geological profile of Bolu Tunnels. Personal Communications.

Idriss, I.M. and Sun, J.I., 1992. SHAKE: A computer program for conducting equivalent linear seismic response analysis of horizontally layered soil deposits. Center for Geotechnical Modeling, Department of Civil & Environmental Engineering, University of California, Davis, California.

Kramer, S.L., 1996. Geotechnical Earthquake Engineering, Prentice-Hall, pp.340.

Kudo, K., Kanno, T., Okada, H., Özel, O., Erdik, M., Sasatani, T., Higashi, S., Takahashi, M. and Yoshida, K., 2002. Site-specific issues for strong ground motions during the Kocaeli, Turkey, earthquake of 17 August 1999, as inferred from microtremors and aftershocks. Bulletin of Seismological Society of America, Vol.92, No.1, pp.448-465.

Kuhlemeyer, R.L. and Lysmer, J., 1973. Finite Element Method Accuracy for Wave Propagation Problems. Journal of the Soil Mechanics and Foundations Division, 99, 5, pp421-427.

Lanzano, G., Bilotta, E., and Russo, G., 2008. Tunnels under seismic loading: a review of damage case histories and protection methods. Progetto INTERREG MEETING, Università del Molise: report finale, Fabbrocino & Santucci de Magistris eds., pp 65-74.

Lettis, W. & Asssociates Inc. and Barka, A., 2000. Geologic Characterisation of Fault Rupture Hazard, Gümüşova-Gerede Motorway project report.

Nishiyama, S., Muroya, K., and Haya, H., 1999. Seismic Design of cut and cover tunnel based on damage analyses and experimental studies. Quarterly Report of Railway Technical Research Institute, Vol.40, pp. 158-164.

Owen, G.N. and Scholl, R.E., 1981. Earthquake engineering of large underground structures. Report No. FHWA/RD-80/195. Federal Highway Administration and National Science Foundation.

Park, D. and Hashash, Y.M.A., 2004. Soil Damping Formulation in Nonlinear Time Domain Site Response Analysis. Journal of Earthquake Engineering, Vol.8, No.2, pp.249-274.

Penzien, J. and Wu, C.L., 1998. Stresses in linings of bored tunnel. Earthquake Engineering and Structural Dynamics, Vol.27, pp. 283-300.

Penzien, J., 2000. Seismically induced rocking of tunnels. Earthquake Engineering and Structural Dynamics, Vol.29, pp. 683-691.

Pitilakis, K., Alexoudi, M., Argyroudis, S., Monge, O., and Martin, C., 2006. Earthquake Risk Assessment of Lifelines, Bulletin of Earthquake Engineering, Vol.4, pp.365-390.

Pitilakis, K., Alexoudi, M., Argyroudis, S., Monge, O., and Martin, C., 2008. Vulnerability and risk assessment of lifelines. Chapter II: Vulnerability Assessment, C.S. Oliveira, A. Roca and X. Goula (eds.). Assessing and Managing Earthquake Risk, Springer, pp.185-211.

PLAXIS-b.v., 2007. PLAXIS: Finite Element Package for Analysis of Geotechnical Structures, Delft, Netherland.

Power, M.S., Rosidi, D., Kaneshiro, J., Gilstrap, S.D. and Chiou, S., 1998. Summary and evaluation of procedures for the seismic design of tunnels. MCEER Final Report for Task 112-D-5.3(c), FHWA Contact Number DTFH61-92-C-00112, University at Buffalo, State University of New York.

Rathje, E.M., Stokoe, K.H., and Rosenblad, B., 2003. Strong motion station characterization and site effects during the 1999 earthquakes in Turkey. Earthquake Spectra, Vol.19, No.3, pp.653-675.

Rathje, E.M., Stewart, J.P., Baturay, M.B., Bray, J.D. and Bardet, J.P., 2006. Strong ground motions and damage patterns from the 1999 Düzce Earthquake in Turkey. Journal of Earthquake Engineering, Vol.10, No.5, pp. 693-724.

Rosenblad, B., Rathje, E. and Stokoe, K.H., 2001. Shear wave velocity profiling by the SASW method at selected strong-motion stations in Turkey. Final Report to Pacific Earthquake Engineering Research Center, Berkeley.

Scandella, L., Harmandar, E., Faccioli, E., Paolucci, R., Durukal, E. and Erdik, M., 2007. Numerical evaluation of earthquake induced ground strains: The case of Düzce. Proceedings of the Fourth International Conference on Earthquake Geotechnical Engineering.

Schubert, P., Moggioli, M., Brandl, J., and Golser, J., 1997. Extraordinary difficulties driving the motorway tunnels through Bolu Mountains, Turkey. Felsbau, Vol.15, No.5, pp. 351-356.

Seed, H.B. and Idriss, I.M., 1982. Ground motions and soil liquefaction during earthquakes. EERI Monograph Series, Berkeley, CA.

Seed, H.B., Wong, R.T., Idriss, I.M., and Tokimatsu, K., 1986. Moduli and damping factors for dynamic analyses of cohesionless soils. Journal of Geotechnical Engineering, ASCE, Vol.
112, No.11, pp.1016-1032.

Sharma, S. and Judd, W.R., 1991. Underground opening damage from earthquakes. Engineering Geology, Vol.30, pp. 263-276.

Shimizu, I., Osawa, H., Seo, T., Yasuike, S. and Sasaki, S., 1996. Earthquake-related ground motion and groundwater pressure change at the Kamaishi Mine. Engineering geology, Vol.43, pp.107-118.

Strasser, F.O. and Bommer, J.J., 2009. Review: Strong ground motions – Have we seen the worst. Bulletin of Seismological Society of America, Vol.99, No.5, pp.2613-2637.

St John, C.M. and Zahrah, T.F., 1987. Aseismic Design of Underground Structures. Tunnelling and Underground Space Technology. Vol.2, No.2, pp.165-197.

Sucuoğlu, H. and Yılmaz, T., 2001. Düzce, Turkey: A city hit by two major earthquakes in 1999 within three months. Seismological Research Letters, Vol.72, No.6, pp.679-689.

Sun, J.I., Golesorkhi, R., and Seed, H.B., 1988. Dynamic moduli and damping ratios for cohesive soils. Report No. EERC-88/15, Earthquake Engineering Research Center, University of California, Berkeley.

Tokgözoğlu, F. and Işık, S., 2002. Seismic consideration of Bolu Tunnels after Düzce Earthquake and Possible Solution Proposal. International Conference/Workshop and Exhibition on Tunnelling and Underground Space Use.

Turkish Earthquake Code (TEC), 2007. Specifications for structures to be built in disaster areas. Ministry of Public Works and Settlement Government of Republic of Turkey.

Unterberger, W. and Brandl, J., 2000. The effects of the recent earthquake in Turkey on the Bolu Tunnels. Felsbau, Vol.18, No.2, pp.50-54.

Wang, J., 1993. Seismic design of tunnels. Parsons Brinckerhoff Quade & Douglas, Inc.

Visone, C., Bilotta, E. and Santucci de Magistris, F., 2010. One-Dimensional Ground Response as a Preliminary Tool for Dynamic Analyses in Geotechnical Earthquake Engineering. Journal of Earthquake Engineering, Vol.14, pp.131-162.

Vucetic, M. and Dobry, R. 1991. Effect of soil plasticity on cyclic response. Journal of Geotechnical Engineering, ASCE, Vol.117, No.1, pp. 89-107.

Yüksel Proje, 2001. Old and new alignments of Bolu Tunnels. Personal Communications.

Yüksel – Rendel Engineers, 1999. Damage assessment report for Bolu Tunnels following Kaynaşlı Earthquake of 12th November 1999.

APPENDIX A

EXAMPLE CALCULATION SHEET FOR ANALYTICAL SOLUTION

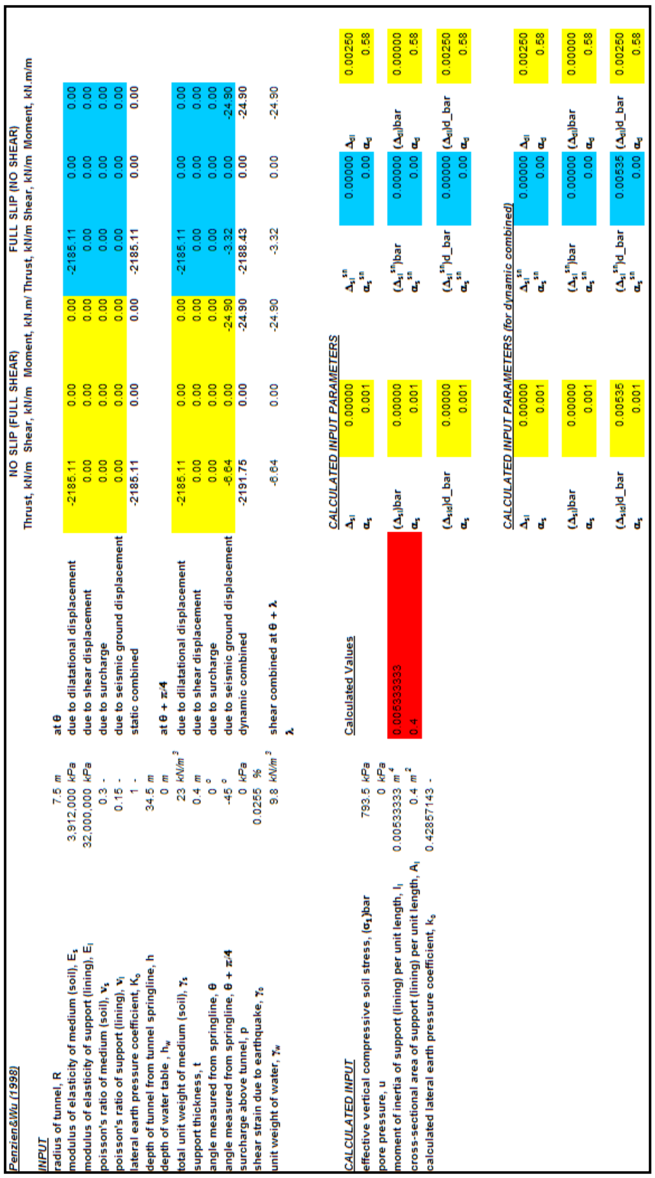

Penzien&Wu (1998)

INPUT		
radius of tunnel, R	7.5	m
modulus of elasticity of medium (soil), E_s	3,912,000	kPa
modulus of elasticity of support (lining), E_l	32,000,000	kPa
poisson's ratio of medium (soil), ν_s	0.3	-
poisson's ratio of support (lining), ν_l	0.15	-
lateral earth pressure coefficient, K_o	1	-
depth of tunnel from tunnel springline, h	34.5	m
depth of water table, h_w	0	m
total unit weight of medium (soil), γ_s	23	kN/m^3
support thickness, t	0.4	m
angle measured from springline, θ	0	°
angle measured from springline, θ + π/4	-45	°
surcharge above tunnel, p	0	kPa
shear strain due to earthquake, γ_c	0.0255	%
unit weight of water, γ_w	9.8	kN/m^3

	NO SLIP (FULL SHEAR) Thrust, kN/m	Shear, kN/m	Moment, kN.m/	FULL SLIP (NO SHEAR) Thrust, kN/m	Shear, kN/m	Moment, kN.m/m
at θ						
due to dilatational displacement	-2185.11	0.00	0.00	-2185.11	0.00	0.00
due to shear displacement	0.00	0.00	0.00	0.00	0.00	0.00
due to surcharge	0.00	0.00	0.00	0.00	0.00	0.00
due to seismic ground displacement	0.00	0.00	0.00	0.00	0.00	0.00
static combined	-2185.11	0.00	0.00	-2185.11	0.00	0.00
at θ + π/4						
due to dilatational displacement	-2185.11	0.00	0.00	-2185.11	0.00	0.00
due to shear displacement	0.00	0.00	0.00	0.00	0.00	0.00
due to surcharge	0.00	0.00	0.00	0.00	0.00	0.00
due to seismic ground displacement	-6.64	0.00	-24.90	-3.32	0.00	-24.90
dynamic combined	-2191.75	0.00	-24.90	-2188.43	0.00	-24.90
shear combined at θ + λ	-6.64	0.00	-24.90	-3.32	0.00	-24.90
λ						

CALCULATED INPUT			Calculated Values
effective vertical compressive soil stress, (σ_1)bar	793.5	kPa	
pore pressure, u	0	kPa	
moment of inertia of support (lining) per unit length, I_l	0.00533333	m^4	0.005333333
cross-sectional area of support (lining) per unit length, A_l	0.4	m^2	0.4
calculated lateral earth pressure coefficient, k_o	0.42857143	-	

CALCULATED INPUT PARAMETERS

Δ_{sl}	0.00000	Δ_{sl}^{ss}	0.00000	Δ_{sl}	0.00250
α_s	0.001	α_s^{ss}	0.00	α_s	0.58
(Δ_{sl})bar	0.00000	(Δ_{sl}^{ss})bar	0.00000	(Δ_{sl})bar	0.00000
α_s	0.001	α_s^{ss}	0.00	α_s	0.58
(Δ_{sld})d_bar	0.00000	(Δ_{sl}^{ss})d_bar	0.00000	(Δ_{sl})d_bar	0.00250
α_s	0.001	α_s^{ss}	0.00	α_s	0.58

CALCULATED INPUT PARAMETERS (for dynamic combined)

Δ_{sl}	0.00000	Δ_{sl}^{ss}	0.00000	Δ_{sl}	0.00250
α_s	0.001	α_s^{ss}	0.00	α_s	0.58
(Δ_{sl})bar	0.00000	(Δ_{sl}^{ss})bar	0.00000	(Δ_{sl})bar	0.00000
α_s	0.001	α_s^{ss}	0.00	α_s	0.58
(Δ_{sld})d_bar	0.00535	(Δ_{sl}^{ss})d_bar	0.00535	(Δ_{sl})d_bar	0.00250
α_s	0.001	α_s^{ss}	0.00	α_s	0.58

Figure A.1 Example calculation sheet for analytical (simplified) solution

APPENDIX B

DETAILED CONSTRUCTION DRAWINGS OF TUNNELS

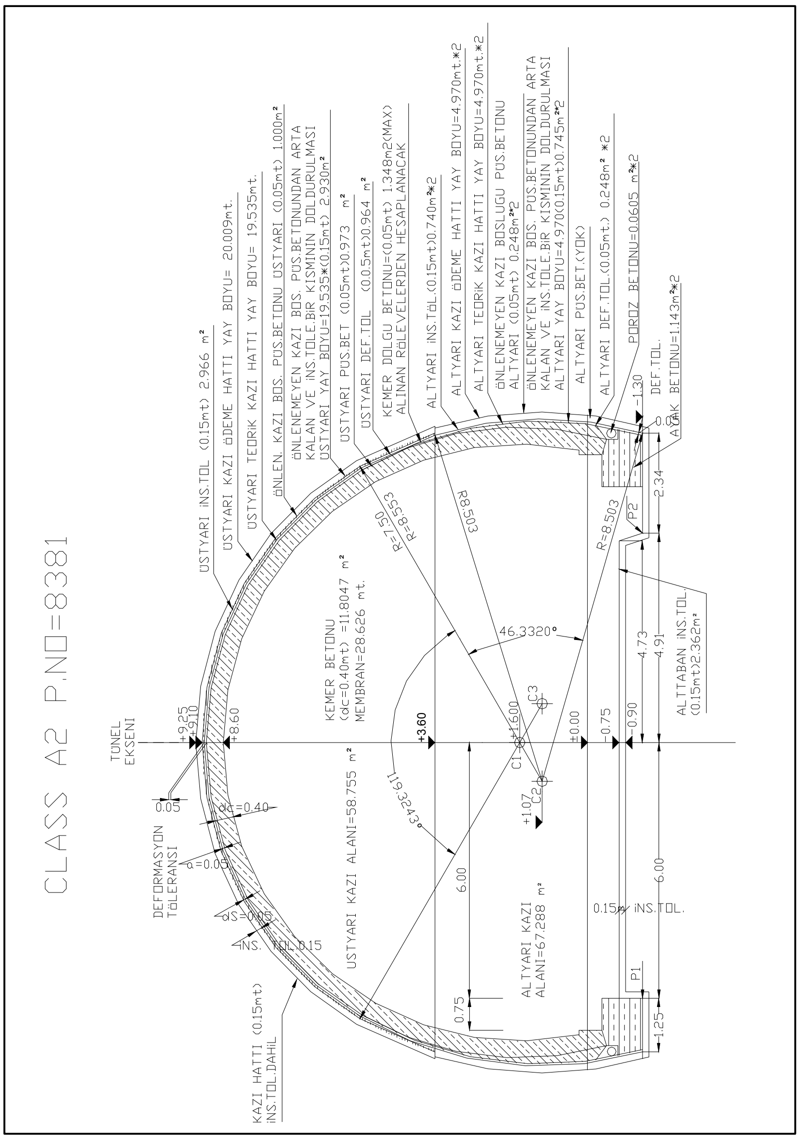

Figure B.1 Details of A2 support-class (after Astaldi SpA, 1993-2006)

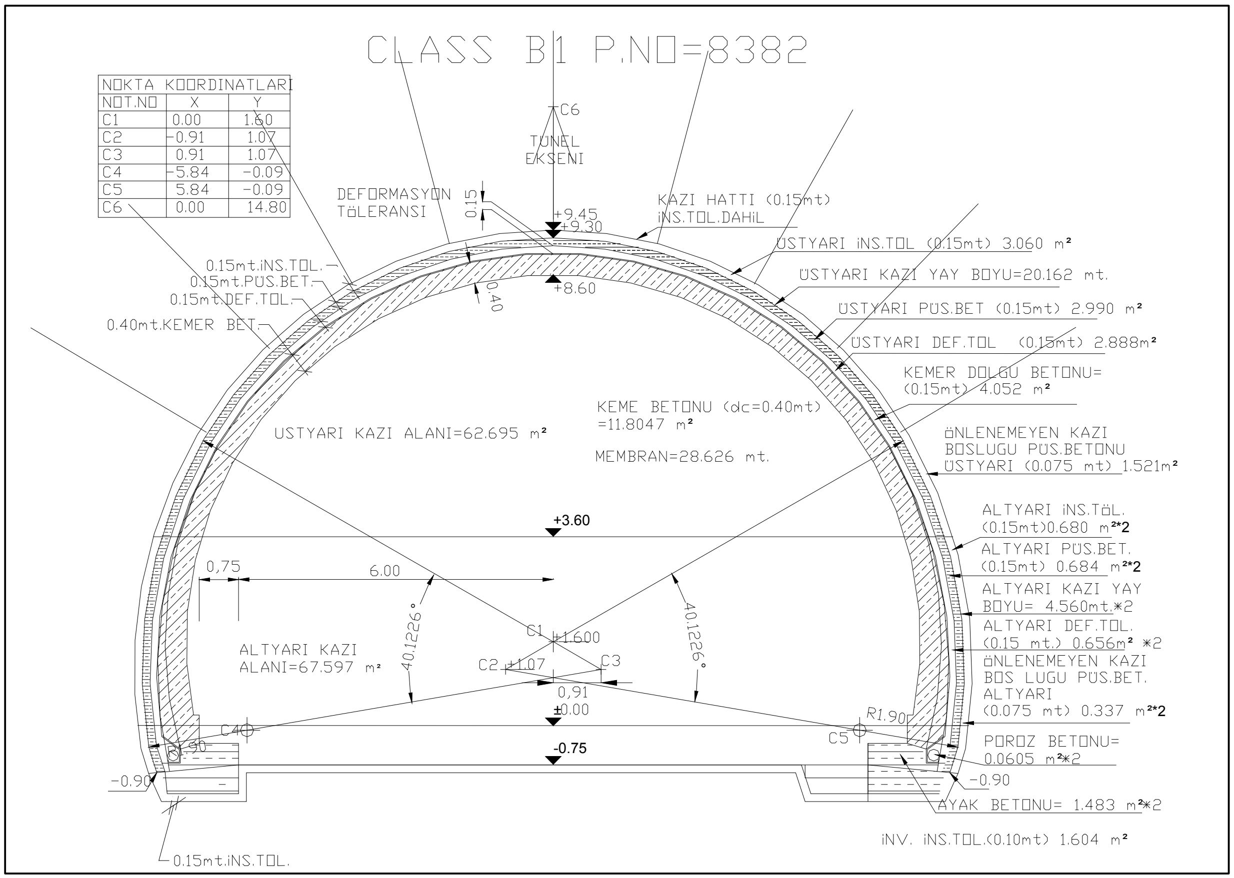

Figure B.2 Details of B1 support-class (after Astaldi SpA, 1993-2006)

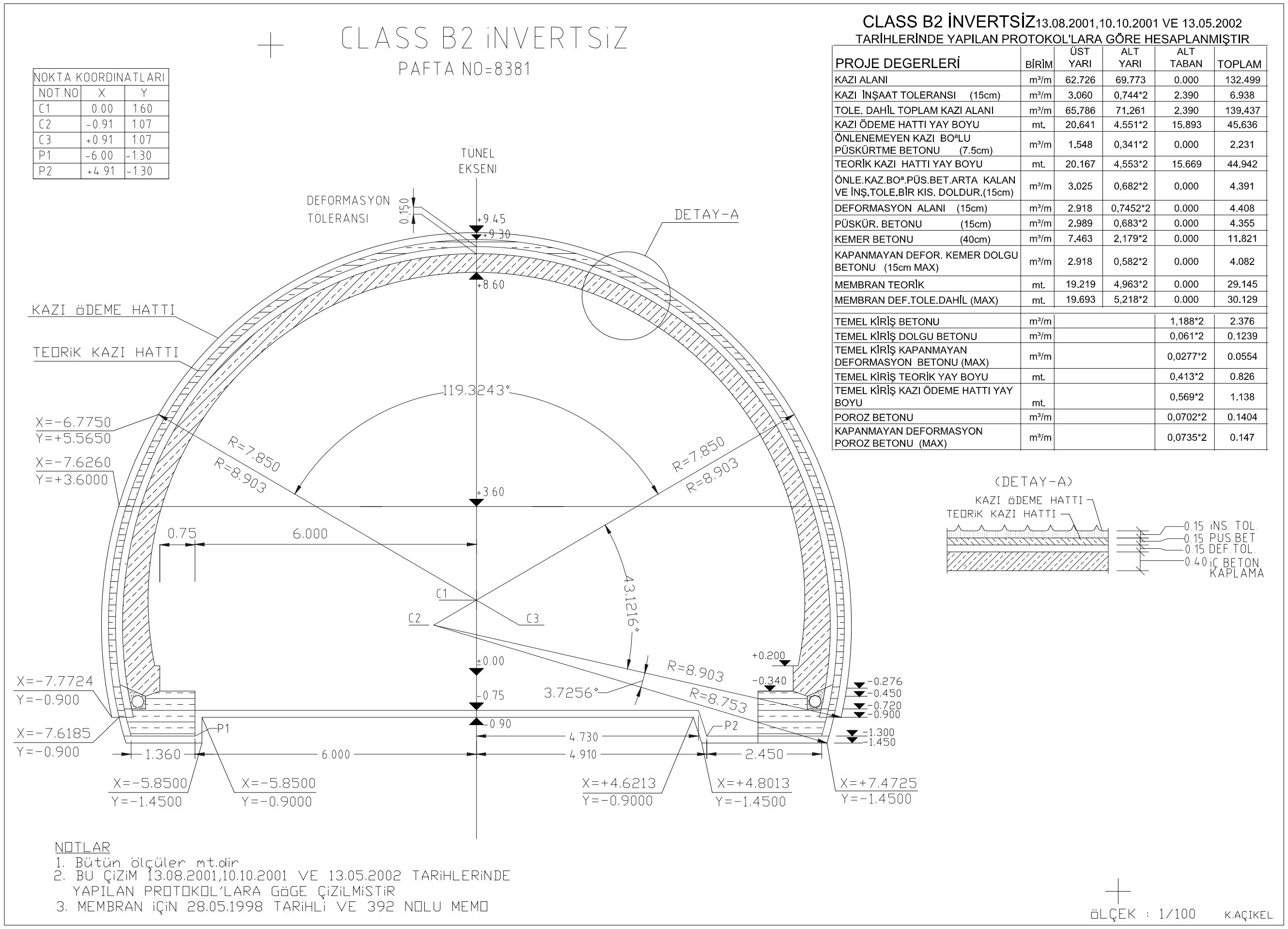

NOKTA KOORDINATLARI

NOT.NO	X	Y
C1	0.00	1.60
C2	-0.91	1.07
C3	+0.91	1.07
P1	-6.00	-1.30
P2	+4.91	-1.30

CLASS B2 İNVERTSİZ 13.08.2001,10.10.2001 VE 13.05.2002 TARİHLERİNDE YAPILAN PROTOKOL'LARA GÖRE HESAPLANMIŞTIR

PROJE DEGERLERİ	BİRİM	ÜST YARI	ALT YARI	ALT TABAN	TOPLAM
KAZI ALANI	m³/m	62.726	69.773	0.000	132.499
KAZI İNŞAAT TOLERANSI (15cm)	m³/m	3.060	0,744*2	2.390	6.938
TOLE. DAHİL TOPLAM KAZI ALANI	m³/m	65.786	71.261	2.390	139.437
KAZI ÖDEME HATTI YAY BOYU	mt.	20.641	4.551*2	15.893	45.636
ÖNLENEMEYEN KAZI BOªLU PÜSKÜRTME BETONU (7.5cm)	m³/m	1.548	0,341*2	0.000	2.231
TEORİK KAZI HATTI YAY BOYU	mt.	20.167	4,553*2	15.669	44.942
ÖNLE.KAZ.BOª.PÜS.BET.ARTA KALAN VE İNŞ.TOLE.BİR KIS. DOLDUR.(15cm)	m³/m	3.025	0,682*2	0.000	4.391
DEFORMASYON ALANI (15cm)	m³/m	2.918	0,7452*2	0.000	4.408
PÜSKÜR. BETONU (15cm)	m³/m	2.989	0,683*2	0.000	4.355
KEMER BETONU (40cm)	m³/m	7.463	2,179*2	0.000	11.821
KAPANMAYAN DEFOR. KEMER DOLGU BETONU (15cm MAX)	m³/m	2.918	0,582*2	0.000	4.082
MEMBRAN TEORİK	mt.	19.219	4,963*2	0.000	29.145
MEMBRAN DEF.TOLE.DAHİL (MAX)	mt.	19.693	5,218*2	0.000	30.129
TEMEL KİRİŞ BETONU	m³/m			1,188*2	2.376
TEMEL KİRİŞ DOLGU BETONU	m³/m			0,061*2	0.1239
TEMEL KİRİŞ KAPANMAYAN DEFORMASYON BETONU (MAX)	m³/m			0,0277*2	0.0554
TEMEL KİRİŞ TEORİK YAY BOYU	mt.			0,413*2	0.826
TEMEL KİRİŞ KAZI ÖDEME HATTI YAY BOYU	mt.			0,569*2	1.138
POROZ BETONU	m³/m			0,0702*2	0.1404
KAPANMAYAN DEFORMASYON POROZ BETONU (MAX)	m³/m			0,0735*2	0.147

Figure B.3 Details of B2 support-class (after Astaldi SpA, 1993-2006)

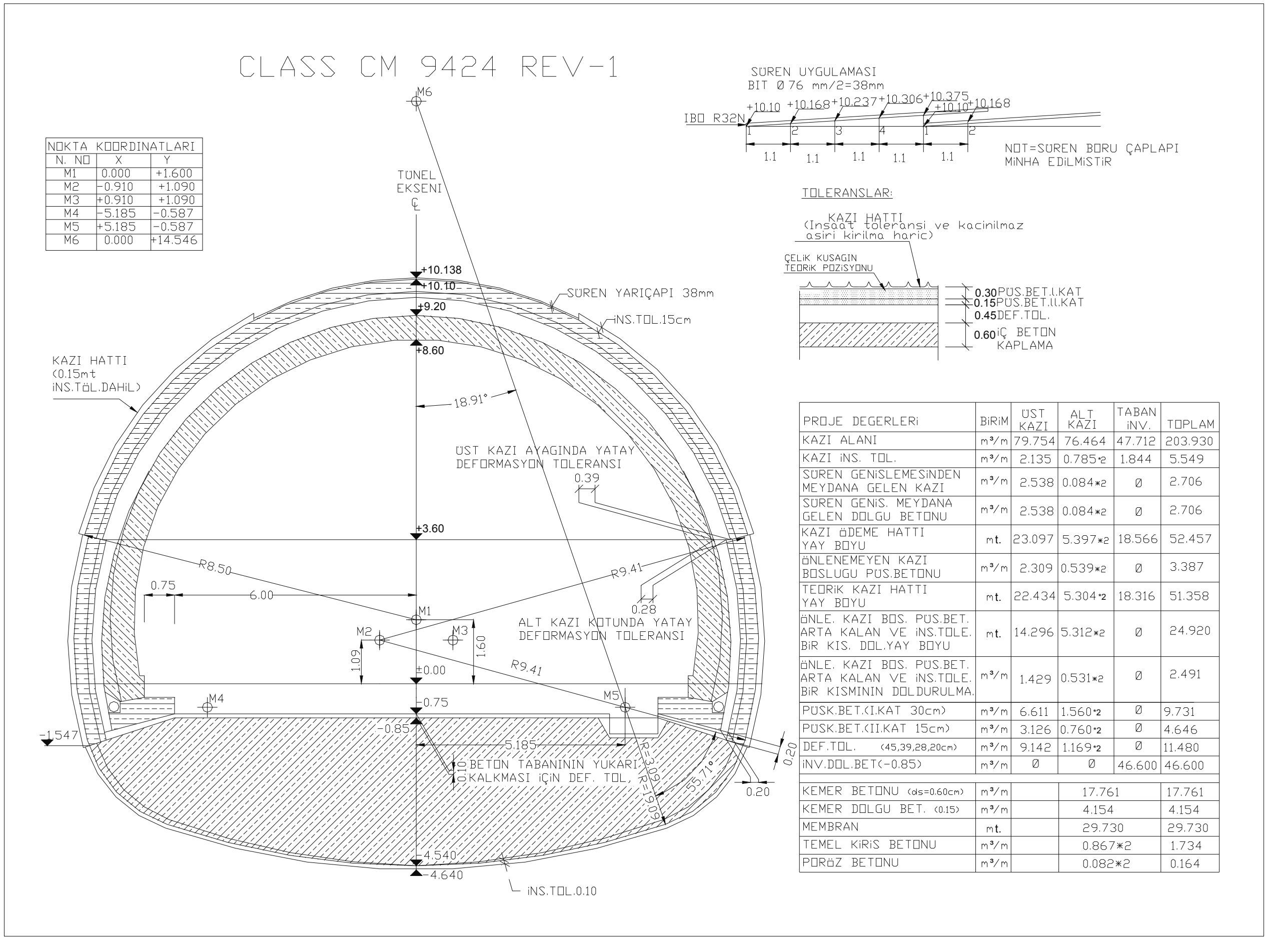

Figure B.4 Details of CM support-class (after Astaldi SpA, 1993-2006)

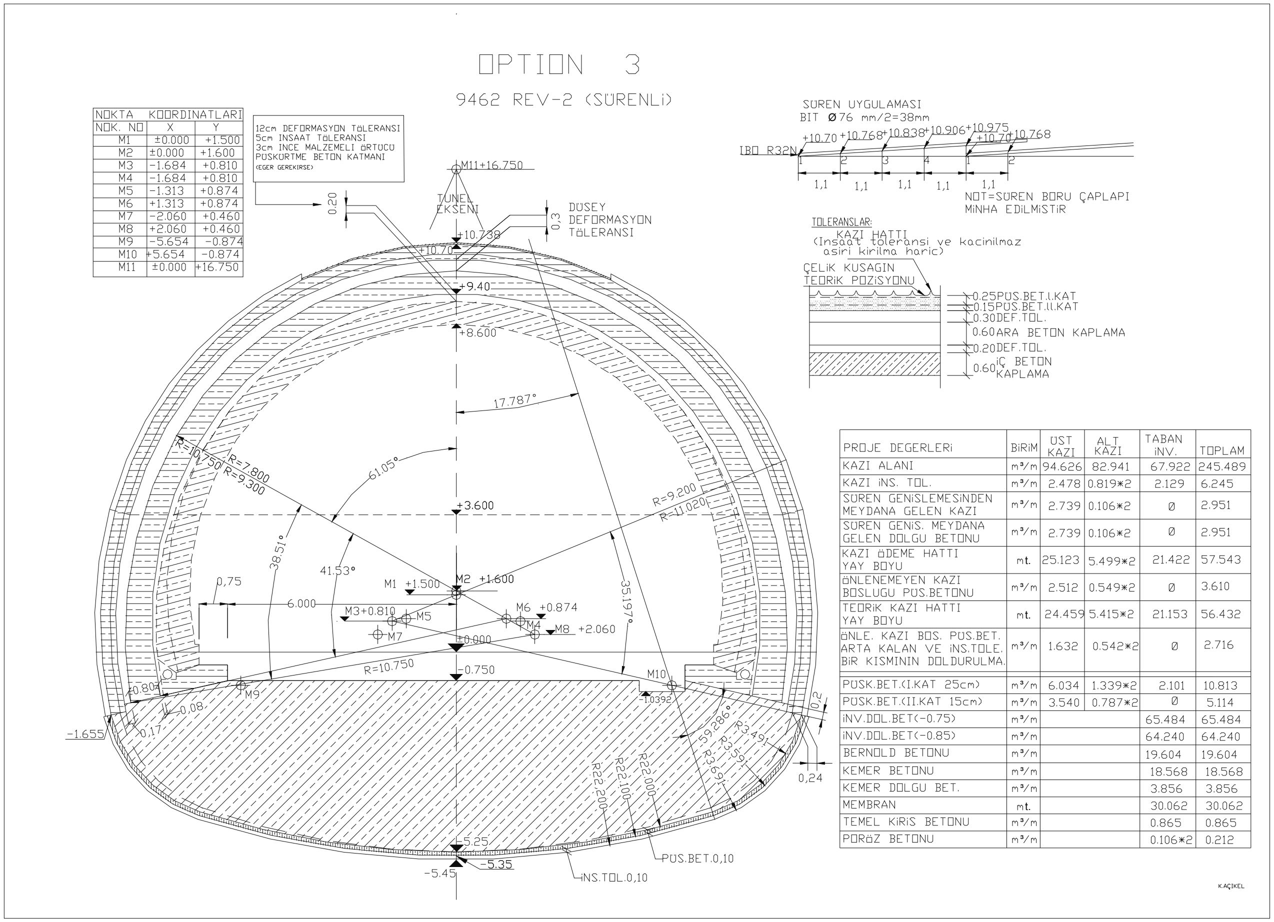

Figure B.5 Details of Option-3 support-class (after Astaldi SpA, 1993-2006)

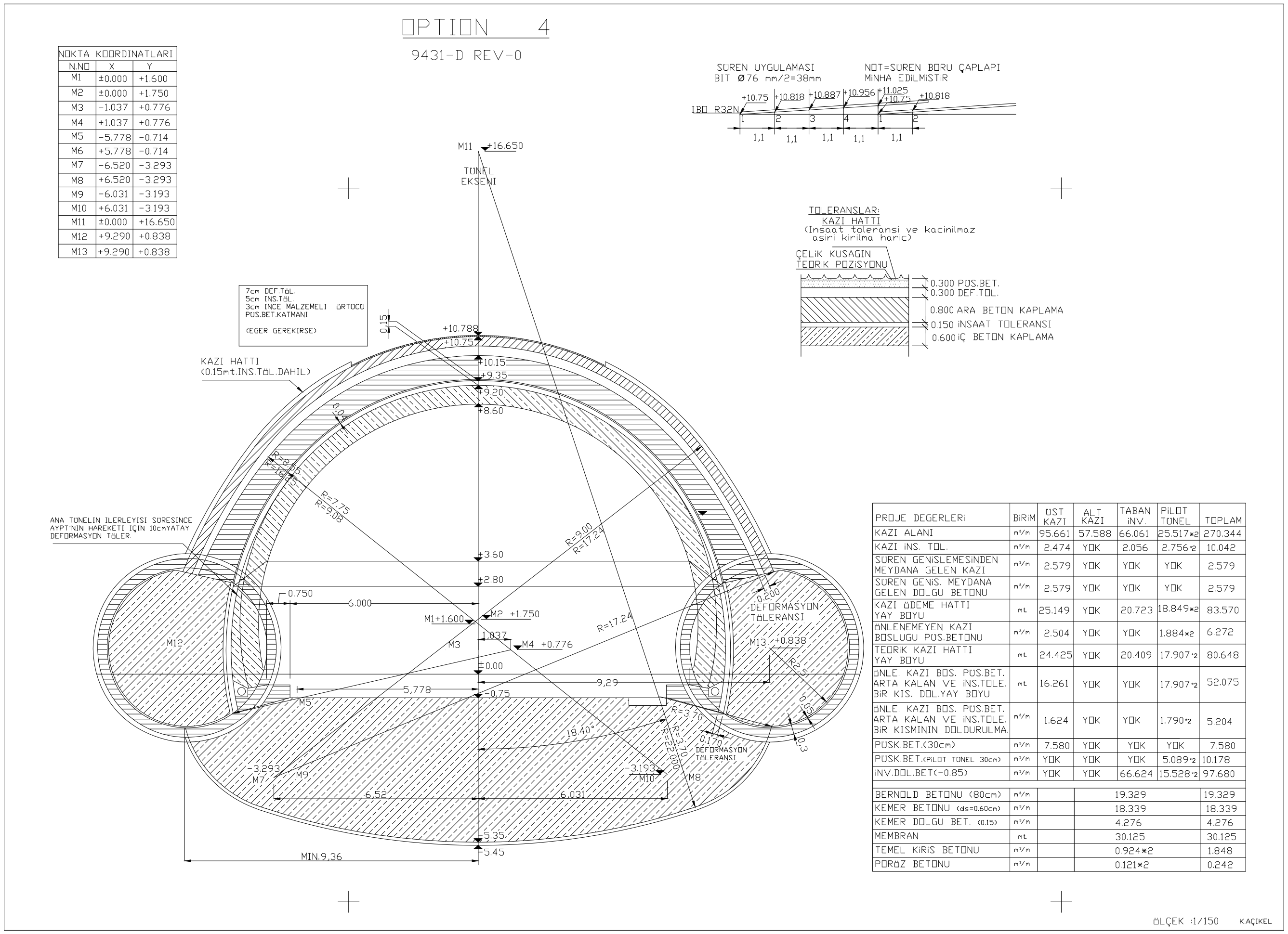

Figure B.6 Details of Option-4 support-class (after Astaldi SpA, 1993-2006***)***

APPENDIX C

DETAILED GEOLOGICAL PROFILES OF BOLU TUNNEL

Figure C.1 Detailed geological profile of initial alignment Bolu Tunnels (after Astaldi SpA, 1993-2006)

Figure C.2 Detailed geological profile of final alignment of Bolu Tunnels – LEFT TUBE (after Astaldi SpA, 1993-2006)

Figure C.3 Detailed geological profile of final alignment of Bolu Tunnels – RIGHT TUBE (after Astaldi SpA, 1993-2006)

APPENDIX D

BOREHOLE LOGS OF DÜZCE STATION

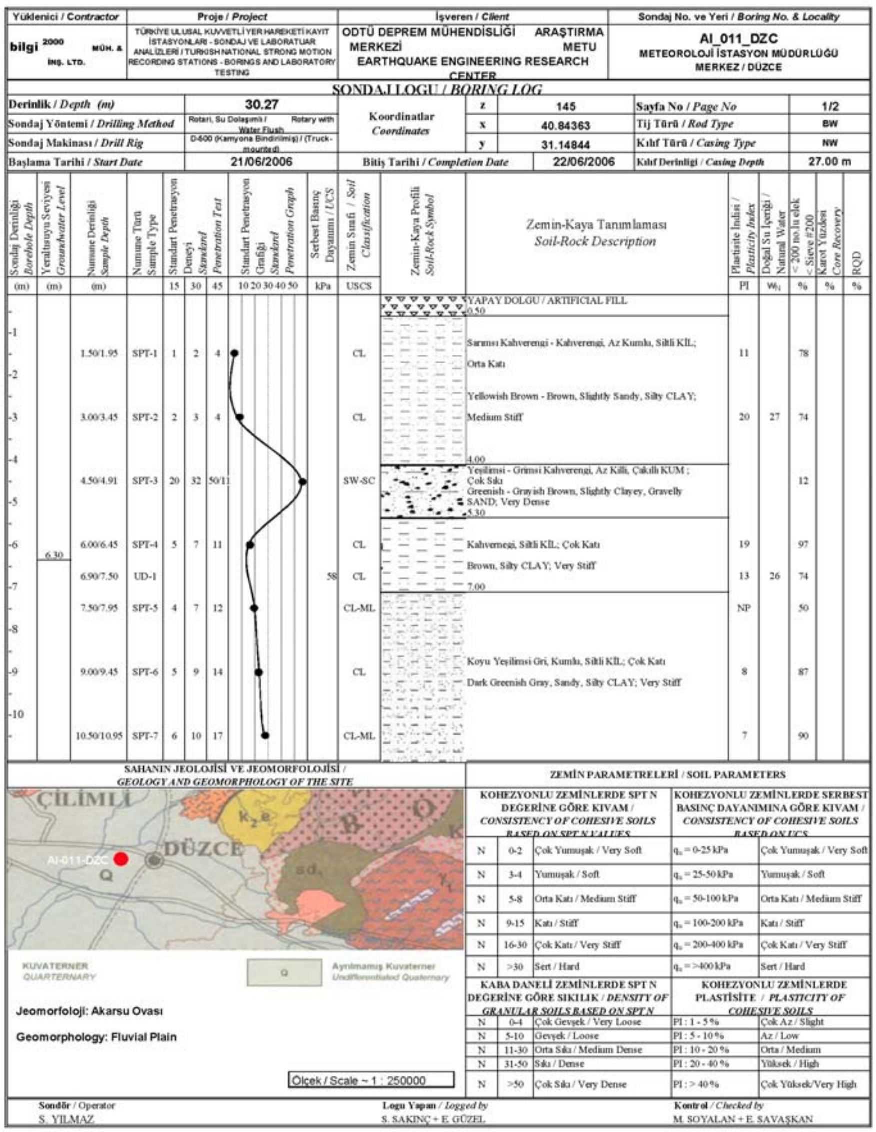

Figure D.1 Borehole logs of Düzce Station, pg.1/2 (after ERD and EERC, 2009)

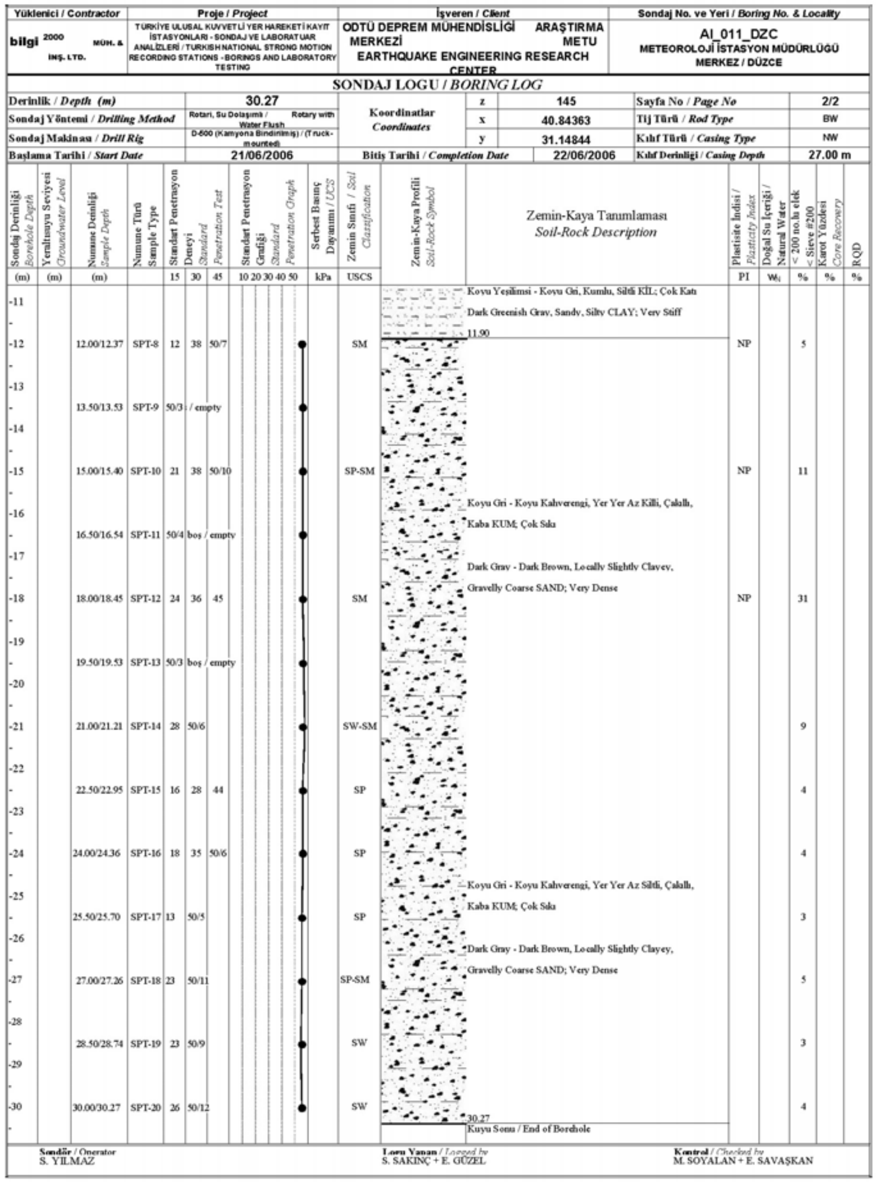

Figure D.2 Borehole logs of Düzce Station, pg.2/2 (after ERD and EERC, 2009)

APPENDIX E

BOREHOLE LOGS OF BOLU STATION

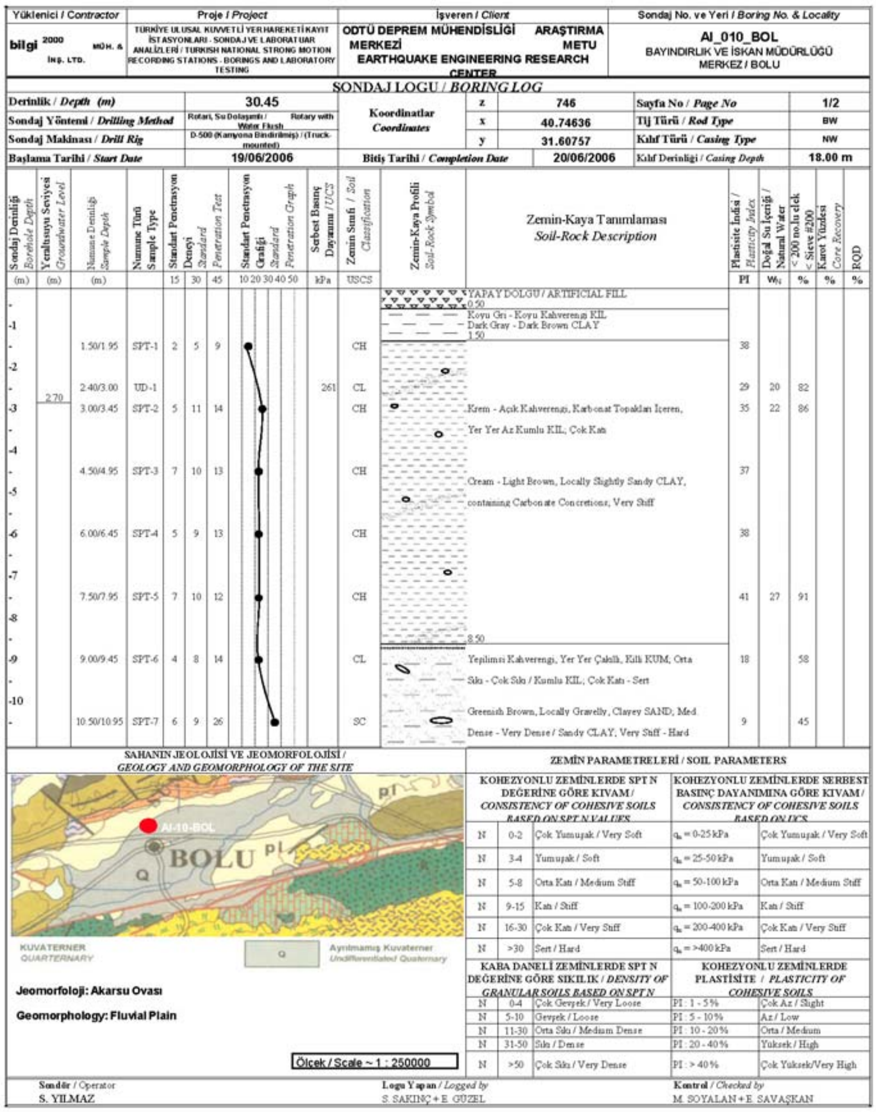

Yüklenici / *Contractor*	Proje / *Project*	İşveren / *Client*	Sondaj No. ve Yeri / *Boring No. & Locality*
bilgi 2000 MÜH. & İNŞ. LTD.	TÜRKİYE ULUSAL KUVVETLİ YER HAREKETİ KAYIT İSTASYONLARI - SONDAJ VE LABORATUAR ANALİZLERİ / TURKISH NATIONAL STRONG MOTION RECORDING STATIONS - BORINGS AND LABORATORY TESTING	ODTÜ DEPREM MÜHENDİSLİĞİ ARAŞTIRMA MERKEZİ METU EARTHQUAKE ENGINEERING RESEARCH CENTER	AI_010_BOL BAYINDIRLIK VE İSKAN MÜDÜRLÜĞÜ MERKEZ / BOLU

SONDAJ LOGU / *BORING LOG*

Derinlik / *Depth (m)*	30.45	Koordinatlar *Coordinates*	z	746	Sayfa No / *Page No*	1/2
Sondaj Yöntemi / *Drilling Method*	Rotari, Su Dolaşımlı / Rotary with Water Flush		x	40.74636	Tij Türü / *Rod Type*	BW
Sondaj Makinası / *Drill Rig*	D-500 (Kamyona Bindirilmiş) / (Truck-mounted)		y	31.60757	Kılıf Türü / *Casing Type*	NW
Başlama Tarihi / *Start Date*	19/06/2006	Bitiş Tarihi / *Completion Date*		20/06/2006	Kılıf Derinliği / *Casing Depth*	18.00 m

Sondaj Derinliği *Borehole Depth* (m)	Yeraltısuyu Seviyesi *Groundwater Level* (m)	Numune Derinliği *Sample Depth* (m)	Numune Türü *Sample Type*	Standart Penetrasyon Deneyi *Standard Penetration Test* 15	30	45	Serbest Basınç Dayanımı / *UCS* kPa	Zemin Sınıfı / *Soil Classification* USCS	Zemin-Kaya Tanımlaması *Soil-Rock Description*	Plastisite İndisi / *Plasticity Index* PI	Doğal Su İçeriği / *Natural Water* W_N	< 200 no.lu elek < Sieve #200 %	Karot Yüzdesi *Core Recovery* %	RQD %
									YAPAY DOLGU / ARTIFICIAL FILL 0.50					
-1									Koyu Gri - Koyu Kahverengi KİL Dark Gray - Dark Brown CLAY 1.50					
		1.50/1.95	SPT-1	2	5	9		CH		38				
-2														
	2.70	2.40/3.00	UD-1				261	CL		29	20	82		
-3		3.00/3.45	SPT-2	5	11	14		CH	Krem - Açık Kahverengi, Karbonat Topakları İçeren, Yer Yer Az Kumlu KİL; Çok Katı	35	22	86		
-4		4.50/4.95	SPT-3	7	10	13		CH	Cream - Light Brown, Locally Slightly Sandy CLAY, containing Carbonate Concretions; Very Stiff	37				
-6		6.00/6.45	SPT-4	5	9	13		CH		38				
-7		7.50/7.95	SPT-5	7	10	12		CH	8.50	41	27	91		
-9		9.00/9.45	SPT-6	4	8	14		CL	Yeşilimsi Kahverengi, Yer Yer Çakıllı, Killi KUM; Orta Sıkı - Çok Sıkı / Kumlu KİL; Çok Katı - Sert	18		58		
-10		10.50/10.95	SPT-7	6	9	26		SC	Greenish Brown, Locally Gravelly, Clayey SAND; Med. Dense - Very Dense / Sandy CLAY; Very Stiff - Hard	9		45		

SAHANIN JEOLOJİSİ VE JEOMORFOLOJİSİ / *GEOLOGY AND GEOMORPHOLOGY OF THE SITE*

ZEMİN PARAMETRELERİ / SOIL PARAMETERS

KOHEZYONLU ZEMİNLERDE SPT N DEĞERİNE GÖRE KIVAM / *CONSISTENCY OF COHESIVE SOILS BASED ON SPT N VALUES*			KOHEZYONLU ZEMİNLERDE SERBEST BASINÇ DAYANIMINA GÖRE KIVAM / *CONSISTENCY OF COHESIVE SOILS BASED ON UCS*	
N	0-2	Çok Yumuşak / Very Soft	q_u = 0-25 kPa	Çok Yumuşak / Very Soft
N	3-4	Yumuşak / Soft	q_u = 25-50 kPa	Yumuşak / Soft
N	5-8	Orta Katı / Medium Stiff	q_u = 50-100 kPa	Orta Katı / Medium Stiff
N	9-15	Katı / Stiff	q_u = 100-200 kPa	Katı / Stiff
N	16-30	Çok Katı / Very Stiff	q_u = 200-400 kPa	Çok Katı / Very Stiff
N	>30	Sert / Hard	q_u = >400 kPa	Sert / Hard

KABA DANELİ ZEMİNLERDE SPT N DEĞERİNE GÖRE SIKILIK / *DENSITY OF GRANULAR SOILS BASED ON SPT N*			KOHEZYONLU ZEMİNLERDE PLASTİSİTE / *PLASTICITY OF COHESIVE SOILS*	
N	0-4	Çok Gevşek / Very Loose	PI : 1 - 5%	Çok Az / Slight
N	5-10	Gevşek / Loose	PI : 5 - 10%	Az / Low
N	11-30	Orta Sıkı / Medium Dense	PI : 10 - 20%	Orta / Medium
N	31-50	Sıkı / Dense	PI : 20 - 40%	Yüksek / High
N	>50	Çok Sıkı / Very Dense	PI : > 40%	Çok Yüksek/Very High

Sondör / Operator: S. YILMAZ — Logu Yapan / *Logged by*: S. SAKINÇ + E. GÜZEL — Kontrol / *Checked by*: M. SOYALAN + E. SAVAŞKAN

Figure E.1 Borehole logs of Bolu Station, pg.1/2 (after ERD and EERC, 2009)

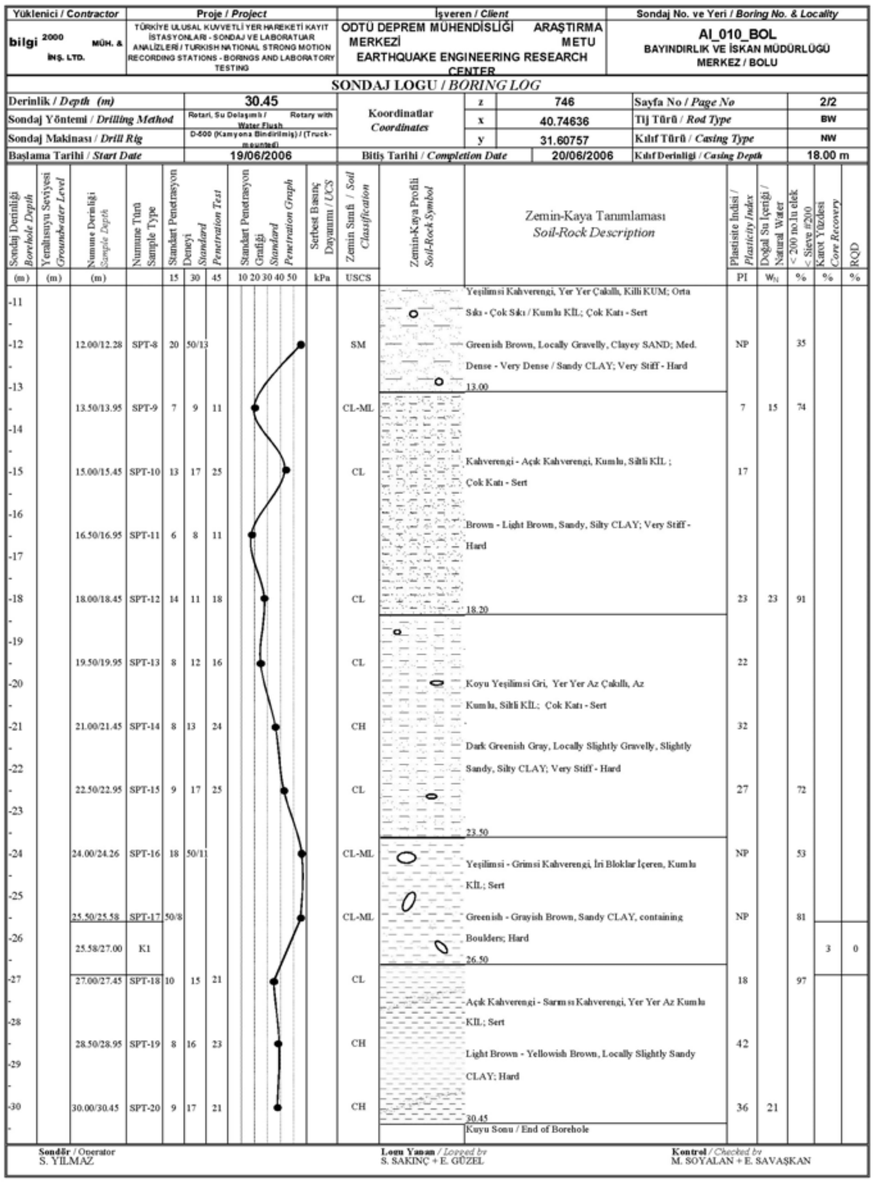

Figure E.2 Borehole logs of Bolu Station, pg.2/2 (after ERD and EERC, 2009)

APPENDIX F

MODULUS REDUCTION AND DAMPING CURVES

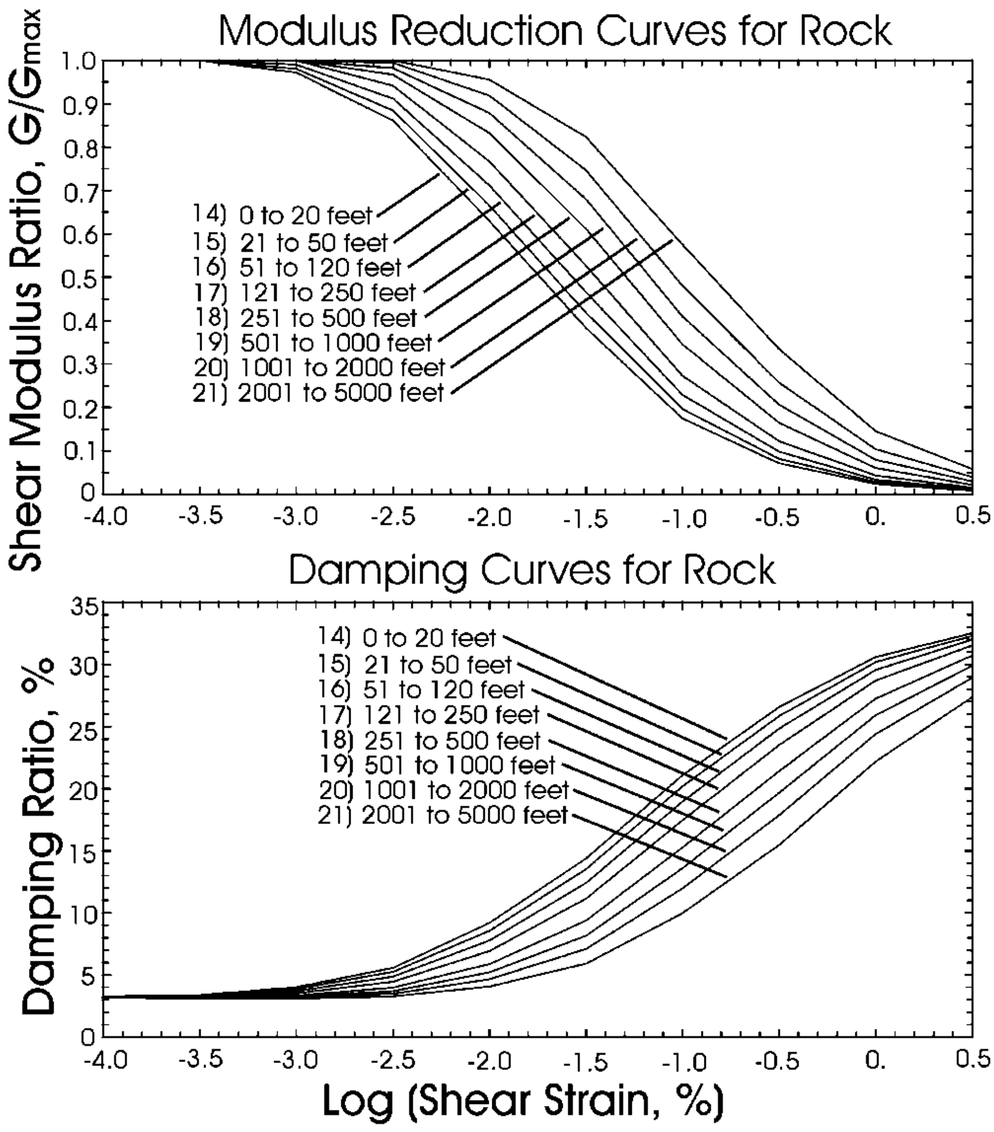

Figure F.1 EPRI (1993) Modulus reduction and damping curves for rock (quoted by Hartzell, 2004)

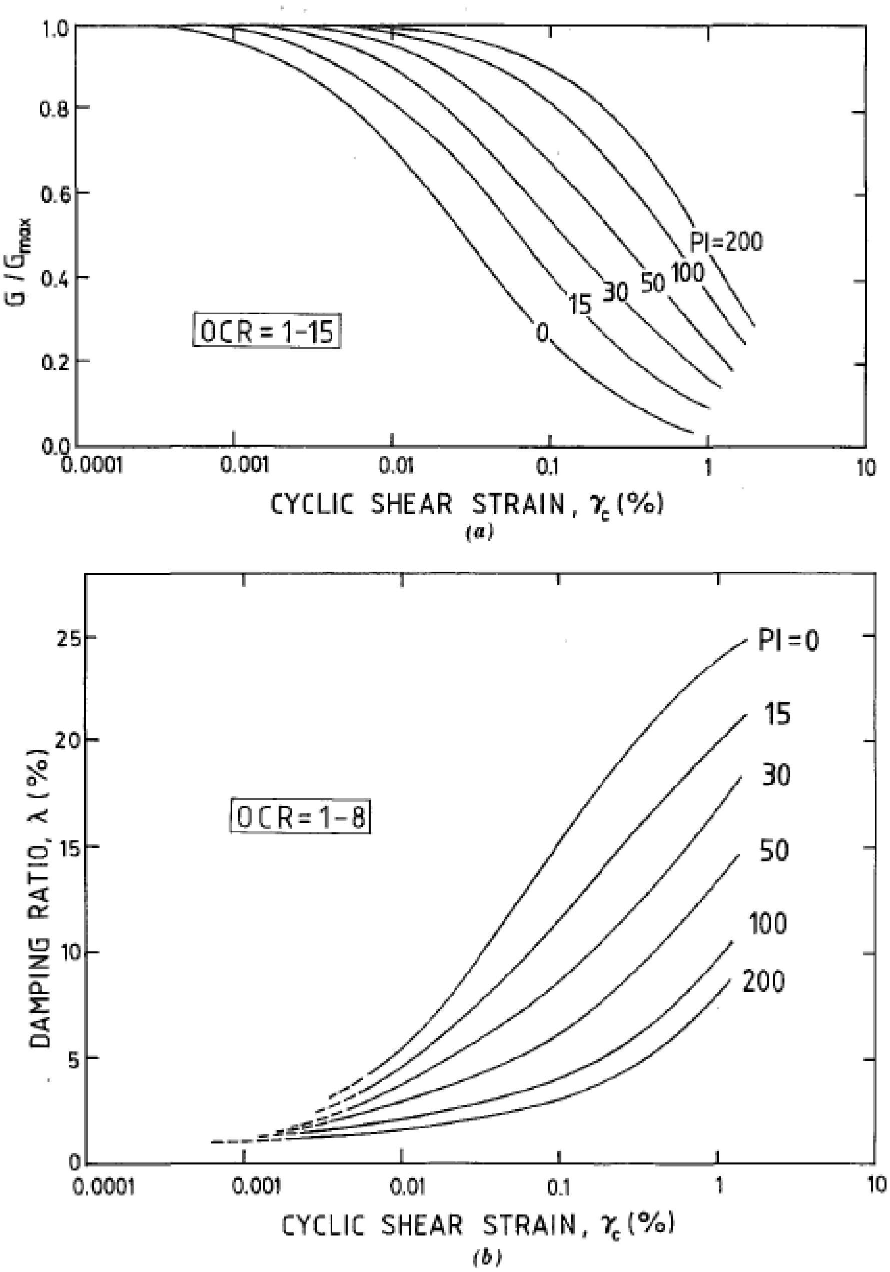

Figure F.2 Relations between G/G_{max} versus γ_c and λ versus γ_c curves and soil plasticity for normally consolidated and overconsolidated soils (after Vucetic and Dobry, 1991)

APPENDIX G

SHEAR WAVE VELOCITY PROFILES OF ANALYZED SECTIONS

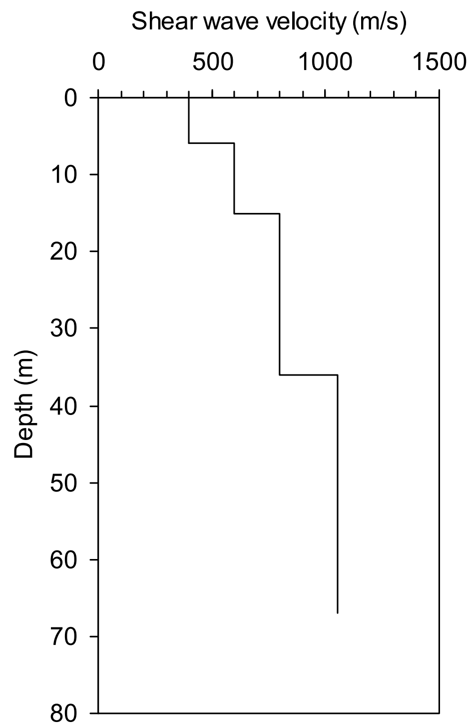

Figure G.1 Shear wave velocity profile of Section No.1

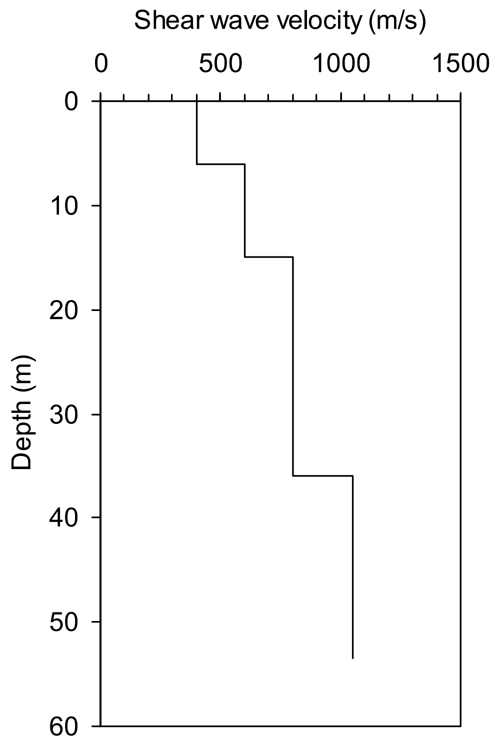

Figure G.2 Shear wave velocity profile of Section No.2

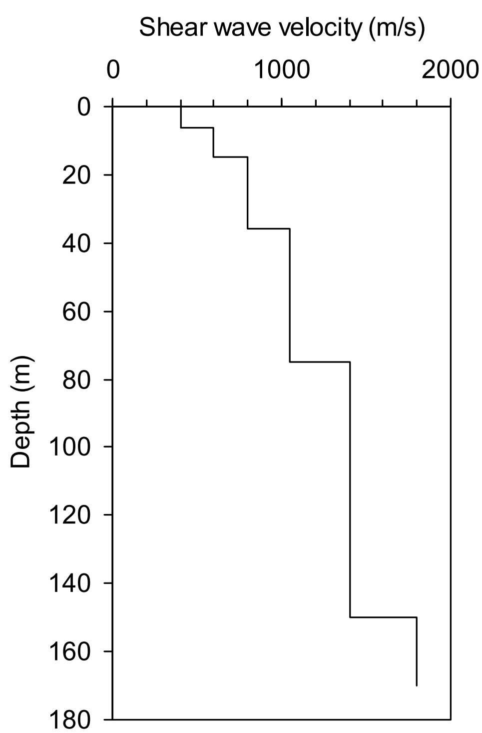

Figure G.3 Shear wave velocity profile of Section No.3

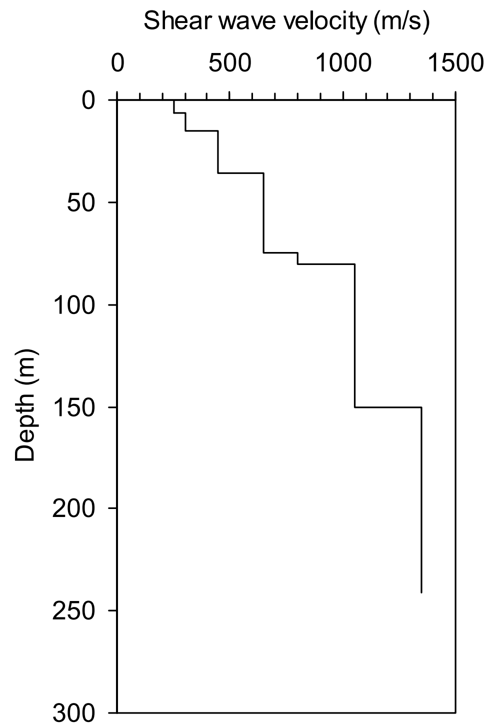

Figure G.4 Shear wave velocity profile of Section No.4

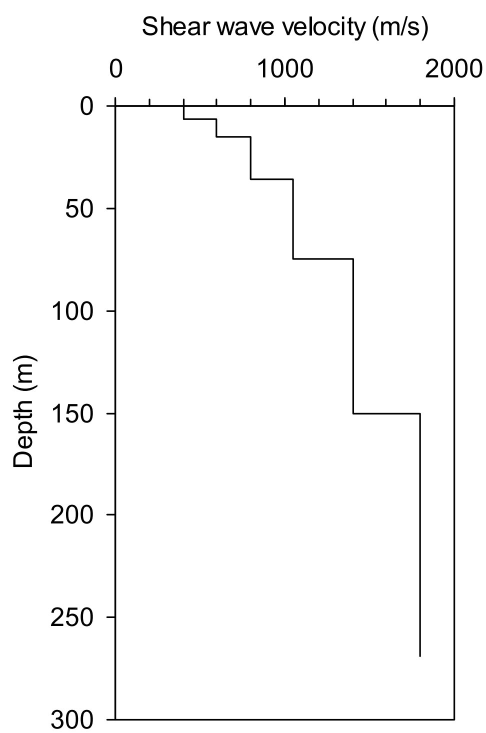

Figure G.5 Shear wave velocity profile of Section No.5

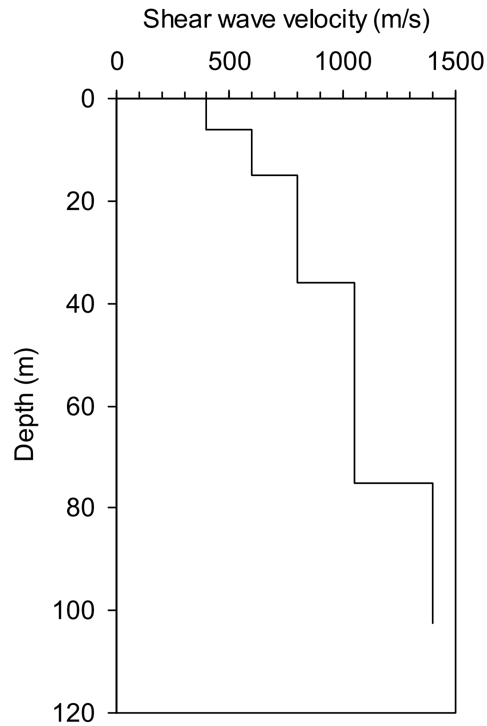

Figure G.6 Shear wave velocity profile of Section No.7

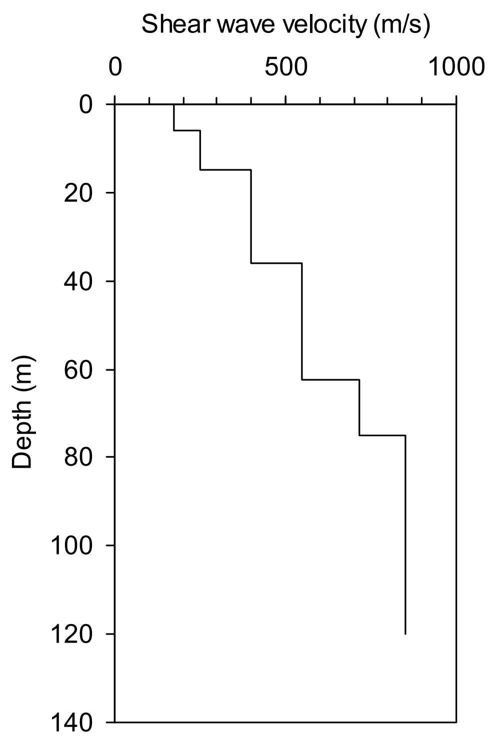

Figure G.7 Shear wave velocity profile of Section No.25

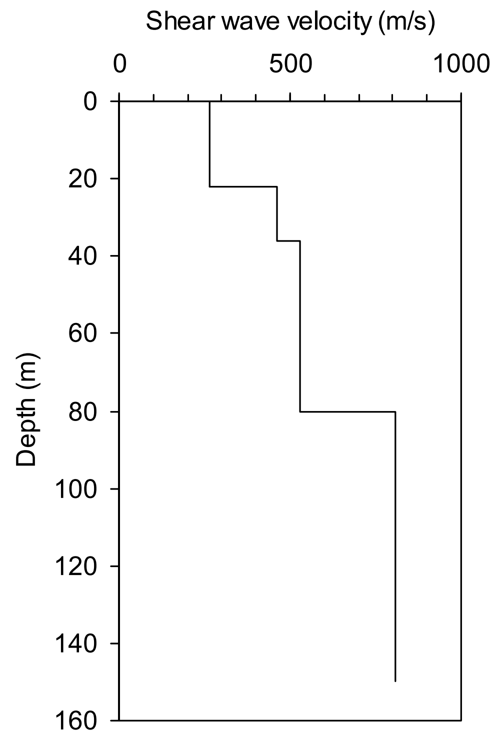

Figure G.8 Shear wave velocity profile of Section No.26

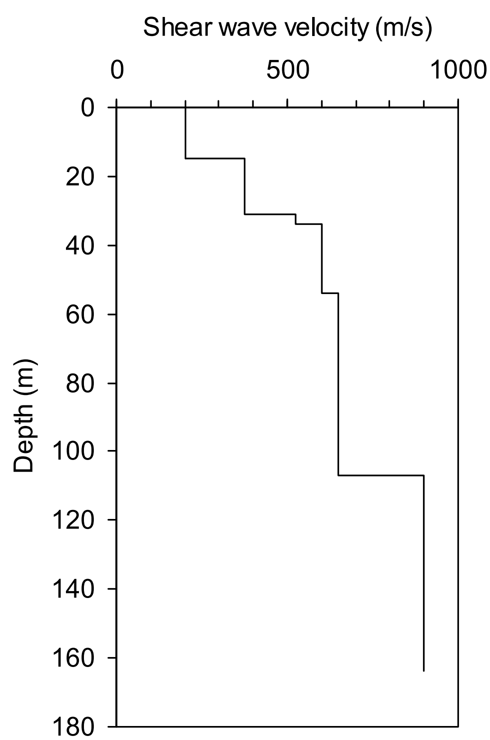

Figure G.9 Shear wave velocity profile of Section No.27

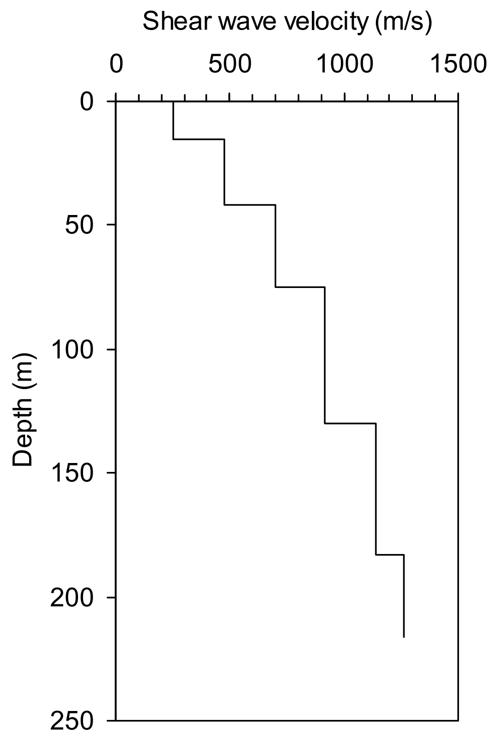

Figure G.10 Shear wave velocity profile of Section No.29

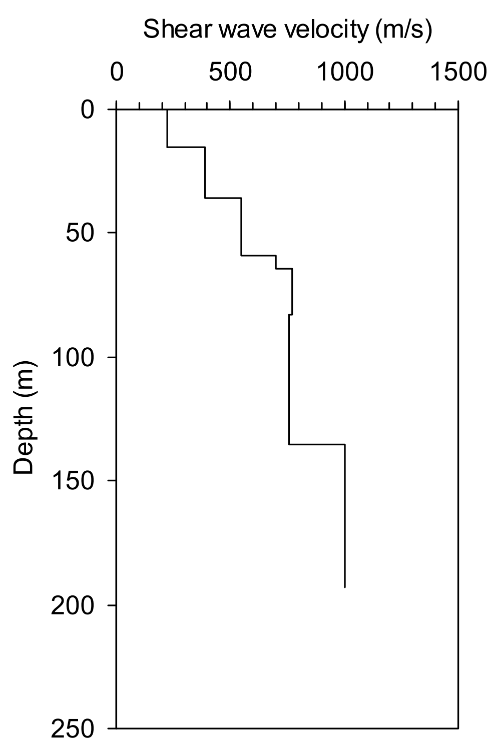

Figure G.11 Shear wave velocity profile of Section No.30

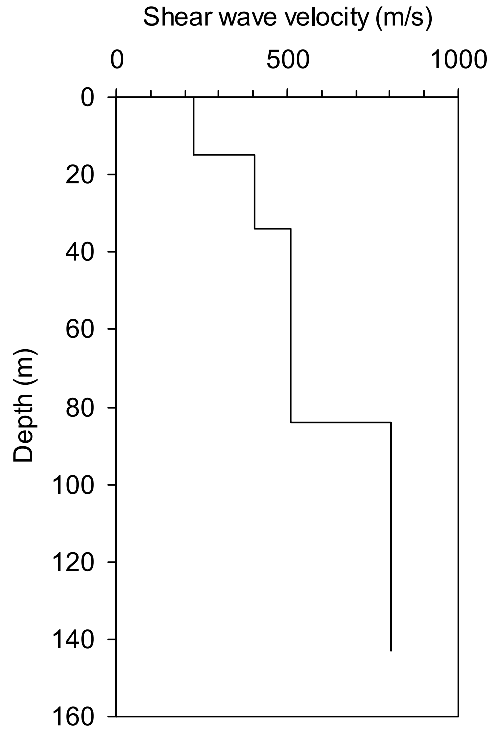

Figure G.12 Shear wave velocity profile of Section No.31

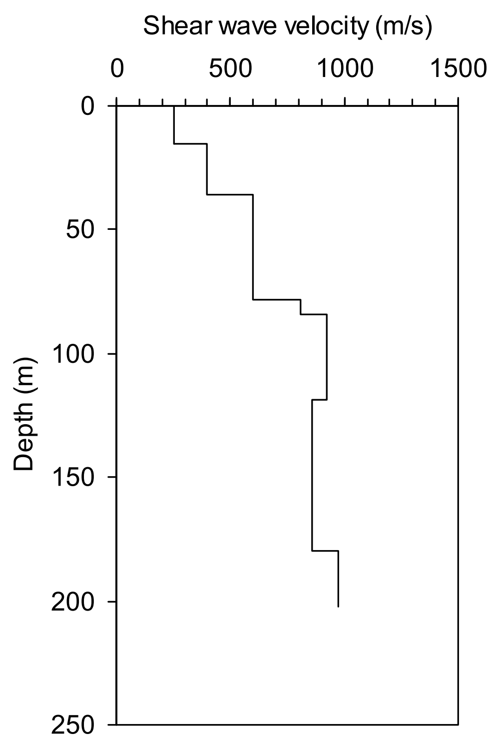

Figure G.13 Shear wave velocity profile of Section No.32

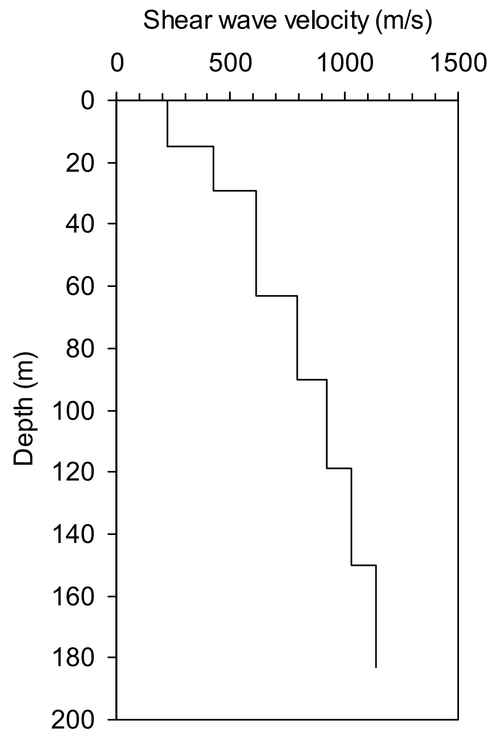

Figure G.14 Shear wave velocity profile of Section No.33

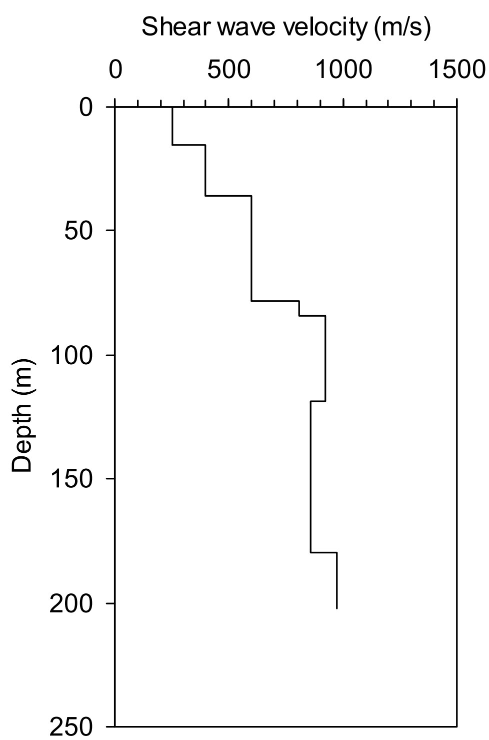

Figure G.15 Shear wave velocity profile of Section No.34

APPENDIX H

FINITE ELEMENT MODELS OF SOLVED TUNNEL SECTIONS

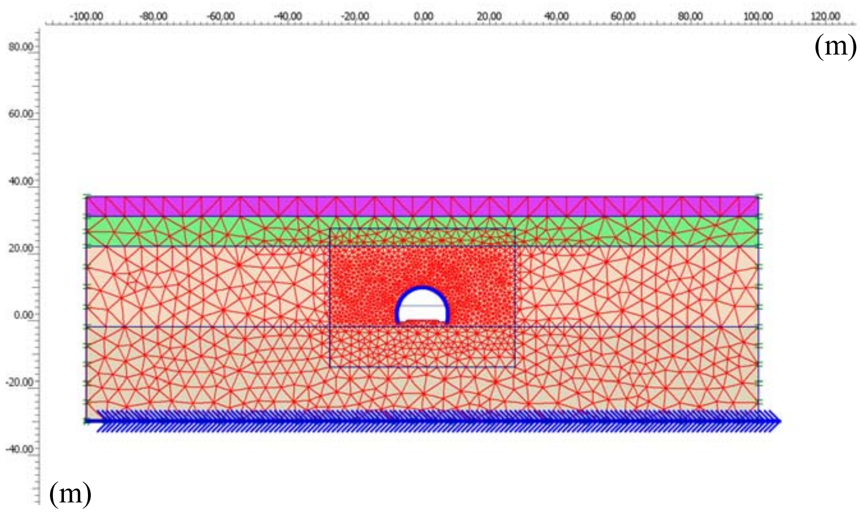

Figure H.1 Full-dynamic FE model for Section No.1 (Rock Class A2)

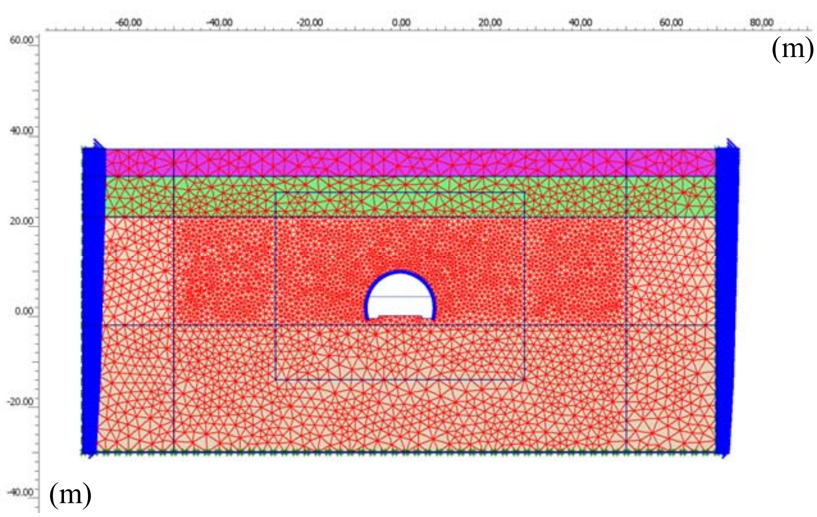

Figure H.2 Pseudo-static FE model for Section No.1 (Rock Class A2)

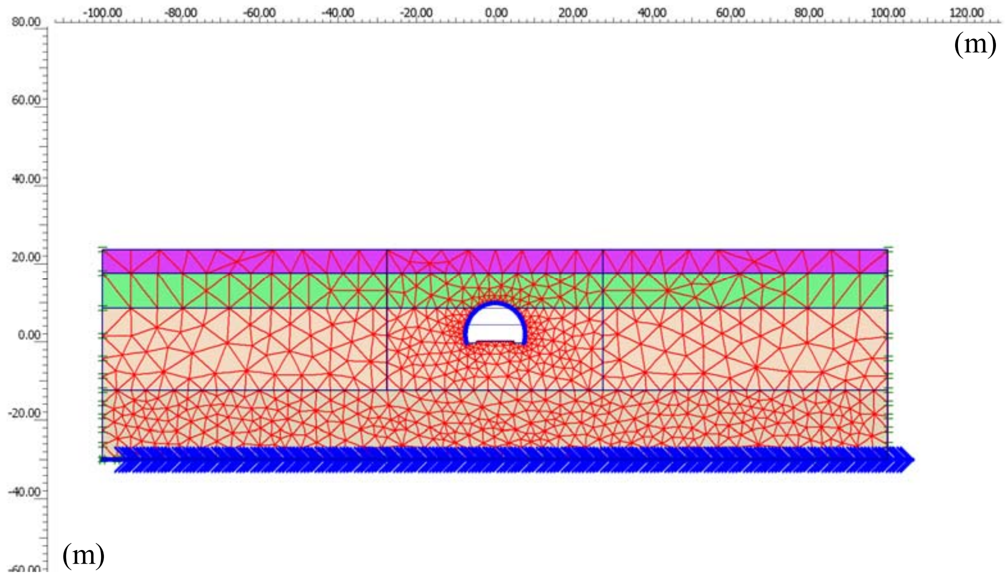

Figure H.3 Full-dynamic FE model for Section No.2 (Rock Class A2)

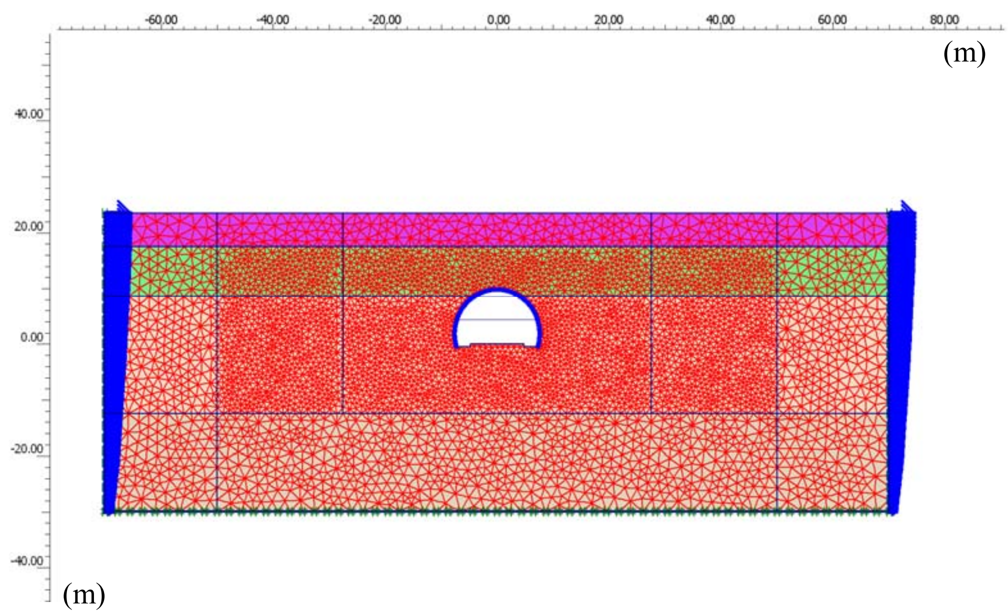

Figure H.4 Pseudo-static FE model for Section No.2 (Rock Class A2)

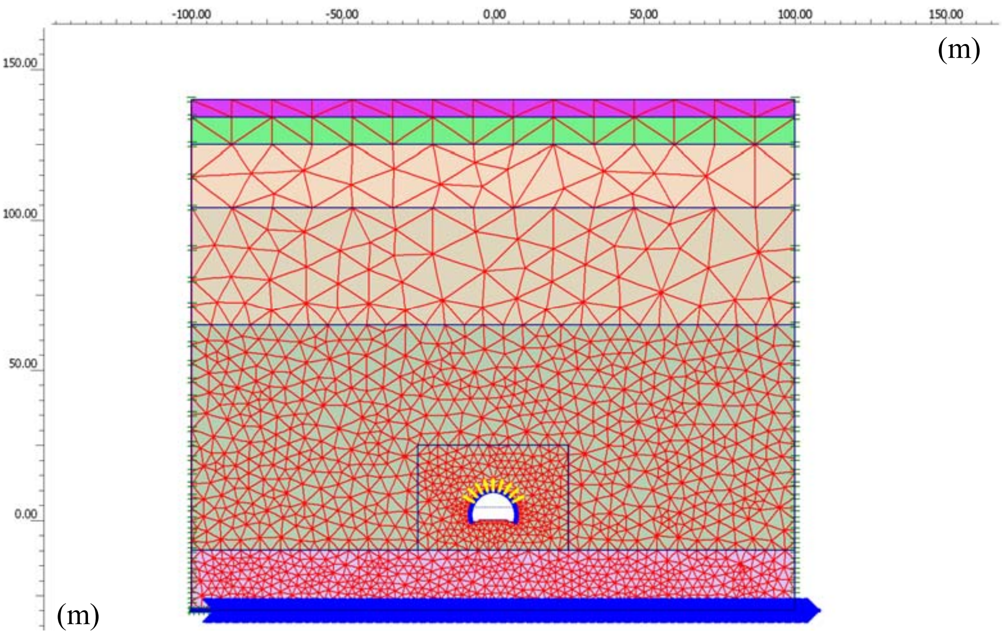

Figure H.5 Full-dynamic FE model for Section No.3 (Rock Class B1)

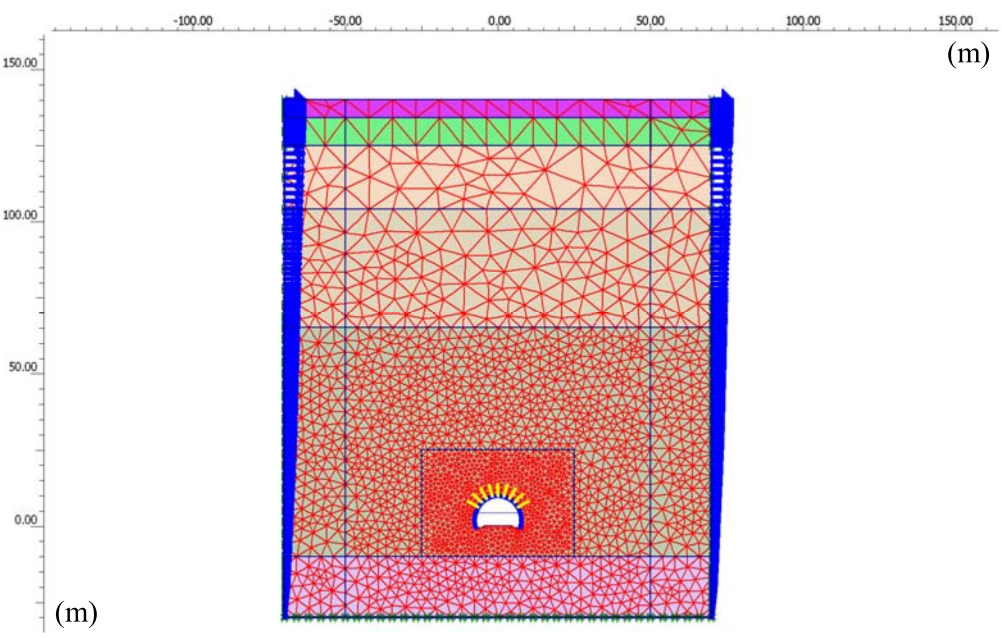

Figure H.6 Pseudo-static FE model for Section No.3 (Rock Class B1)

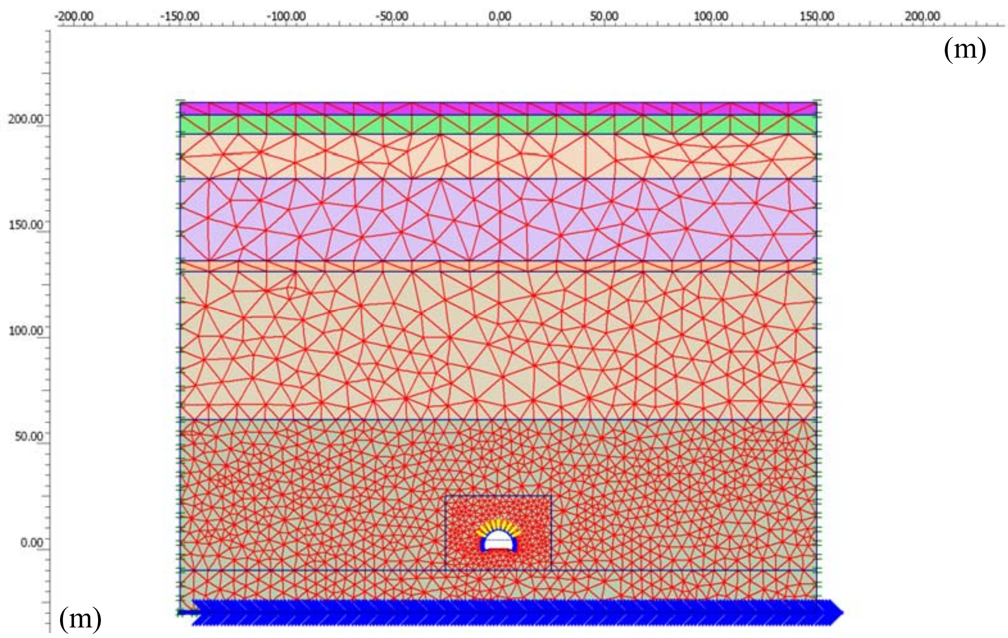

Figure H.7 Full-dynamic FE model for Section No.4 (Rock Class B1)

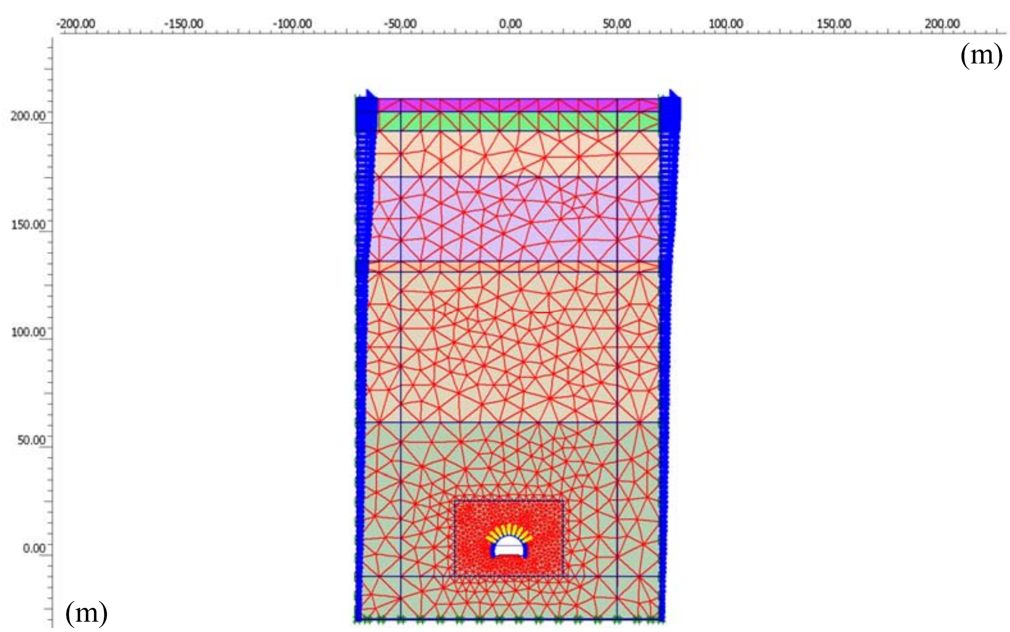

Figure H.8 Pseudo-static FE model for Section No.4 (Rock Class B1)

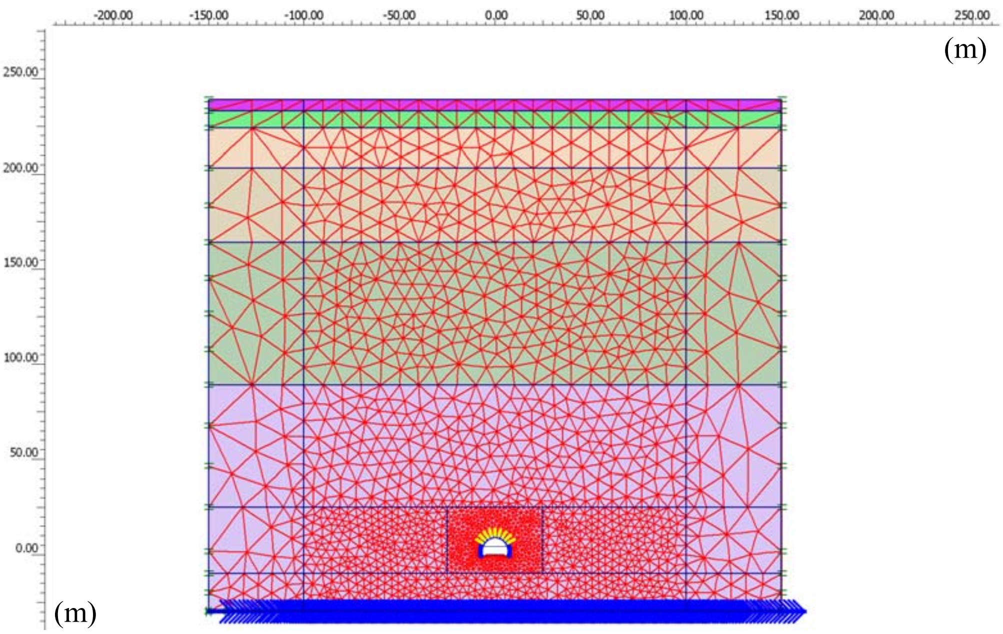

Figure H.9 Full-dynamic FE model for Section No.5 (Rock Class B1)

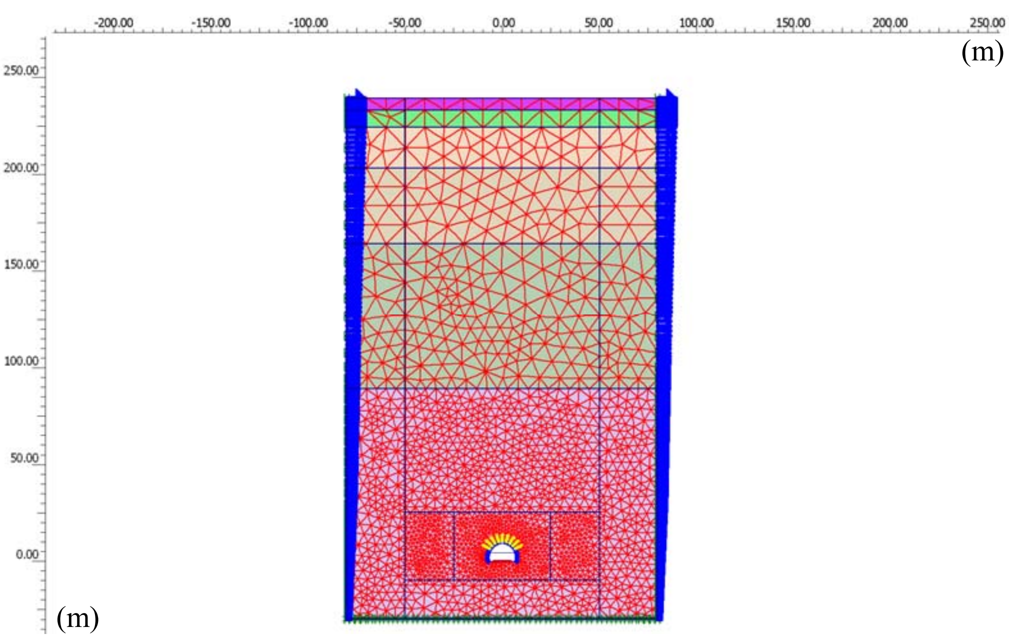

Figure H.10 Pseudo-static FE model for Section No.5 (Rock Class B1)

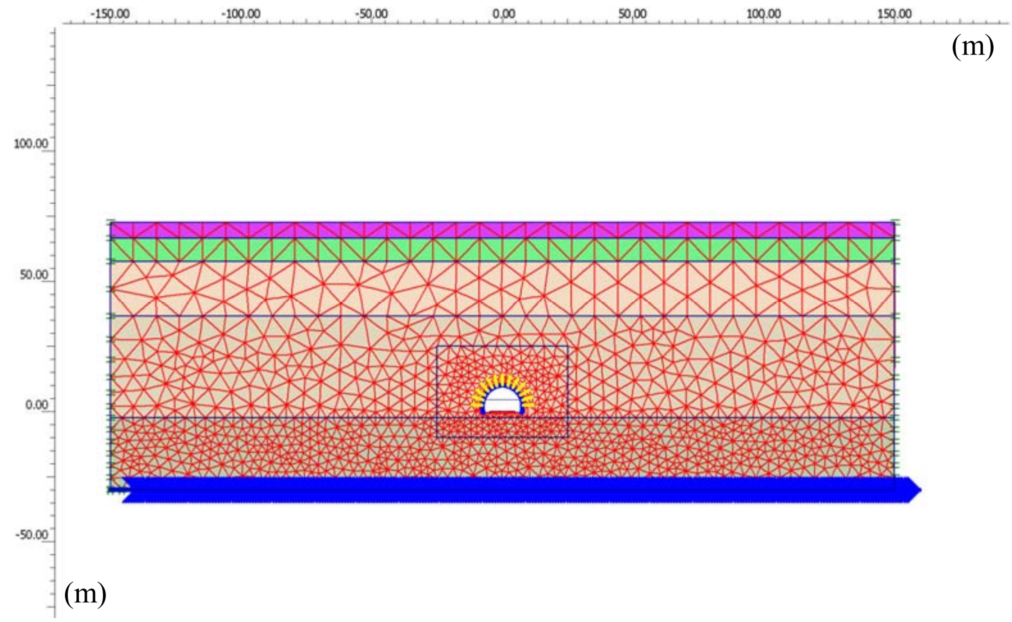

Figure H.11 Full-dynamic FE model for Section No.7 (Rock Class B2)

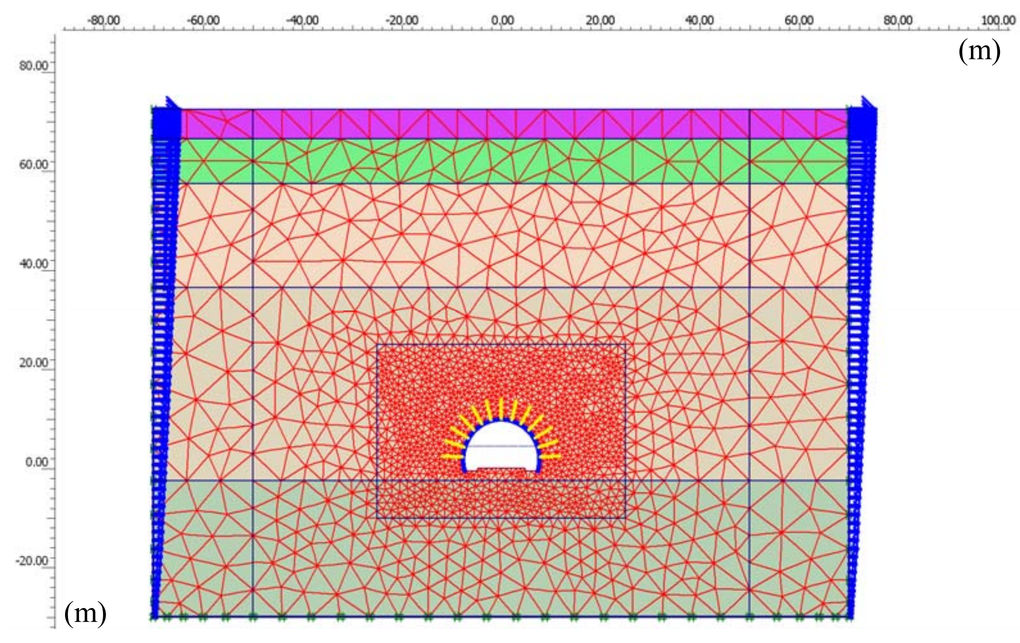

Figure H.12 Pseudo-static FE model for Section No.7 (Rock Class B2)

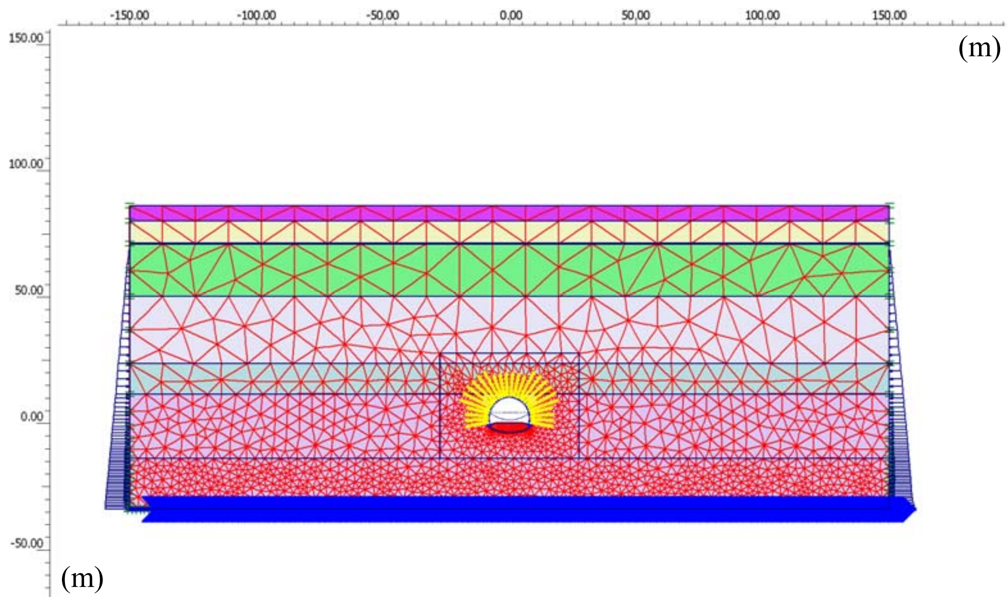

Figure H.13 Full-dynamic FE model for Section No.25 (Rock Class CM)

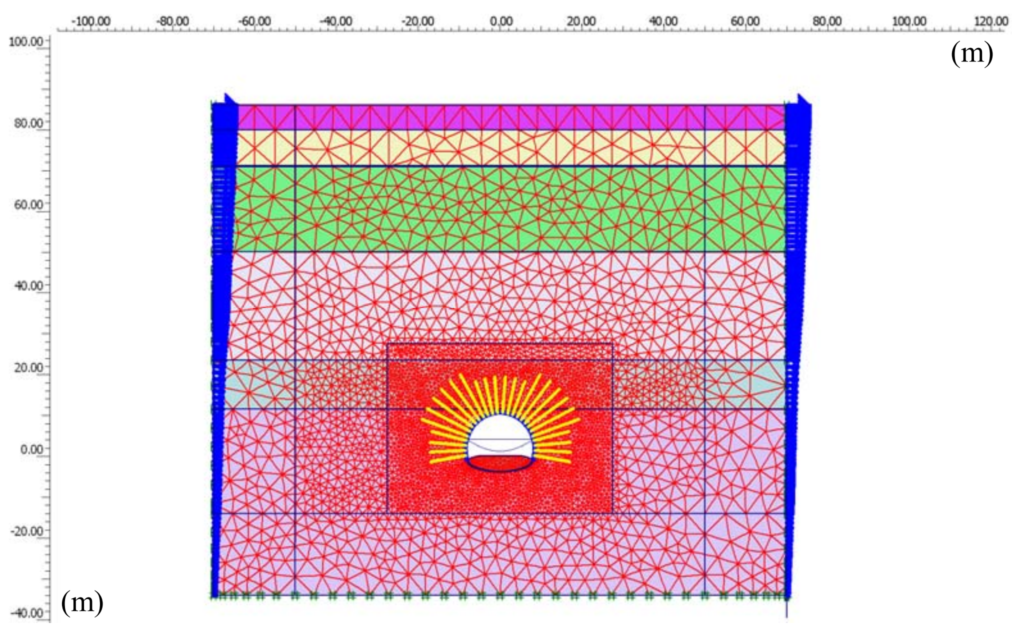

Figure H.14 Pseudo-static FE model for Section No.25 (Rock Class CM)

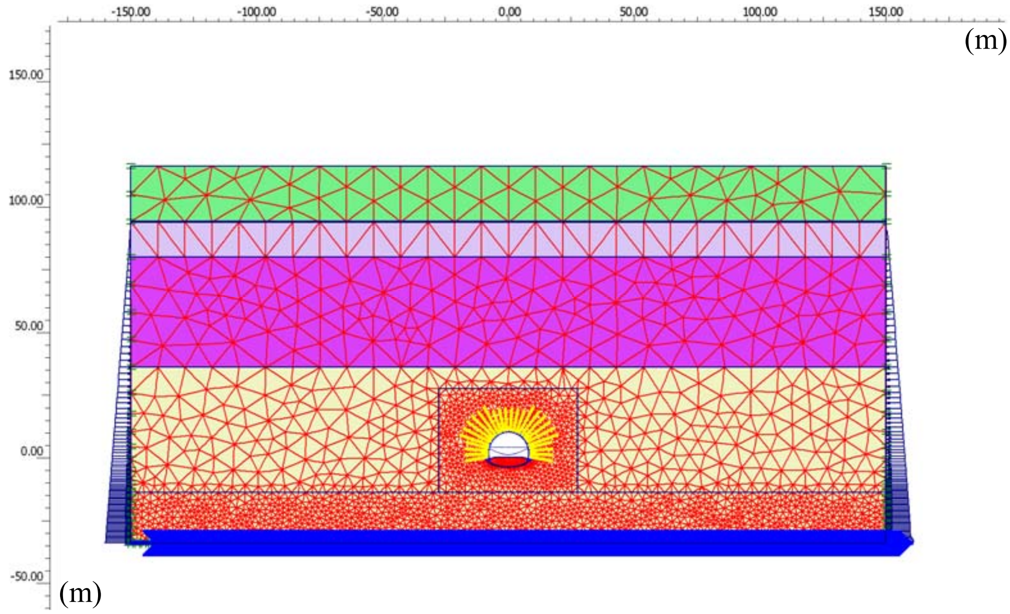

Figure H.15 Full-dynamic FE model for Section No.26 (Rock Class CM)

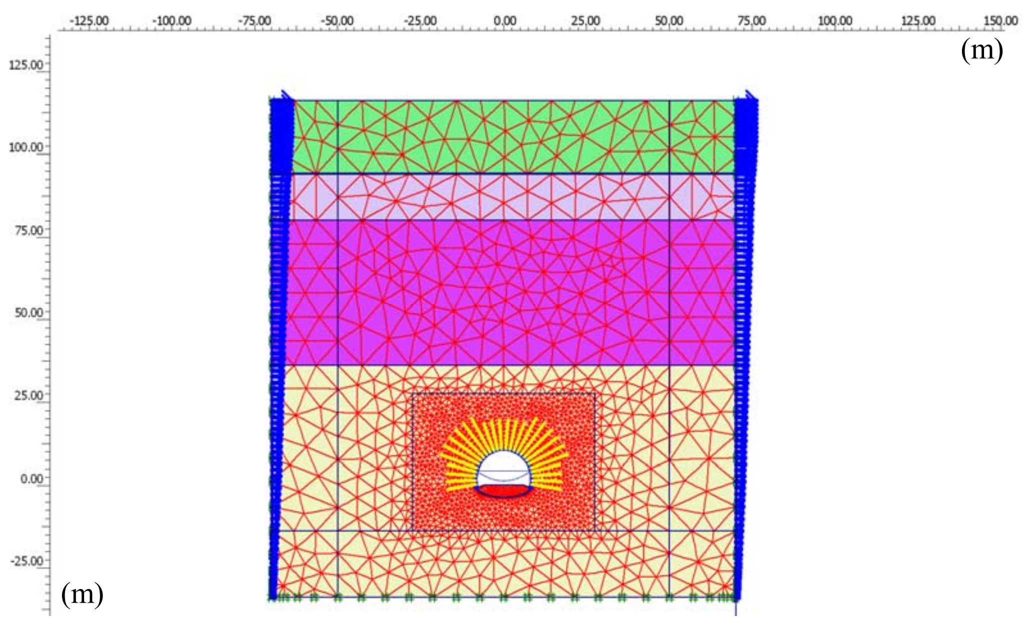

Figure H.16 Pseudo-static FE model for Section No.26 (Rock Class CM)

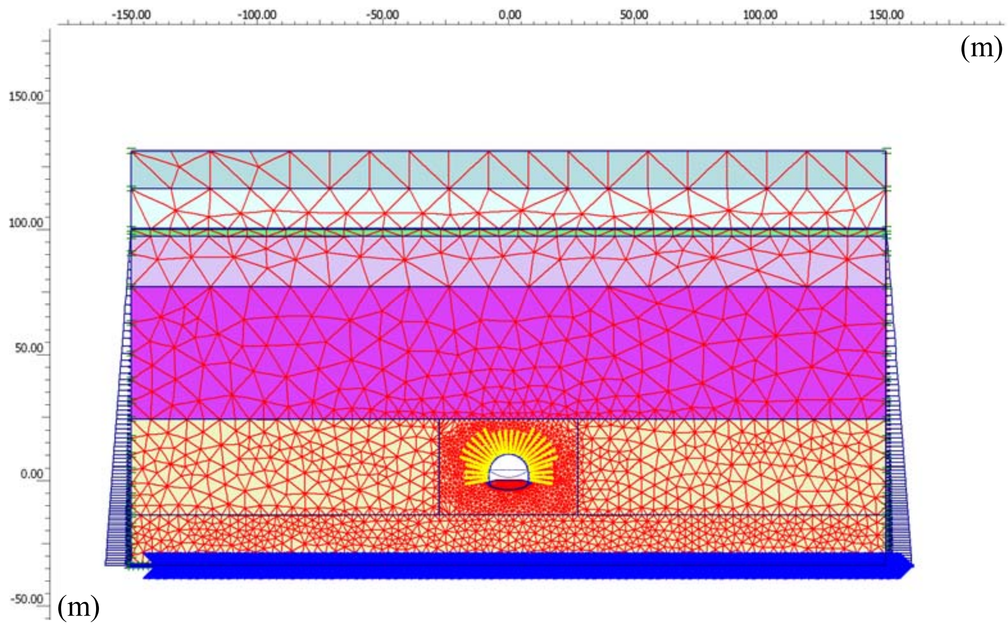

Figure H.17 Full-dynamic FE model for Section No.27 (Rock Class CM)

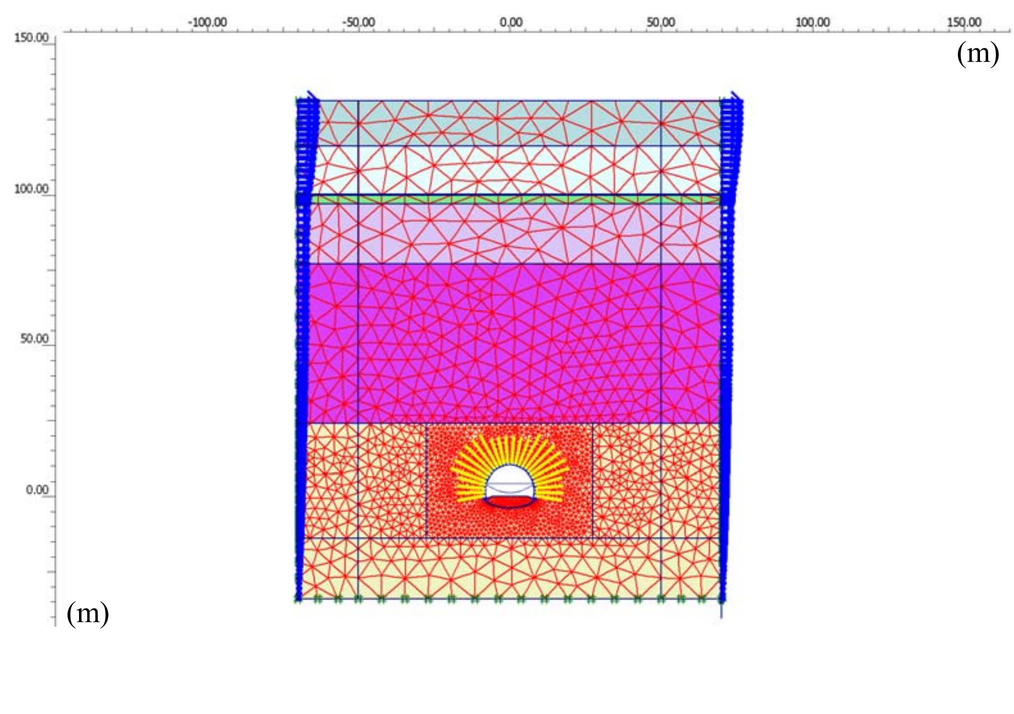

Figure H.18 Pseudo-static FE model for Section No.27 (Rock Class CM)

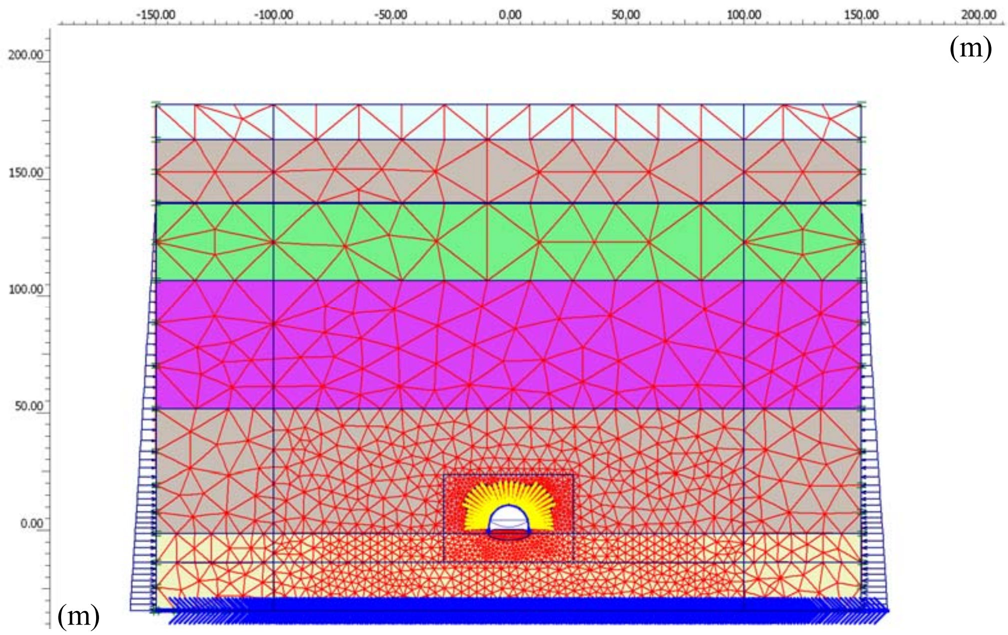

Figure H.19 Full-dynamic FE model for Section No.29 (Rock Class Option-3)

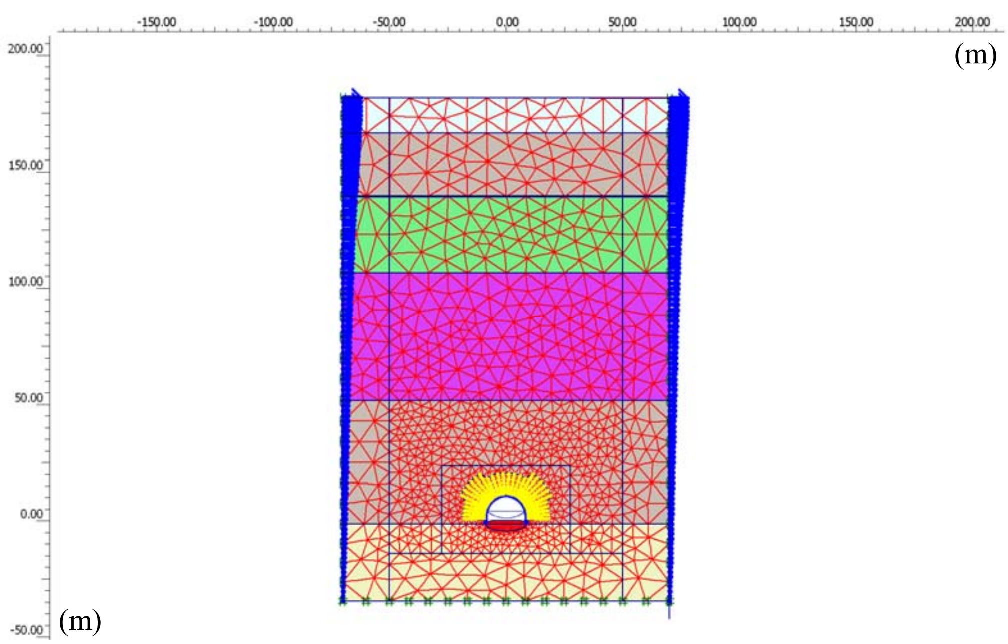

Figure H.20 Pseudo-static FE model for Section No.29 (Rock Class Option-3)

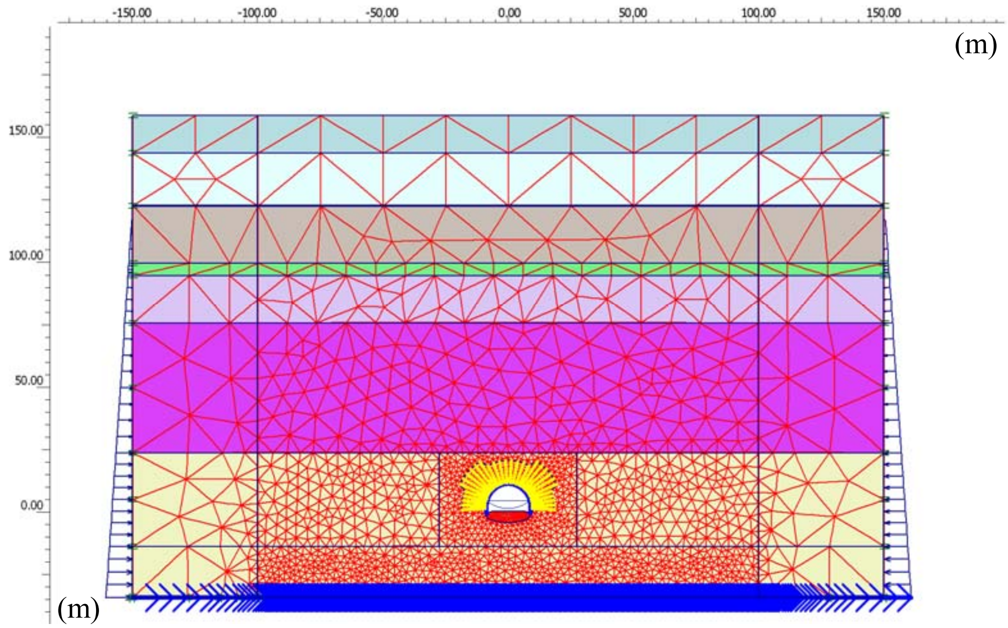

Figure H.21 Full-dynamic FE model for Section No.30 (Rock Class Option-3)

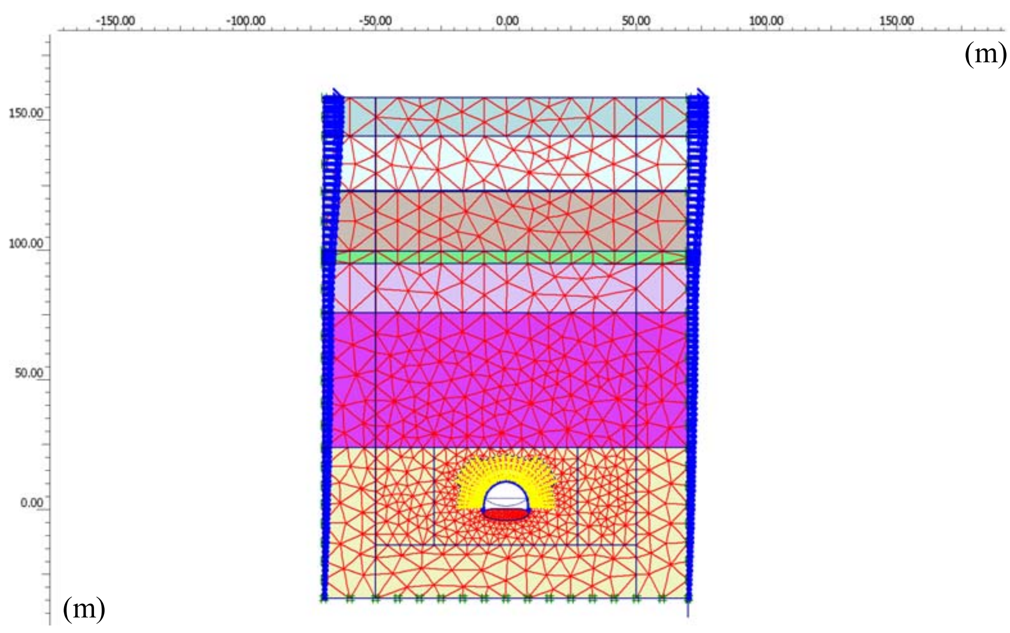

Figure H.22 Pseudo-static FE model for Section No.30 (Rock Class Option-3)

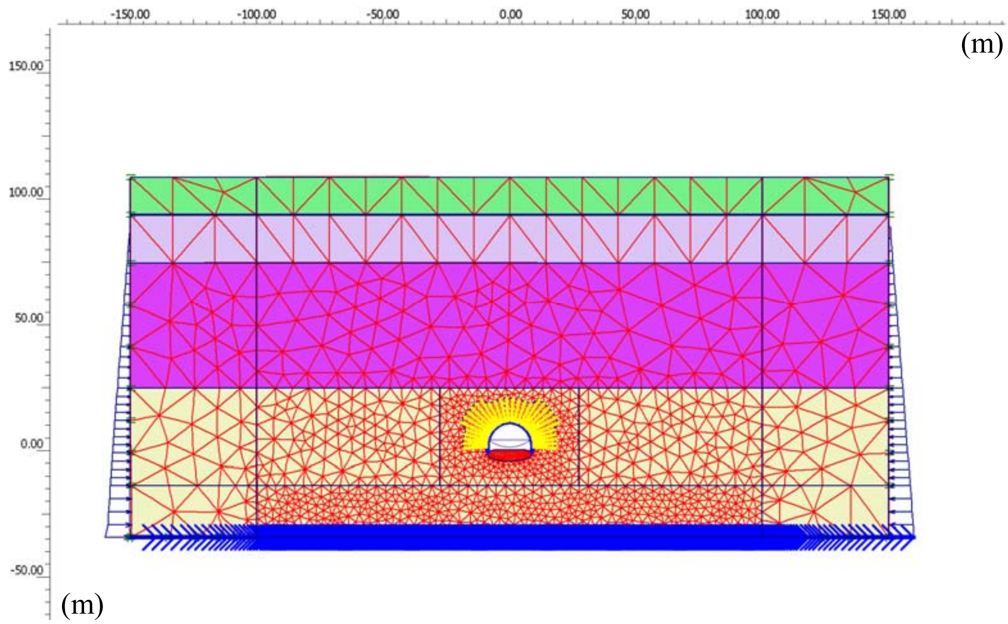

Figure H.23 Full-dynamic FE model for Section No.31 (Rock Class Option-3)

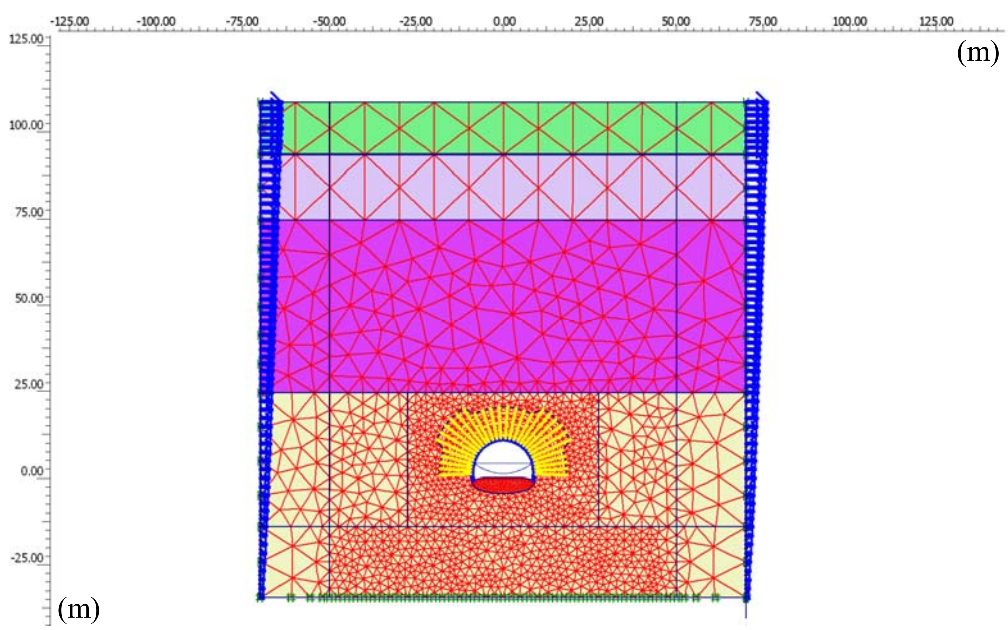

Figure H.24 Pseudo-static FE model for Section No.31 (Rock Class Option-3)

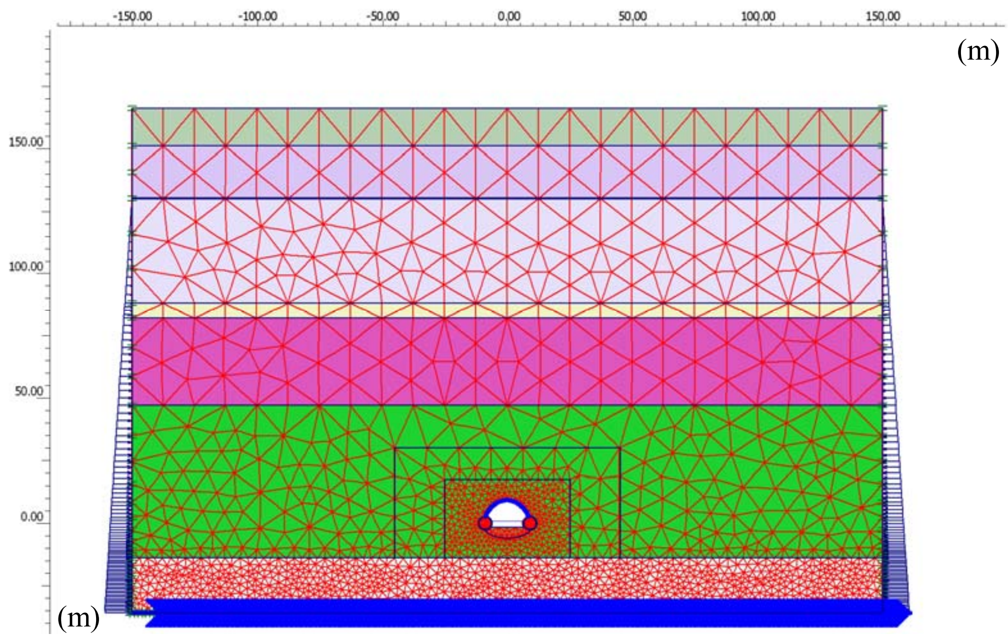

Figure H.25 Full-dynamic FE model for Section No.32 (Rock Class Option-4)

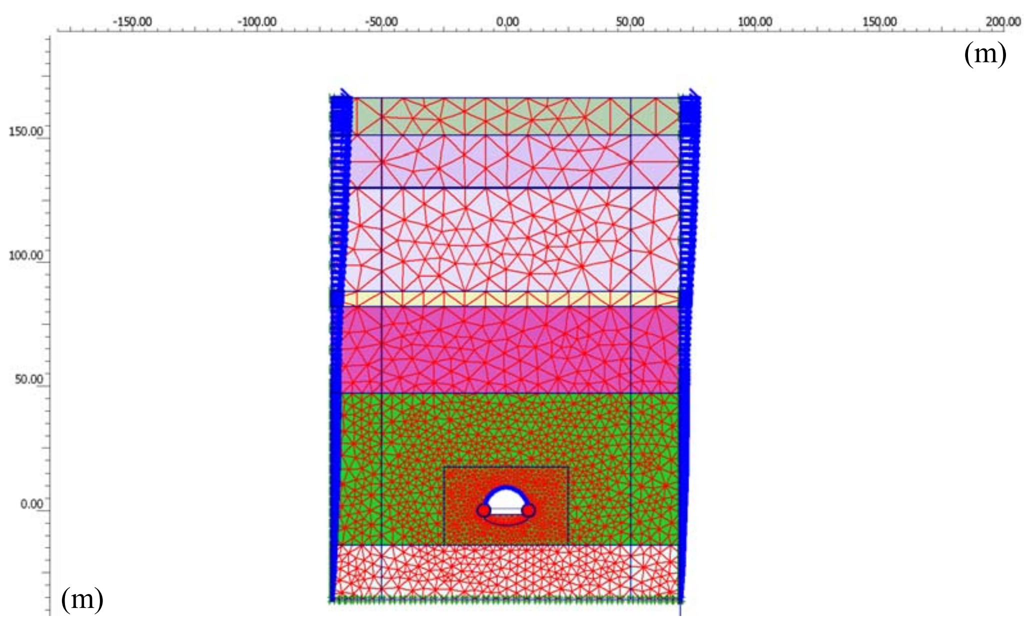

Figure H.26 Pseudo-static FE model for Section No.32 (Rock Class Option-4)

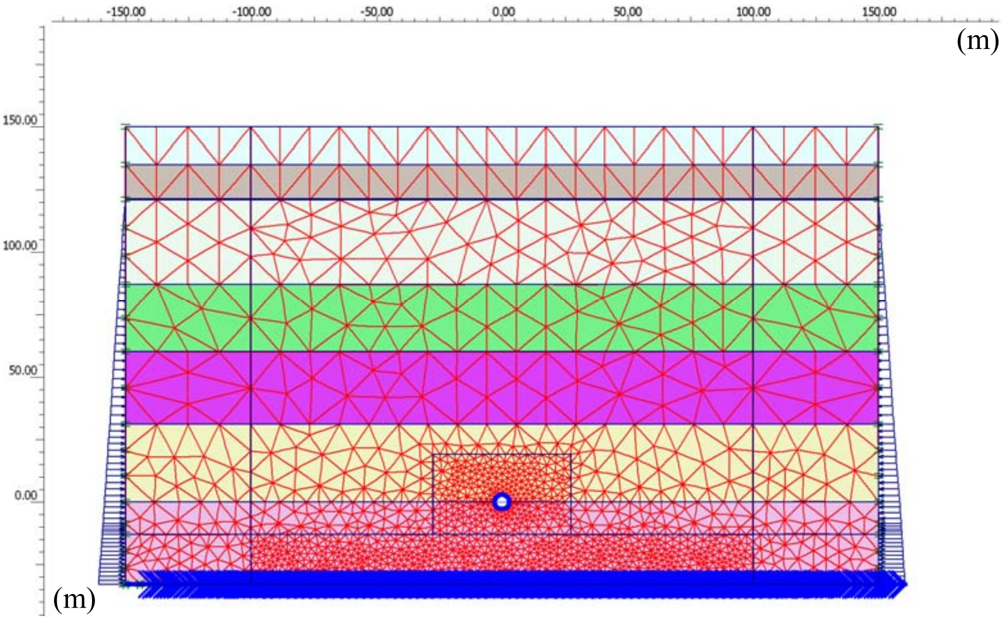

Figure H.27 Full-dynamic FE model for Section No.33 (Rock Class CM Pilot T.)

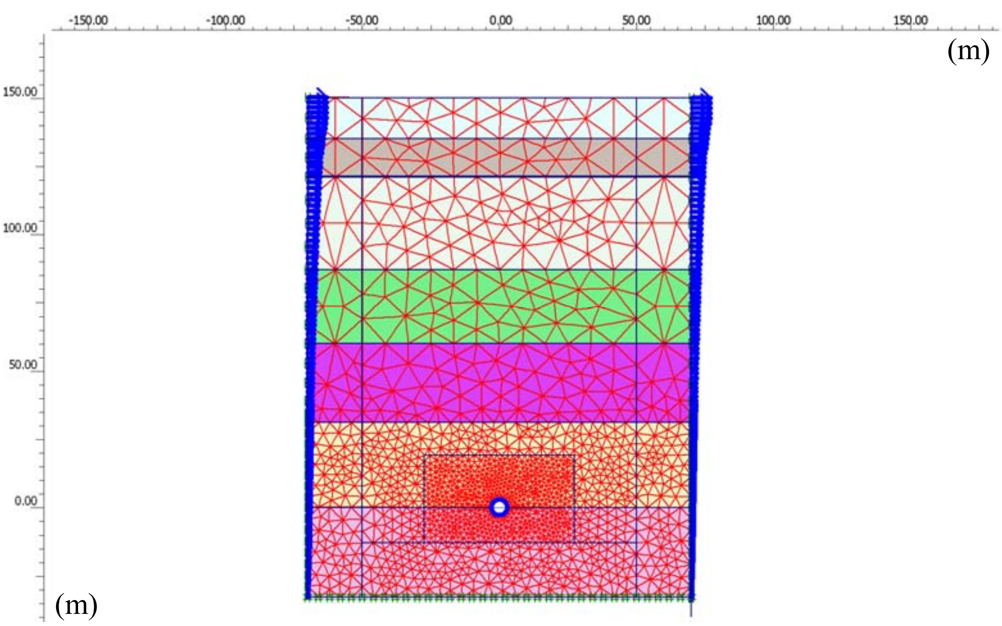

Figure H.28 Pseudo-static FE model for Section No.33 (Rock Class CM Pilot T.)

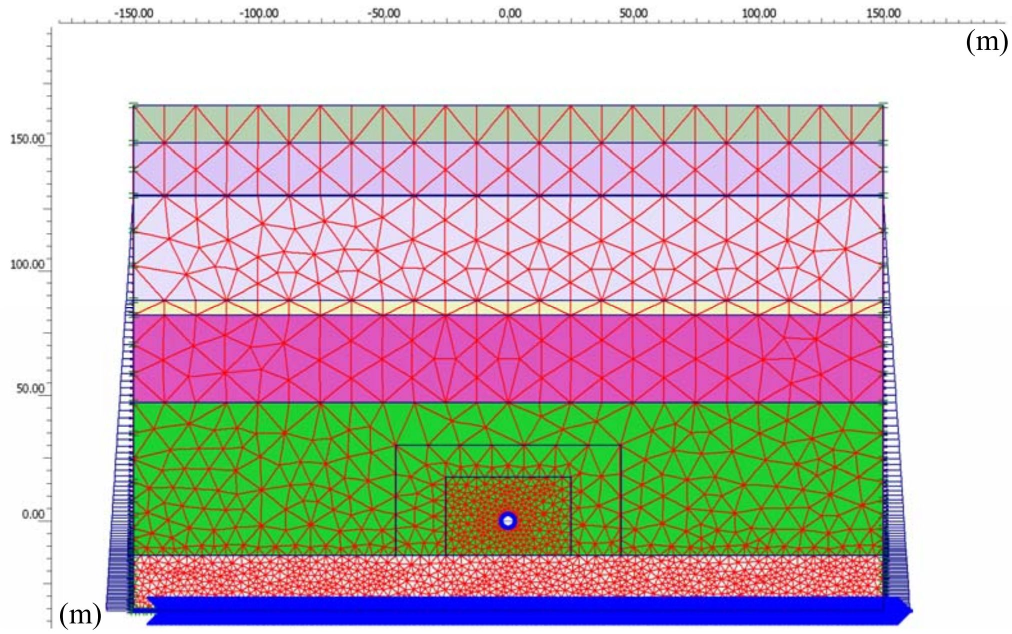

Figure H.29 Full-dynamic FE model for Section No.34 (Rock Class CM Pilot T.)

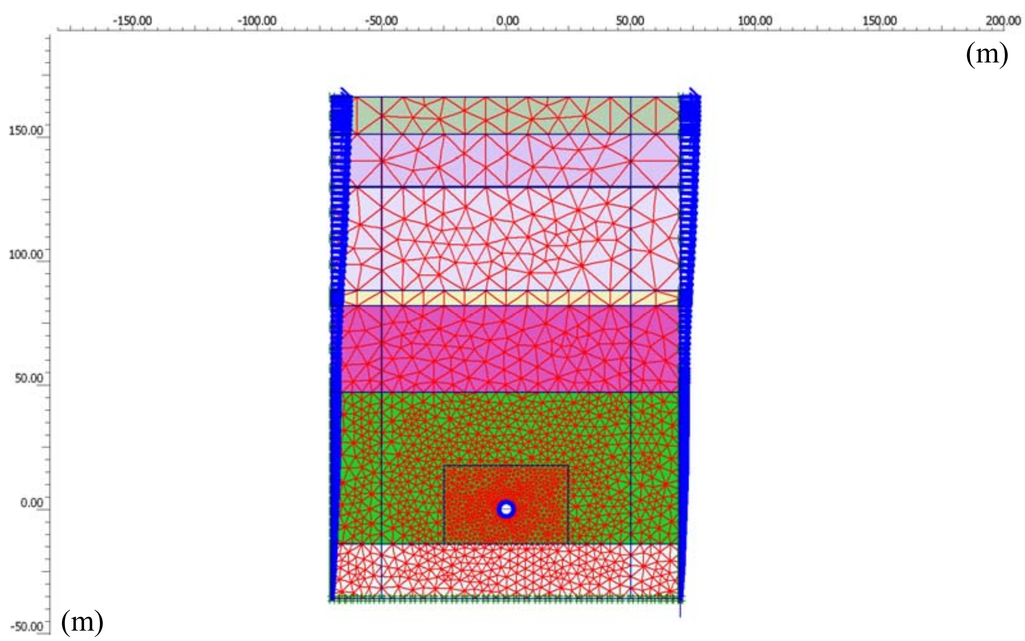

Figure H.30 Pseudo-static FE model for Section No.34 (Rock Class CM Pilot T.)

APPENDIX I

MOMENT INTERACTION DIAGRAMS

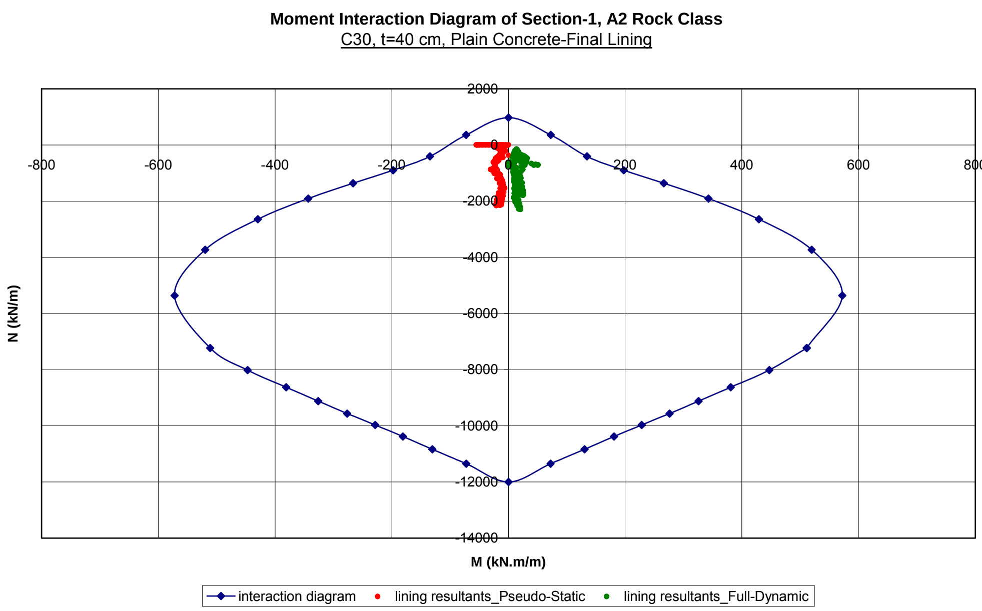

Figure I.1 Moment interaction diagram of Section No.1

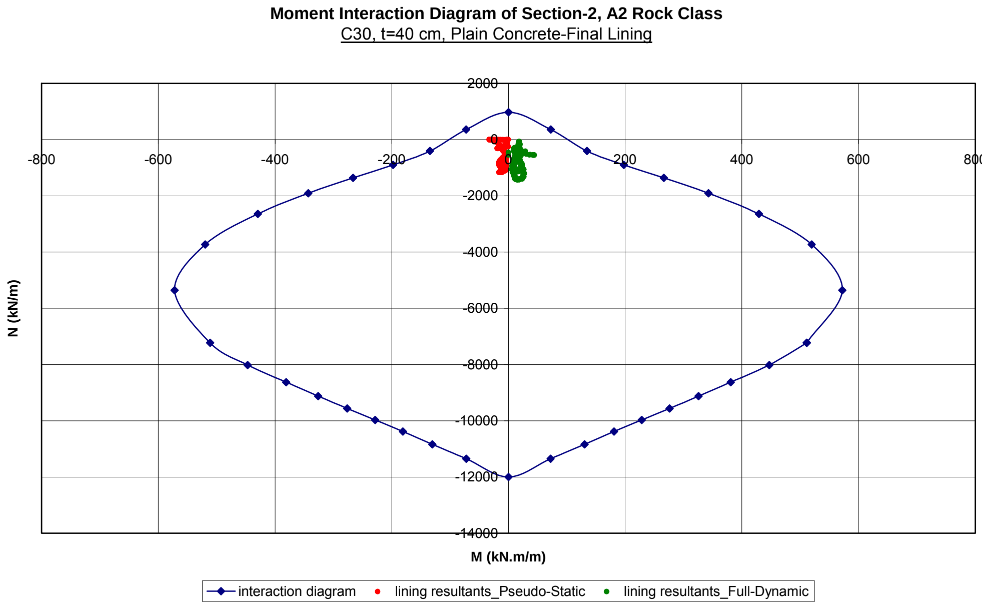

Figure I.2 Moment interaction diagram of Section No.2

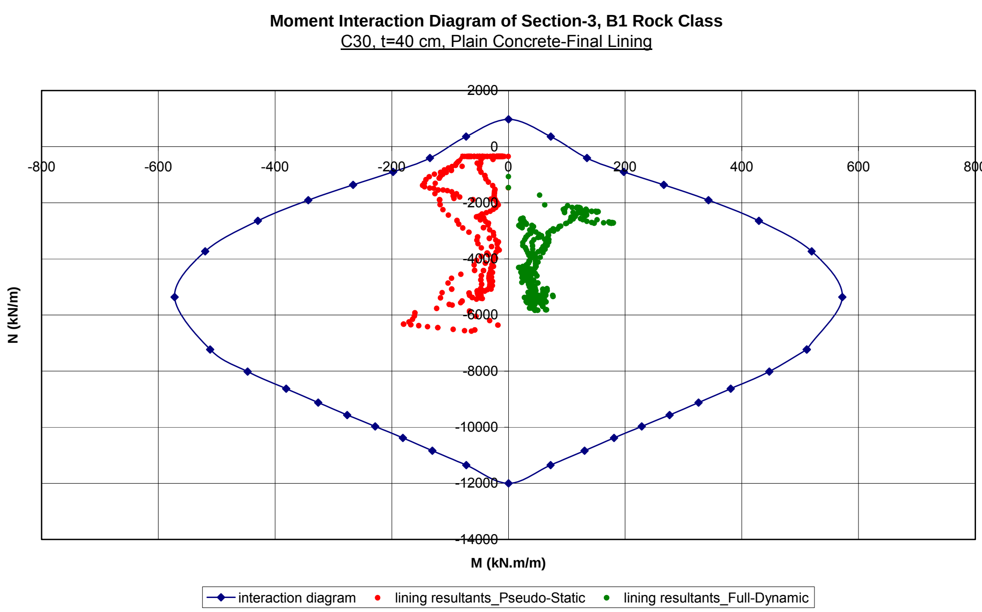

Figure I.3 Moment interaction diagram of Section No.3

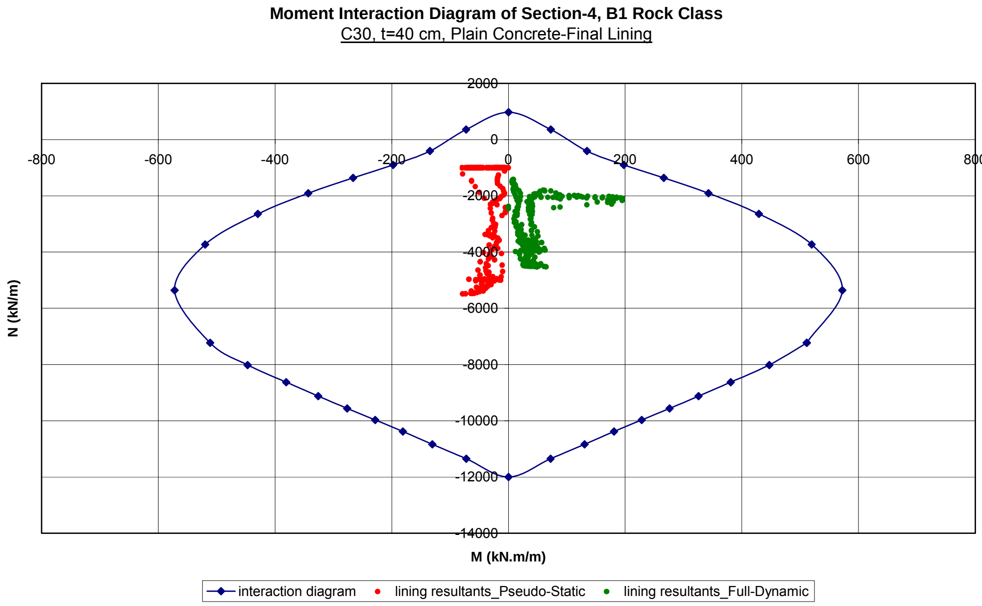

Figure I.4 Moment interaction diagram of Section No.4

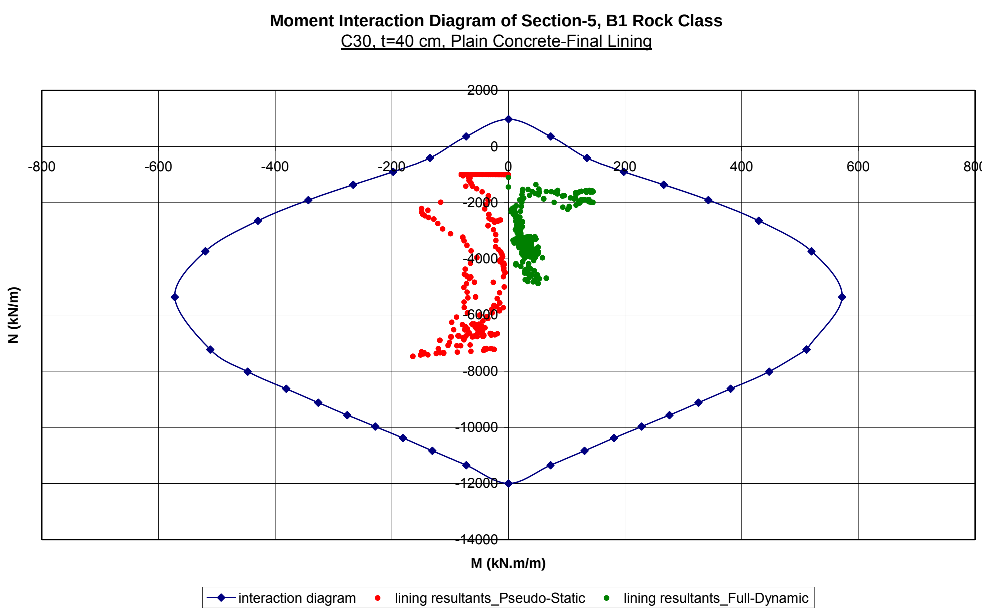

Figure I.5 Moment interaction diagram of Section No.5

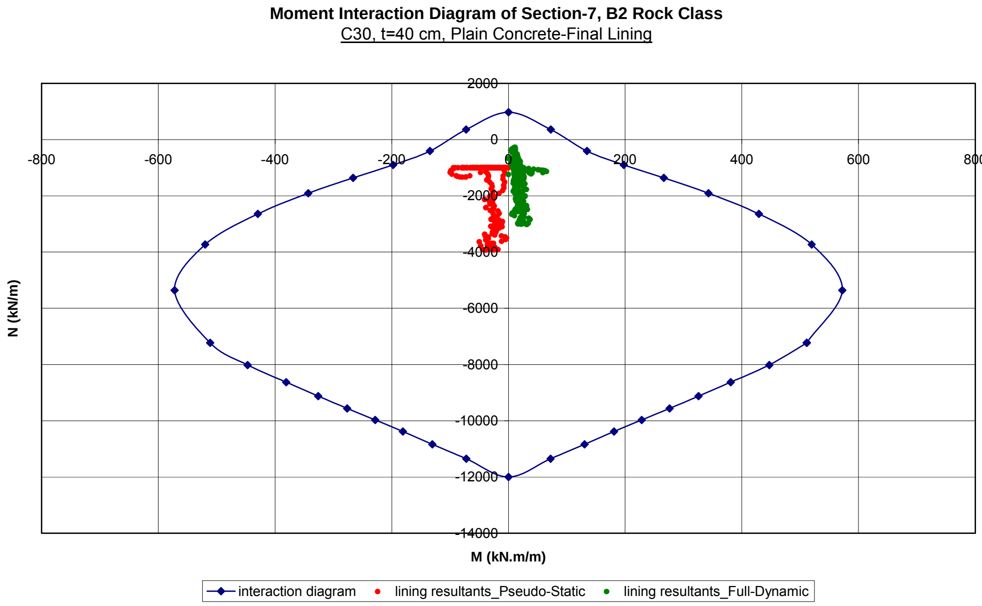

Figure I.6 Moment interaction diagram of Section No.7

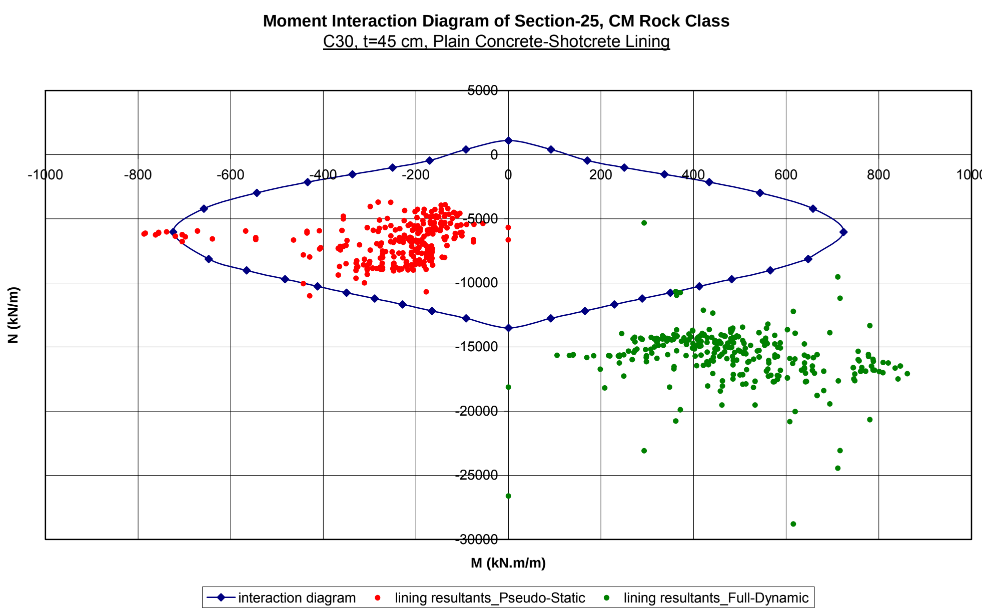

Figure I.7 Moment interaction diagram of Section No.25

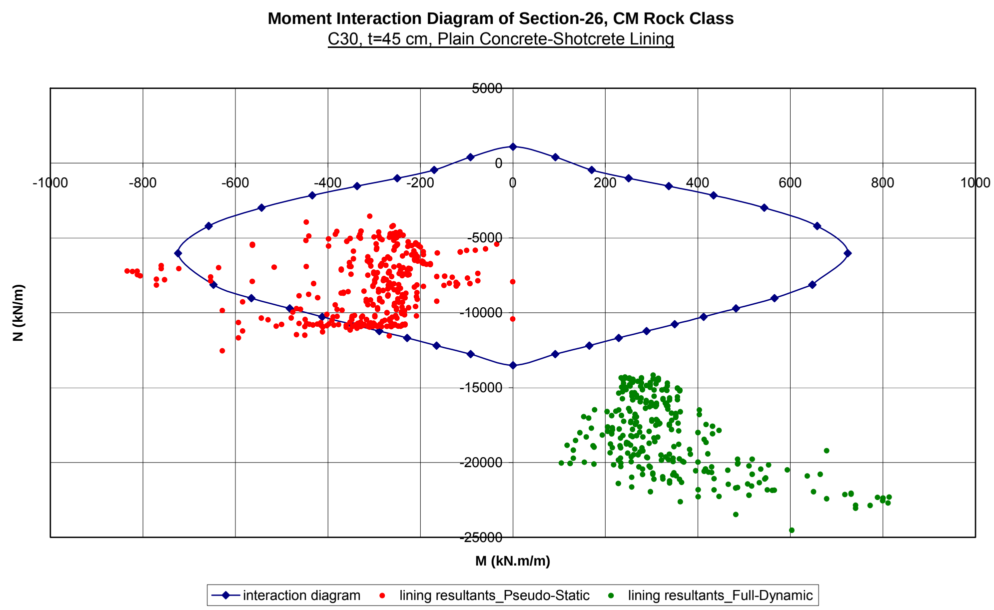

Figure I.8 Moment interaction diagram of Section No.26

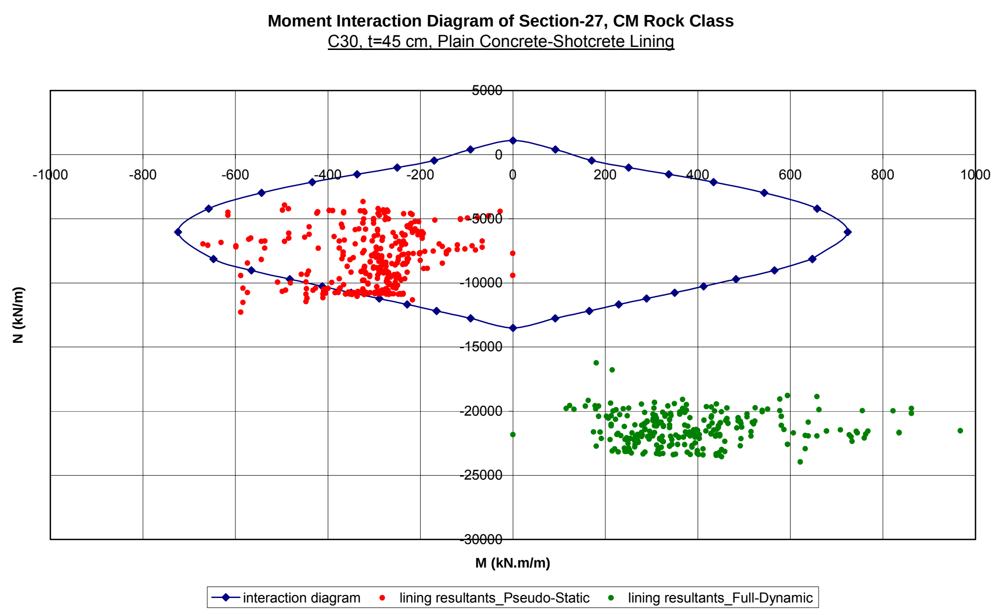

Figure I.9 Moment interaction diagram of Section No.27

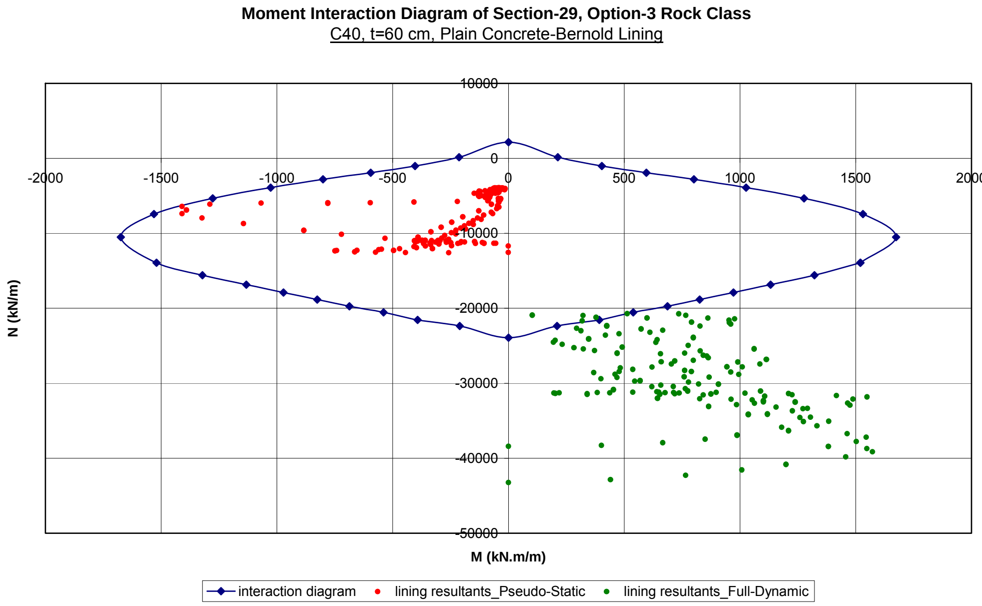

Figure I.10 Moment interaction diagram of Section No.29

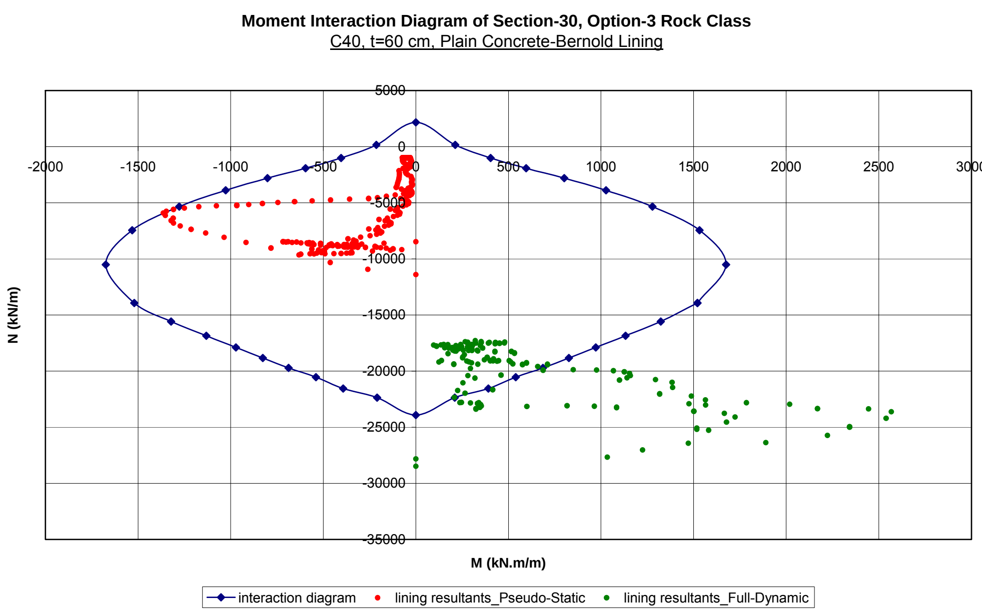

Figure I.11 Moment interaction diagram of Section No.30

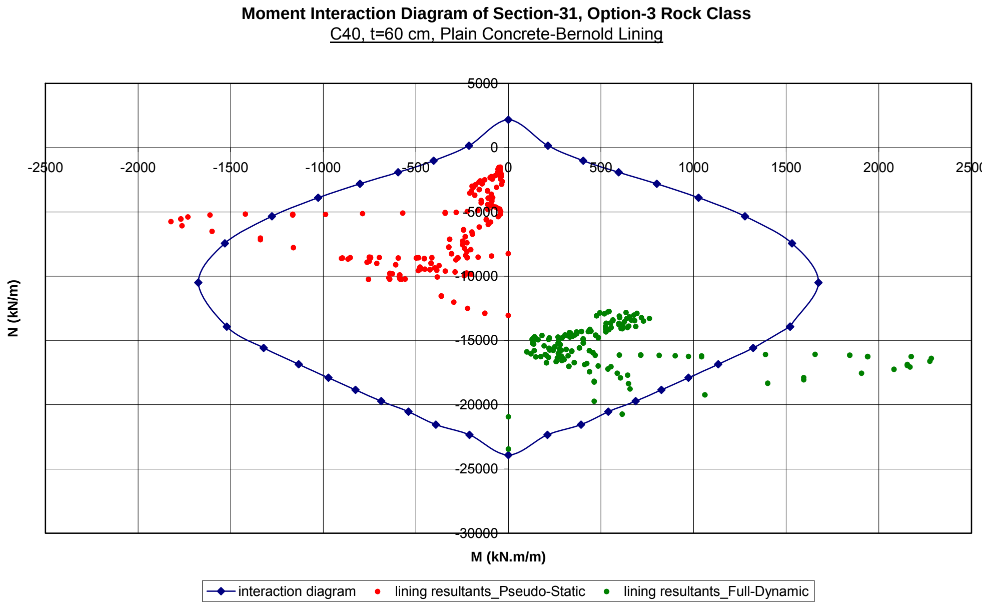

Figure I.12 Moment interaction diagram of Section No.31

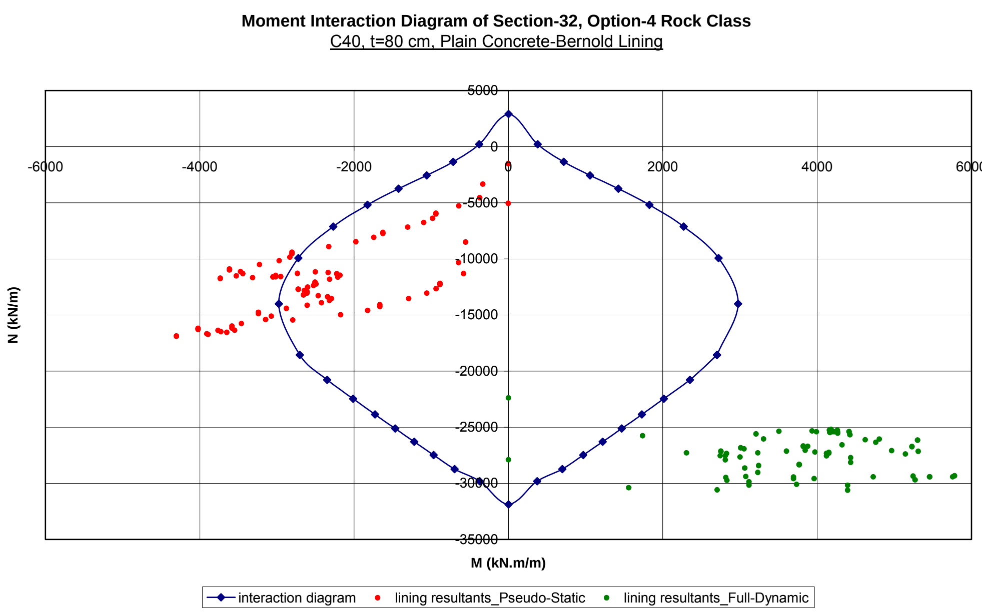

Figure I.13 Moment interaction diagram of Section No.32

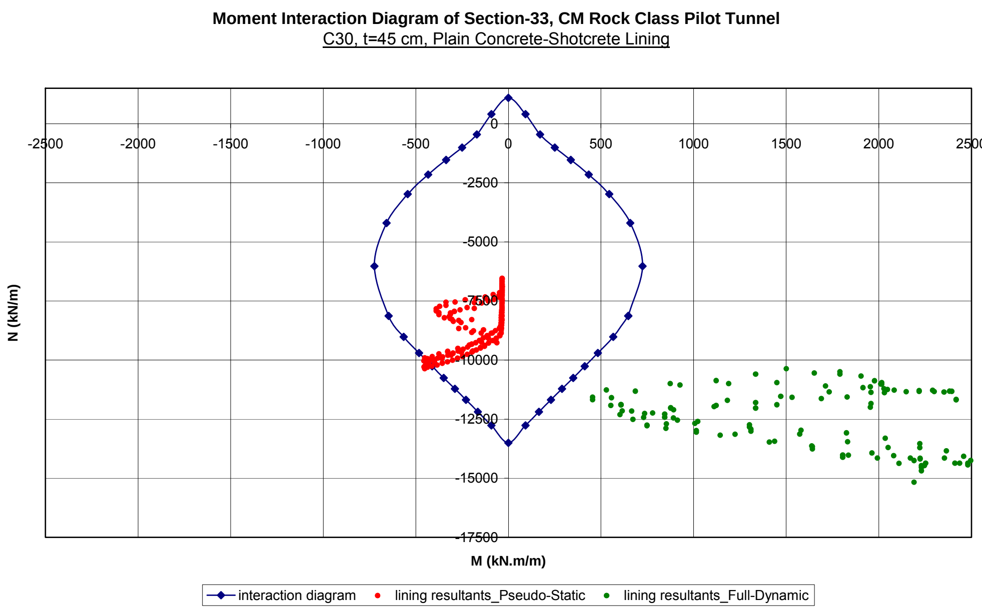

Figure I.14 Moment interaction diagram of Section No.33

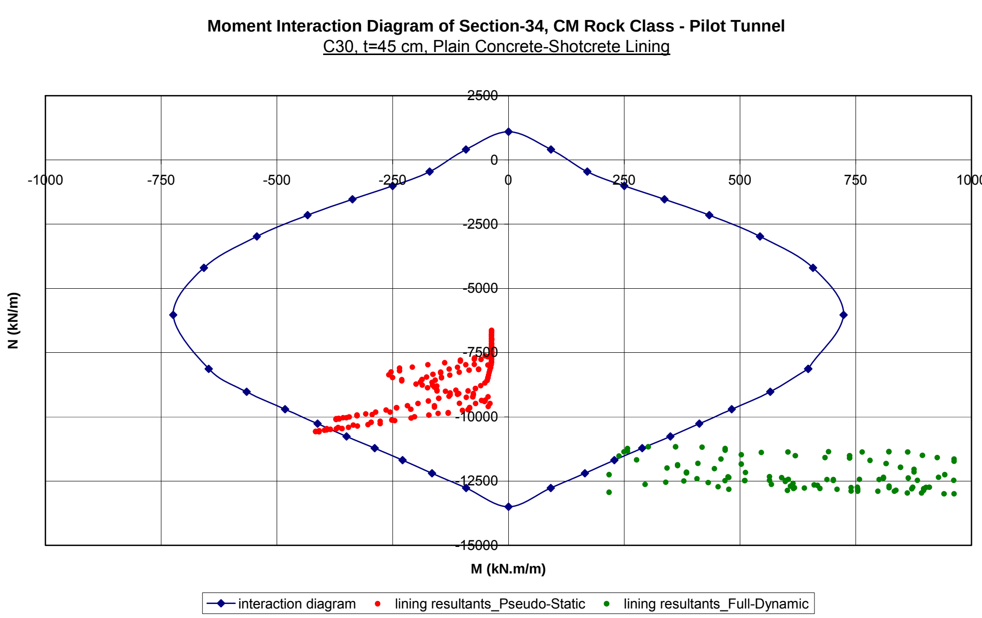

Figure I.15 Moment interaction diagram of Section No.34

APPENDIX J

FRAGILITY CALCULATIONS

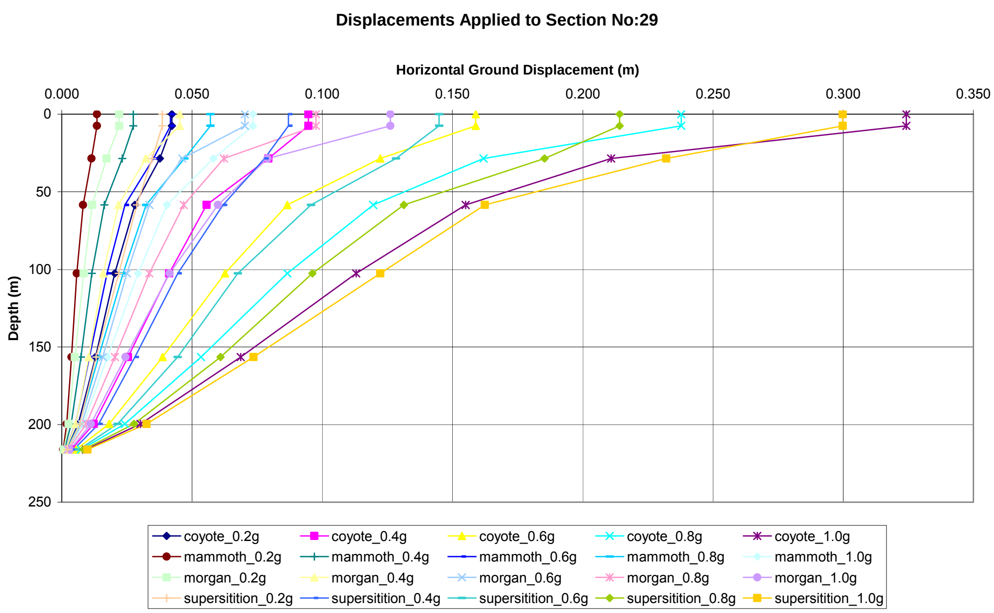

Figure J.1 Displacements calculated using 1-D site response analysis that are applied to Section No.29 for vulnerability assessment

Table J.1 Calculated damage indexes for Section No.29

Section-29

Earthquake		***Damage indexes according to PGAs of earthquakes*** 0.2g	0.4g	0.6g	0.8g	1.0g
Supersitition	DI(M_{eq}/M_{rd})	0.32	0.71	1.01	1.50	1.78
Mammoth_Lake		0.19	0.25	0.33	0.38	0.47
Morgan_Hills		0.23	0.29	0.47	0.53	0.64
Coyote		0.32	0.83	1.22	1.69	1.78

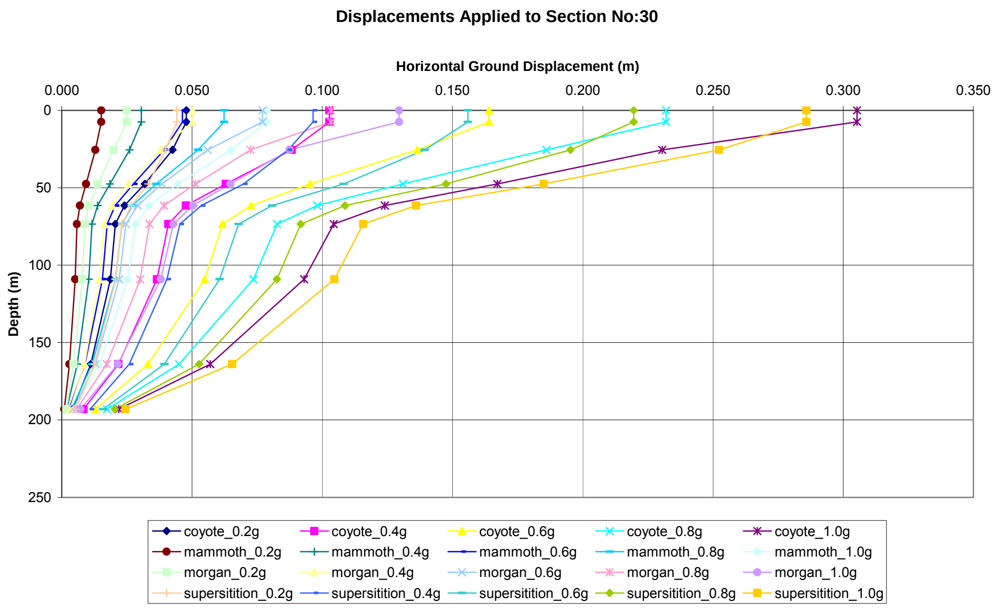

Figure J.2 Displacements calculated using 1-D site response analysis that are applied to Section No.30 for vulnerability assessment

Table J.2 Calculated damage indexes for Section No.30

		Section-30				
		Damage indexes according to PGAs of earthquakes				
Earthquake		**0.2g**	**0.4g**	**0.6g**	**0.8g**	**1.0g**
Supersitition	**DI(M_{eq}/M_{rd})**	0.23	0.63	0.96	1.33	1.69
Mammoth_Lake		0.12	0.17	0.20	0.26	0.29
Morgan_Hills		0.16	0.22	0.24	0.44	0.65
Coyote		0.24	0.63	0.97	1.43	1.84

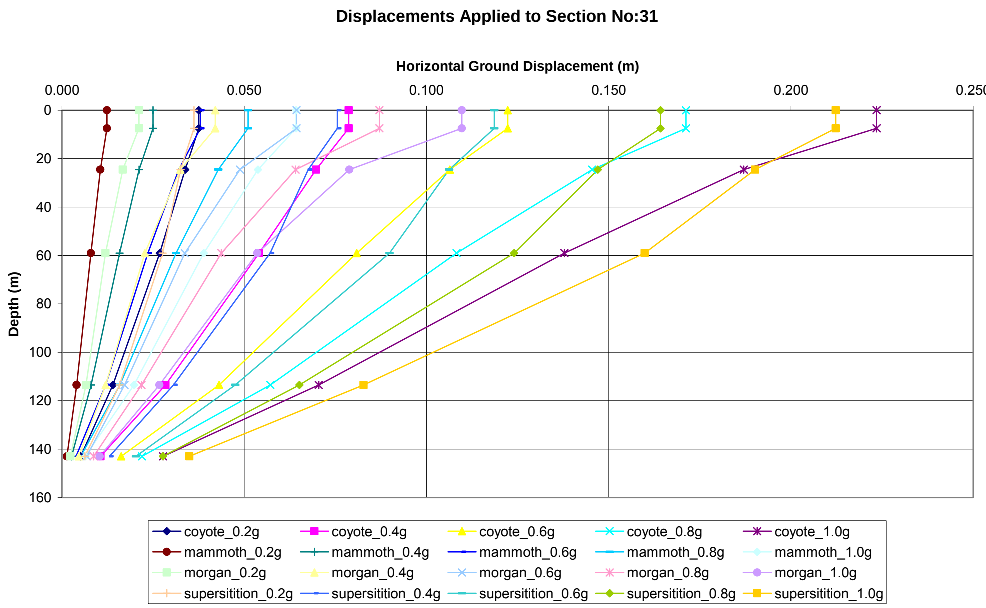

Figure J.3 Displacements calculated using 1-D site response analysis that are applied to Section No.31 for vulnerability assessment

Table J.3 Calculated damage indexes for Section No.31

		Section-31				
		Damage indexes according to PGAs of earthquakes				
Earthquake		**0.2g**	**0.4g**	**0.6g**	**0.8g**	**1.0g**
Supersitition	**DI(M_{eq}/M_{rd})**	0.32	0.89	1.29	1.65	1.95
Mammoth_Lake		0.17	0.18	0.28	0.40	0.57
Morgan_Hills		0.20	0.26	0.48	0.68	0.84
Coyote		0.36	0.89	1.20	1.56	1.90

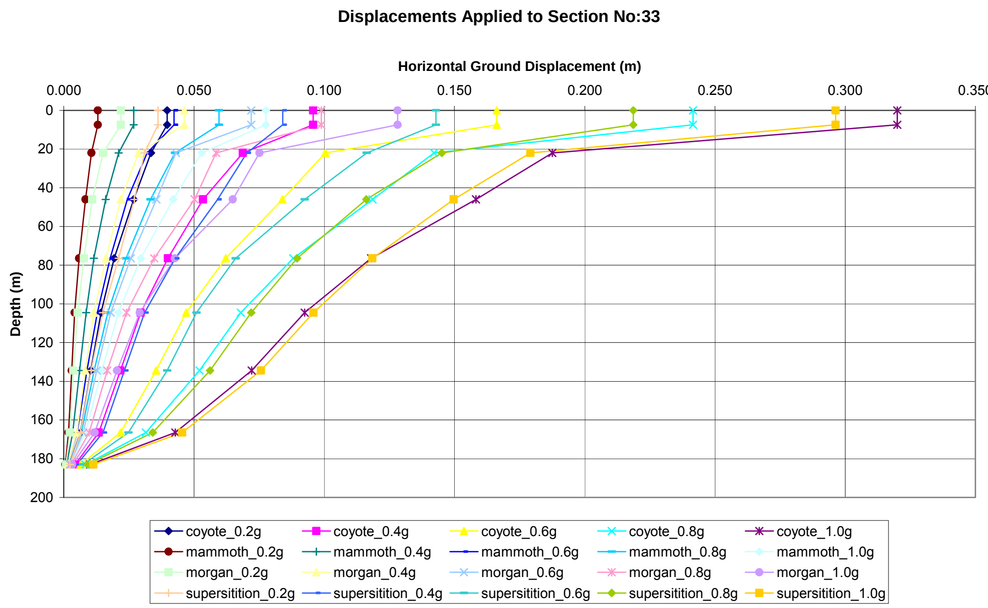

Figure J.4 Displacements calculated using 1-D site response analysis that are applied to Section No.33 for vulnerability assessment

Table J.4 Calculated damage indexes for Section No.33

		Section-33				
		Damage indexes according to PGAs of earthquakes				
Earthquake		**0.2g**	**0.4g**	**0.6g**	**0.8g**	**1.0g**
Supersitition	**DI(M_{eq}/M_{rd})**	0.10	0.38	2.00	3.92	5.72
Mammoth_Lake		0.06	0.07	0.09	0.11	0.13
Morgan_Hills		0.06	0.07	0.09	0.16	0.27
Coyote		0.09	0.40	1.83	5.00	6.70

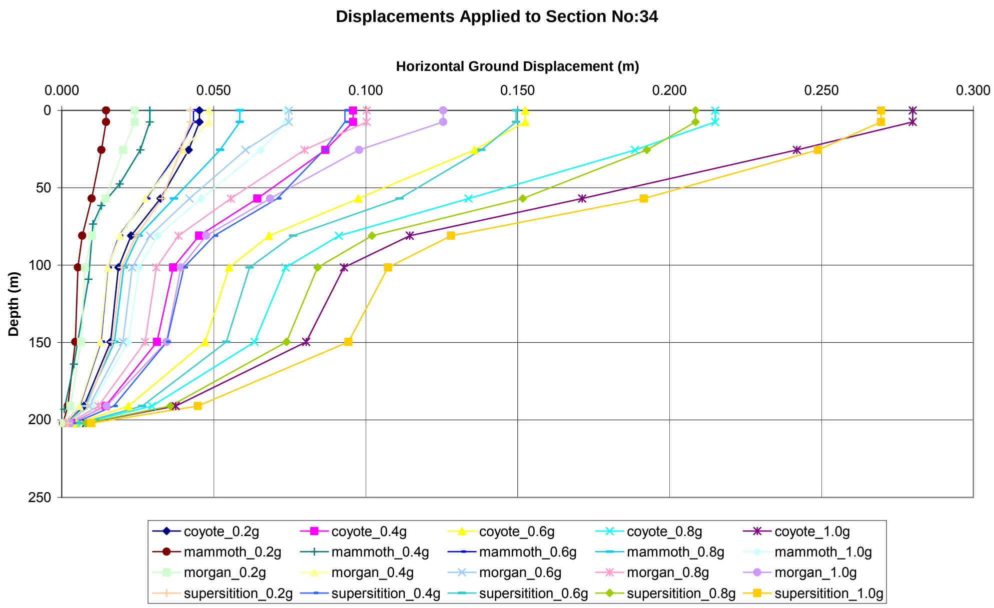

Figure J.5 Displacements calculated using 1-D site response analysis that are applied to Section No.34 for vulnerability assessment

Table J.5 Calculated damage indexes for Section No.34

		Section-34				
		Damage indexes according to PGAs of earthquakes				
Earthquake		**0.2g**	**0.4g**	**0.6g**	**0.8g**	**1.0g**
Supersitition	**DI(M_{eq}/M_{rd})**	0.11	0.24	1.00	3.10	5.85
Mammoth_Lake		0.06	0.08	0.09	0.11	0.13
Morgan_Hills		0.06	0.09	0.11	0.17	0.03
Coyote		0.09	0.31	1.43	3.20	6.00

APPENDIX K

EXAMPLE DAMAGE INVENTORY

Table K.1. Properties of tunnels which hit by earthquakes (after ALA, 2001)

ID	Earthquake	Name of Tunnel	Location	Use	Length (m)	Cross Section Width x Height (m)	Liner System	Liner Thickness (cm)	Geological Feature	Cover (m)
1	1923 Kanto	Hakone No. 1 (up)	Yamakita-Yaga	RR	284.7	4.3 x 4.7	4	34 - 57	marlstone, soil	
		(down)	(on Tokaido [Gotemba] Line)		285.2	4.6 x 5.0	4	23 - 46		
2	1923 Kanto	Hakone No. 3 (up)	Yamakita-Yaga	RR	312.0	4.3 x 4.7	4	23 - 57		4 - 47
		(down)	(on Tokaido [Gotemba] Line)		318.1	4.6 x 5.0	4	23 - 46		
3	1923 Kanto	Hakone No. 4 (up)	Yamakita-Yaga	RR	269.9	4.3 x 4.7	4	23 - 57		4 - 53
		(down)	(on Tokaido [Gotemba] Line)		306.8	4.6 x 5.0	4	23 - 57		
4	1923 Kanto	Hakone No. 7 (up)	Yaga – Surugaoyama	RR	211.2	4.6 x 5.0	4	34 - 46		
		(down)	(on Tokaido [Gotemba] Line)		232.9	4.3 x 4.7	4	34 - 57		
5	1923 Kanto	Nagoe (up)	Kamakura – Zushi	RR	442.6	4.9 x 6.0	4-5	34 - 46	mudstone	
		(down)	(on Yokosuka Line)		344.3	4.3 x 5.6	4-5	23 - 57		
6	1923 Kanto	Komine	Odawara – Hayakawa	RR	260.5	9.1 x 6.0 (box)	4-5	126 - 137	soil	1 - 17
			(on Atami Tokaido] Line)			8.5 x 6.9 (tube)				
7	1923 Kanto	Fudoyama	Hayakawa – Nebukawa	RR	100.6	8.7 x 6.9	4-5	69 - 114	red agglomerate	4 - 20
			(on Atami Tokaido Line)							
8	1923 Kanto	Nenoueyama	Hayakawa – Nebukawa	RR	105.6	8.7 x 6.9	4-5	91	black agglomerate,	12 - 17
			(on Atami Tokaido Line)						pyroxene andesite	
9	1923 Kanto	Komekamiyama	Hayakawa – Nebukawa	RR	278.6	8.7 x 6.9	4-5	57 - 103	pyroxene andesite,	2 - 51
			(on Atami Tokaido Line)						agglomerate, volcanic ash	
10	1923 Kanto	Shimomakiyayama	Hayakawa – Nebukawa	RR	160.9	8.7 x 6.9	4-5	69 - 103	pyroxene andesite,	14 - 31
			(on Ataini [Tokaido] Line)						volcanic ash	
11	1923 Kanto	Happonmatan	Nebukawa – Manazurn	RR	76.4	8.7 x 6.9	4-5	69 - 91	loose agglomerate	< 17
			(on Atami [Tokaido] Line)							
12	1923 Kanto	Nagasakayama	Nebukawa – Manazurn	RR	673.9	8.5 x 6.9	4-5	57 - 91	agglomerate	11 - 94
			(on Atami Tokaido] Line)							
13	1923 Kanto	Yose	Sagainiko – Fujino	RR	292.6	4.6 x 5.0	4	46 - 69	soil	4 - 21
			(on Chuo Line)							

Table K.1 continued

ID	Earthquake	Name of Tunnel	Location	Use	Length (m)	Cross Section Width x Height (m)	Liner System	Liner Thickness (cm)	Geological Feature	Cover (m)
14	1923 Kanto	Toke	Toke – Ohami (on Boso [Sotobo] Line)	RR	353.3	4.3 x 4.5	4	34 - 46	mudstone	12 - 20
15	1923 Kanto	Namuya	Iwal – Tomiura (on Hojo [Uchibo] Line)	RR	740.3	4.9 x 6.0	4-5	30 - 57	shale, tuffite	9 - 70
16	1923 Kanto	Mineokayama	Futorni - Awakamogawa (on Awa [Uchibo] Line)	RR	772.5	4.9 x 6.0	4	30 - 47	sandstone, shale, gabbro	
17	1930 Kita-Izu	Tanna	Atami – Kannami (on Atami [Tokaido] Line)	RR	7804.0	8.5 x 6.4	4-5	32 - 136	amdesite, agglomerate	
18	1961 Kita-Mino	I Power Plant	upperstream of Tedori River	WT	2538.0	2.1 x 2.2 2.4 x 2.45	5 5	20 - 40 20 - 40	sandstone, soil	
19	1964 Niigata	Budo	Murakami – Buya (on Route 7)	HW	320.0	8.6 x 5.8	5	50 - 60	rhyolite, talus, perlite clay	
20	1964 Niigata	Terasaka	Nezugaseki - Koiwagawa (on Uetsu Line)	RR	79.4		4-5	47 - 107	soft mudstone	
21	1964 Niigata	Nezugaseki	Nezugaseki - Koiwagawa (on Uetsu Line)	RR	104.0				soft mudstone	
22	1968 Tokachi-oki	Otofuke	Nukabira – Horoka (on Shihoro Line)	RR	165.0	4.8 x 5.2	4-5	25 - 60	tuff	< 50
23	1978 Izu-Oshima-kinkai	Inatori	Inatori – haihatna (on Izu-kyuko Une)	RR	906.0	4.4 x 5.1	5	40 - 70	metamorphic andesite solfataric clay	< 90
24	1978 Izu-Oshima-kinkai	Okawa	Okawa – Hokkawa (on Izu-kyuko Une)	RR	1219.5				andesite, fault clay	
25	1978 Izu-Oshima-kinkai	Atagawa	Atagawa - Kataseshirata (on Izu-kyuko Une)	RR	1277.0				andesite, solfararic clay	
26	1978 Izu-Oshima-kinkai	Shiroyama	Imaihama – Kawazu (on Izu-kyuko Line)	RR						
27	1978 Izu-Oshima-kinkai	Tomoro	Shirata – Inatori (on Higashi-Izu Toll Road)	HW	425.5		5		andesite	

Table K.1 continued

ID	Earthquake	Name of Tunnel	Location	Use	Length (m)	Cross Section Width x Height (m)	Liner System	Liner Thickness (cm)	Geological Feature	Cover (m)
28	1978 Izu-Oshima-kinkai	Shirata	Shirata – Inatori (on Route 135)	HW	88.7				audesite	
29	1978 Izu-Oshima-kinkai	Joto	Shirata - Inatori (on Route 135)	HW	127.3		4-6		audesite	
30	1978 Izu-Oshima-kinkai	Kurone	Shirata - Inatori (on Route 135)	HW	400.0				andesite, scoria	
31	1978 Miyagiken-oki	Nakayama No.2	Naruko - Nakayamadaira (on Rikuu-east Line)	RR	262.1	4.9 x 6.1	4-5	59 - 69		
32	1984 Naganoken-seibu	Otakigawa Dam	Otaki, Nagano	UT		2.7 x 3.0	5		sandstone, shale	
33	1993 Notohanto-oki	Kinoura	Orido, Suzu, Ishikawa Shimamaki Village	HW	76.0	6.8 x 5.1	5		mudstone, tuff	< 26
34	1993 Hokkaido-nansei-oki	Shiraito No. 2	(on Route 229)	HW	1463.0		6	60	talus	

Table K.2. Damage information of tunnels which hit by earthquakes (after ALA, 2001)

ID	Earthquake	Name of Tunnel	Damage at Portals	Damge within 30 m of portals	Damage to Liner > 30 m from portal	Notes
1	1923 Kanto	Hakone No. 1 (up) (down)	2	2	1	
2	1923 Kanto	Hakone No. 3 (up) (down)	4 - slide	3	1	
3	1923 Kanto	Hakone No. 4 (up) (down)	4 - slide	3	1	Damage varies from Table C-2.
4	1923 Kanto	Hakone No. 7 (up) (down)	2	4	1	lesser damage to down (mountain side) Damage varies from Table C-2.
5	1923 Kanto	Nagoe (up) (down)	1	2	3	Damage varies from Table C-2.
6	1923 Kanto	Komine	4 (Box section)	4 (box section)	3 (tube section)	liner type depends on location
7	1923 Kanto	Fudoyama	2	2	1	
8	1923 Kanto	Nenoueyama	4 - slide	3	4	steep slope
9	1923 Kanto	Komekamiyama	4	3	1	liner with invert arch
10	1923 Kanto	Shimomakiyayama	4 - slide	4	1	steep slope Damage varies from Table C-2.
11	1923 Kanto	Happonmatan	4 - slide	3	1	steep slope
12	1923 Kanto	Nagasakayama	2	3	4	Damage varies from Table C-2.
13	1923 Kanto	Yose	1	2	4	collapse accident reported during construction
14	1923 Kanto	Toke	1	1	4	
15	1923 Kanto	Namuya	2	3	4	steep slope, landslide suspected,

Table K.2 continued

ID	Earthquake	Name of Tunnel	Damage at Portals	Damge within 30 m of portals	Damage to Liner > 30 m from portal	Notes
						water acceident reported during construction
16	1923 Kanto	Mineokayama	2	3	4 of drift	under construction at time of earthquake, progressive failure after the main shock
17	1930 Kita-Izu	Tanna	1	1	4	under construction at time of earthquake, earthquake fault crossing the tunnel
18	1961 Kita-Mino	I Power Plant	1	1	3	cracking 32% of whole length longitudinal crck dominant
19	1964 Niigata	Budo	1	2	2	under construction at time of earthquake cracking on the ground surface
20	1964 Niigata	Terasaka	1	3	3	landslide area cracking on the ground
21	1964 Niigata	Nezugaseki	2	2	2	landslide area
22	1968 Tokachi-oki	Otofuke	1	1	3	landslide area, slope
23	1978 Izu-Oshima-kinkai	Inatori	3	2	3	earthquake fault crossing the tunnel trouble with geology during construction
24	1978 Izu-Oshima-kinkai	Okawa	1	1	2	damage over 60 m long
25	1978 Izu-Oshima-kinkai	Atagawa	1	1	2	damage over 400 m long
26	1978 Izu-Oshima-kinkai	Shiroyama	4	1	1	a gigantic rock crashed and blocked the portal
27	1978 Izu-Oshima-kinkai	Tomoro	3	3	3	cracking on the ground surface
28	1978 Izu-Oshima-kinkai	Shirata	4 - slide	2	3	steep slop cracking on the ground surface
29	1978 Izu-Oshima-kinkai	Joto	4 - slide	1	4	steep slope cracking on the ground surface
30	1978 Izu-Oshima-kinkai	Kurone	4 - slide	2	1	

Table K.2 continued

ID	Earthquake	Name of Tunnel	Damage at Portals	Damge within 30 m of portals	Damage to Liner > 30 m from portal	Notes
31	1978 Miyagiken-oki	Nakayama No.2	1	1	3	
32	1984 Naganoken-seibu	Otakigawa Dam	1	1	2	earthquake fault crossing suspected
33	1993 Notohanto-oki	Kinoura	2	4	3	collapse extended by aftershocks
34	1993 Hokkaido-nansei-oki	Shiraito No. 2	1	1	4	falling rock hit the exposed tunnel lining

FUN: Function of tunnel
- AC = Particle accelerator
- HW = Highway
- RE = Railroad
- UT = Utility
- WT = Water

Liner / support system
- 1 = Unlined 2 = Rock Bolt 3 = Timber 4 = Masonry/brick
- 5 = Unreinforced concrete 6 = Reinforced Concrete 7 = Steel pipe 9 = Unknown

Rock / Soil
- R = Rock S = Soil

COVER: Depth of cover above tunnel (meters)
PGA : Peak Ground Acceleration in g

DM : Damage State
- 1 = none
- 2 = slight (cracks, displacement, deformation)
- 3 = moderate (severe cracks, falling out, arch hanging down, swelling, invert cut)
- 4 = heavy (collapse)

CURRICULUM VITAE

PERSONEL INFORMATION

Surname, Name: Üçer, Serkan
Nationality: Turkish (TC)
Date and Place of Birth: 16.11.1978, KIRIKKALE
Marital Status: Single
Phone: +90 312 2157921
GSM: +90 533 510 97 37
e-mail: ucer.serkan@gmail.com

EDUCATION

Degree	Institution	Year of Graduation
MS	METU Civil Engineering	2006
BS	METU Civil Engineering	2002
High School	Kırıkkale Anatolia High School	1997

WORK EXPERIENCE

Year	Place	Enrollment
2010-Present	Üçer Engineering	Free-lance Consultant
2005-2010	METU Civil Engineering Department	Research Assistant
2004-2005	Su-Yapı Engineering	Geotechnical Engineer
2003-2004	STFA Temel Pile Construction	Chief Site Engineer
2002-2003	DOLSAR Engineering	Project Engineer

FOREIGN LANGUAGES

Fluent English, Intermediate Russian, Intermediate German

PUBLICATIONS

1. Üçer, S., Sağlam, S. and Bakır, B.S., 2009. Seismic slope stability assessment of a construction site at Bandırma, Turkey. Second International Conference on New Developments in Soil Mechanics and Geotechnical Engineering, Nicosia, North Cyprus.

2. Üçer, S., Işık, S. ve Bakır, B.S., 2008. Comparison of 2d and 3d Finite Element Modeling of Tunnel Advance in Soft Ground A case study: Bolu tunnels. 12th National Congress of Soil Mechanics and Foundation Engineering, 16-17 October 2008, Selçuk University, Konya, Turkey.

HOBBIES

Latin Dances, Gourmet, Billards, Darts, Travelling, Movies, Music